The Effects of Tibial Tray Rotation and Posterior Slope on Knee Kinematics Following Total Knee Replacement

By

Mr. Amer Karim, MBBS, FRCS (Tr & Orth), FRSA

A Thesis Submitted in Fulfilment of the
Requirements for the Degree of
Doctor of Medicine MD(Res)

Department of Mechanical Engineering
Imperial College London

May 2010

ABSTRACT

Aims

To determine the effects of tibial component rotation and posterior slope on kinematics following Scorpio CR navigated TKR in cadaver specimens.

Methods & Results

Knee kinematics were monitored using a validated IR Navigation System. Ten normal comparable cadaver specimens were mounted in a custom rig allowing assessment of kinematics under various loading conditions. The specimens then underwent Navigated TKR. The surgery was performed as per normal operating surgical protocols by an expert knee surgeon. However an augmented tibial component was implanted allowing the researchers to precisely modify its rotation and posterior slope. A pneumatic cylinder attached to the quadriceps tendon was then used to repetitively flex and extend the knee with a variety of applied loads.

Kinematics were different after TKR. Increasing posterior slope resulted in increasing posterior position of the femur, particularly at maximum flexion. Posterior slope also resulted in a deviation of the neutral path of motion and alteration of the normal envelope of laxity. Tibial component malrotations over 5 degrees resulted in deviations of the neutral path of motion without affecting the envelope of laxity. Combined malrotations over 10 degrees with posterior slopes over 6 degrees resulted in prosthetic subluxation under certain loading conditions.

Discussion

Knee kinematics are different after TKR. Increasing internal and external malrotation as well as the addition of posterior slope resulted in deviations of TKR kinematics through alteration of the neutral path of movement and or the envelope of laxity. Combined misalignments of slope and rotation resulted in the greatest deviations from normal kinematics, and in some cases, prosthetic subluxation. Incompatibilities of alignment may result in increased ligament tension and component articulation dysfunction that may contribute to premature wear and loosening. Surgeons should be aware of this when considering the addition of posterior slope or assessing tibial component positioning in TKR.

ORIGINALITY STATEMENT

I hereby declare that this submission is my own work and to the best of my knowledge it contains no materials previously published or written by another person, or substantial proportions of material which have been accepted for the award of any other degree or diploma at Imperial College London or any other educational institution, except where due acknowledgement is made in the thesis. Any contribution made to the research by others, with whom I have worked at Imperial College London or elsewhere, is explicitly acknowledged in the thesis. I also declare that the intellectual content of this thesis is the product of my own work, except to the extent that assistance from others in the project's design and conception or in style, presentation and linguistic expression is acknowledged.

DEDICATION

This thesis is dedicated with love and gratitude to my Mother for her extraordinary commitment to my education. Without her constant encouragement and support, I would not have had the courage to pursue my education to this level.

TABLE OF CONTENTS

ACKNOWLEDGEMENTS

Although this work carries my name, it is made possible only through the concerted efforts and the support of the many people who motivated me and assisted me to complete it, and to whom I am deeply indebted.

- Professor Andrew Amis
- Mr. Neil Thomas
- Dr. Anthony Bull
- Mr. Oliver Kessler
- Mr. Duncan Lucas
- Mr. Philip Wilson
- Mr. James Stoddard

The project was kindly funded by Stryker (Europe) Corporation.

PEER REVIEWED PUBLICATIONS

1. A. Karim, AMJ Bull, O Kessler, NP Thomas, AA Amis: The Effects of Tibial Tray Rotation and Posterior Slope on Knee Kinematics Following Total Knee Replacement – Abstract published in Journal of Bone and Joint Surgery (British Edition), Autumn Research Supplement.

2. A. Karim, AMJ Bull, O Kessler, NP Thomas, AA Amis: The Effects of Tibial Tray Rotation and Posterior Slope on Knee Kinematics Following Total Knee Replacement - Abstract published in Journal of Bone and Joint Surgery (British Edition), ISAKOS Supplement.

3. A. Karim, AMJ Bull, O Kessler, NP Thomas, AA Amis: The Effects of Tibial Tray Rotation and Posterior Slope on Knee Kinematics Following Total Knee Replacement - Abstract published in Journal of Bone and Joint Surgery (British Edition), EFORT Supplement.

4. A. Karim, AMJ Bull, O Kessler, NP Thomas, AA Amis: The Effects of Tibial Tray Rotation and Posterior Slope on Knee Kinematics Following Total Knee Replacement - Abstract published in Journal of Bone and Joint Surgery (British Edition), Annual Congress Supplement.

5. A. Karim, AMJ Bull, O Kessler, NP Thomas, AA Amis: The Effects of Tibial Tray Rotation and Posterior Slope on Knee Kinematics Following Total Knee Replacement – Extended abstract published in Journal of Mechanical Engineering IMECH Research Supplement.

6. A. Karim, AMJ Bull, O Kessler, NP Thomas, AA Amis: The Effects of Tibial Tray Rotation and Posterior Slope on Knee Kinematics Following Total Knee Replacement - Abstract published in Journal of Bone and Joint Surgery (British Edition), British Orthopaedic Research Society Supplement.

7. A. Karim, AMJ Bull, O Kessler, NP Thomas, AA Amis: The Effects of Tibial Tray Rotation and Posterior Slope on Knee Kinematics Following Total Knee Replacement - Abstract published in Journal of Bone and Joint Surgery (British Edition), Computer Assisted Orthopaedic Surgery Supplement.

PRESENTATIONS TO LEARNED SOCIETIES

- The Effects of Tibial Tray Rotation and Posterior Slope on Knee Kinematics Following Total Knee Replacement: British Orthopaedic Association 2009 Annual Congress, Manchester - Poster Presentation

- The Effects of Tibial Tray Rotation and Posterior Slope on Knee Kinematics Following Total Knee Replacement: British Orthopaedic Research Society Annual Meeting, Newcastle University June 2009 - Oral Podium Presentation

- The Effects of Tibial Tray Rotation and Posterior Slope on Knee Kinematics Following Total Knee Replacement: IMECH Knee Arthroplasty meeting, 30 April – 2 May 2009, The Royal College of Surgeons of England, London - Oral Podium Presentation

- The Effects of Tibial Tray Rotation on Knee Kinematics Following Total Knee Replacement: 10th EFORT Congress, 3–6 June 2009 in Vienna, Austria - Electronic Poster Presentation

- The Effects of Tibial Tray Posterior Slope on Knee Kinematics Following Total Knee Replacement: 10th EFORT Congress, 3–6 June 2009 in Vienna, Austria - Electronic Poster Presentation

- The Effects of Tibial Tray Rotation on Knee Kinematics Following Total Knee Replacement: 7th Biennial ISAKOS Congress, April 2009 in Osaka, Japan – Electronic Poster Presentation

- The Effects of Tibial Posterior Slope on Knee Kinematics Following Total Knee Replacement: 7th Biennial ISAKOS Congress, April 2009 in Osaka, Japan – Electronic Poster Presentation

- The Effects of Tibial Tray Rotation on Knee Kinematics Following Total Knee Replacement: 13’th ESSKA 2000 Conference, Porto, May 2008 – Oral Podium Presentation

- The Effects of Tibial Posterior Slope on Knee Kinematics Following Total Knee Replacement: 13’th ESSKA 2000 Conference, Porto, May 2008 – Oral Podium Presentation

- The Effects of Tibial Tray Rotation and Posterior Slope on Knee Kinematics Following Total Knee Replacement: Gauvain Society Meeting, Basingstoke, June 2007 – Prize Winning Oral Podium Presentation

- The Effects of Tibial Tray Rotation and Posterior Slope on Knee Kinematics Following Total Knee Replacement: ESSKA Travelling Fellows Meeting, London, March 2007 – Oral Presentation

LIST OF FIGURES

INTRODUCTION

More than 100 types of arthritis now afflict almost a billion people worldwide ([5]). In the majority of cases, this results in progressive joint destruction in which the articular cartilage is worn away resulting in a bone on bone articulation. This is very painful, not only when the patient is active, but at rest as well. Uneven wear in the joint can result in deformity and patients can become immobile and lose their independence and ability to perform basic activities of daily living ([15]).

The commonest form, Osteoarthritis (OA), affects over 45 million people in the USA alone ([15]). Studies indicate that primary OA is acquired and probably results from a combination of metabolic, genetic, chemical, and mechanical factors. Secondary OA usually follows an identifiable predisposing event (most commonly trauma, congenital deformity, or obesity) and leads to similar degenerative changes as the primary version, but at an earlier age. Osteoarthritis may first appear between the ages of 30 and 40, and is present in almost everyone by the age of 70. Before the age 55, it affects men and women equally, but after the age of 55, the incidence is higher in women and is thought to be related to changes in hormone profile following menopause.

The commonest site for OA is the knee joint with a symptomatic incidence of 1% per year and a radiographic incidence of 2% per year ([47]). Although the majority of patients with OA may be managed with medical treatment, analgesics and lifestyle changes, an increasing number of cases frequently require Total Knee Replacement (TKR) using implants made from cobalt-chrome or titanium alloys with polyethylene inserts (Figure 1). The polyethylene takes the place of the cartilage in the normal knee, and provides a low friction surface for the contacting surfaces of the implant components. The number of total joint replacements performed per year is growing rapidly. In 1998, an estimated 400,000 total knee replacements were performed in the United States alone, a 285% increase from the start of the decade ([4;74]), with numbers continuing to grow and estimated to reach 3.5 million new procedures per year in the United States alone by 2030 ([74]).

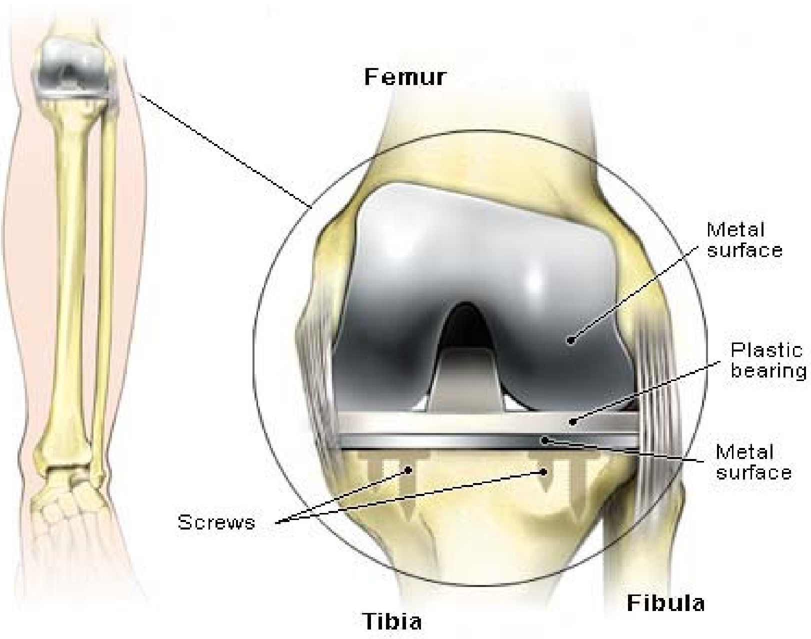

Figure 1: Simplified View of Modern Total Knee Prosthesis ([9])

Although artificial knee joints are expected to last over 15 years ([100]), research indicates that some implants fail within 10 years ([76]). In addition, implants do not allow the full functionality of normal joints, in terms of range of motion ([39]) and the types of activities that can be supported ([39]), with several studies reporting subjective dissatisfaction rates of 20% to 40% ([11;48;96]). Better implant designs are needed that have improved performance, longevity and patient satisfaction.

The Evolution of Knee Replacements

The concept of replacing damaged or worn out knee joints is not a new one. In the mid 19th Century, surgeons tried to apply the principles learnt from the hip replacements of the time to develop knee replacements. However, major differences exist in the mechanics of each joint: The ball and socket joint of the hip, driven by the surrounding muscles, is intrinsically stable when compared to the knee joint, which depends on its intra-articular and extra-articular ligaments for stability. In addition, the knee joint is not just a simple hinge joint as was first thought, but undergoes a complex series of movements that incorporate rolling as well as sliding motions across the joint in a normal flexion extension cycle.

The initial work upon which arthroplasty of the knee is based, focused upon a material for interposition between the articular surfaces of the femur and the tibia. Autologous tissue was first used as early as 1840 with *Verneviul* reporting the first interposition knee arthroplasty using joint capsule ([139]). Fifty years later, in a series of lectures in Berlin in 1890, *Thermestocles Gluck* described a total joint replacement fashioned from solid ivory and stabilized in bone with a cement fashioned from plaster of Paris, pumice and colophony ([140]). *Gluck's* concepts were excellent and very radical for a time when knee arthrodesis remained the only effective procedure for people with arthritis and dysfunction. Unfortunately, the materials science required for his concept was not available at the time, and his ideas were therefore discarded for nearly a century. *Verneviul's* interpositional arthroplasty efforts were revisited in the second decade of the twentieth century by *Murphy* and *Putti* ([105;112]) with fat and fascia lata interpositions in 1913 and 1920, again unsucessfully.

In the 1940's, attempts to copy the more advanced Total Hip Replacements of the time, resulted in the development of isolated femoral condyle moulds. These free floating acrylic discs failed frequently and early, and made subsequent revision surgery difficult or impossible due to the significant ligament and bone resections necessary for their insertion. *Sampson* tried cellophane for this purpose in I949 ([117]), with co-workers *Kuhan* and *Potter* using sheets of nylon in 1950 ([72]). Despite an evolution in materials and techniques, the results of interpositional knee arthroplasty remained unpredictable with high failure rates and poor clinical outcomes.

Arthrodesis remained the treatment of choice for the moderately destroyed knee in the mid-decade of this century,

The first use of metallic implants was reported by *Smith-Peterson* and *Harold Boyd,* who both inserted femoral moulded Vitallium interposition plates at the Massachusetts General Hospital in 1953 ([62]). Metal tibial plateau inserts were used in the late 1950's by *Mcintosh* ([85]). Although better than acrylic or nylon, the results of metallic interpositional arthroplasty were still too inconclusive to replace arthrodesis.

The concept of hinged knee replacements was being developed by *Judet* and *Crepin* as early as 1947 ([63]), with *Magnoni* reporting the first successful implantation in 1949 ([88]). The initial prostheses were made of acrylic but were replaced by metal hinged prosthesis in London in 1958 by *Walldius* ([141]), who accumulated the first ever large series of successful knee replacements till that time. By the 1960's, the hinged metal knee prosthesis had become an acceptable treatment for certain abnormalities of the knee.

The greatest advance in Total Knee arthroplasty came about in the 1960's with the development of materials science, engineering and a spin off the pioneering work in hip replacement surgery by *John Charnley* ([31]) and *G. K. McKee* ([95])*;* their discovery that prosthetic components could be secured in bone with methylmethacrylate; and that high molecular weight (medium density) polyethylene, stainless steel and cobalt chrome alloys were acceptable materials for arthroplasty. Two of the three obstacles to knee arthroplasty had now been solved; the materials to construct the prostheses and the cement fixation in the bone. The remaining challenge of providing motion and stability was to come in the next decade.

The first non hinged knee unit was designed and then used by *Frank Gunston*, who perfected his concept during his stay with *John Charnley* in Wrightington, England in 1968. *Gunstons's* concept was a knee with separate components, constrained within the soft tissue envelope of the knee's collateral ligaments and stabilized by the cruciate ligaments. He produced a design that resurfaced the knee rather than replaced it, with his implants utilizing the minimal amount of metallic component possible to reduce operative complications and permit arthrodesis should the implant fail. Following the development of his prosthesis on cadaver specimens, he performed his first polycentric knee arthroplasty in February 1968 (figure 2) at Wrightington and had performed 15 more by May 1969.

Gunston later revised his design in 1971 ([52]) to improve the implant kinematics. In this later model, he further reduced the metal content of the replacement and included a larger more anatomical polyethylene insert; the result was less friction and a greater range of movement, allowing flexion to 130º. By recognizing the importance and impact of kinematics on knee replacement, *Gunston's* designs led the way for a whole new generation of cemented polythene on metal knee implants, and also opened the world's eyes, to the importance of the understanding and development of knee kinematics.

A year later in 1972, an Englishman living in New York City, *John Insall*, designed what has become the prototype for all current total knee replacement prostheses, the Total Condylar Prosthesis (figure 3); with three separate components to resurface the three wearing surfaces of the knee, the femur, tibia and the patella. The implants were fixed to the bone with cement as before. But the key difference was in the implantation; this was the first total knee replacement complete with specific instruments for accurate bone cutting and implantation, with truly outstanding results! *Ranawat et al.* reported a survivorship of 94.6% at 15 years of follow-up which until recently was the most impressive reported series in the world to date ([113]).

This realisation of the critical importance of kinematics and implantation (figure 4) on the function and longetivity of knee implants through the work of G*unston* and *Insall*, in combination with advances in computer aided design, manufacturing and materials science in the 80's and 90's, spawned a whole new industry. Designs changed radically and implant companies began to explore design modifications to further improve kinematics. These modifications included the use of mobile bearing prostheses, posterior stabilised implants and full radius designs to name a few, as well as new materials science and minimal access instrumentation techniques.

Today with metal backed high molecular weight and highly cross linked polyethylene components, an increased inventory of appropriate sizes of implants, and markedly better instruments to perform the procedure as well as computer navigation, knee replacement results have now equalled or surpassed those of hip replacement ([4]).

Figure 2: Knee implants (from left): a Macintosh spacer, 1953; a Gunston polycentric femoral component, 1969; a Geomedic (Zimmer) with an unsupported all polyethylene tibial insert and a femoral component that does not replace the patella-femoral articulation, 1976; a Kinemax (Howmedica) with a tibial insert supported by a metal tray and a femoral component with an anterior flange for the patella-femoral articulation, 1983 ([6]).

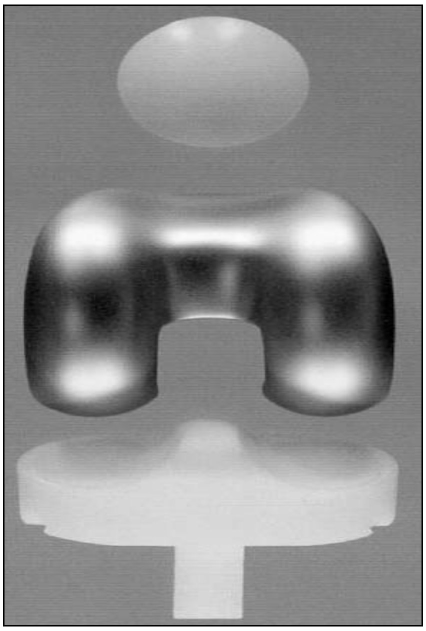

Figure 3: John Insall's "Total Condylar Prosthesis " total knee replacement, of which he successfully implanted over 300 by 1976 ([6])

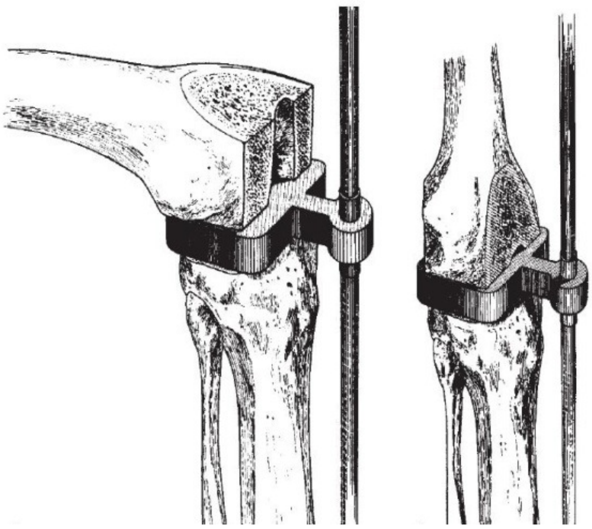

Figure 4: In 1974, Insall first coined the terms flexion and extension gap. He described the use of an alignment rod and spacer block to achieve the properly balanced gaps between the femur and tibia ([6]).

Knee Kinematics

Kinematics is the branch of mechanics that studies the motion of a body or a system of bodies; without consideration given to its mass or the forces acting on it. As applied to the knee joint, it describes the three dimensional envelope of movement that occurs at the knee joint. Normal knee kinematics allows for increased surface conformity and subsequent balanced implant loading throughout the range of motion ([102]).

There have been significant evolutions in the concepts of normal knee kinematics from a simple hinge joint as suggested in the late 19th Century ([153]), to the recently understood complex joint, with kinematics in all three orthogonal planes. This multiple axis movement results from the asymmetric bony and soft tissue anatomy described below (figures 5, 6).

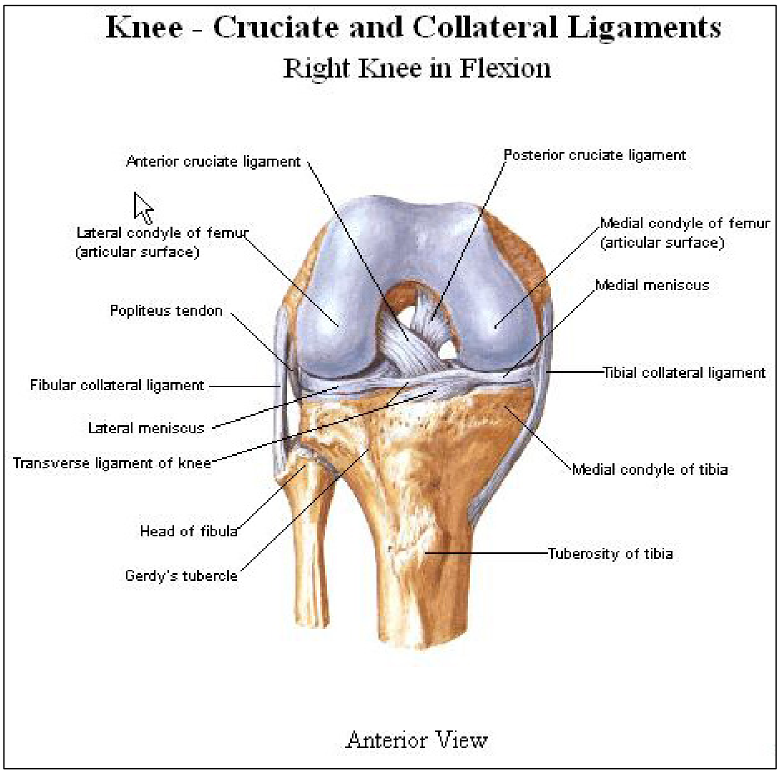

Figure 5: anterior view of knee in flexion ([6])

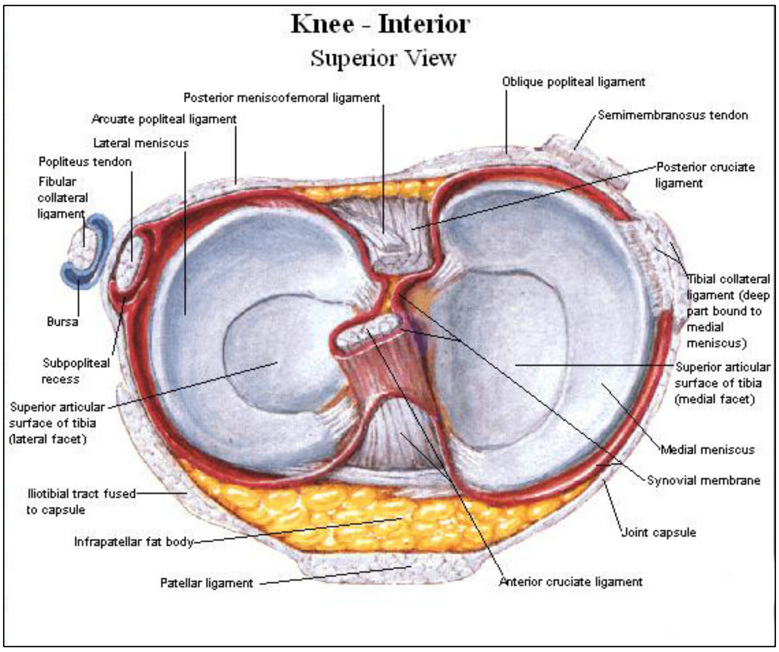

Figure 6: Superior view of the tibial plateau ([6])

Movement of the knee joint can be classified as having six degrees of freedom, three translations: anterior/posterior, medial/lateral, and inferior/superior and three rotations: flexion/extension, internal/external, and abduction/adduction. The movements of the knee joint are determined by the shape of the articulating surfaces of the tibia and femur, the muscular and gravitational forces imposed and the orientation of the four major ligaments of the knee joint: the anterior and posterior cruciate ligaments and the medial and lateral collateral ligaments.

The normal angulation of the distal femur ([16]) results in the knee joint being in 5º to 7º of valgus, depending on sex, height and race. The medial femoral condyle is larger and more spherical than the lateral condyle, resulting in a deeper and wider articulation compared to the lateral side. The medial and lateral menisci differ in shape, size and mobility ([33]), creating a concave medial tibial plateau that is deepened by the medial meniscus. In comparison, the deeper lateral meniscus rests on a laterally concave saddle shaped tibial plateau ([33]). There are also differences in the ligamentous architecture between the medial and lateral collateral ligaments, and the Anterior Cruciate Ligament (ACL) and the Posterior Cruciate Ligament (PCL), with regard to their bony attachments and individual tensions through a flexion-extension cycle ([53;150]).

The net result is an axis of tibial rotation close to the tibial attachment of the ACL at 0º of flexion, which moves towards the tibial attachment of the PCL at 45º of flexion ([93]); and an envelope of rotation laxity that allows 8.3º of tibial rotation at 0º of flexion, increasing to 31.7º at 30º of flexion and decreasing to 24.8º at 90º of flexion ([93]). This ACL tethered tibial external rotation is termed the "screw-home mechanism" and is a physiological rotation between the tibia and femur and occurs automatically between full extension (0^o) and 20^o of knee flexion. It is attributed to the function of the ACL in the presence of the asymmetry of the medial and lateral condyles and a resultant movement in full extension[9]. This external rotation helps to lock the knee when in full extension, providing a stable construct for locomotion (figure 7).

Knee flexion also results in a physiological posterior translation of the femoral condyles termed "femoral roll back". This mechanism is due to the asymmetry between the lateral and medial femoral condyles and occurs automatically from approximately 20º of knee flexion. The actions of the PCL in flexion produce a medially anchored knee with some lateral mobility in the antero-posterior plane. The observed posterior translation of the femur in flexion increases the range of knee flexion by increasing the clearance of the tibia and preventing impingement in deep flexion ([81;103]). It also serves to translation the tibia anteriorly, increasing the moment arm and efficiency of the quadriceps muscles in deep flexion (Figure 8).

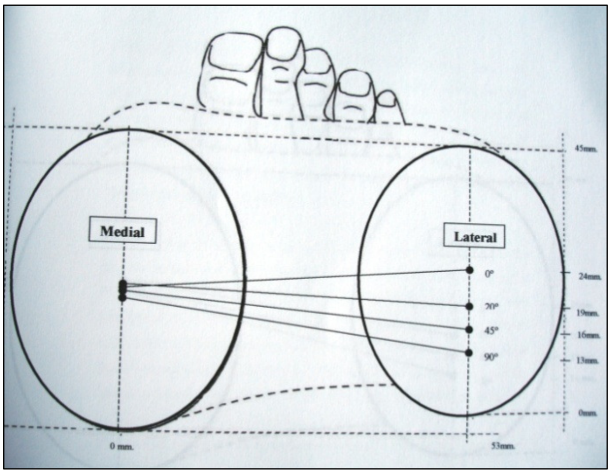

Figure 7: Diagram illustrating the medially anchored femoral condyle, while the lateral condyle glides across the tibia through the flexion extension range [93]

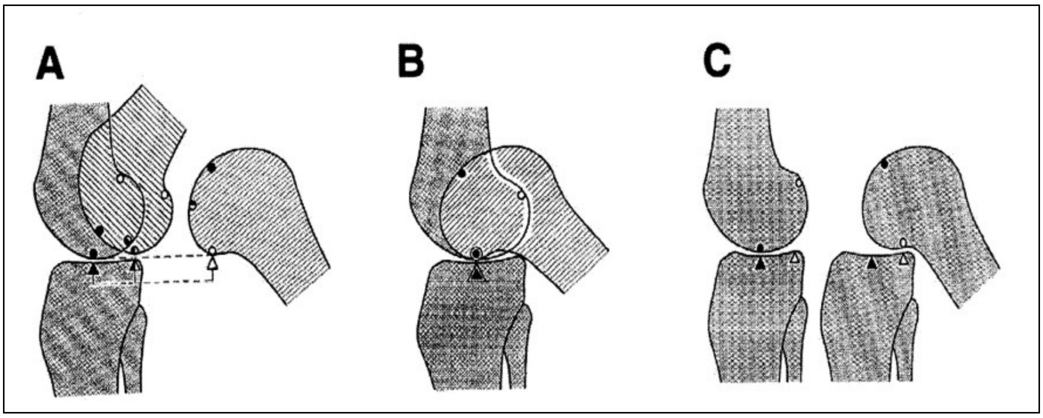

Figure 8: Diagram illustrating femoral roll and glide as the knee approaches full flexion [81]

Following TKR, prosthetic articulation geometries and residual ligamentous support can vary substantially from the normal knee and between different prostheses, altering the subsequent knee kinematics.

Uvehammer et al used roentgenstereophotogrammetric analyses to demonstrate that both cruciate retaining and sacrificing knee designs exhibited abnormal kinematics, with abnormal tibial AP motion in knee extension, compared with control subjects ([137;138]). Banks and Hodge ([19]) found a closer reproduction of knee kinematics with cruciate sacrificing designs utilising an average medial centre of axial rotation during extension. However, applying the same principals to a cruciate retaining design resulted in a paradoxical medial femoral condylar roll forward with knee flexion ([19;80;128;129]). Abnormal rolling forces and sliding forces have also been demonstrated after TKA ([148]) due to the relatively high coefficient of friction of artificial joints (u = 0.03-0.01 ([49])) compared to the native knee joint (u = 0.002-0.03 ([40])), these findings accounting for some of the observed abnormal kinematics.

Implant choice, surgical technique and component positioning therefore play crucial roles in the mechanics and function of the prosthetically replaced knee. Incompatibilities of alignment, joint loading or implant geometry will produce abnormal knee kinematics. This may manifest clinically through subjective dissatisfaction ([11;48;96]) or mechanically through abnormal joint contact forces that may ultimately result in early implant failure due to loosening or wear ([142;149]). If implants can be designed that better replicate normal knee kinematics, then this may improve the satisfaction, performance and longevity of implants.

Measuring Knee Kinematics

Over the last few centuries, our understanding of human locomotion and movement at the knee has been a function of the methods available at the time, with the expanding need for enhancing our understanding of normal and pathological human movement driving the introduction of new technologies and methods.

The *Weber brothers* (1836) reported one of the first quantitative studies of the temporal and distance parameters during human locomotion ([143]). Their work established a model for subsequent quantitative studies of human locomotion.

During the 1950's there was a need for an improved understanding of locomotion for the development of prosthetics to treat the injured veterans following the Second World War. The classic work at the University of California ([41]) provided a tremendous resource of knowledge related to the mechanics of human movement. This work, formed the basis for many of the fundamental techniques currently used for the study of human locomotion (Figure 9).

More recently, instrumentation and computer technologies have provided new opportunities for the advancement of the study of human locomotion. The limitations with respect to automated motion capture as well as measurement reduction no longer exist. New methodology has made it feasible to extend the application of kinetic analysis to clinical problems. Mathematical models have been developed for the knee and leg that contain numerous equations of motion (*e.g.*, up to 30 ([71])), but these need empirical data to determine key parameters, in order to study the effects of real-life activities (walking, stair climbing, etc.) on component position and wear. It is critical to analyze joint kinematics dynamically under a variety of loading conditions that replicate the effects of muscle loads and soft tissue constraints as would be present in patients both with and without knee pathology.

Several evaluation techniques exist and have had variable levels of success in providing either in vivo or dynamic capabilities. These have included cadaveric simulations ([14;26;146;147]), subject gait labs ([104]), externally worn goniometric devices ([119]), dynamic and static Radio Stereo-Metric Analyses ([14;18]), open MRI and CT scanners ([79;101;118;124]), industrial robot movement systems or simulators ([71]) and computer navigation tracking systems ([107;152]).

Gait Labs and Goniometric Analyses

With the development of photography in the late 1800's, it became possible to capture image sequences which reveal the details of human locomotion not noticeable by the human eye alone ([64]). The first research was done using plate cameras and stroboscopes; however these were subsequently superseded with film cameras. This technology dubbed "gait lab" and the subsequent branch of "goniometric analysis", evolved rapidly as it was popularized by medical research in the 1980's (figure 9).

Knee kinematics can be recorded utilising this technology in a variety of systems and methodologies:

1. Plain photography, which is the most basic method, often augmented with strobe lighting at a known frequency to improve the image quality.

2. Video recording using footage from single or multiple cameras, aided by the development of analysis software that allows for analysis in 3 dimensions.

3. Active or passive marker systems, worn by the subject: The numerous "hot points" are then tracked by multiple motion or infra red (IR) cameras and the data combined in a computer to provide 3 dimensional movement data.

4. Goniometric devices, again worn by the subject: These contain rotating platforms in single or multiple planes that transduce a subject's movement either in space or across a joint, into an electrical signal that is recorded and then processed by a

computer. When multiple signals are combined, a 3 dimensional movement simulation is obtained.

The above methods record only the movement of the subject in space. In order to calculate the kinematics, the labs utilise a floor load transducer or force platform. This measures the ground reaction forces magnitude and direction. A computer then combines the data sets to calculate the true kinematics ([8]).

Three major factors make the routine use of gait analysis for knee kinematics impractical, particularly in individuals with poor walking ability: The first is the setting up of the lab walk-way which requires considerable physical space and effort to place and calibrate all the cameras accurately in relation to one another. The second is the time and effort required for setting up and testing a subject and the associated burden to that person; depending on the particular protocol, the apparatus attached to the subject is frequently heavy and constrains joint movement itself. The final major limitation is the time and efforts required to process and analyze the data. Errors due to skin movement artefact and the unreliability of data acquisition and processing methods require an inordinate number of trials, burdening both the subjects being tested as well as the recording staff.

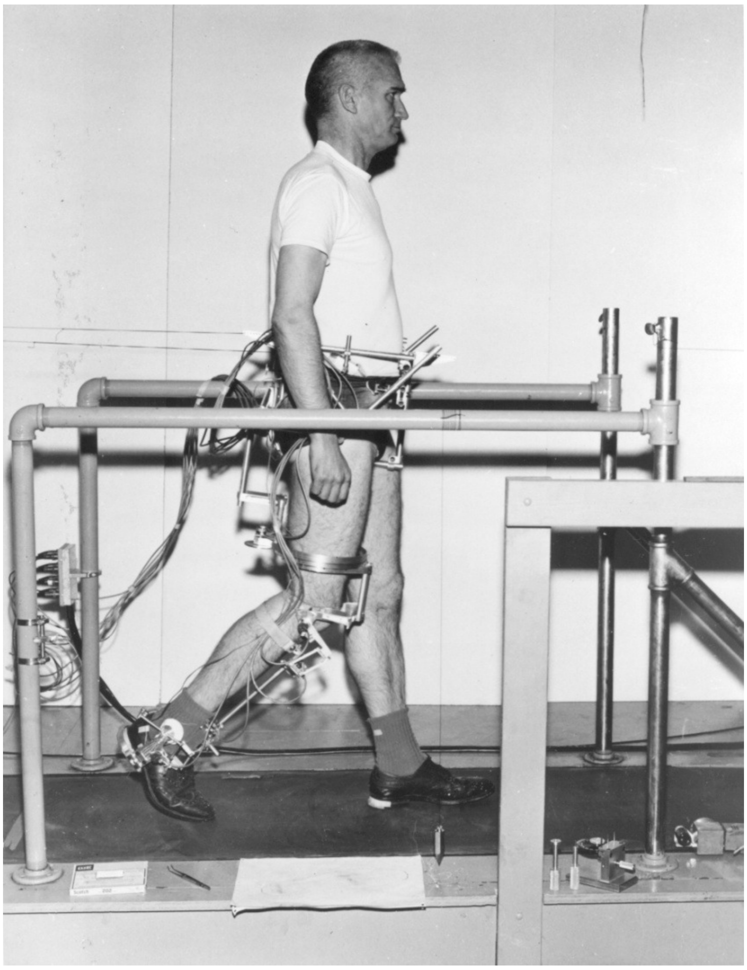

Figure 9: A photograph of the exoskeletal goniometer as used in the pioneering work and subsequent thesis “Experimental Kinematics of Human Walking”, University of California at Berkeley, 1970 ([6]).

RSA – Radio Stereo-Metric Analysis

Roentgen stereophotogrammetry (RSG) is a technique for measuring the three-dimensional (3-D) position of an object in space using 2 or more X-rays taken at an angle to each other (figure 10). Although the history of RSG dates back to the invention of X-rays ([35]), the broad application of modern RSG started after the technique was further developed by *Göran Selvik* in 1972 in Lund, Sweden ([122]). Selvik named his method Roentgen Stereophotogrammetric Analysis (RSA) ([121]). Selvik's original experiments utilised Vitallium as a radio-marker, however he swapped over to tantalum because of its increased density (atomic number 73) and its enhanced biocompatibility.

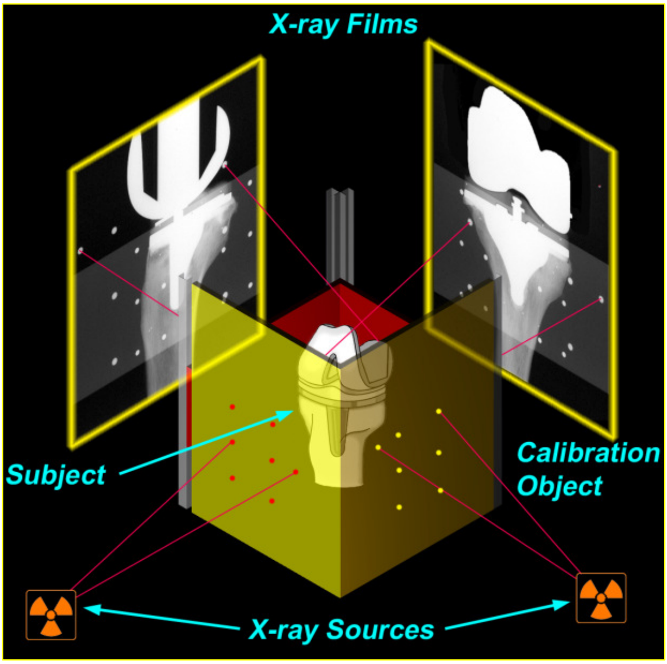

Figure 10: Diagrammatic view of a typical RSA setup with 2 X-ray beams projecting the same subject at right angles to each other at the same projected distance ([6]).

RSA, though usually limited to the study of static objects in 3D space, has also been used to assess joint kinematics dynamically. The first study on knee joint kinematics was initiated as early as 1986 on cadaver specimens ([36]), utilising a pair of film exchangers allowing sequential exposures at a rate of 4 exposures per second.

Traditionally for the analysis of knee movements, spherical radio-opaque markers are attached to implant components (figure 11) or inserted into the host bones to define these objects for kinematic measurements. One limitation of this technique is that markers can be obscured by metallic components of the implant rendering them invisible in X-ray images. Also, the addition of markers to modern implants is often impractical as they are difficult to attach and may interfere with the movements and design. Model based approaches to RSA require precise implant computer modelling which is expensive and time consuming. There is also the issue of significant radiation exposure during the analysis both to the subject and to the operators of the equipment.

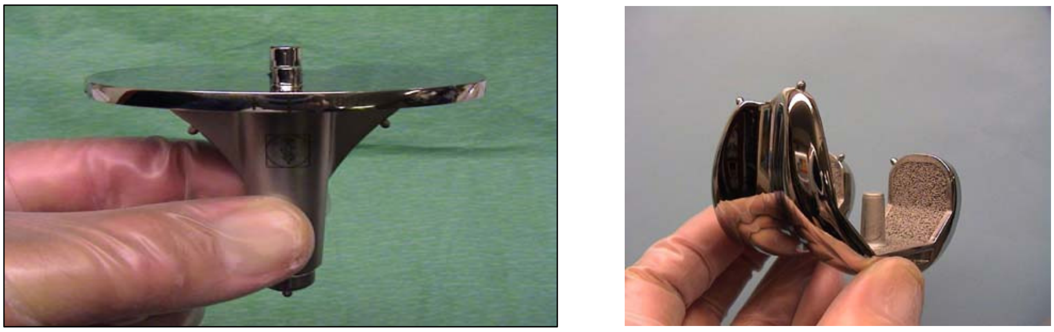

Figure 11: Examples of implants that have been modified to include attached spherical tantalum beads ([6]).

X-ray Fluoroscopy

New developments in fluoroscopic technology have shown X-ray video fluoroscopy to be a useful tool for kinematic analysis of the knee joint ([42;75]).

A fluoroscope consists of a radiation source and an image intensifier. X-rays leave the radiation source, pass through the subject matter and strike the input phosphor of the image intensifier. The X-ray image is processed on a phosphor screen and the developed image is then recorded by a video camera. The result is essentially an X-ray "movie" which can be viewed on a monitor and transferred to a video tape or computer (figure 12).

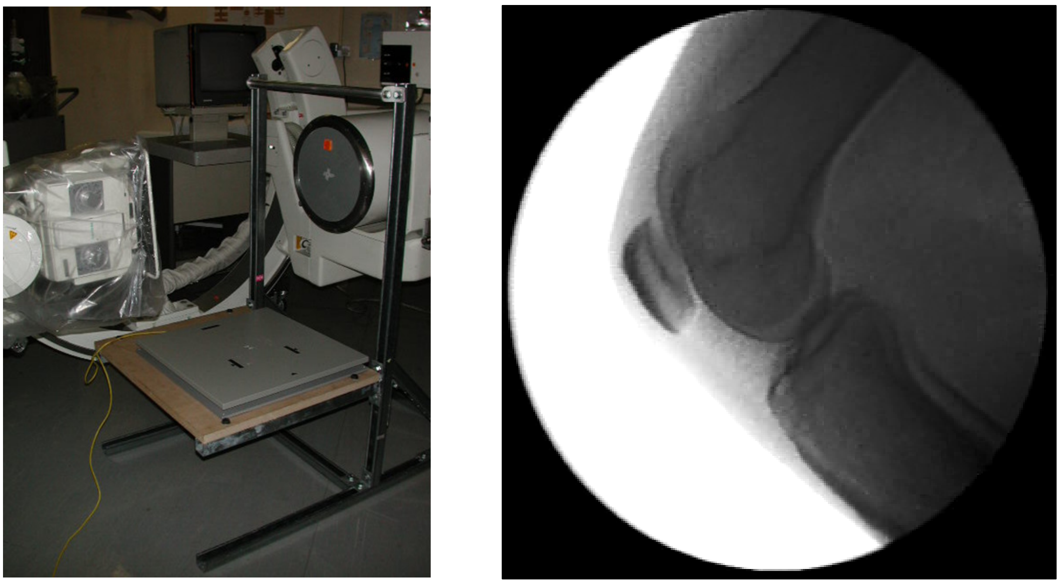

Figure 12: A typical fluoroscopic setup; the subjects knee joint is raised on a fixed platform such that the centre of the knee remains in the in the centre of the Image Intensifier beam. Knee movements are then screened and recorded by the X-ray beam ([6]).

Fluoroscopic setups allow the patient to perform real-life load-bearing activities (within the working volume of the fluoroscope) such as a deep knee flexion. However due to the relatively poor resolution of the images and low frequency of images, it is limited to patients with implants that interpret more clearly than the native joint. Fluoroscopic images are also only two-dimensional and therefore suffer with errors of subject rotation in the X-ray beam. A few authors claim to have been able to obtain all three-dimensions ([37;54]), but only after CT scanning and CAD modelling of the subjects (which is an entire project on its own). As with RSA there is also the issue of significant radiation exposure during the analysis both to the subject and to the operators of the equipment

Open MRI and Computer Tomography (CT) Scanners

MRI and CT scanners provide detailed images of the body in any single plane and have been used for kinematic analysis of the knee joint ([42;71]). MRI has the advantages of much greater soft tissue contrast compared to CT and does not expose the subject to ionizing radiation.

Kinematic analysis of the knee using single plane imaging is difficult. The contacts between the tibia, femur, and patella impose complicated nonlinear constraints on their positions and orientations throughout a flexion extension cycle. In order to create a true 3D motion sequence, multiple scanning runs through different planes with identical knee movements and loads have to be performed and the various knee constraints have to be computed numerically with constraints and variables to motion varying between subjects. Also due to the space constraint of both scanners, kinematic protocols are limited to: passive positioning, active isotonic movement within the confines of the scanner and isometric contractions against resistance. These protocols are often combined with positioning devices to guide the joint in a specific plane of imaging. These devices may constrain the free movement of the knee and bias the kinematic results (figures 13, 14).

With regard to total knee kinematics, both MRI and CT images suffer with significant artefacts related to the prosthesis. These artefacts can be reduced with software manipulation, but at the cost of degradation of the final image sequences.

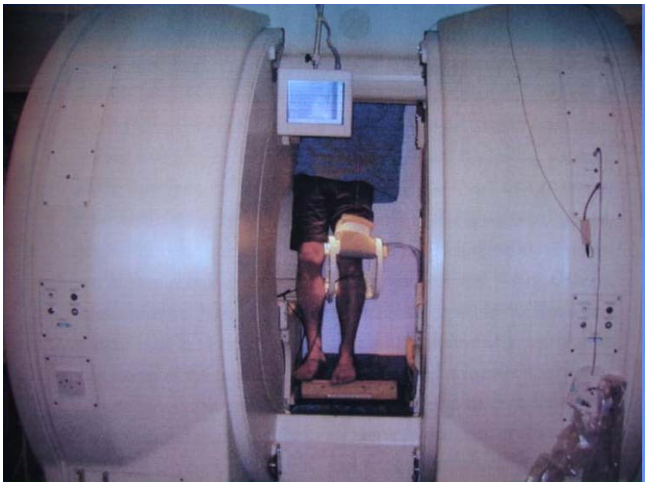

Figure 13: Picture of an open MRI scanner with a subject undergoing constrained movement-against-resistance knee kinematics analysis ([6])

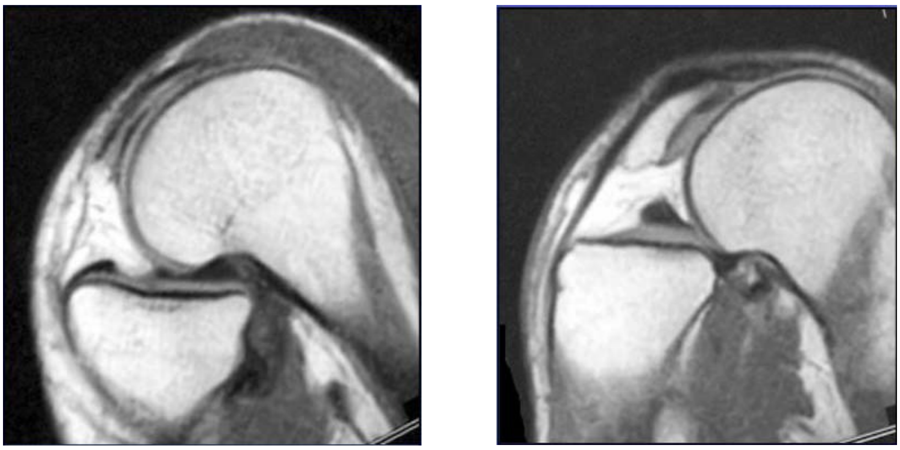

Figure 14: Two dynamic MRI Images demonstrating femoral roll back in deep flexion([6])

Computerised Navigation Systems

The use of computerised navigation in orthopaedic surgery is well established and has been shown to increase the accuracy of component and instrument placement when compared to standard jig based systems ([21;44;86;110;135]). This ability of a navigation system to triangulate and precisely guide a target object in three dimensions can be used in reverse to precisely track a target object's movement and record precise kinematic data.

These advances in computer navigational tracking are possible through the development of compact six degrees of freedom orientation and position trackers and respective high frequency tracking cameras. The trackers are attached to the bones either side of the joint being analysed and register themselves in free space through an infrared, optical or magnetic tracking system.

Infra Red (IR) systems utilise an LED generated IR pulse in the range of 50 to 150 Hz. The pulse can either be emitted directly by the battery-powered tracker (direct transmission), or from an emitter contained within an overhead boom (reflected transmission).

In direct transmission systems, the emitted IR pulse is identified by a spaced array of IR cameras in an overhead boom. In reflected transmission systems, the bone mounted trackers consist of a set of reflective spheres. The reflected IR pulse is identified by a spaced array of IR cameras in the same overhead boom containing the emitter. The computer system then triangulates the source of the pulse by simple spatial calculation and converts the analogue position to a digital signal that can be viewed on a monitor and recorded for analyses.

Optical tracking systems triangulate and process positional data in a similar way to the IR systems, but utilise a series of optical image recognition stereo metric cameras on an overhead boom. The tracker arrays are then composed of a set of three spheres arranged in a triangular formation. This array is then tracked by the optical tracking system and the size and relative position of the three spheres is used to calculate the position in three dimensions by the computer system.

Electromagnetic navigation systems work via an electromagnetic field generated by a stationary emitter, which is positioned near the operating field. The surgical instruments and jigs are each equipped with a magnetic coil designed to work with the system. As each one is introduced, it disrupts the predetermined electromagnetic field. The system's computer then recognizes the instrument due to its unique magnetic signal and calculates its three-dimensional location in the surgical field.

Misalignment and Implant Failure

Although total knee implants have revolutionized orthopaedic health care, enabling millions of people to walk again, there remain some significant problems. The most serious of these problems is premature failure. Despite continued improvements in component design, surgical technique and cementing technology, after infection, misalignment and aseptic loosening are still the most frequent reasons for revision surgery following TKA ([34;116]).

Premature wearing of the polyethylene inserts (figure 15) due to repeated frictional contact generates loose particles which lead to inflammation of the joint, osteolysis, and eventual implant loosening ([151]). It has been shown that the kinematics of artificial knees involve excessive sliding and rotational motions ([108]) which may lead to high shear stresses through the polyethylene bearing, particularly if there is compounding misalignment of the components as well.

Figure 15: Polyethylene wear in total knee replacement inserts affects the direct functioning of the implant, with the released wear debris resulting in osteolysis and implant loosening([6]).

Nevertheless, misalignment in isolation also causes premature failure through instability, dislocation, stiffness and pain, necessitating revision surgery, even in the absence of loosening or wear. Reported revision rates following TKA are as high as 9% ([73]) and cost more than £3 billion per year in the USA alone ([25]).

Tibial component misalignment encompasses component varus & valgus position, correct coronal positioning, component fit, rotational alignment and tibial slope. Any significant tibial component misalignment will produce abnormal knee kinematics, contact forces and may ultimately result in implant failure due to loosening or excessive wear ([142;149]).

Varus & valgus component misalignment is common in primary TKA (figure 16) with 5º of post operative varus or valgus misalignment present in up to 17% of implanted joints ([126]). Experimentally in cadavers, a varus or valgus misalignment of only 3º has demonstrated significant alterations in medial and lateral compartment loading ([144]) that would ultimately affect component survival. Poor surgical technique, improper jig use and utilization of an intra-medullary technique in the presence of excessive tibial bowing have all been cited as causes for the surgical bone resection errors ([134]) that commonly result in a varus or valgus misalignment. Slotted tibial cutting guides ([111]), the use of an intra-medullary technique with accurate entry points and the use of larger intra-medullary rods, have all been shown to improve varus and valgus alignment ([87]) in TKA.

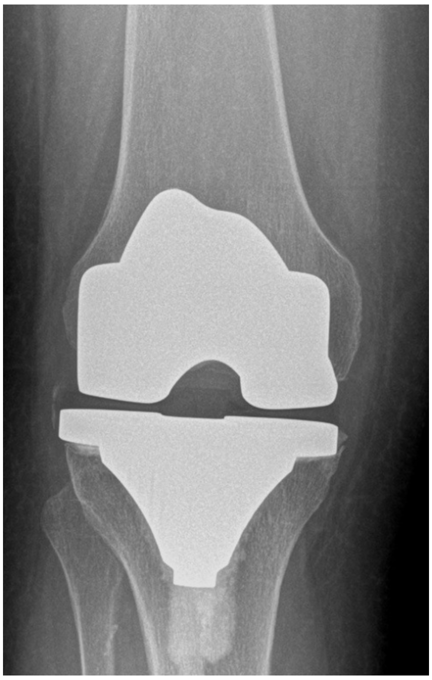

Figure 16: AP weight bearing radiograph of TKR demonstrating slight valgus component misalignment.

Coronal tibial component positioning, tibial tray internal and external rotation, tibial try fit, tibial posterior slope and tibial tray overhang are important variables in the outcome of TKA. Ideally, the tibial component should cover as much of the cancellous and cortical shell of the tibia as possible, to allow optimal weight distribution, without overhanging at any point. Alignment should optimise kinematics, and allow satisfactory patello-femoral capture and tracking, even in the presence of physiological tibial torsion.

Tibial component malrotation is the commonest positioning error in TKA, with studies demonstrating as much as 96% of components incorrectly placed in a wide range; from 10º of external rotation to 28º of internal rotation ([56;92;115]). Even a small error in the rotation of the tibial tray may result in altered patello-femoral kinematics, causing patellar tilt (figure 17) and anterior knee pain ([92]) and even cases of patellar fracture. Tibial cortex laser strain studies have demonstrated that tibial-femoral rotational misalignments as small as 2º caused abnormal tibial torques in excess of 4 Nm, which increased to over 8 Nm at 10º of rotational misalignment ([67]). Component retrieval studies have also confirmed that critical wear can be associated with even slight rotational misalignment of the tibial component ([142]).

The high prevalence of tibial component malrotation is often due to unidentified factors including missed, and therefore uncorrected tibial torsion at the time of surgery, purposeful and wrongful surgical overcompensation to enhance patella capture and tracking, and femoral component malposition. The common, well established technique of "floating" the tibial component into position using the aligning forces of the femoral component through the full range of knee motion, can successfully locate the best kinematic position for the tibial component; but only if the femoral component is precisely positioned and the tibial and femoral components are highly conforming. But even in experienced hands, significant isolated femoral component misalignment is present in up to 25% of cases, and can vary from 9º of internal rotation to 14º of external rotation ([98]). These errors in femoral component positioning are subsequently compounded when positioning the tibial tray, resulting in total prosthesis misalignment. As the patella is still normally aligned, its tracking and kinematics are significantly compromised with increased shear forces in early flexion ([70]).

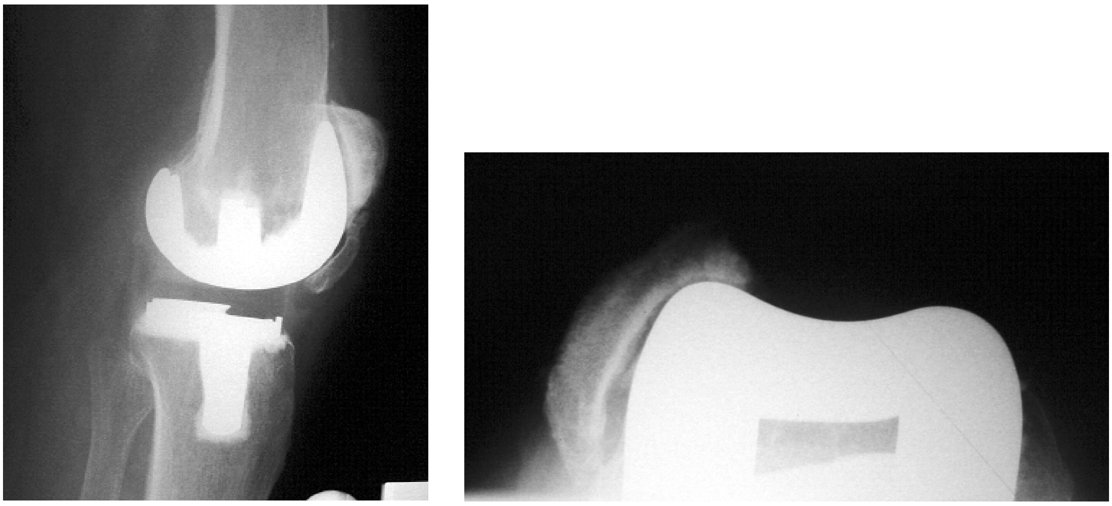

Figure 17: Lateral and skyline radiographs demonstrate patella subluxation as a result of component malrotation ([10]).

Tibial component positioning resulting in poor coverage, fit or overhang is also undesirable and has been shown to increase component subsidence and migration ([92]) (figure 18). The recovery of the stabilising soft tissues is also affected, resulting in stiffness and decreasing the range of knee movements post operatively ([87]). Careful component sizing and trialling prior to definitive fitting should allow an achievable average coverage in excess of 80% with no overhang, in the majority of cases ([70]). With regard to symmetry, no significant differences in component fit have been demonstrated between symmetrical and asymmetrical components so far, in either experimental or clinical studies ([98]).

Figure 18: Lateral radiograph demonstrating total knee dislocation following subsidence and collapse of the tibial tray secondary to malposition. The posterior overhang of the component has resulted in anterior under hang of the tibial component with subsequent subsidence resulting in failure ([10]).

The role of posterior slope in tibial component positioning is still controversial, with some published clinical studies showing no advantage from the addition of tibial slope ([12;66;68;97;120]). However other studies suggest that the addition of some of tibial slope can be help balance the knee in the presence of PCL tightness ([50;82]). A TKA retrieval study suggested that knees implanted with excessive posterior slope suffer from posterior loading of the tibial insert with subsequent increased wear ([142]). This has also been shown in biomechanical experimental studies ([17]). Posterior loading observed with posterior slope ([29]), can also compromise the PCL if it is left intact post-TKA, inducing excessive posterior laxity ([27;94]), as well as increasing the varus, valgus and rotational laxity of the knee ([61;145]). This can result in instability, poor patellar tracking or subsequent dislocation. A posterior position of the femur can also compromise the function of the quadriceps muscles, particularly in deep flexion ([109]).
One study has demonstrated an advantage from tibial slope, with gains of 1.7º of extra flexion per degree, to a maximum slope of 7º ([23]). These gains in flexion were

achieved by reducing direct component impingement in deep flexion, and by dealing with the recurrent paradoxical tibial up slope and unevenness of cut obtained when cutting with a flexible saw blade ([23;84;136]).

The Scorpio Cruciate Retaining TKR System

The Scorpio prosthesis was designed by *Dr. Schmalzried*, and first implanted at the Joint Replacement Institute in 1996 ([2]). It has since undergone many modifications and improvements. To date, more than half a million Scorpio knee prostheses have been implanted worldwide (figure 19).

Figure 19: Stryker Scorpio total knee replacement implant ([130]) .

The implants are made from a Vitallium-cobalt-chrome-molybdenum alloy and are available as cemented or interference fit (uncemented) implants. In both cases, the femoral joint articulating surfaces are highly polished and articulate with a high molecular weight polyethylene insert. The cemented implants have a grit blasted back surface finish and femoral pegs to allow good adherence to the cement. The implant volume is also slightly reduced compared to the bony resections to allow for a 2 mm cement mantle. The uncemented implants have porous coated backs to allow bony in-growth and slightly greater volume compared to the bony resections. They are designed to be implanted tightly to provide an initial interference fit while biological fixation is achieved. The tibial inserts for the fixed and mobile designs are manufactured from ultra high molecular weight polyethylene (poly) and are secured into the Vitallium tibial component with a fixed keel, using an anterior metal circlip.

The Scorpio CR femoral component is a single axis or full radius design, based on the philosophy that there exists a single flexion / extension axis in the knee that is equivalent to the transepicondylar axis ([57]). The implant has been designed around this perceived centre of rotation, optimising its kinematics in a fixed bearing system ([123]), and reducing mid flexion instability by maintaining ligament isometry throughout the flexion / extension cycle ([22]). The femoral component also has the added benefits of a longer moment arm that has been shown to reduce the patello-femoral joint reaction force and reduce anterior knee pain compared with other implants ([89]). It also has a patellar groove and anterior patella recess that allows better patellar capture and tracking ([89]) (figure 20).

Figure 20: Full radius profile of Scorpio femoral component with patello-femoral recess and groove ([130]).

The superior surface of the Scorpio CR fixed tibial tray insert has a dished symmetrical medial / lateral design which is congruent with the single radius design of the femoral component. The anterior sulcus of the insert is raised and sloped posteriorly. This helps to prevent excessive posterior subluxation and reduces PCL stress. The insert also has 4º of posterior slope built into the design to allow deep flexion, and a relatively flat central eminence designed to allow up to 15º of internal and external rotation to compensate for anatomical variations and minor degrees of misalignment. The inferior surface of the insert is grooved on the anterior and posterior aspect of the insert. These grooves correspond to lips on the tibial tray, allowing the insert to be securely clipped into the tibial insert with an anterior stainless steel circlip. The tight peripheral lock of the insert prevents accidental release of the insert and also minimises micro motion of the insert within the tibial tray (figure 21).

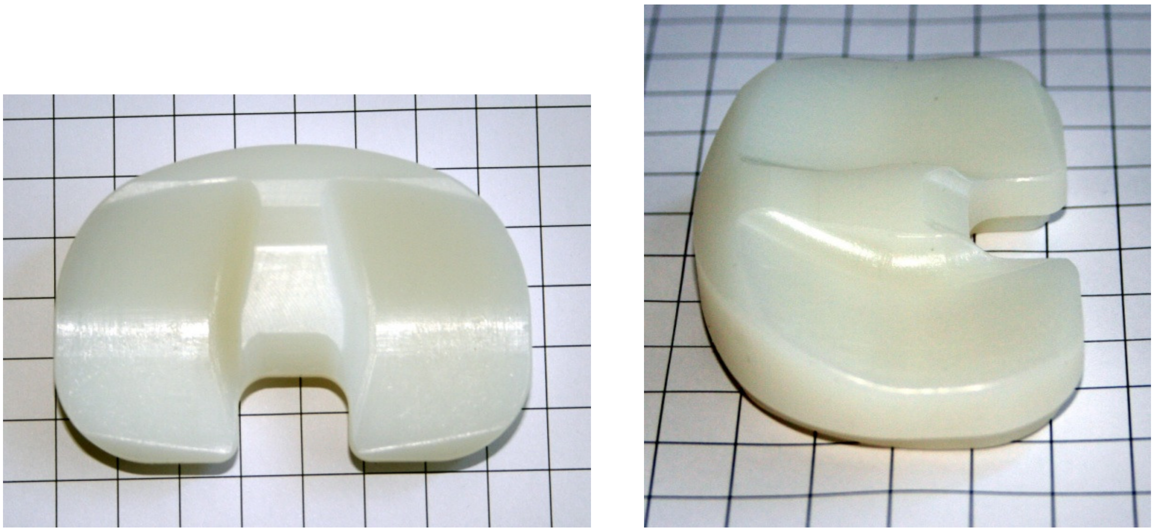

Figure 21: Photographs of a Stryker Scorpio CR polyethylene tibial insert.

The Scorpio CR tibial tray component is a symmetrical central keeled tibial tray with a posterior central recess for the PCL. The keel is 3cm deep to engage the cancellous bone in the tibia. The triangular fins that arise from the central keel span almost the whole width of the tibial implant and are ridged to provide rotational stability whilst minimising bone loss.

The Scorpio resurfacing domed patella is machined from solid polyethylene and available in a range of sizes to allow the closest fit to the bony margins of the patella. It has 3 pegs on the underside to aid fixation and is cemented into the pre prepared patella.

The Stryker Scorpio's modular single radius design, multiple sizing options for close anatomical fit, options for navigated or instrument implantation and proven clinical success with 9 year survival rates in excess of 95% ([90]), continue to make it a popular and successful choice of implant for primary total knee arthroplasty

Computer Assisted Surgery

Computer assisted surgery or "navigation" has been in existence in some form or other now for more than 10 years in many areas of medicine and has been used to help guide the placement of needles, cutting guides, instruments, and implants. In TKA, navigation systems have been shown to improve the accuracy of tibial and femoral bone resections, improve component positioning ([21;44;86;110;135]) and help with soft tissue balancing; while avoiding instrumentation of the fat and marrow cavities of the intramedullary canal that can result in potentially fatal emboli ([46]) (figure 22). Un-navigated extramedullary guides are available from most knee implant manufacturers and are frequently used for tibial alignment, but have been found to be grossly inaccurate when applied to the femur ([77]) due to the larger soft tissue envelope. Both tibial and femoral extramedullary guide inaccuracies were also found to be magnified in obese patients ([77]).

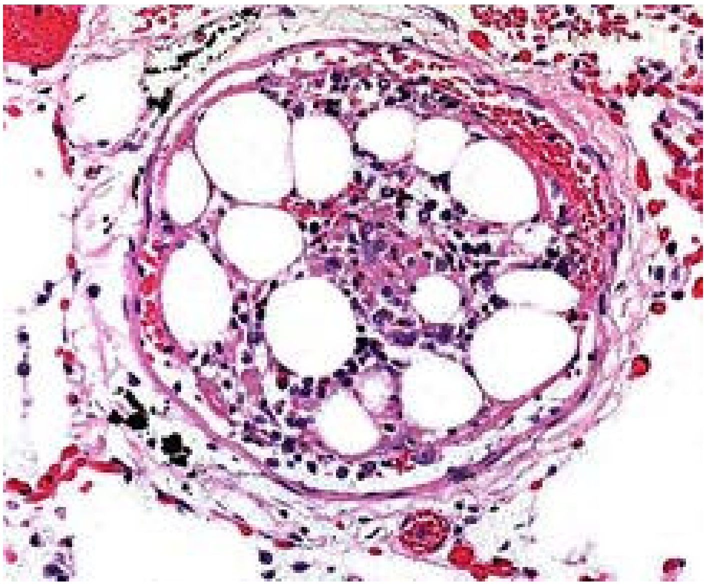

Figure 22: A red stain demonstrates a lung capillary occluded with a globule of fat following knee replacement surgery in this histological specimen ([10]).

There are several navigation systems manufactured by different companies on the market today, and the numbers are growing annually. Some are generic machines while others are prosthesis specific. They work by utilising a three dimensional (3D) map of landmarks digitised preoperatively or intra-operatively by the surgeon.

Preoperative anatomical references can be obtained by Computed Tomography (CT), or Magnetic Resonance Image (MRI) scans of the leg ([78]). Images of the femoral head, knee, and the distal tibia are normally taken with a slice thickness of 2 mm ([106]). This data is then used to construct a 3D model of the femur and tibia, from which the mechanical, transepicondylar and rotational axes are computed, along with reference points for validation during surgery (figure 23). During the operative procedure, the validation points are then entered using an infrared (IR) system or an optical recognition system. Utilising a 3D pointer, trackers applied to the femur and tibia reference off each other and the pointer to create a 3D grid of the limb. The navigation system then applies the previously calculated axes and CT data to the limb and feeds back information regarding the position of the pointer in 3D space. This is then used to guide the bony resections.

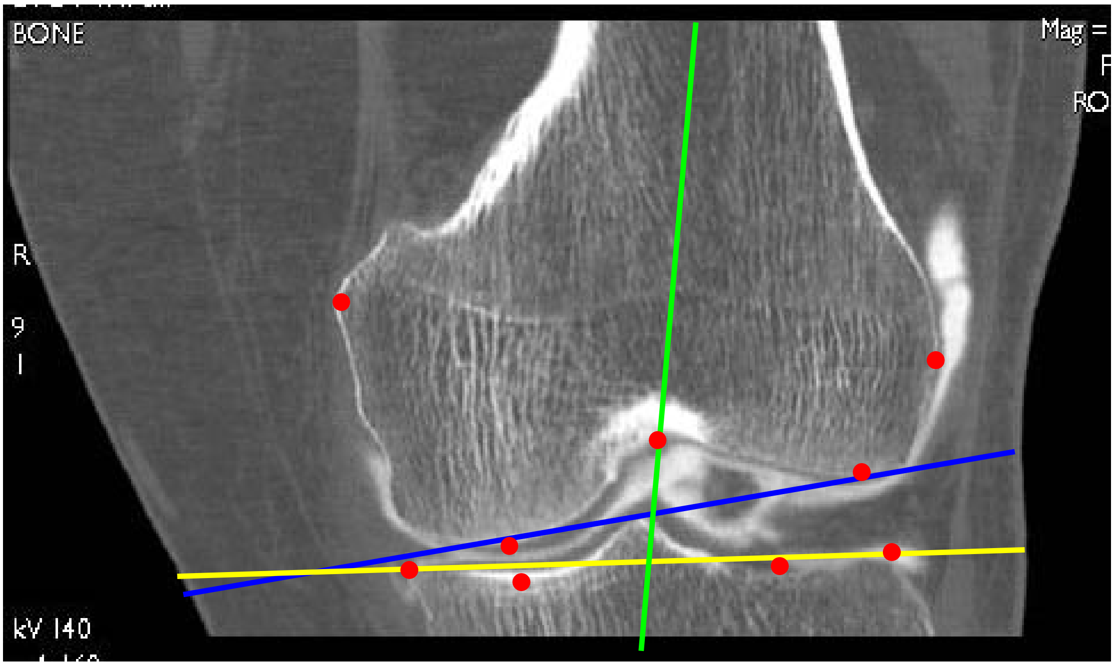

Figure 23: Preoperative CT scan image of the knee used to acquire and digitise bony landmarks for reference in future surgery ([10]).

IR tracking systems utilise trackers fitted with light emitting diodes (LED) that emit a pulse of IR light. These pulses are detected by a receiver that is usually mounted on an overhead moveable boom. This boom is positioned before surgery such that it can "see" the trackers throughout the whole range of movement of the limb during the procedure without having to be moved. Optical recognition tracking systems work on the same principles but instead of trackers with IR LEDs, the trackers have a series of reflective spheres on the end of the femoral and tibial pins. These spheres and their precise alignment with respect to each other are recognised by video cameras mounted in an overhead boom (figure 24).

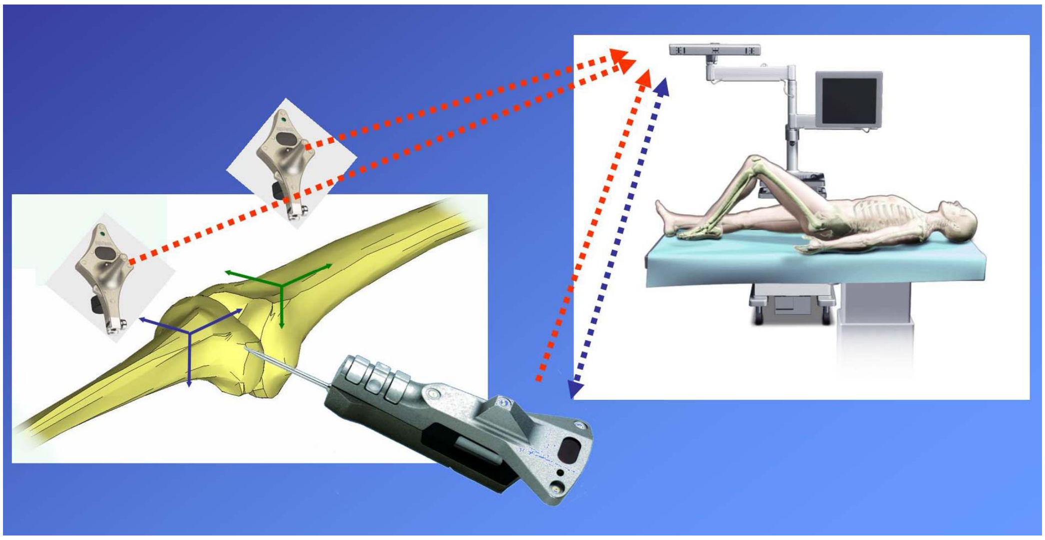

Figure 24: Stryker Knee Navigation System utilising a boom mounted IR camera and bone fixed infrared LED femoral and tibial trackers and an LED pointer ([10]).

The alternative method of Intra-operative Fluoroscopic Navigation utilises captured images acquired during surgery ([114]). The navigation computer then calculates the reference axes from the data, which is relayed back to the surgeon by an IR or optical tracking system to determine the position of the leg. This is then combined with identifiable bony landmarks about the knee to determine the bony resections.

In addition to preoperative computerized tomography and intra-operative fluoroscopy, a third method dubbed morphing surface navigation or non-image computer-assisted surgery (CAS) also exists. This method does not require images be obtained preoperatively or intra-operatively ([60;69]), instead, the manufacturer of the CAS system obtains CT scans from a large number of patients and stores them in an anatomical database on the CAS unit. During the surgical procedure, an IR or optical tracking system are used to digitise multiple landmarks and surface points from the distal femur, femoral condyles, tibial plateau, the medial and lateral epicondyles and ankle joint. These are compared with the database to help create a computerised model of the femur and tibia best fitting the digitized surface points.

All types of navigation systems require the position of the centre of the femoral head to allow the computer to construct the mechanical axis of the leg. Earlier systems utilised a tracking pin placed in the pelvis above the hip and or preoperative CT data to help determine the femoral head position ([125]). This technique has now been abandoned in favour of a kinematic determining method ([125]). Once the femoral tracking pin has been inserted, the leg is moved in a circular manner through multiple arcs of circumduction. The computer analyses these arcs of motion and calculates the most likely centre of rotation of the hip. However, this method is only accurate if there is normal hip movement and the pelvis is fixed and does not move during the calibration procedure. Pelvic pins are still necessary in patients with abnormal hip motion such as in severe osteoarthritis (OA), ankylosis, or severe hip dysplasia.

The goal of navigation is to increase surgical accuracy and reduce the chance of misalignment of the implants. Misalignment has been shown to increase the risk of implant failure and early loosening ([83]). *Fehring et al* ([46]) and *Jeffery et al* ([59]) demonstrated how implants misaligned by more than 3° had a 24% loosening rate by 3 years after surgery. The loosening for correctly aligned implants was only 3% ([46;59]). In addition, the computer aided navigation systems also allow the progress of the numerous bone resections in TKA to be checked at every stage of the operation, decreasing the incidence of a compounding error earlier in the surgical procedure ([20]).

Several studies have demonstrated that the use of a computer navigation system improves the accuracy of implant positioning when compared to a standard jig navigated system ([30;43]).

In theory, better kinematics attributable to precise component positioning with the aid of computer assistance, should result in lower incidences of loosening and wear, but so far there has not yet been sufficient follow up or evidence to support this conclusively.

AIMS

The aims of this project were to determine the kinematics and acceptable error margin for tibial tray rotation and posterior slope for the Scorpio CR TKR prosthesis when implanted and loaded in cadaver specimens.

OBJECTIVES

To achieve our stated aims, many difficult steps and challenges were encountered. Some had been anticipated while others were an unexpected and complete surprise. As a result, a list of important objectives were drawn up:

- To become familiar with the use of an IR navigation tracking system, such that it could be used to accurately record the movement of one tracker relative to another in three dimensions of space.

- To modify the aforementioned IR trackers such that they could be securely fastened to the tibias and femurs cadaver knee specimens. This would allow the movement of the tibia to be recorded relative to the movement and position of the femur.

- To design or modify a suitable rig that would allow cadaver knee specimens to be mounted to allow a full range of flexion and extension with a clear line of sight to allow the recording of movement data using the aforementioned navigation system.

- To design a jig system that would allow precise rotational misalignment and posterior slope to be applied via external controls to a Scorpio CR tibial base plate without having to repeatedly reopen the knee joint.

- To design a suitable protocol of active loading cycles that would allow us to determine the envelope of laxity of an implanted knee, as well as to design a suitable protocol of misalignment and posterior slope as is commonly found in the current orthopaedic literature.

- To perform the dissection, digitisation and implantation experimentation in fresh frozen cadaver specimens.

- To compare and contrast the kinematics and envelopes of movement of normal knees before and after Scorpio CR cemented TKRs through a variety of loading cycles.

- To determine the effect, if any, of rotational misalignment of the tibial tray in isolation on the kinematics and envelopes of movement of Scorpio CR cemented TKRs through a variety of loading cycles.

- To determine the effect, if any, of posterior slope in isolation on the kinematics and envelopes of movement of Scorpio CR cemented TKRs through a variety of loading cycles.

- To determine the effect, if any, of rotational misalignment combined with posterior slope on the kinematics and envelopes of movement of Scorpio CR cemented TKRs through a variety of loading cycles.

METHODS

Ethical Approval

Before the study could commence, an application detailing the research proposal was submitted to the National Research Ethics Committee ([1]) and to the Ealing Hospital Research Ethical Committee ([1]). Following an interview and discussion of the research with the committee, full ethical approval was granted for the study to proceed.

Cadaver Specimens

Our study utilized ten whole fresh-frozen left human cadaver legs. These were supplied disarticulated at the hip joint and complete with feet. The specimens were obtained from a fully registered tissue bank within the United States of America, where they were selected at random from the bank and were not affected by gross arthritic defects or previous knee surgery. They were considered to be "normal" for an elderly population or a population that would require or benefit from total knee replacement surgery. The specimens were couriered by air in a freezer compartment and were folded into full flexion and wrapped several times over in insulating wool and plastic sheeting before being sealed in large plastic bags for protection.

At the time of arrival at Imperial College London, all the specimens were checked and found to still be appropriately frozen. The specimen bags were recorded and marked and the specimens placed into a locked freezer at -20ºC. During the course of the study, the specimens were defrosted slowly as required over a twelve hour period in a locked fridge at 4ºC just prior to the experimentation. This procedure ensured that the specimens were fresh at the time of experimentation and that there was no damage to the soft tissues from rapid thawing or residual ice. During the experiments, the specimens were kept out of direct sunlight and moist by spraying them at regular intervals with a fine sprayer containing tap water.

Following completion of the experiments, all tissue from the specimens was appropriately bagged and disposed of as per guidelines issued by Imperial College London in the appropriate facility.

The Navigation System

A commercially available Stryker IR (non image) CAS Navigation System (Image Guided Technologies, California, USA. Serial number 422523) (figure 25) was used to guide the bony resections and the implantation of the Scorpio CR TKRs. Its software had also been modified to also allow movement data collection from the trackers during the study.

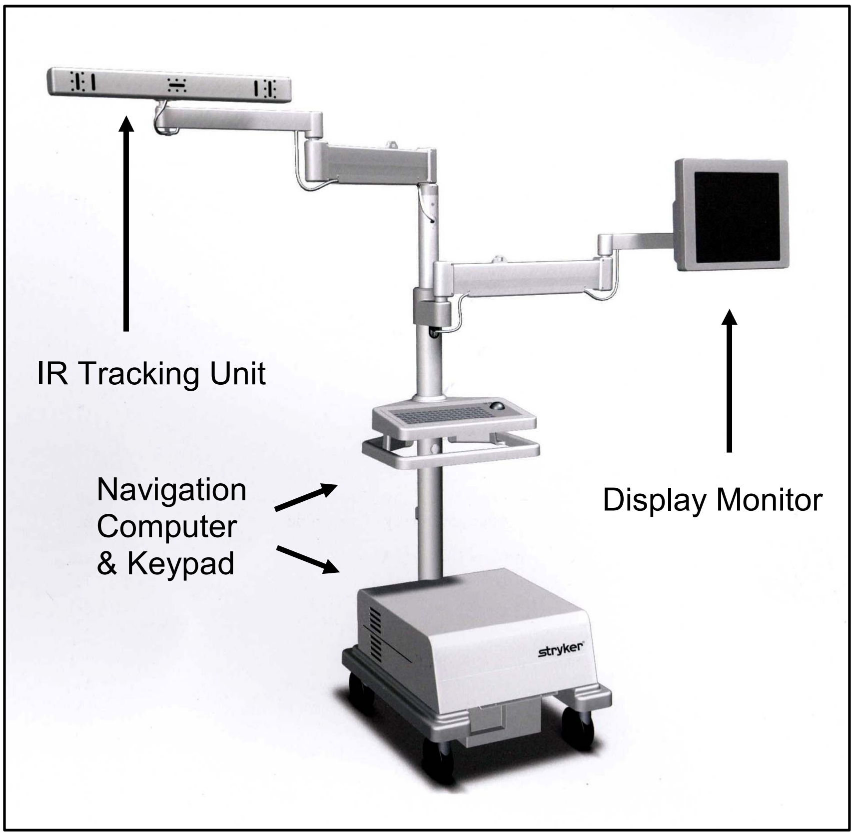

Figure 25: The Stryker Navigation system stack complete with a mobile IR tracking boom, Display monitor and computer system and keyboard

The Navigation system was comprised of an IR tracking unit, a display monitor, two LED trackers, an LED pointer and a navigation computer in the form of a laptop:

The IR tracking unit was composed of three individual IR sensors mounted 25cm apart on a mobile adjustable boom. The three individual sensors utilise a computerised triangulation system to determine the position of the IR pulse emitting trackers and pointer. For the digitisation and experiments, the tracking unit was set up approximately two hundred centimetres to the left side of and above the specimen such that all three IR sources could be clearly detected throughout the whole procedure.

A mobile display monitor was used to display the details of the navigation software that guided the bony resections for the TKR implantation. It was also used for the system calibration and allowed the progress of the recorded movement data from the experiments to be followed closely.

The femoral and tibial trackers were battery operated pulsed IR emitters. They each consisted of an arrangement of five IR LED's. Four were arranged in a single plane in a rhomboid arrangement, with a central solitary LED elevated on a pedestal. This allowed its position to be identified relative to the position of the plane of the other 4 LED's (figure 26).

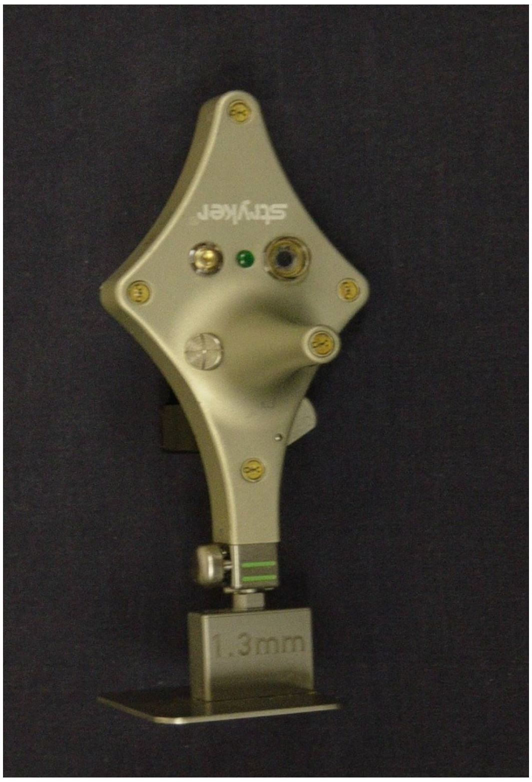

Figure 26: Photograph illustrating the spatial arrangement of the IR LEDs on the femoral and tibial trackers.

In normal surgical protocol, the tibial and femoral trackers are secured to the tibia and femur with two drilled bi-cortical screws on a height adjustable assembly. Any slight movements or deviations of the tracker positions through loosening of the fixation would result in significant compounding errors in the movement data collection. Purpose built, machined steel augments were therefore used in their place and will be discussed in more detail later.

The remote IR pointer was also battery operated and utilised a similar 5 LED configuration. Its purpose was to digitise the bony landmarks and joint surfaces for the navigation. It was also used to remotely make selections and advance screens on the navigation computer via several buttons on the pointer, as well as provide a plane of reference for checking the bony resections and implantation of the Scorpio CR TKR (figure 27).

Figure 27: The Stryker remote IR pointer with an identical spatial arrangement of IR LEDs on the handle as on the IR bone trackers.

As mentioned above, the trackers and remote pointers were battery powered. The batteries (Duracell C4) were readily available and typically lasted 6 hours. Because the experiments were frequently over 10 hours, two or three battery changes were performed during the course of the digitisation and experimentation to ensure the trackers maintained a strong signal. The process of changing the batteries in the trackers did not affect the data collected or outcome of the experiments.

Throughout the implantation procedure, the plane of angulation and positions of the resection guide slots and cut bony surfaces were checked and confirmed using the resection plane probe. The probe consisted of a flat mounting plate upon which a navigation tracker (either tibial or femoral depending on position) was attached. The flat surface of the probe was thin enough to slot into the resection guides and wide enough to verify the cut surfaces during implantation (figure 28).

Figure 28: The Stryker resection plane probe

Finally, a navigation computer in the form of a Pentium 4 laptop PC with 2GB of RAM and a hard disc drive was used to run the navigation software and record the movement data from the experiments.

Misalignment Protocols

To investigate the effects of isolated tibial tray rotational misalignment on kinematics, the protocol included a navigated implant position (with no rotational misalignment); as well misaligned rotations that would cover the range of commonly reported series in the current literature:

- 10º external rotation of the tibial tray
- Normal rotational alignment of the tibial tray
- 10º internal rotation of the tibial tray

In order to investigate the effect of isolated tibial slope on kinematics, the protocol included a navigated implant position (with no posterior slope) ; as well as posterior slope values that would cover the range of commonly reported posterior slope in the current published literature:

- 0º posterior slope of the tibial tray
- 3º posterior slope of the tibial tray
- 6º posterior slope of the tibial tray

To investigate the extreme effects of misalignment in isolation, a further category of extreme component positions was selected as follows:

- 20º external rotation of the tibial tray
- 20º external rotation of the tibial tray
- 9º posterior slope of the tibial tray

To investigate the combined effects of rotational misalignment and posterior slope, it was decided to use the extremes of rotation and slope to produce a dramatic translation in kinematics.

- 20º external rotation of the tibial tray combined with 9º of posterior slope of the tibial tray
- 20º internal rotation of the tibial tray combined with 9º of posterior slope of the tibial tray

The rotation of the tibial tray component was controlled by a custom made jig that allowed precise misalignment of the tibial tray without the need to reopen the knee repetitively. It was initially hoped to incorporate into this rotation jig, a mechanism to allow the posterior tibial tray slope to be altered as well. However, producing an accurate device for precisely altering the posterior slope without affecting the height of the joint line was difficult and complicated and would have required extensive resection of the proximal tibia beyond that normally required for TKA. As a result, it was decided to incorporate the tibial posterior slope into the polyethylene tibial inserts. This allowed the tibial posterior slope to be precisely set whilst still maintaining the same joint line height and bony resections as found in a routine TKR surgical protocol. The knee would have to be opened more frequently than originally planned to change the inserts for the adjustment of the tibial posterior slope, but after consulting the senior supervising surgeon (Mr. Neil Thomas), it was determined that with a meticulous repair, the soft tissue envelope would not be significantly adversely affected by this.

Details of the jig, polyethylene inserts and their development will be discussed in a later chapter.

Tibial Tray Polyethylene Insert Modification

For reasons discussed in the previous chapter, it was decided to use modified tibial tray inserts to allow the addition of posterior slope. This would allow a standard flat (0º) navigated resection of the tibial plateau to accommodate a modified standard tibial tray as per normal TKR surgical protocol.

The geometry of the polyethylene inserts were calculated using CAD software to create 3º, 6º and 9º of posterior slope without affecting the central level of the joint line (figures 29, 30, 31).

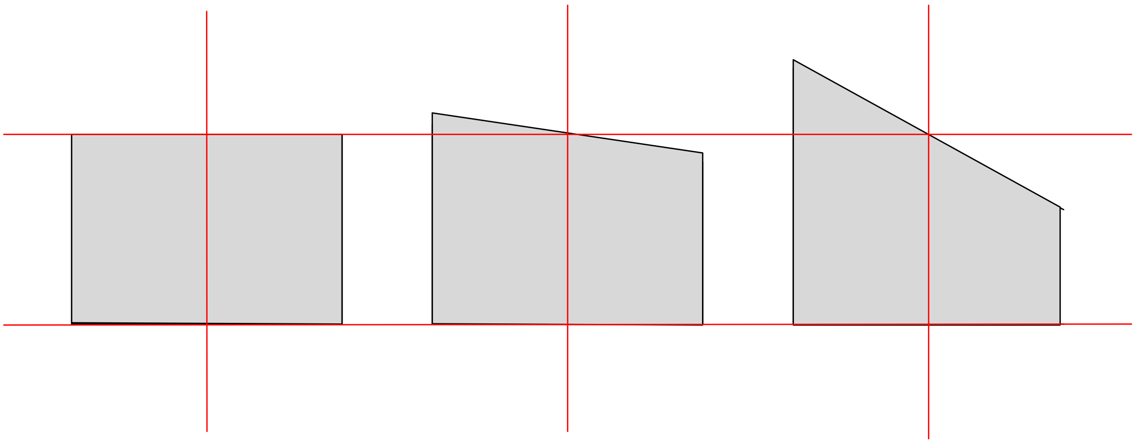

Figure 29: Dramatised drawing demonstrating the principal of changing the posterior slope of the insert without changing the central level of the joint line by differential machining of the inset.

The resulting designs utilised a 12 mm standard dished polyethylene insert (as used in normal surgical protocol). For the 0º slope, this insert was used unmodified. The subsequent production and differential machining of the inserts was performed by Stryker to the requested specifications for the full range of commercially available Scorpio TKR tibial insert sizes 3, 5, 7, 9 and 11.

On receipt of the machined inserts, all sizes and slopes were checked and the tibial inserts stamped on their under surface to identify the size and slope to prevent any errors in identification. A small 5 mm diameter by 3 mm deep cavity in the centre of the under surface of the inserts was also removed using a router. This allowed the insert to sit flat on the tray when the tray was attached to the intramedullary jig using a screw.

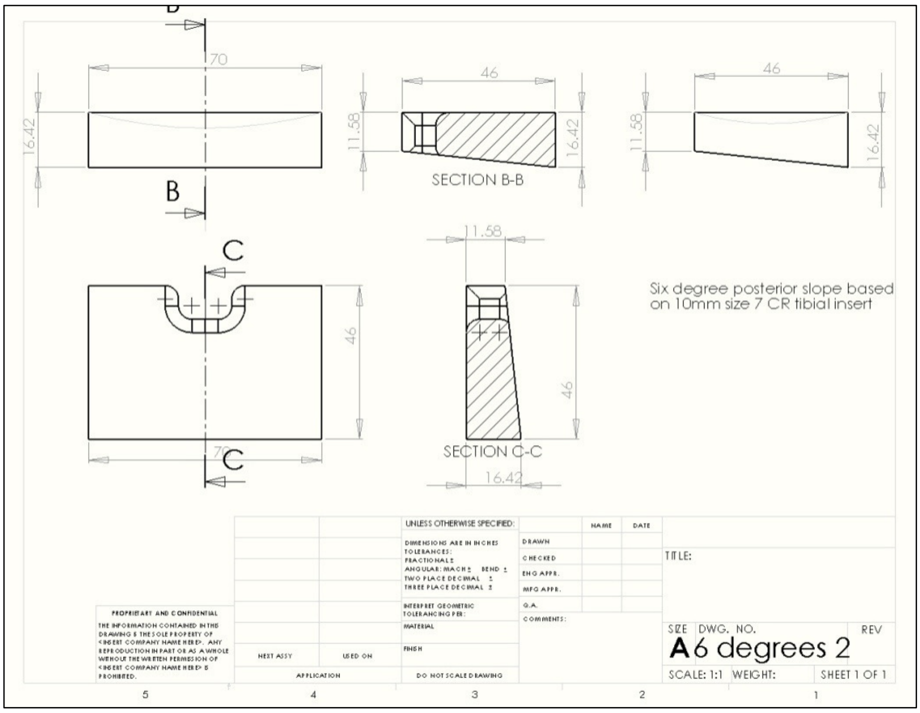

Figure 30: CAD drawings of an example 6º posterior slope tibial size 7 tibial insert

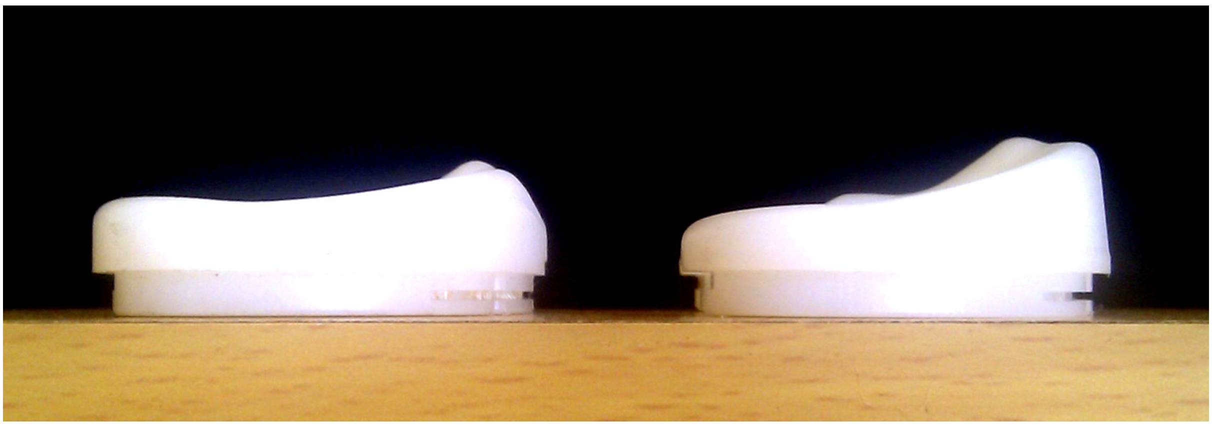

Figure 31: Photograph of a side view of two tibial inserts used in the experiments, a standard tibial insert on the left compared with a 6 degrees posterior sloped insert on the right.

Development of the Test Rig

In order to achieve the aims and record the true envelope of laxity of the cadaver knees, the rig had to allow unconstrained movement of one bone relative to the other in 6 degrees of freedom during a flexion-extension cycle whilst also being loaded.

The 6 degrees of freedom rig had to allow three translations and three rotations (figure 32):

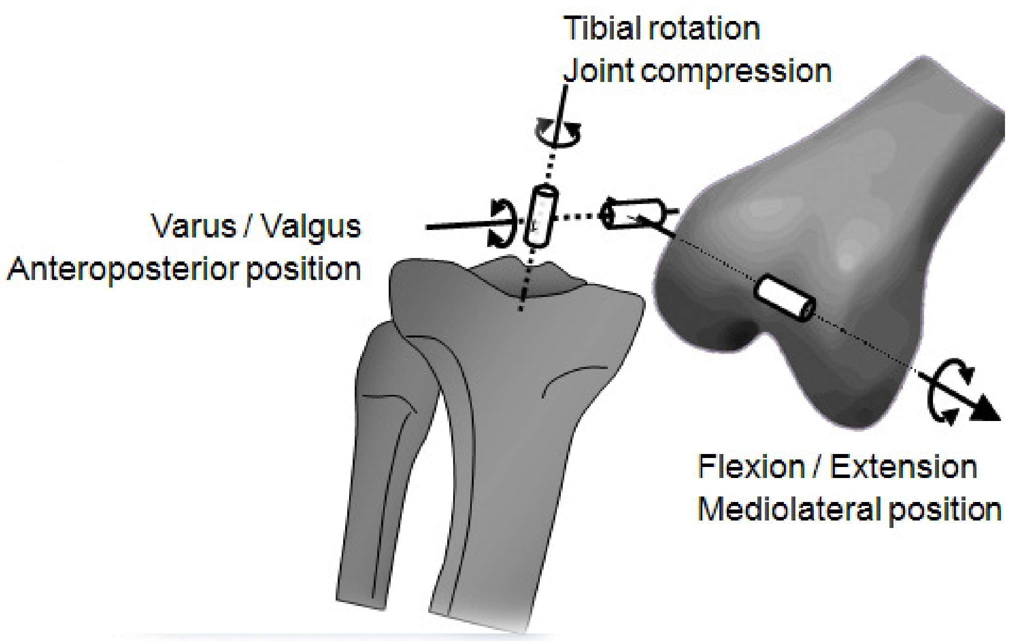

Figure 32: Diagram illustrating the six degrees of freedom of motion around the knee joint ([28])

This aim was to be achieved by fixing the femur to a custom made hinged rig that allowed flexion and extension, with simulated quadriceps contraction loading, while still allowing the tibia to hang freely and unconstrained below it. The unconstrained tibia would then be free to be loaded. The motion of the femur and the tibia during flexion and extension would then be recorded in 6 degrees of freedom by the navigation system (figure 33).

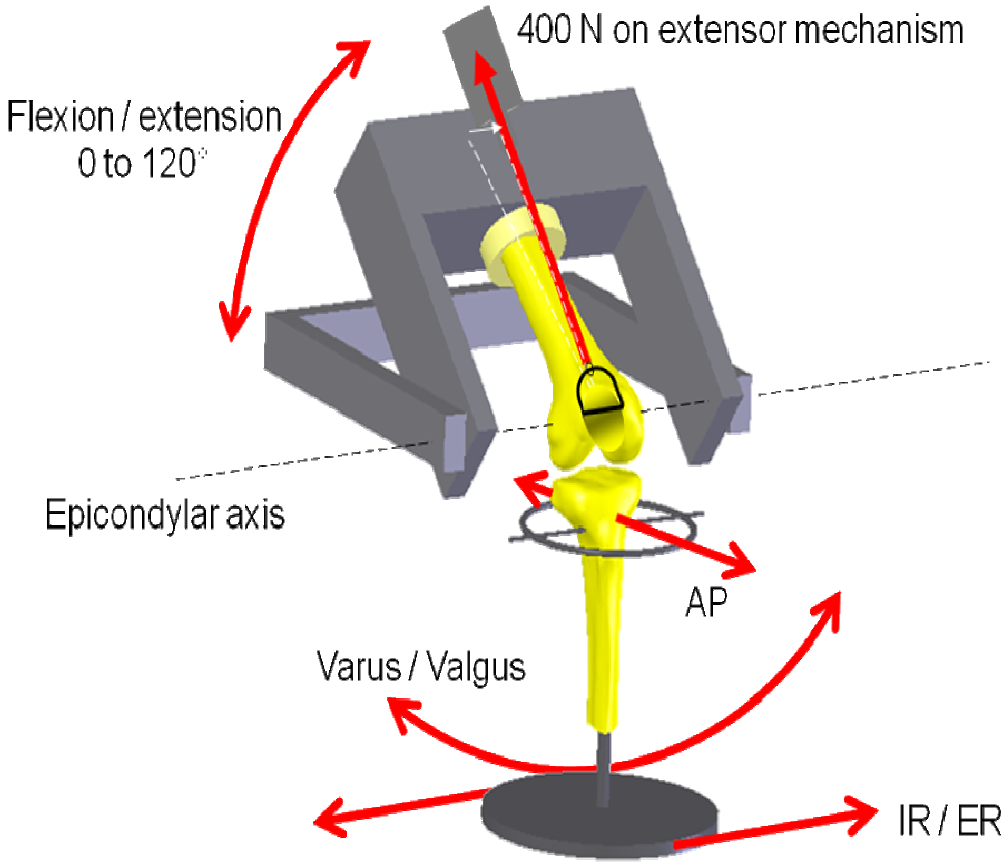

Figure 33: A CAD drawing of the initial rig concept ([28]).

The testing rig was made from steel and consisted of a large steel base that was firmly attached to the end of the work bench. From this base, two symmetrical and parallel vertical arms projected 50 centimetres upwards and outwards at right angles, overhanging the edge of the bench by approximately 50 centimetres. To complete this flexion / extension hinge, a third U shaped assembly was mounted in-between the two arms and supported at each end by nylon washer lubricated partially threaded locked bolts. These allowed the middle U section to hinge freely and with minimal resistance between the two arms of the rig. The U section also had two adjustable end cross bars with bolts to allow the secure fixing of a specimen's potted femur, whilst ensuring that the axis of flexion and extension (epicondylar axis) matched the hinge axis of movement of the rig. The middle hinged section could then be extended and flexed by hand, to flex and extend the knee (figure 34).

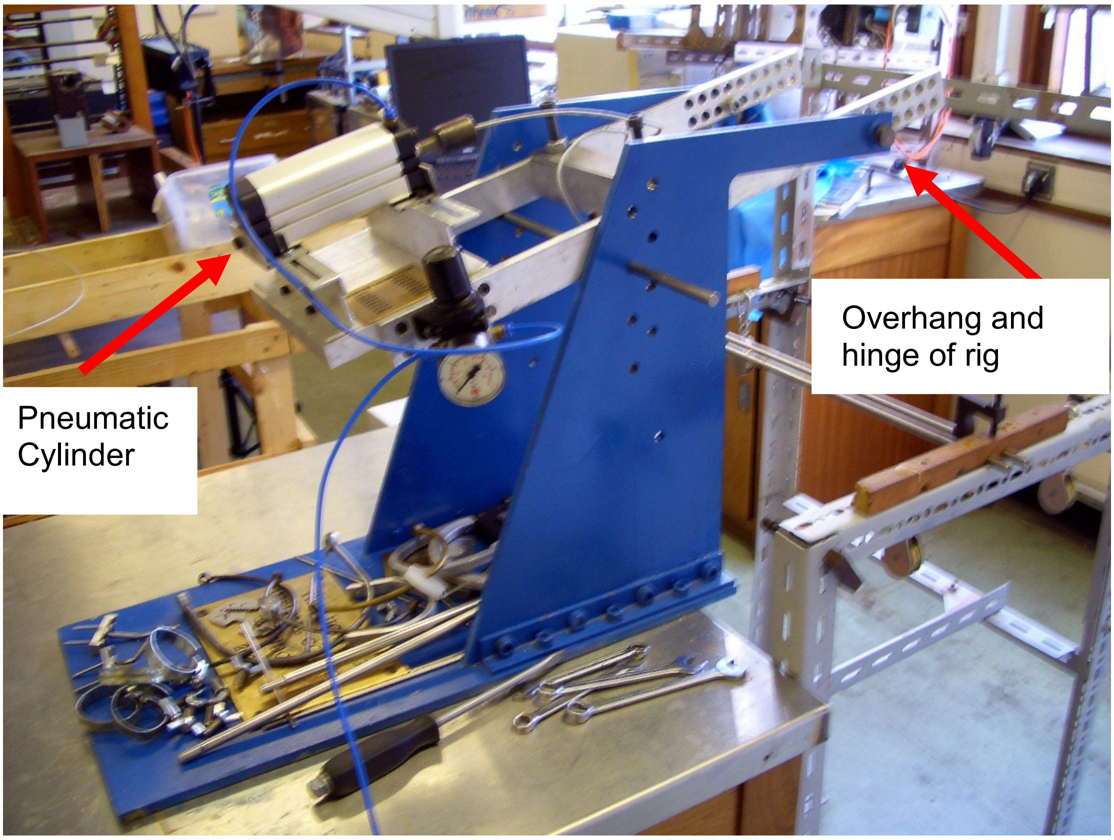

Figure 34: Side view of the test rig demonstrating the described overhang, hinge mechanism and quadriceps force simulating pneumatic cylinder

For the tibia, a steel angle frame was constructed and fixed to the work bench below the cantilevering arms of the rig. It had two polished stainless steel rods that ran transversely across the box frame that were fixed 5 centimetres apart in a small jig. This jig was adjustable and could be moved in the sagittal plane so that the mounted specimen's tibia hung vertically at the centre of the box frame. An intramedullary rod cemented into the centre of the distal tibia sat in-between the two polished stainless rods, when the knee was at rest. Its purpose was to allow simulated quadriceps contraction whilst still allowing the tibia to remain sufficiently unconstrained to demonstrate the other 5 degrees of freedom during a controlled flexion / extension cycle (figure 35, 36).

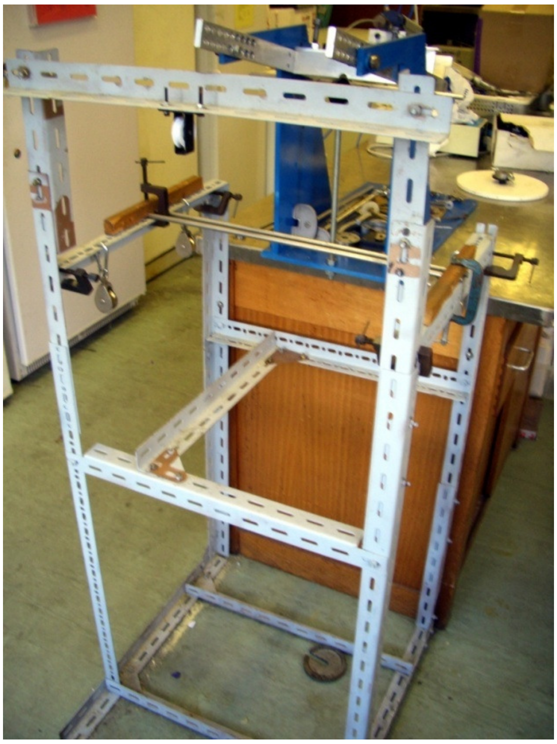

Figure 35: Photograph of the front of the steel angle frame demonstrating the transverse stainless rods and pulleys used to simulate the various loading conditions

To provide the simulated quadriceps contraction force, a pneumatic cylinder was mounted to the end bar of the U section, with a pull parallel to the long axis of the femur; this was used to apply a continuous simulated quadriceps force of 400N through the patella by means of a trans-osseous pin attached to a semicircular yoke and steel cable assembly.

A simulated quadriceps contraction force of 400N was utilised as this equated to half the anticipated body weight for an average 80Kg human being. This value did not approach the predicted 3.1 times body weight when walking and 5.4 times body weight when stair climbing, as suggested by *Taylor et al* ([133]). However, the standardised load of 400N was used as it was felt that this value provided sufficient quadriceps simulation to ensure a compressive joint load while still allowing the envelope of laxity to be investigated using moderate precise loading forces in the other planes of movement. It was known from prior experience that larger forces led to a risk of failure of the trans-osseous pin in the porotic patellae of the elderly knees available and used in the experiments.

Figure 36: The rig in action, with the knee mounted with the epicondylar axis coincident with the rig axis. The simulated quadriceps contraction force of 400N provided by the pneumatic piston provides an axial joint load and is sufficient for the knee to hold itself and the weight of the test rig in an extended position.

Other loads were also applied to the tibia: varus and valgus moments, internal and external rotational torques, anterior and posterior drawer forces and combinations of the above were applied with the use of cables, weights and pulleys. Six small ball bearing greased pulleys, a large machined nylon disc and a reel of nylon monofilament line (breaking strain in excess of 150N) were used to apply the loads.

Development of the Tibial Tray Test Jig

Having developed a rig suitable for the flexion and extension of the knee specimens under load, a tibial tray jig was required that would allow precise rotational misalignments of the tibial tray around its predetermined centre axis whilst still holding the tray firmly in position to prevent artefact during the various loading cycles. Ideally, the jig would also allow the adjustment of the rotational misalignment and the addition of posterior slope without having to repeatedly open and close the knee. This would avoid the inter-test variability caused by the soft tissues and save experimental time and preserve the soft tissue envelope as much as possible.

After some initial drawings and experiments in the laboratory, an intramedullary jig system was devised. It was designed to fit within the intramedullary canal of the tibia and allow adjustment of the prosthesis through a control rod protruding through the bottom of the resected tibia. The resection would follow the digitisation of the distal bony landmarks around the ankle required for the navigation system and is discussed in more detail later.

This rig consisted of a 10 mm solid stainless steel machined rod snugly contained within a 12 mm diameter tube. The hollow tube’s wall was 1 mm thick, allowing the tube to resist loads applied across it, while also allowing the exterior surface to be roughened (to permit interlocking with the bone cement). At 12 mm in diameter, the tube was thin enough to fit and be cemented into the intramedullary canal of the tibia utilising Poly-methyl-methacrylate bone cement (PMMA).

PMMA was chosen and used to cement the tibial tube into the intramedullary canal because it was readily available in the laboratory and the researchers had past experience with handling it safely. Its properties of high compression resistance were suitable for the task and it was safe to use and handle (with gloves and appropriate eye protection). It was easily mixed to a runny consistency to allow 360º cementing of the rod and previous experiments in the laboratory demonstrated that it adhered satisfactorily to the roughened steel tube to allow firm fixation during the loading experiments. Once completed, it could also be completely removed from the metal surfaces of the jig, ready for the next specimen, without marking or damaging the rig.

The tibial steel tube was approximately 35cm in length and the lower 10cm was split with a saw, removing 2 mm and creating a slot to allow compression and clamping of the inner rod (figure 37).

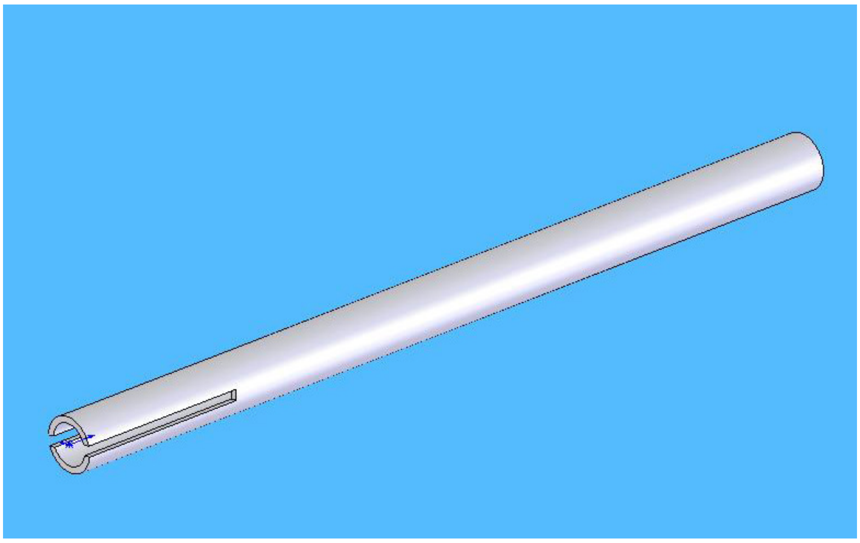

Figure 37: CAD drawings of the slotted steel tube

The machined nylon rotation disc was firmly fixed to the steel tube using a machined bushing and a pair of grub screws. A second bushing with two facing screws was also manufactured and used to compress the steel tube across the split portions to clamp the rod firmly (figure 38).

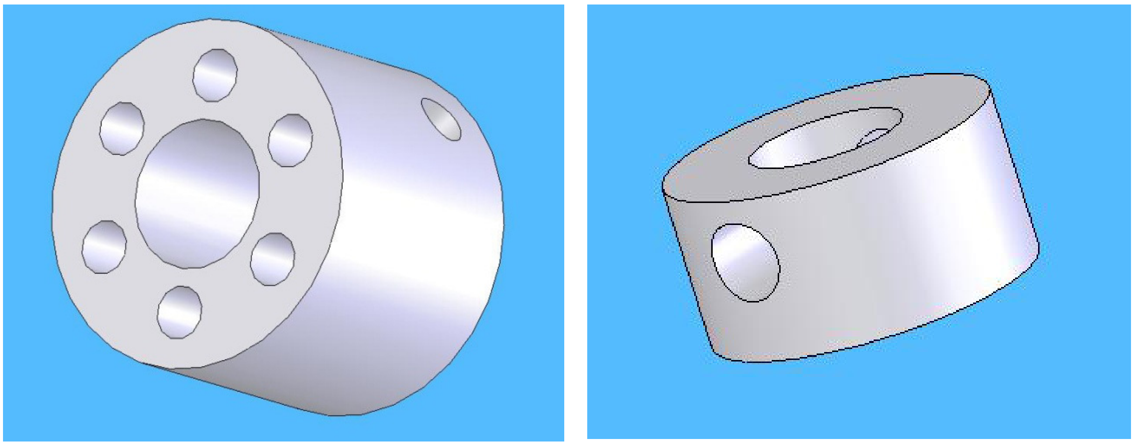

Figure 38: CAD drawings of the tibial rotation disc bushing and the slotted section compression bushing

To further secure the steel tube in the tibia, a de-rotation steel augment was manufactured and firmly TIG welded to the top of the steel tube. Its purpose was to provide a platform for smooth rotation of the tibial tray as well as to further secure the steel tube in the tibia. The augment was 3.5cm in diameter and flat on its upper surface with a central 12 mm diameter hole to contain the tibial tube and welding (figure 39).

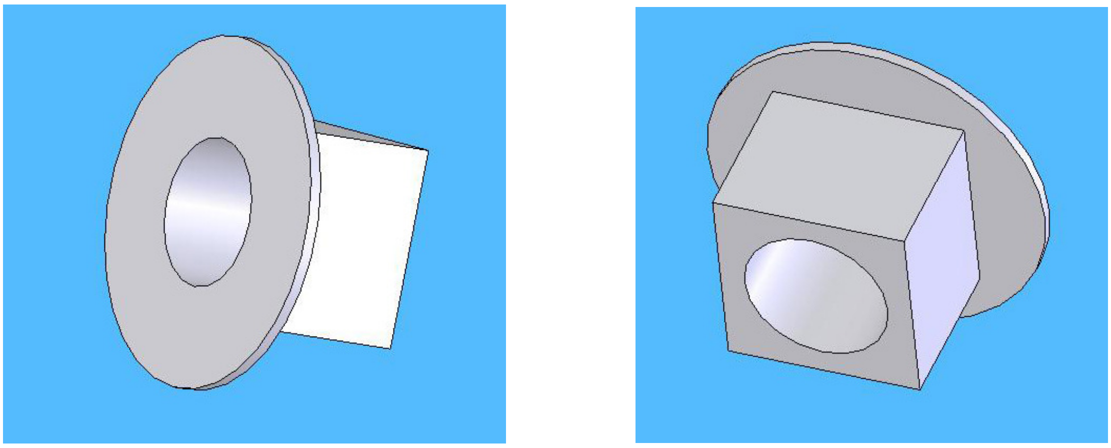

Figure 39: CAD drawings of the de-rotation tibial tube augment. This was welded to the tibial steel tube and cemented into the tibial metaphysis.

The inner solid rod was 40cm in length and machined down to a diameter of 10 mm so that it fitted snugly and could be easily rotated within the steel tibial tube. The top of the rod was vertically drilled and tapped to accommodate a 6 mm x 20 mm hexagon socket machine screw. The bottom of the rod was transversely drilled and tapped with an M8 Thread 1cm from the end of the rod. This allowed the control rod to be screwed into the inner rod.

The control rod was also machined from stainless steel to a diameter of 10 mm with a male threaded M8 portion of 2 cm at one end. This was screwed into the tibial rod and allowed the rotation of the inner rod and prosthesis to be precisely controlled and measured.

The entire jig was assembled and tested to ensure it was satisfactory and durable for the subsequent experiments (figures 40, 41).

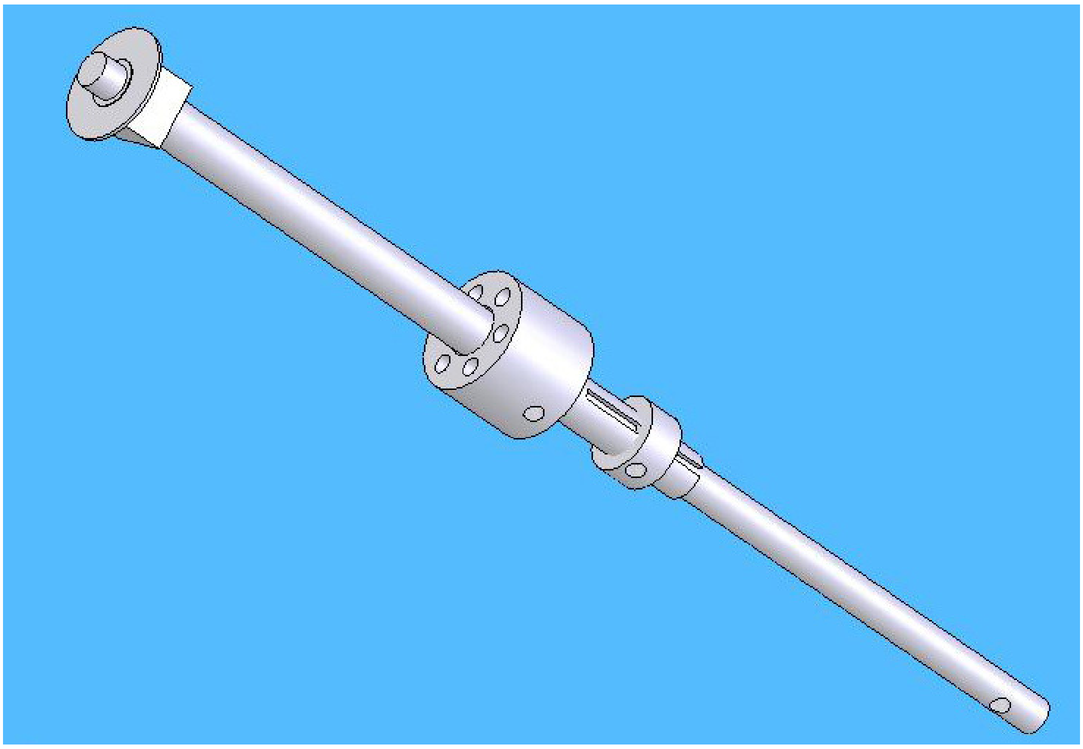

Figure 40: CAD drawings of tibial jig assembly minus rotation disc and tibial tray

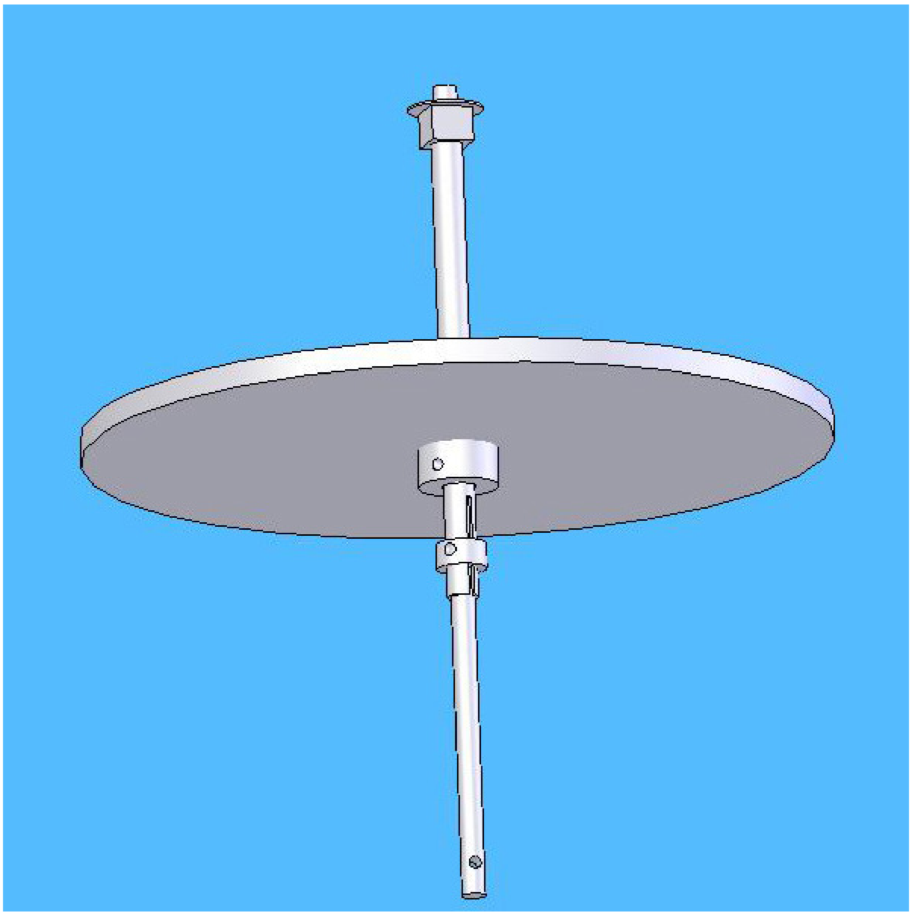

Figure 41: CAD drawings of entire assembly minus tibial tray

Tibial Tray Modification

Stryker CR tibial tray prostheses are manufactured from a cobalt-chrome-molybdenum alloy and possess a 50 mm wide by 30 mm deep tapered central keel. To allow rotation of the tibial tray on the flat navigation guided resected tibial surface via the inner rod, the implant keel had to be removed and a central hole drilled in the tibial tray. To allow for a variation in tibial size of the cadaver specimens, five different component sizes were cut and machined (3, 5, 7, 9 & 11).

Due to the hardness of the alloy and difficulty with machining, the components were cut immersed in oil using a spark gap machine and plasma cutter (figure 42).

Figure 42: Photographs of the spark gap cutting procedure necessary to modify the tibial trays

Anterior and Posterior Loading

For the experiments, a 70N anterior and posterior translation (drawer) force was applied to the tibia via a trans-osseous threaded pin inserted medial to lateral, through the centre of the tibial condyles 5 cm below the joint line of the knee (figure 43). Two half ring round rod attachments (one anteriorly and one posteriorly), with circular hoops at each end were threaded onto the trans-osseous pin on both sides of the tibia. These allowed an antero / posterior draw to be applied in a constant true AP plane whilst still allowing the tibia to remain unconstrained and to rotate freely under the applied loading conditions. The actual load itself was applied using a 70N weight attached to a nylon monofilament that ran through ball bearing greased pulley assemblies mounted to the front and back of the steel box section assembly. The heights of the pulleys were adjusted so that the pull of the nylon monofilaments was parallel to the floor and hence perpendicular to the tibia.

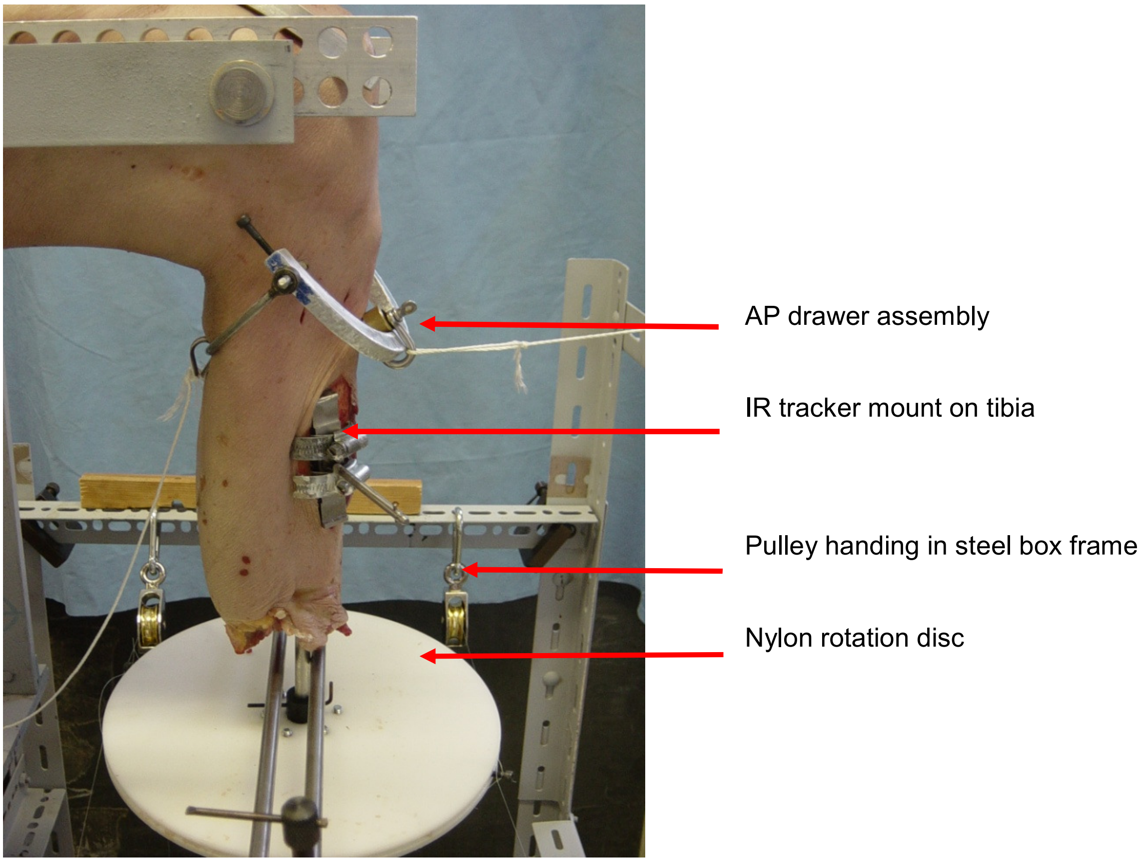

Figure 43: A mounted specimen in the rig illustrating the steel box angle frame, mounted nylon rotation disc and anterior and posterior drawer half rings and pulley assembly. Note that the pull of the monofilaments was at the same level as the pulley and transverse K-wire so that they ran parallel to the ground when applying rotational torque, A-P drawer or varus / valgus load.

To prevent any sliding resistance from the filament / rod interface and to facilitate smooth movements, the nylon filament was attached to the semi-circular hoops rods via a custom made ball bearing assembly block. This consisted of a small machined hollow enclosure containing a single mounted wide lubricated bearing. The weighted nylon monofilament was secured to a hook screwed into the outside of the enclosure opposite the bearing. During loading, the bearing was pulled tight against the inside of the semi-circular hoops allowing a smooth, low friction interface between the rod and the loaded nylon monofilament during rotation of the tibia (figure 44).

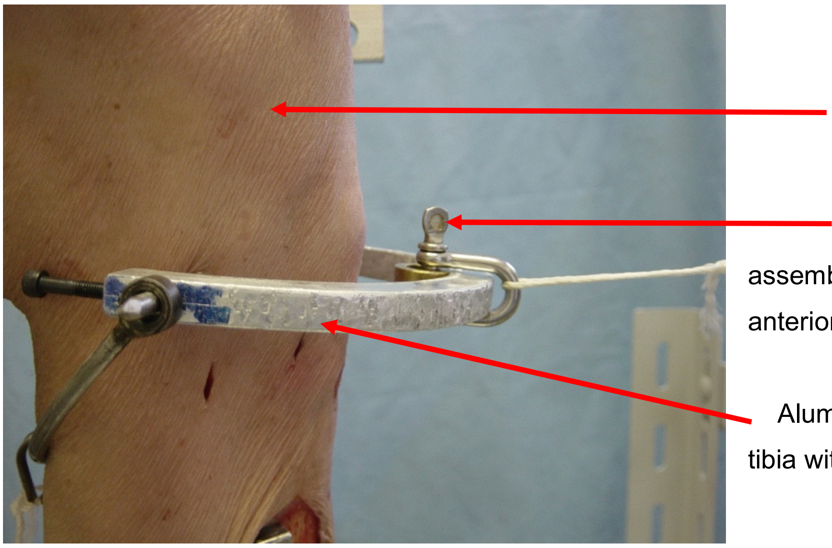

Figure 44: Low friction bearing assembly running on half ring allowed low friction tibial rotations without artefact in the presence of an AP drawer of 70N.

Internal and External Rotational torque:

Rotational torque was applied to the tibia through a 10 mm thick solid nylon circular rotation disc. This was designed and machined to be low in weight with a circumferential deep pulley line retaining groove and was also of sufficient diameter to apply a 5Nm torque about the axis of the tibia. It was attached to the tibia by means of a 12 mm steel bushing that was bolted onto the underside of the centre of the rotation disc using 6 nuts and bolts. A 12.25 mm hole was then drilled through the centre of the rotation disc and bushing assembly. The bushing itself was further drilled and tapped in the 3 O'clock and 9 O'clock positions (relative to the anterior tibial plane). This allowed its height relative to the steel box frame and cadaver leg to be adjusted and so it could be secured to the central 12 mm tube using 2 bolts (the central 12 mm tube was to be subsequently cemented into the base of the tibia of the cadaver specimens for the experiments). The 5Nm moment was applied through the rotation disc by the application of two nylon monofilament threads attached at the 12 O'clock and 6 O'clock positions (relative to the anterior tibial plane) on the rotation disc. The nylon monofilaments were then each passed around the machined outer groove of the rotation disc, either clockwise or counter clockwise as appropriate to the desired moment (internal or external rotation). These filaments were then each passed through 1 of 2 pulleys on each side of the steel box frame, depending on the desired moment (internal or external rotation). The height of the pulleys and rotation disc were adjusted so the tensioned monofilaments ran parallel to the ground during loading (figure 45).

Figure 45: The grooved nylon rotation disc, box frame and pulley assembly. Note that the pull of the monofilaments was at the same level as the pulleys so that they ran parallel to the ground when applying rotational torque or varus / valgus load.

Varus and Valgus Loading

Varus and Valgus moments of 5Nm were applied to the tibia 1 metre below the knee via a monofilament loop placed around the 12 mm steel rod that was cemented into the centre of distal tibia. The ends of the monofilament were then passed through ball bearing greased pulleys on the steel box frame. The monofilament was secured around the steel rod such that the pull of the monofilaments was parallel to the ground and 2.5 Newton weights were hung on each free end.

Characterization of the Normal Knee

The first stage of the experiments was to define the knee laxity characteristics for all of the normal native knee specimens. These had undergone no implantation surgery, but had been subject to the same tracker mounting dissection procedure on the femur and tibia as well as a simple arthrotomy to allow digitisation of the knee for the navigation tracking system.

Constraint to Movement, Neutral Path and Envelope of Laxity

Constraint when applied to TKR, describes the resistance to displacement, rotation and angulation between the femoral and tibial components when forces and moments are applied to the knee joint. In TKR, these constraints can be attributed to the component articulation, the frictional forces between the components and the tension in the surrounding soft tissues, joint capsule and ligaments. For this study, the terms:

- “Neutral path” is used to describe the observed displacement, rotation and angulation of the tibia (driven by the component articulation, joint friction and tension in the soft tissues), for any given degree of knee flexion, when only the simulated quadriceps extension force of 400N was applied to the knee.

- “Envelope of laxity” is used to describe the boundaries of potential displacement, rotation and angulation of the tibia (constrained by the component articulation, joint friction and tension in the soft tissues) in any given plane of movement for any given degree of knee flexion when the simulated quadriceps extension force of 400N was applied in combination with the probing force / torque applied in the plane of movement.

The primary variables for the neutral path and envelope of laxity could be subdivided into the 6 degrees of freedom of movement:

- Anterior / Posterior (AP) envelope
- Varus / Valgus (abduction / adduction) envelope
- Internal / External rotation envelope
- Flexion / Extension envelope
- Compression / Distraction envelope
- Medial / lateral translation envelope

For the purpose of this experiment, two degrees of freedom, compression / distraction and medial / lateral translation were deemed very closely related to the geometry of the articulating surfaces of the knee and were therefore unlikely to contribute significantly to the overall envelope of laxity of the knee. These were therefore not specifically tested or modified and, although the navigation system measured them, they were excluded from the study.

Loading cycles used to characterise the envelopes of laxity

The 3 Dimensional kinematic analysis of the envelope of laxity was performed through a full flexion / extension cycle (0º to 120º) after the initial arthrotomy of the native knee and at each stage of the tibial component augmentation after the navigated knee arthroplasty surgery. The following forces and torques were standardised and used for all the stages of the experiment.

- Axial force of 400N only
- Axial force of 400N and anterior drawer force of 70 N
- Axial force of 400N and posterior drawer force of 70 N
- Axial force of 400N and internal rotation torque of 5 Nm
- Axial force of 400N and external rotation torque of 5 Nm
- Axial force of 400N and varus moment of 3.5 Nm
- Axial force of 400N and valgus moment of 3.5 Nm

The knee was extended on the rig from 120º of flexion to full extension (0º) slowly with one extension and return flexion cycle lasting approximately 30 seconds. For each load and implant state, the extension and flexion cycles were repeated three times to increase the data collected for reliability by averaging.

System Setup

The cadaver specimens were placed on a scientific working table with the long axis of the legs oriented with the long axis of the table. The rig assembly required for the experiments was firmly bolted to the end of the table. The navigation system was placed on one side of the table while the scientists worked from the other side. The initial arthrotomy, IR tracker fixation and calibration was performed free hand on the table. The rest of the experimentation, including the implantation, was performed with the specimen mounted in the rig assembly.

Arthrotomy

All the knees underwent a standard median parapatellar arthrotomy. With the leg in full extension a skin incision was made from the medial border of the quadriceps tendon, along the medial edge of the patella and down to the medial edge of the patellar tendon, extending 3 cm onto the anterior tibial surface. The subcutaneous fat was also incised along the same line. The deeper capsular incision was then performed along the junction of the middle and central third of the quadriceps tendon, to the superior medial corner of the patella and distally, medial to the patella (ensuring an adequate cuff was present to allow re-approximation) and down along the medial border of the patellar tendon. This allowed the patella to be fully everted in flexion exposing the whole knee for the surgical procedure and calibration stages of the experiments (figure 46).

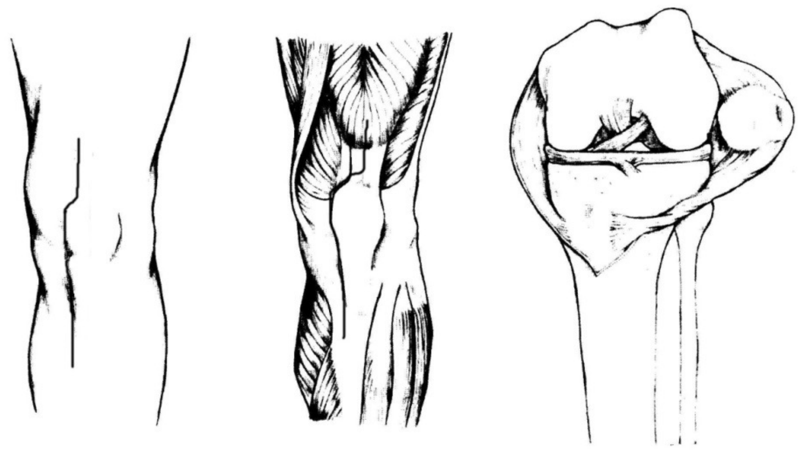

Figure 46: Diagram of medial parapatellar approach used for arthrotomy of surgical specimens and subsequent patellar eversion and joint exposure ([130;131]).

The arthrotomy wounds were closed anatomically in layers using commercially available absorbable dyed braided polygalactin suture utilising a reverse cutting needle for the capsule and subcutaneous tissues and a non absorbable polyamide monofilament suture with a reverse cutting needle for the skin. All the sutures were instrument tied utilising at least 4 sequentially laid reef knots per suture and the closure was performed meticulously with surgical instruments.

Bone Tracker Mounting

Several simple experiments were performed in the laboratory utilising synthetic human Sawbones ([3]). These demonstrated that the standard bi-cortical pin fixation of the trackers and their adjustable height assembly was susceptible to loosening and was not able to resist even minor collisions.

In addition, because the aim was to utilise intramedullary jigs to allow precise rotational misalignment and posterior slope of the tibial component, bi-cortical pin fixation would not have been appropriate for the tibial tracker. Therefore, an alternative method of fixation was devised. This consisted of a rectangular stainless steel block, 10 mm x 50 mm x 10 mm; two 10 mm notches half the thickness of the original block were machined at two positions equidistant from the block's centre. A standard tracker coupling stalk was then drilled and welded into the centre of the block (figure 47).

These blocks were then secured to the cortical surface of the tibia and femur with two circumferential Jubilee circlips that ran in the notches of the blocks. This method of fixation proved to be successful in all the experiments, being both secure and not interfering with the intramedullary instrumentation (figure 48).

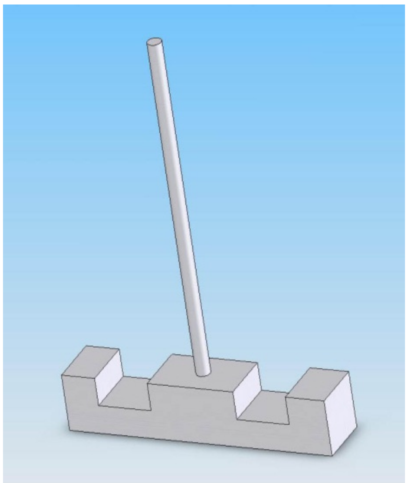

Figure 47: Computer aided drawing of the tracker mounting blocks manufactured and used to secure the IR trackers to the tibia and femur for the purposes of the experiments.

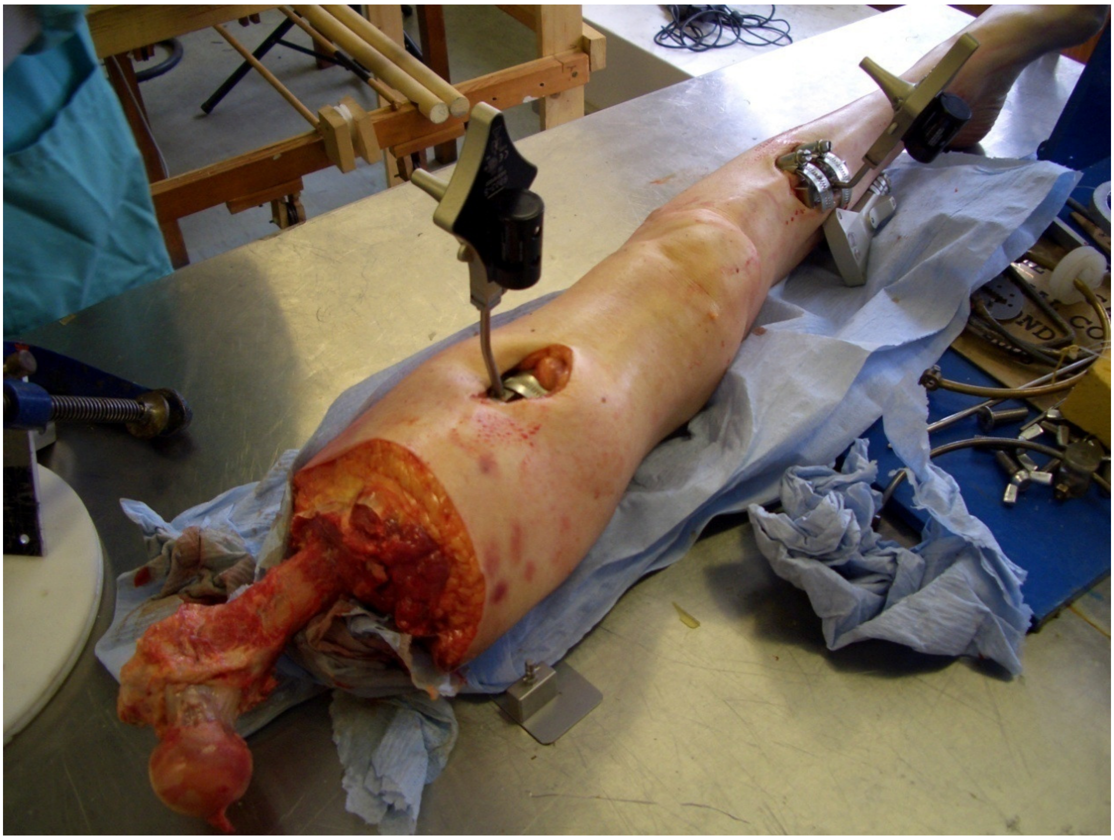

Figure 48: Photograph of specimen with tracker mounting blocks and trackers attached, ready for initial digitisation procedure

Infra Red Tracker Tool Initialisation

When activated, the Stryker Navigation System required an initialisation and validation process to be performed prior to use on each occasion. This took approximately 30 minutes to complete and was performed on each occasion after the initial arthrotomy.

For the initialisation procedure, a C4 compact battery was inserted into the battery holder of each of the two trackers and the IR pointer. The LED arrays were then aimed at the tracking boom and the activation switch on the IR pointer was depressed. An audible sound and visualisation of their relative 3D positions on the monitor display confirmed initialisation of the IR devices . The validation step then involved touching the tip of the IR pointer against a validation point on the femoral tracker and pressing the activation switch. The IR pointer was then validated and its end position was also visible on the monitor display (figure 49).

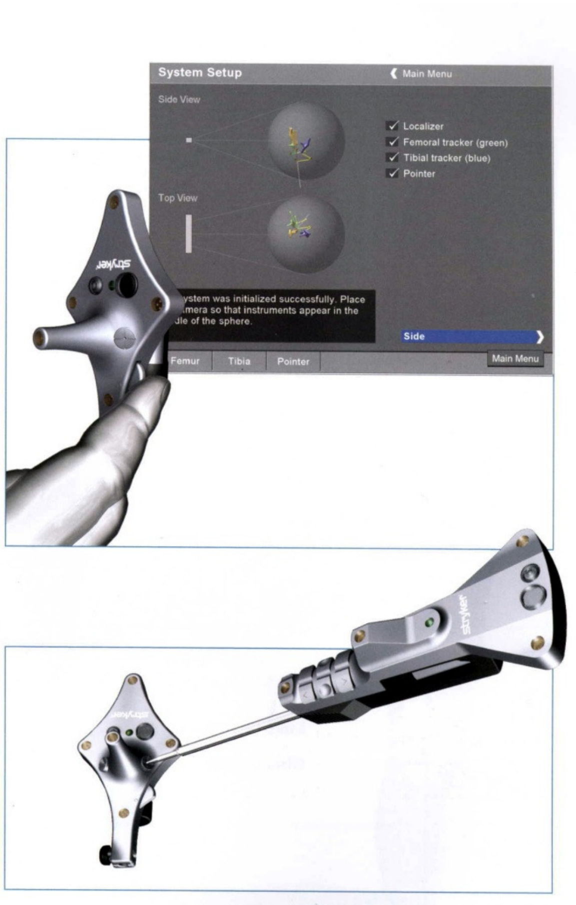

Figure 49: Pictures illustrating the initialisation process required to activate the trackers and locate them in free space. The subsequent validation process registered the tip of the IR pointer in a similar fashion. Confirmation and the relative positions of the trackers and IR pointer were then displayed on the display monitor ([130;131]).

Definition of Mechanical Axes

The femoral mechanical axis was defined by a line passing through the centre of the femoral head and the centre of the knee. The hip centre of rotation was determined by the system using motion analysis of the leg. The centre of the knee was digitised using the IR pointer; the exact steps will be described below.

The tibial mechanical axis was defined by a line passing through the digitised centre of the tibia and the centre of the ankle. In order to define the centre of the ankle, the system created a frontal ankle plane from the centre of the proximal tibia and the digitised malleoli. The centre of the ankle was derived from the average of the intersection point of the IR pointers axis, pointing to the ankle centre, on the frontal ankle plane and the mid-point of the inter-malleolar line calculated from the digitisation of the medial and lateral malleolus.

During the navigated procedure, the computer system calculated the desired alignment and necessary bone resections for the tibia and femur.

Definition of Rotational Axes

The navigation system analysed the digitised epicondyles of the femur to calculate the transepicondylar axis. This axis and the perpendicular line to the digitised preliminary AP axis were averaged by the computer system to define the internal / external rotation axis of the femur. The tibial rotational axis was defined by the IR pointers axis when pointing along the anatomical AP axis of the knee in line with the posterior cruciate ligament (figure 50).

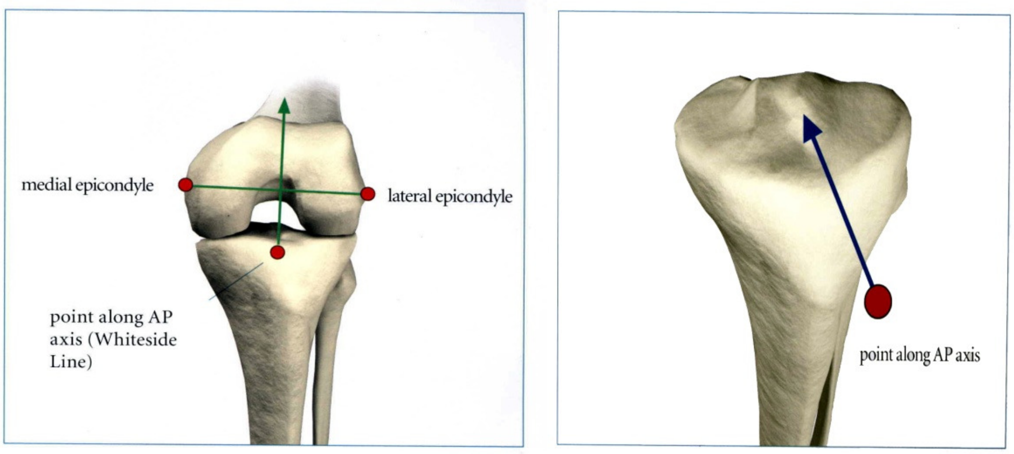

Figure 50: diagrams illustrating the navigation systems definition of femoral and tibial rotation ([130;131]).

Calibration - Anatomic survey of the Femur

The calibration process in vivo would normally have the femoral head located within a stable acetabulum. The cadaver specimens were supplied disarticulated at the hip joint, and it was therefore necessary to fashion an acetabular substitute for the purposes of calibration. Therefore an anatomically verified Sawbone Pelvis ([7]) was firmly mounted into a bench vice on the cadaver working table and the left acetabulum was lightly greased to permit smooth movements of the cadaver hip.

The relative position of the tibial and femoral trackers was then assessed by the registration of the knee position at 20º and 45º of flexion, by depressing the selection switch on the IR pointer (figure 51).

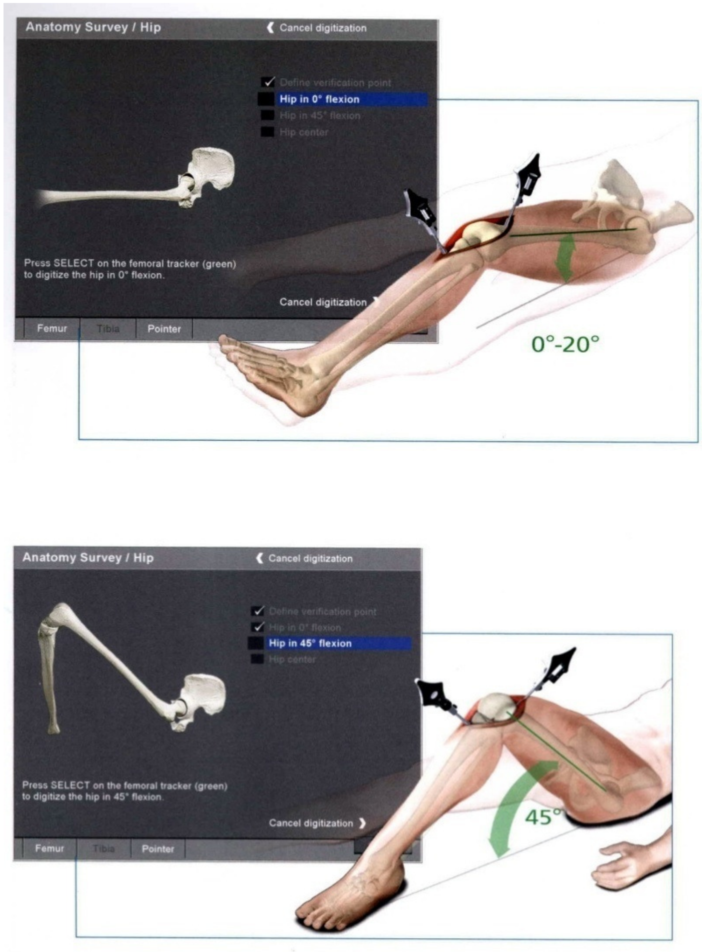

Figure 51: Digitisation of the hip in 20**º** and 45º of flexion respectively ([130;131]).

The acquired data was then used by the computer system to calculate an approximate centre of the femoral head by denoting two reference positions that are conferred to the limb by movement at the hip joint. The limb was then circumducted smoothly (figure 52) to replicate normal hip movements but without any movement of the Sawbone pelvis. The navigation system recorded 200 points of reference of the femoral tracker about its centre of rotation (the centre of the femoral head) and produced a 'best fit' pattern of the movement data that averaged the data points to eliminate and compensate for any inadvertent artefact. This calculated centre of rotation was displayed on the monitor as a 3-Dimensional plot of the calculated centre of rotation. Aberrant movements were also depicted on the monitor and a cut off limit of 100% was employed to prevent wayward determinations that required hip centre recalibration.

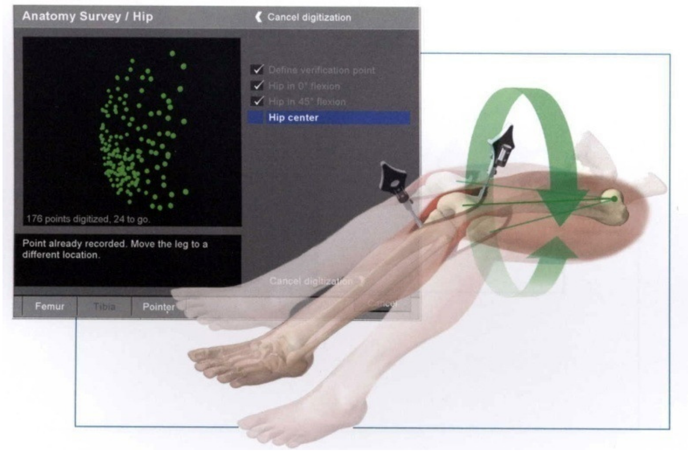

Figure 52: Slow circumduction of the knee within the Sawbone pelvis acquired 200 points from which the centre of femoral head was calculated by the computer system ([130;131]).

Having determined the centre of rotation for the hip joint, the software required several predetermined landmarks to be input into the computer system utilising the IR pointer. Data points were acquired by pointing or tracing the IR pointer over the bone and joint surface. These were then used to generate a static three dimensional model of the bony landmarks of the distal femur and proximal tibia.

Digitisation of Bony Landmarks

Medial Epicondyle

The prominence of the medial epicondyle was identified and digitised (figure 53).

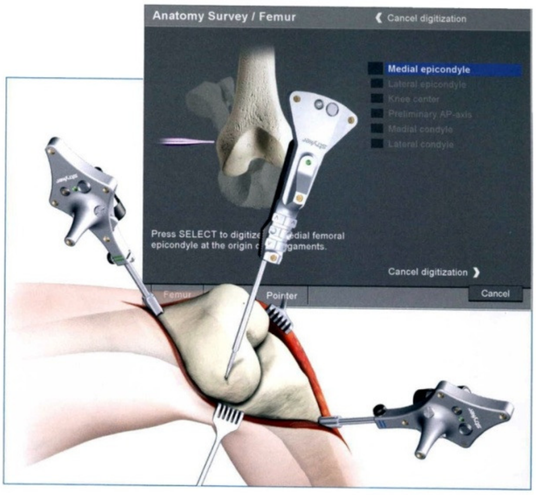

Figure 53: Digitisation of the medial epicondyle ([130;131]).

Lateral Epicondyle

The prominence of the lateral epicondyle was identified and digitised (figure 54).

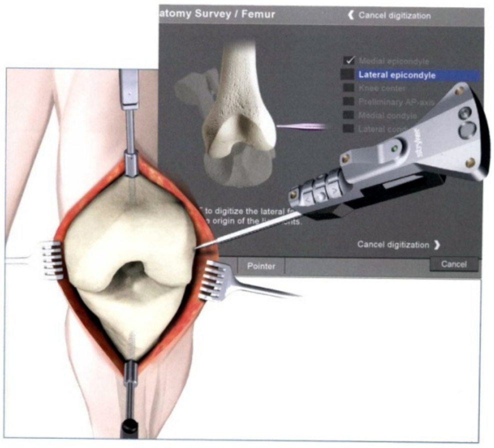

Figure 54: Digitisation of the lateral epicondyle ([130;131]).

Data from the digitisation of the epicondyles was subsequently used by the navigation system to calculate the rotational alignment of the distal femur through calculation of the epicondylar axis. Knee flexion-extension was also measured about this axis.

Centre of the Knee

The centre of the knee was digitised at a point antero-medial to the posterior cruciate ligament insertion into the femur (figure 55).

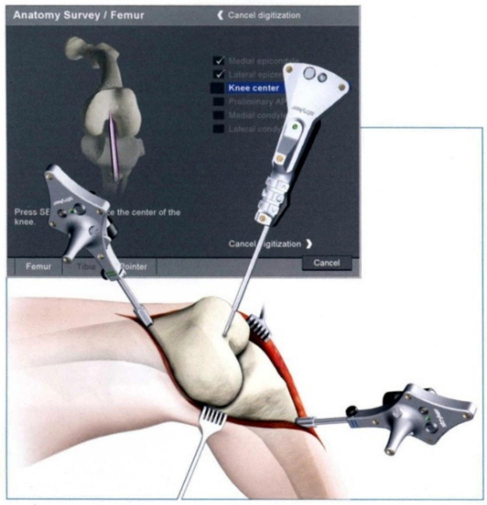

Figure 55: Digitisation of the centre of the knee ([130;131]).

AP Axis

The preliminary AP axis was digitised by aligning the IR pointer with the sulcus of the infra-trochlear groove while ensuring that the straight axis of the pointer was parallel to the neutral axis of the femur. The final AP axis was then calculated by the computer system that averaged the preliminary AP axis and the transepicondylar axis. The system also incorporated a failsafe that issued a warning and or mandated re-digitisation if the rotational deviation of either of the preliminary or final axis was greater than 5º (figure 56).

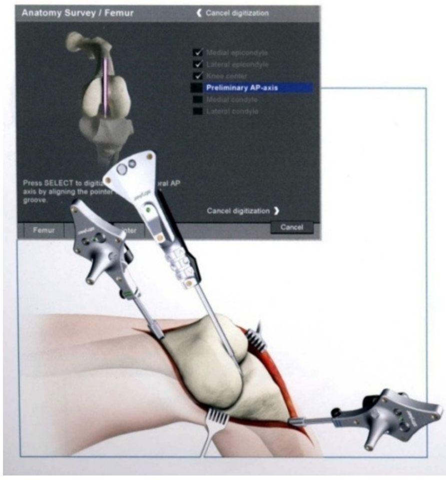

Figure 56: Digitisation of preliminary AP axis ([130;131]).

Medial Condyle

The surface of the medial condyle was then digitised to scan its articular surface. The pointer was moved over the entire surface of the medial condyle of the femur recording over 100 individual points to create a 3D mesh map of the articular surface (figure 57).

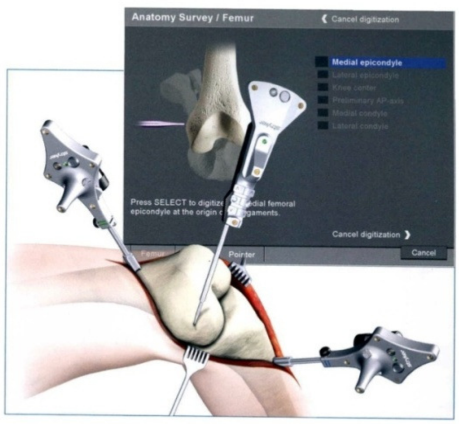

Figure 57: Digitisation of the surface of the medial condyle of the femur ([130;131]).

Lateral Condyle

A similar digitisation procedure was performed on the lateral condyle, recording over 100 individual points to create a 3D mesh map of the articular surface (figure 58).

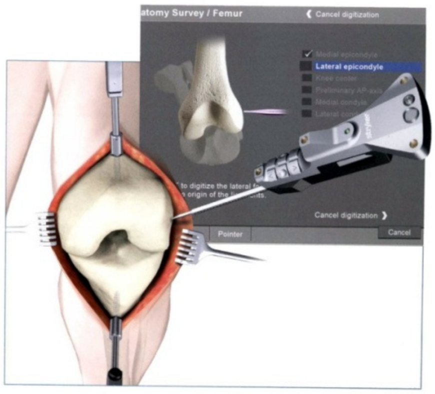

Figure 58: Digitisation of the surface of the lateral condyle of the femur ([130;131]).

Centre of Tibial Plateau

The centre of the tibial plateau was digitised as a point located at the anterior cruciate ligament insertion into the tibial plateau (figure 59).

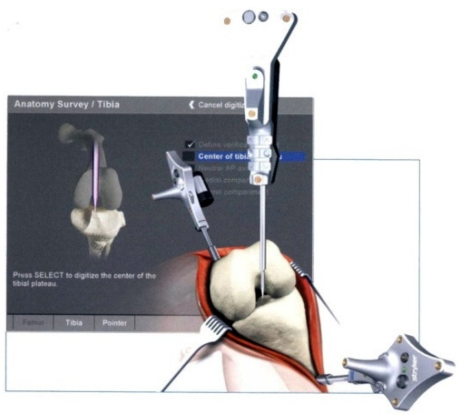

Figure 59: Digitisation of the centre of the tibial plateau ([130;131]).

Neutral AP Axis

The neutral AP axis was digitised by aligning the long axis of the IR pointer with the middle third of the tibial tuberosity and the centre of the posterior cruciate ligament (figure 60).

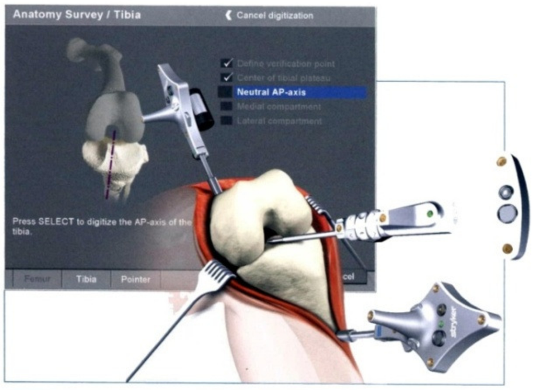

Figure 60: Digitisation of the preliminary neutral AP axis ([130;131]).

Medial and Lateral Compartment

The IR pointer was then moved slowly over the entire articular surface of the medial and lateral tibial plateau in turn. Over 100 points were digitised per compartment creating a 3D mesh map of the articular surface of each compartment (figure 61).

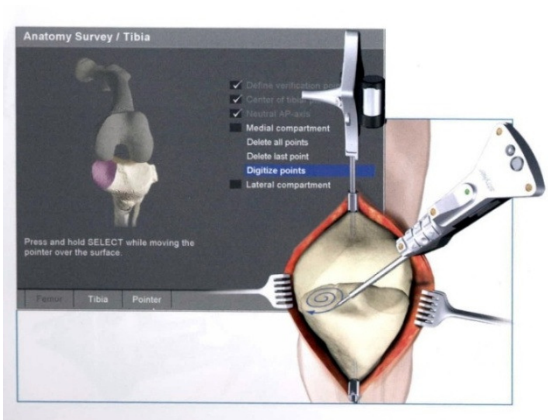

Figure 61: Digitisation of the medial and lateral tibial compartments ([130;131]).

Anatomical Survey of Ankle

The medial and lateral malleoli of the ankle were digitised with the IR pointer (figure 62).

Figure 62: Digitisation of the medial and lateral malleoli of the ankle.

The centre of the ankle was then also digitised by placing the tip of the IR pointer at the perceived ankle centre (figure 63). After digitisation the medial / lateral ratio of the perceived ankle centre was displayed on the monitor.

Figure 63: Digitisation of the perceived ankle centre ([130;131]).

The system also incorporated a failsafe that issued a warning and mandated re-digitisation if the ratio of medial to lateral side to the centre of the ankle was less than 40% or greater than 60%.

Specimen Mounting

Once the digitisation procedure was complete and the navigation system had been set up, the proximal femora were resected to allow the specimen to be mounted in the rig so that the epicondylar axis of the femur was parallel and in line with the hinge of the rig. The distal tibial resections were performed approximately 20cm below the level of the joint line to allow implantation of the jig, operation of the control rod from below and the semi-constrained movement of the tibia in between the stainless steel rods of the box frame.

The resections were performed circumferentially with a scalpel to the bone surface. The periosteum was then incised and the bone cut was completed with a reciprocating cordless saw.

In the case of the femoral resection, a further 3cm of skin and muscle was resected circumferentially from the end of the femur and the periosteum stripped back. The intramedullary canal was then entered and reamed lightly with a pin reamer to remove some of the proximal fat and marrow from within the intramedullary canal. PMMA bone cement was then prepared, poured into the intramedullary canal and pressurised lightly using a gloved finger (figure 64).

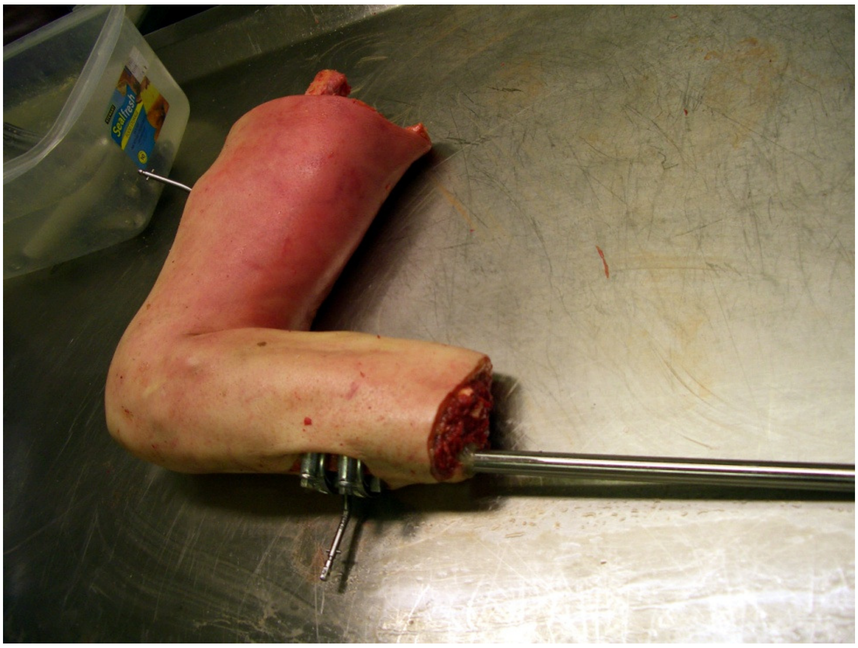

Figure 64: Photograph of calibrated and resected specimen with tibial rod cemented in, prior to femoral potting.

The femur was then potted into a PMMA cement block (4 cm wide x 4 cm tall x 5 cm long) in a neutral vertical alignment with the aid of a potting jig. This consisted of two adjustable lab freestanding bench clamps, a plumb line, a spirit level and a used plastic suture box. The potting procedure involved mounting the specimen femur in a bench clamp such that its alignment when hanging free was vertical as compared to the attached plumb line. The plastic suture box was then sawed in half to the dimensions required (4 cm wide x 4 cm tall x 5 cm long), lightly greased inside with some axle grease and then held with the second bench clamp so that the end of the proximal femur sat within it. PMMA bone cement was then mixed and the box filled. Once the cement had set, the outer suture box was removed, producing a square cement block (figure 65).

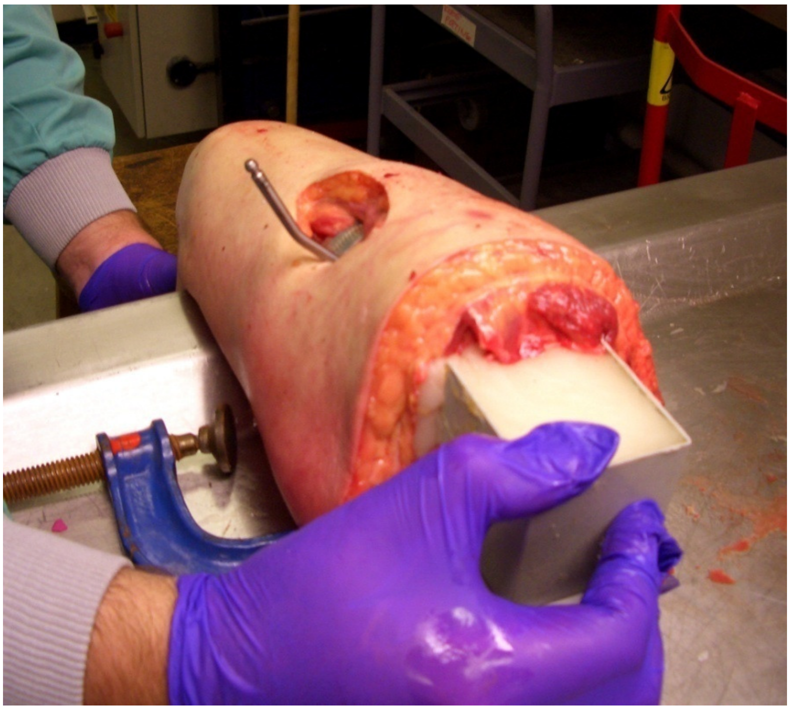

Figure 65: Photograph of the potted femur undergoing removal of the plastic suture box mould.

The potted femur in the square block was then clamped in the rig between two transverse bars using socket-head cap screws. The alignment of the femur was rechecked and adjusted with the femur hanging vertically in the rig to ensure it was vertical and the epicondylar axis was in line with the hinge of the rig (figure 66).

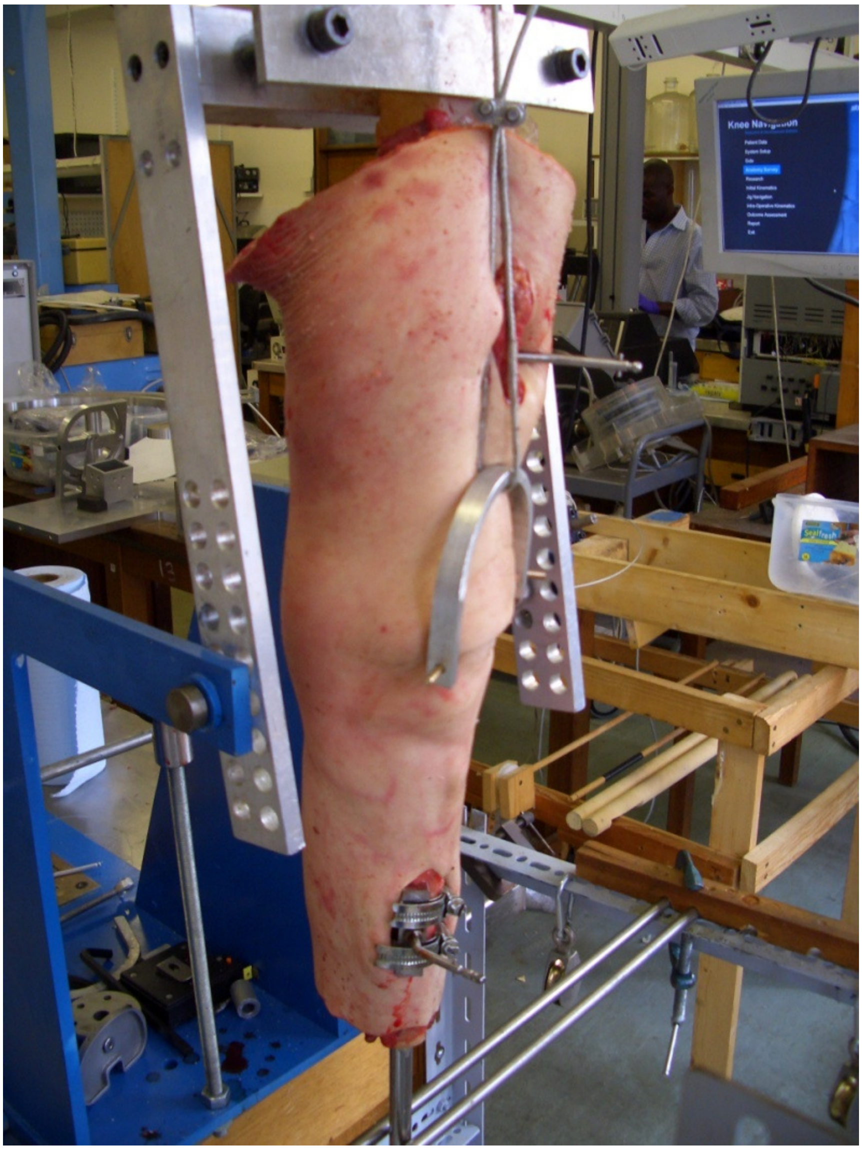

Figure 66: Photograph of a potted and mounted specimen on the rig. Note that the epicondylar axis of the femur is in line with the hinges of the rig and the specimen stands vertically when extended.

Recording of native knee kinematics

The knee kinematics of the specimen were then recorded using the loading cycle protocol as described previously in this chapter. The results were then saved prior to proceeding with the TKR surgical protocol.

Navigated TKR Surgical Protocol

The navigated surgical protocol for TKR for the specimens was identical to the normal operating surgical protocol as described by Stryker in their published Scorpio navigated reference guides([130;131]). Minor modifications to this published technique were necessary to allow the attachment of the IR trackers and insertion of the tibial jig. Normal commercially available instruments and guides as well as a Stryker cordless saw, drill driver, drill bits and blades were used. During the surgical procedure, adequate retraction of the soft tissues was obtained using ring spikes and other surgical retractors so as not to damage the soft tissues. The cementing of the implants was done with premixed PMMA bone cement.

Soft Tissue Dissection and Exposure

The superficial and deep sutures were individually cut and removed from the specimen, reopening the previous arthrotomy. The knee was then flexed and the patella folded over laterally. This allowed good exposure to the joint surfaces of the femur and tibia as well as to the soft tissues within the knee.

The intra-articular anterior fat pad was then excised along with the anterior cruciate ligament and the medial and lateral menisci. Excess synovium was then excised from the medial and lateral walls of the femoral condyles along with the fat and synovium from the anterior surface of the distal femur, exposing the periosteum.

Any visible prominent osteophytes were then excised from the margins of the femur, tibia and patella using a fine straight osteotome.

Femoral Preparation

A 10 mm diameter by 100 mm long drill bit was used to enter the femoral intra-medullary canal on a cordless drill driver. It was positioned 1cm anterior to the femoral attachment of the posterior cruciate ligament (PCL) and slightly medial to the midline of the femur, aiming up towards the hip. Once the drill bit had been inserted to its hilt and was in the intra-medullary canal (signalled by the expression of bone marrow and blood from the drill hole), it was withdrawn whilst toggling the drill slightly in order to slightly enlarge the opening of the hole (figure 67).

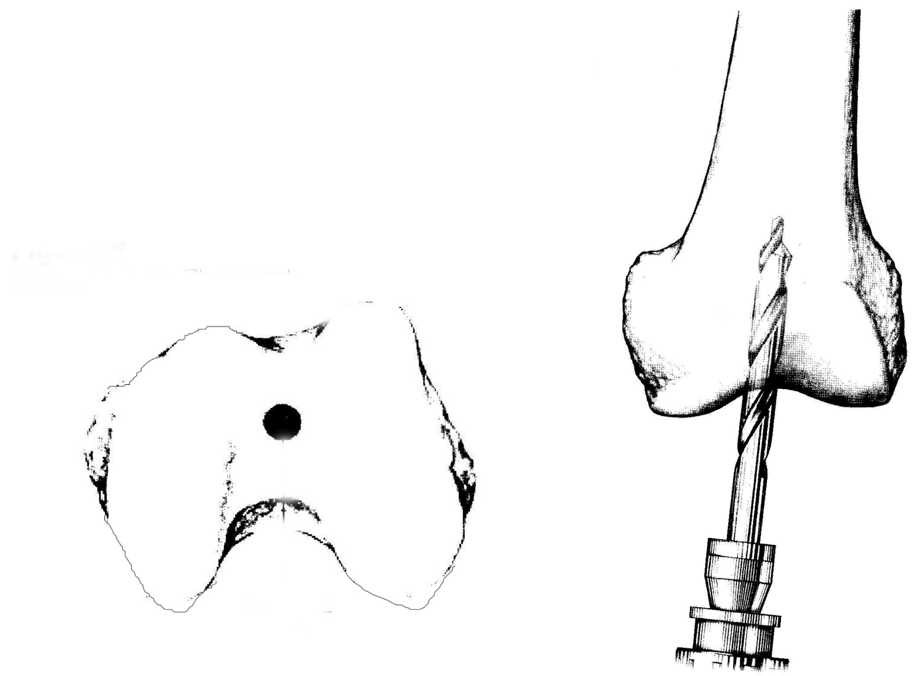

Figure 67: Femoral drill entry point and direction of drill insertion ([130;131]).

Initial alignment for the skim cut of the femur was performed using the epicondylar axis as a guide for femoral rotation. A referencing tool was therefore inserted in the drilled hole and aligned so that its arms were in line with the epicondylar axis of the femur. The cartilage of the femoral condyles was then marked through the slot in the referencing tool with permanent marker ink and the tool removed (figure 68).

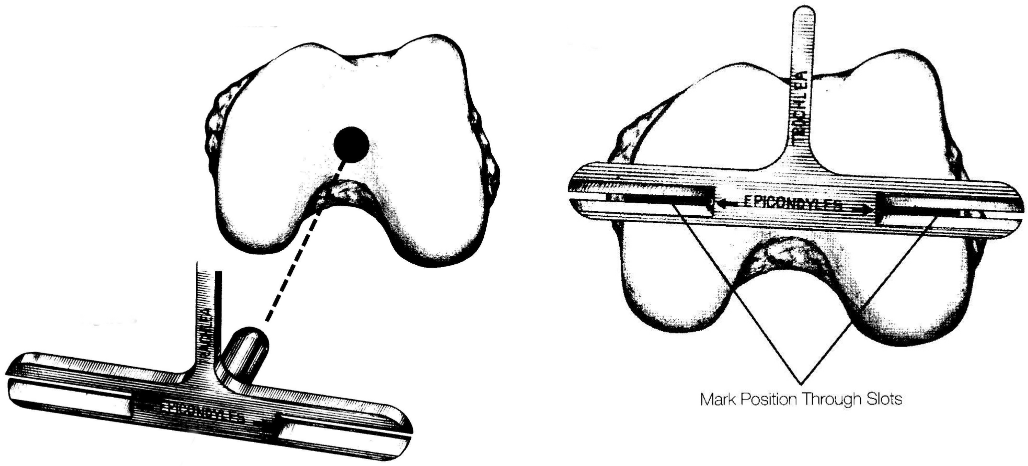

Figure 68: Diagram demonstrating use of the reference guide to determine the initial rotational alignment for the skim cut ([130;131]).

A 10mm x 40cm circular T-handled rod was passed through the left femoral alignment guide and then inserted down the femur through the drill hole. The alignment guide was aligned with the pre-marked epicondylar axis and set to 3º, 5º or 7º of valgus depending on the individual specimen to obtain a best fit on the femoral condyles. 2 threaded pins were then inserted though the alignment guide, securing it firmly in place (figure 70).

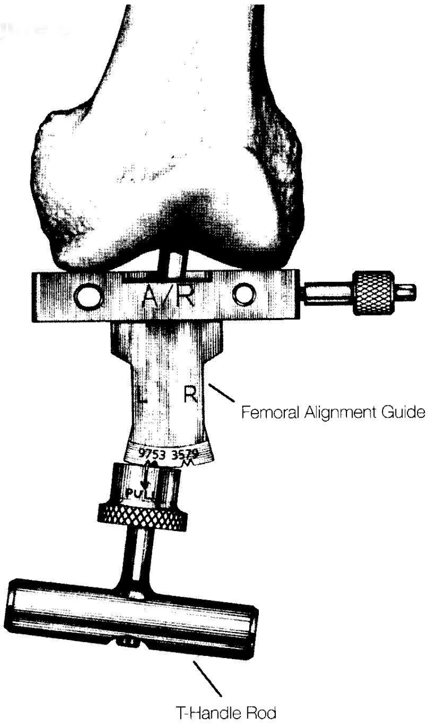

Figure 69: diagram of femoral alignment guide in place on distal femur ([130;131]).

The anterior resection guide was then attached to the dorsal side of the femoral alignment guide and the anterior resection stylus attached. The height of the resection guide was adjusted for an initial skim cut of the anterior trochlea using the stylus placed on the highest point of the anterior femur proximal to the trochlea. This allowed a straight close cut without notching the femur. When satisfactorily set up, the entire assembly was securely tightened using the provided bolts. The blade runner was used to double check the resection level prior to the saw being passed through the resection guide slots to complete the anterior skim cut (figure 70).

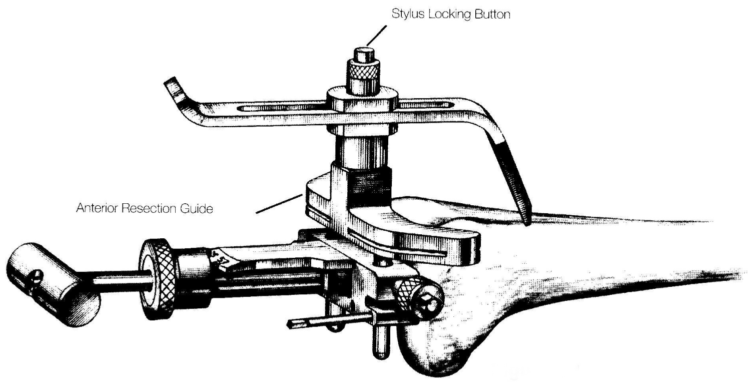

Figure 70: Anterior resection guide and stylus in position ([130;131]).

Once the saw cut was completed, the anterior resection guide was loosened and removed. A 10mm distal resection guide was then assembled by placing the guide over the pegs in the guide stand and engaging the locking pin. The resection guide also incorporated a secondary magnetic alignment system to ensure correct assembly (figure 71).

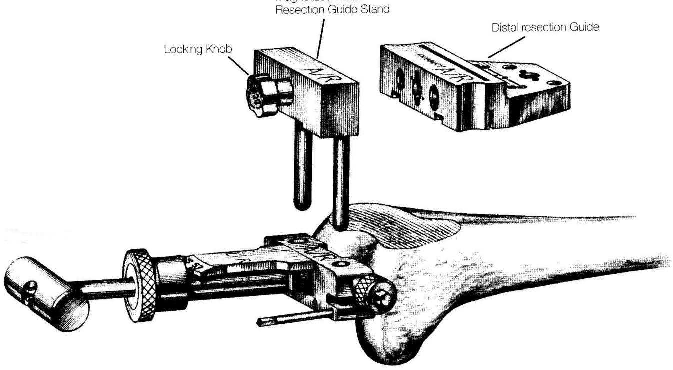

Figure 71: 10mm distal resection guide assembly procedure ([130;131]).

The entire assembly was then securely pressed down onto the anterior femur and pinned in place with two threaded pins (figure 72).

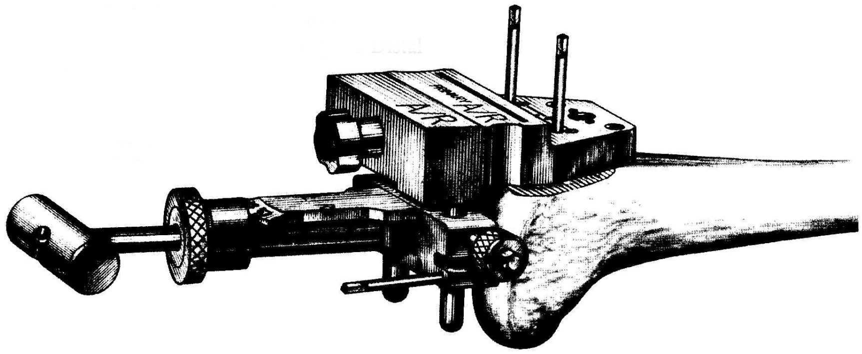

Figure 72: The pinned 10mm distal resection guide ([130;131]).

At this stage the navigation system was used to verify the position and alignment of the distal femoral cut using the tibial tracker and the resection plane probe. By inserting the flat section of the resection plane probe into the saw guide slot, the position and rotation of the resection guide was checked and adjusted so that it was perpendicular to the mechanical axis of the femur prior to final cross pinning and distal femoral resection with the saw (figures 73, 74).

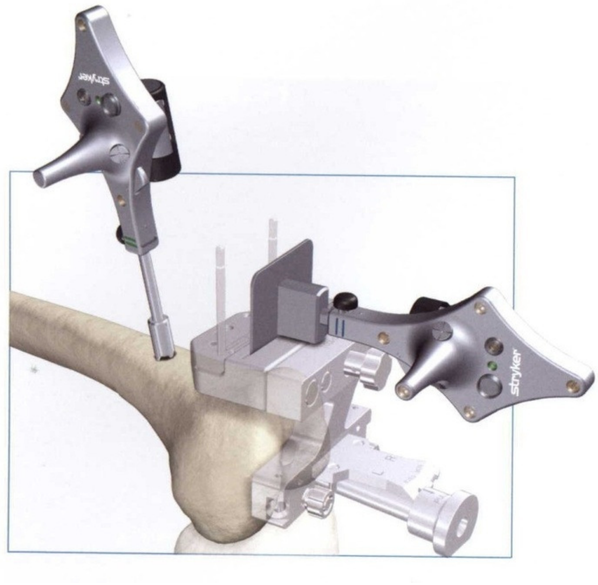

Figure 73: Navigated verification procedure for the distal femoral resection guide prior to cross pinning ([130;131]).

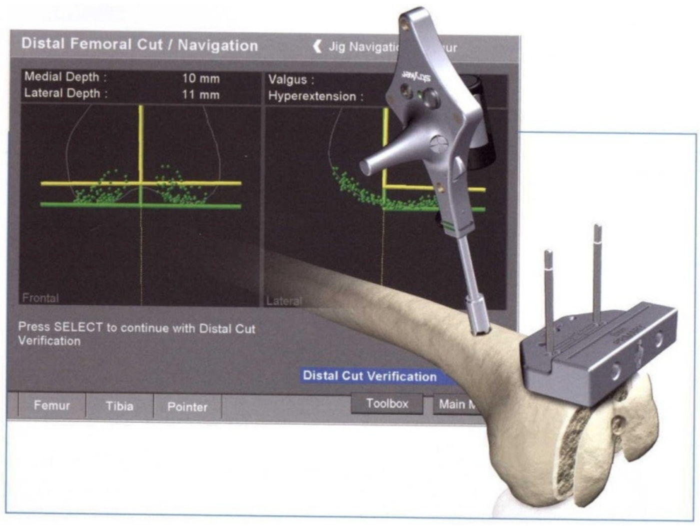

Figure 74: Diagram illustrating navigated alignment verification and subsequent distal femoral resection ([130;131]).

Once the femoral distal cut was completed, the 4 threaded pins, intra-medullary rod and handle and alignment guides were removed and the resection verified by placing the resection plane probe onto the cut surface (figure 75).

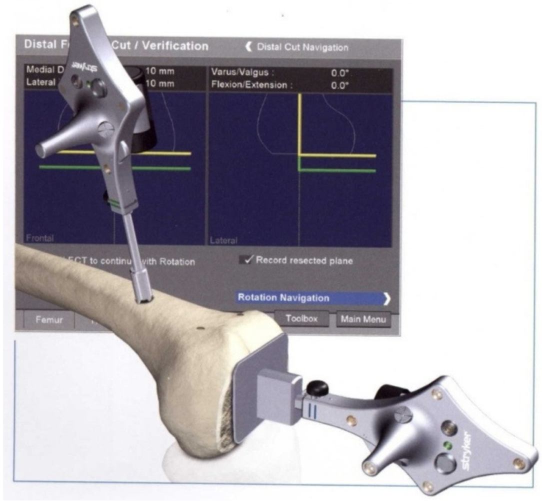

Figure 75: Verification of the distal femoral resection using the navigation system resection plane probe ([130;131]).

The femur was then sized using the femoral sizer (figure 76).

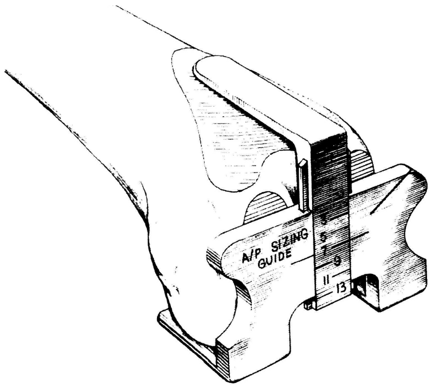

Figure 76: Diagram of femoral sizer. If the measurement read in-between sizes, then the femur was downsized ([130;131]).

The selected sized resection block was then placed flat onto the femur and its position adjusted so that there was no overhang and the block was centrally placed. In the case of 4 of the 10 specimens, the femur was further downsized from the initially selected size to ensure a satisfactory fit with no overhang.

The navigation system was then used to determine the optimal rotational alignment for the femoral resection block. The resection plane probe was inserted into the anterior cortex saw guide slot and the femoral resection block was then rotated until its navigated alignment matched the suggested alignment on the computer monitor (figure 77).

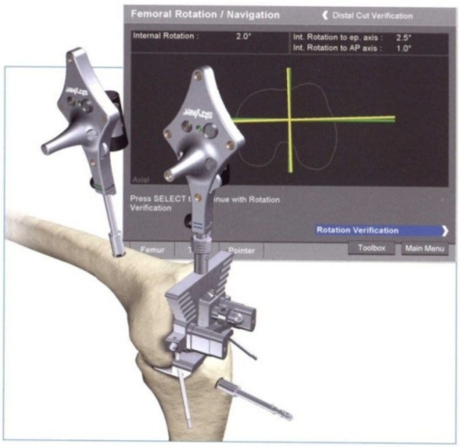

Figure 77: Rotational alignment of femoral resection block determined using the navigation system ([130;131]).

The femoral resection block was then secured using 4 threaded pins and two pairs of spiked towel clips. The blade runner was then used to check that the positions of the guide slots were satisfactory prior to the resections.

The resections were then preformed in the following order (figure 78):

1. Posterior condyles
2. Posterior chamfer
3. Anterior cortex
4. Anterior chamfer

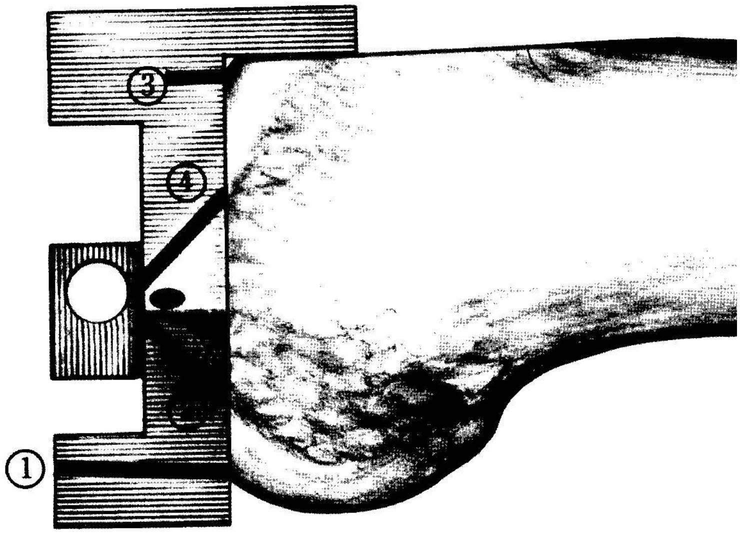

Figure 78: Secured femoral resection block and order of the bone resections ([130;131]).

Once the femoral resections were complete, the femoral resection block was removed and the rotational alignment checked by placing the resection plane probe onto the cut surfaces (figure 79).

Figure 79: Verification of the rotational alignment of the femoral resections using the navigation system resection plane probe ([130;131]).

The next stage in the surgical procedure was to prepare the patellar chamfer. This was performed using the correctly sized notch block (one notch block size for size 3, size 5, and size 7 knee cutting blocks and a second larger sized notch block for the remaining 2 sizes of femoral cutting block) and the patellar groove recess punch. The notch block was placed onto the resected anterior and distal surface of the femur ensuring a snug centered fit on visual inspection. The block was then secured with 4 threaded pins and two pointed towel clips. The appropriately sized patellar groove recess punch (matching the notch block) was then lightly tapped through the predetermined grooves in the notch block, cutting the necessary recess for the patella in the anterior cancellous bone of the femur. The punch was passed both proximally and distally to ensure a smooth even cut (figure 80).

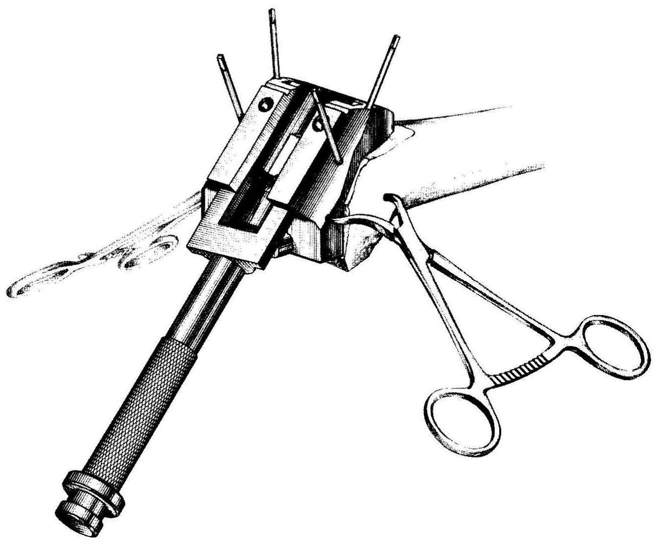

Figure 80: Cutting the patellar groove using the pinned notch block and patellar groove recess punch ([130;131]).

The pins and block were then removed and the loose bone shavings washed off the femur. The appropriately sized femoral trial prosthesis was then lightly impacted centrally onto the femur confirming that all resections were correct and that the femur looked well positioned and stable.

Tibial Preparation

The proximal tibial resection was performed using the 0º proximal tibial resection guide. This was positioned free hand guided by the navigation system, utilizing the femoral tracker mated to the resection plane probe. The probe was inserted into the saw guide slot of the 0º proximal tibial resection guide, allowing the level and angulation of the resection block to be precisely monitored and adjusted. A 12mm resection level with an identical angulation to the computers suggested position was chosen, and the resection guide firmly fixed to the tibia with 3 threaded pins. The blade runner was then used to double check the resection path prior to further fixation of the resection guide with a cross pin. The saw was then carefully passed through the saw guide slot completing the resection of the proximal tibia without affecting the posterior soft tissues (figure 81).

Figure 81: Freehand navigation and pinning of the 0º proximal tibial resection block ([130;131]).

Following the proximal tibial resection, the cutting guide was removed and the cut verified on the navigation system using the resection plane probe (figure 82).

Figure 82: Proximal tibial resection verification using the navigation system ([130;131]).

Once the proximal tibial cut was successfully verified, the best fitting tibial base plate was selected and applied to the proximal tibia. The selected correctly sized tibial base plate provided the greatest cover of the cut tibial surface without any overhang in both the AP and medio-lateral plane. The size of the tibial base plate selected was also no more than one size larger or smaller than the size of the femoral component selected and used on the femur as guided by the Stryker Femoral and Tibial size compatibility table (figure 83).

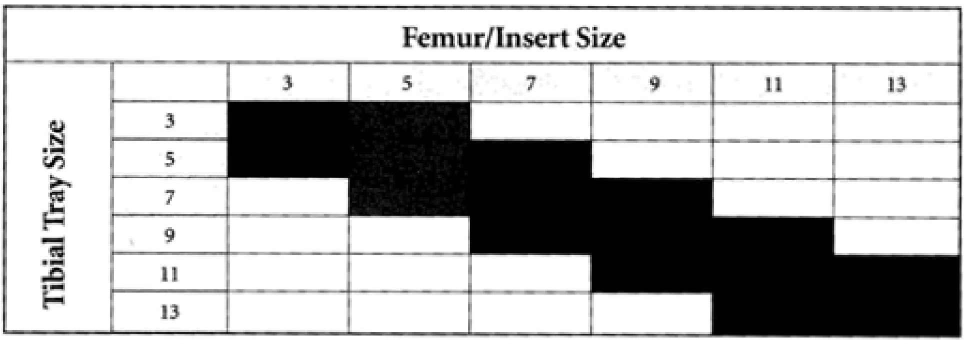

Figure 83: Femoral / tibial sizing chart demonstrating compatible size mismatches between the femoral and tibial component ([130;131]).

The tibial base plate was then mounted to the alignment handle and the femoral navigation tracker attached. The handle was then used to guide the rotational alignment of the tibial tray around its central axis until the alignment matched the calculated AP axis on the navigation system monitor (figure 84).

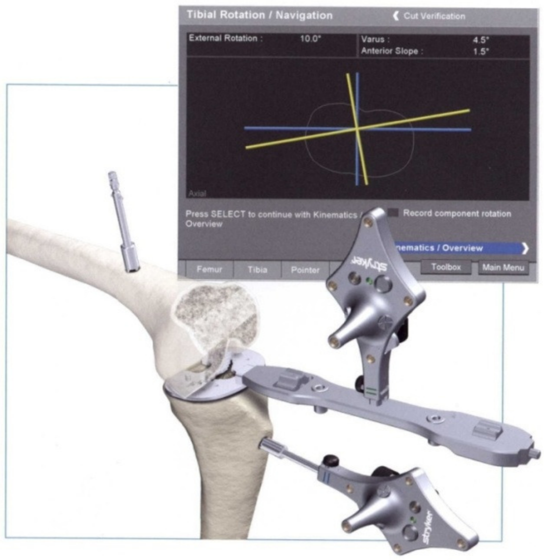

Figure 84: Adjusting the tibial base plate using the alignment handle to determine the optimal rotational alignment of the tibial tray component as defined by the navigation system ([130;131]).

The Anterior tibial cortex was them marked using a fine permanent marker pen in line with the reference marks on the anterior border of the tibial base plate (figure 85).

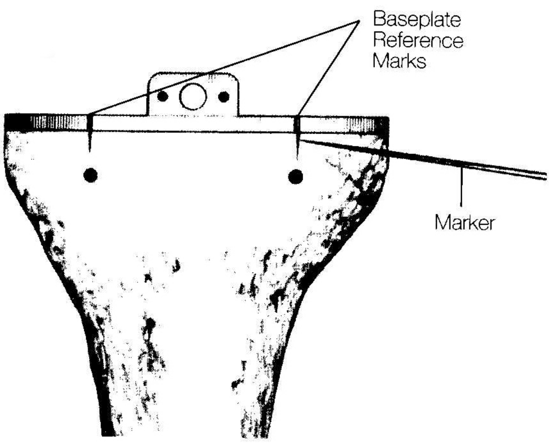

Figure 85: Anterior view of the tibia demonstrating the reference marks for the optimally rotated tibial base plate.

The tibial plate was then pinned into position using 4 short headed pins. The pilot drill hole was marked internally using a permanent marker pen. The drill bushing was then attached to the tibial base plate and the 10 mm drill bit used to open and enter the metaphysis of the tibia (figure 86).

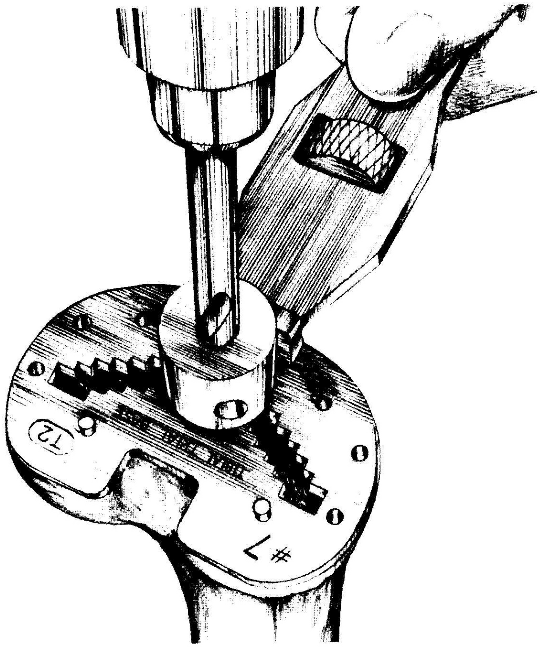

Figure 86: The 10 mm drill bit is used to open the centre of the tibia as directed by the drill bushing attached to the pinned tibial base plate ([130;131]).

The tibial tray bushing was then removed and a T-handled 8mm diameter rigid conical bone reamer was passed down through the drill hole and the intramedullary canal reamed by hand until the tip of the reamer emerged through the bottom of the tibia. This reamed channel was progressively increased in size using sequentially larger reamers to a final diameter of 12mm. The tibial base plate and headed pins were then removed and the 20mm box marked centrally around the reamed channel. This box shape was then excavated using a sharp osteotome so that the outer 12 mm diameter stainless steel tube and de-rotation augment could slip down the reamed channel and be contained within the proximal tibia.

The reamed channel was then flushed with some clean water to remove any loose bone fragments and reamings. Some low viscosity bone cement was mixed and the outer aspect of the 12 mm diameter stainless steel tube and de-rotation augment then cemented into the intramedullary canal and proximal tibial metaphysis. The straight edge of a small steel ruler was placed across the tibial plateau while cementing to ensure that the cut surface of the top of the tibia and the top surface of the de-rotation augment were congruent with no step between them. Once the cement had set, the inner 10 mm rod was passed into the 12 mm tube and checked so that it could rotate freely with little resistance.

The matching size tibial tray to the used best fit tibial base plate was then selected. A 40mm long M5 machine screw was then coated in a commercially available thread locking paste and used to firmly screw the tibial tray on to the 10mm inner rod through the predrilled hole in the centre of the tibial tray. This new construct was then set aside for 10 minutes to allow the thread lock to cure before being inserted into the 12mm outer tube. The construct was thoroughly tested to ensure that the tibial tray was securely fixed and that it could be rotated using the intramedullary 10 mm rod protruding from the distal resected portion of the tibia.

Femoral Implantation

The pre sized femoral component was then selected and the cut surface of the femur was washed with some water to remove any surface blood and bone marrow. The cut surfaces were then dried using paper towels and a double mix of PMMA bone cement applied to the cut surfaces as per a normal surgical cementing technique. The Femoral component was then inserted and impacted into the cement mantle using the femoral impactor with the knee at 90º of flexion. Any excess extruded cement was removed and firm constant pressure was applied to the femoral component in the fitted position until the cement had fully cured. The impactor was then removed and any excess cement removed using a sharp osteotome (figure 87).

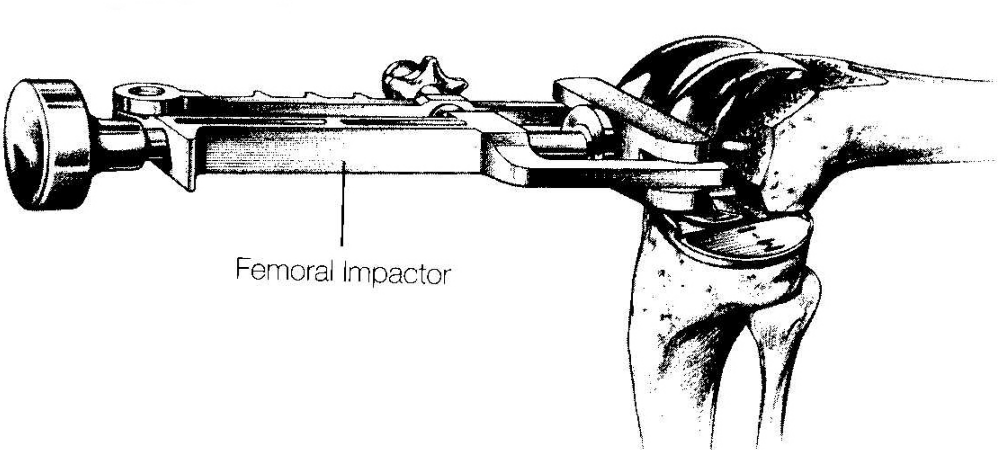

Figure 87: The femoral impactor was used to position and impact the femoral component into cement mantle, and also to apply a constant pressure through the component until the cement had cured ([130;131]).

Tibial Insert Changing Procedure

Insertion and changing of the polyethylene tibial insert was a simple procedure. Both the standard and modified inserts had a slight anterior lip that would lock into a receiving groove on the tibial tray with an audible click. To insert the tibial inserts, they were simply slid into the tray and pressed down on the anterior aspect till they clicked in. To remove the inserts, a Mc-Donald retractor was inserted down the anterior aspect of the tibial tray, releasing the insert from its locking groove and then the insert would pop out easily and undamaged. Repeated testing of the insertion and removal of the inserts in trial tibial trays demonstrated that this was possible with the access available after implantation, and that the function of the inserts was not affected after repeated removals and insertions (figure 88).

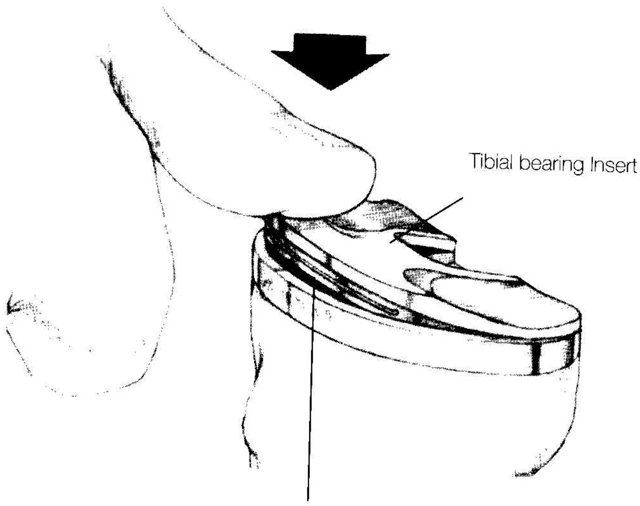

Figure 88: The tibial insert was slid into the tibial tray to engage it posteriorly first. It was then snapped into place anteriorly ([130;131]).

Misalignment Measurement

The rotational misalignment applied to the tibial component was measured with a large custom made protractor. The angle graduations were obtained by scanning a scientific protractor. The obtained image was then enlarged symmetrically so it roughly matched the surface of the nylon rotation disc. The image was then printed and laminated. Once the navigation of the tibial component was completed, using the control rod as a needle, the laminated protractor was lined up at the zero position on the top of the nylon control disc and firmly stuck down with double sided adhesive tape.

The Subsequent rotational misalignments in the experimental protocol were applied and measured without having to reopen the knee. The procedure was straight forward and involved loosening the clamping bolts in the clamping bushing, then using the control rod to rotate the inner rod to the requested angle as read off the protractor on the top of the nylon rotation disc. In order to apply posterior slope, the tibial tray inset (which had previously been differentially machined to apply the slope intrinsically) had to be changed. For this the sutures in the knee were released and the knee reopened. The appropriate tibial insert was selected and changed in the procedure described previously in this chapter. The knee was then meticulously reclosed in layers as described earlier in this chapter.

Misalignment Protocol Order

The final misalignments protocol used for each of the specimens was:

- Native / normal knee
- Navigated knee – zero rotational misalignment, zero posterior slope
- 10º internal rotation misalignment only
- 20º internal rotation misalignment only
- 10º external rotation misalignment only
- 20º external rotation misalignment only
- 3º posterior slope only
- 6º posterior slope only
- 9º posterior slope only
- 20º internal rotation combined with 9º posterior slope
- 20º external rotation combined with 9º posterior slope

Upon completion of the experiments, all trans-osseous pins were removed and the specimens were unclamped from the rig and placed onto the work bench, where an osteotome was used to crack the affixing cement mantles. This allowed all the implants and jigs to be removed intact and undamaged by tapping with a small mallet. The specimens were then appropriately bagged and disposed of as per guidelines issued by Imperial College London in the appropriate facility.

Data Processing

On completion of the experimental protocol for each specimen, a comma spaced value (CSV) data file containing all the movement data and the specimen details was created automatically by the navigation system and saved on the laptop hard disc drive.

The CSV files contained the movement data in 6 degrees of freedom for the three flexion / extension cycles for all the loading conditions for the native knee and all the subsequent TKR component augmentations. This data file was first processed using a series of software algorithms that averaged the three movement cycles and then removed the flexion data, leaving only the averaged extension data in 6 degrees of freedom. This processed data was then split into files each encompassing one of the 7 various loading conditions and the 11 component augmentations, generating a total of 77 files per specimen that were saved in separate folders corresponding to the named specimens. The 616 data spreadsheet files were then sorted and compiled into several master spreadsheets that encompassed all the specimen data according to loading cycle and component augmentation.

The specimen data in the master data sets was averaged and 95% confidence intervals of the data calculated. These were used to construct graphs demonstrating the envelope of laxity in the following planes:

- Tibial internal external rotation
- Varus valgus
- AP translation

Neutral path of motion graphs were also constructed that describe the path of motion followed by the tibia when the knee was extended with only the specimen weight and the simulated 400N quadriceps extension force.

Any displacements noted in the subsequent graphs and results were deemed as movement from the datum "navigated" position and represented translation between the bones of the tibia and femur.

Statistical Analysis

A post hoc power calculation using the standard deviations obtained from the results of the 8 specimens used in the experiment demonstrated an 80% power at the 95% power level with translations of 4 mm or angulations of 7º.

Statistical analyses were performed between the data sets using two-way (paired) t-tests to compare the neutral path of motion and the envelope of laxity between the native knee and the different TKR component augmentations. The 95% confidence bands of the difference between the native knee and the different TKR component augmentations were also calculated and plotted so significant differences could be visually demonstrated as well as statistically demonstrated. A statistically significant difference was inferred with a p value of <0.05.

RESULTS

The results section is been divided into 5 categories:

- Intact knee vs. Navigated implanted knee

- Validation of initial data

- Rotational Misalignment only
    - Navigated vs. 10º external rotation
    - Navigated vs. 20º external rotation
    - 10º external rotation vs. 20º external rotation
    - Navigated vs. 10º internal rotation
    - Navigated vs. 20º internal rotation
    - 10º internal rotation vs. 20º internal rotation

- Posterior Slope only
    - Navigated vs. 3º posterior slope
    - Navigated vs. 6º posterior slope
    - 3º posterior slope vs. 6º posterior slope
    - Navigated vs. 9º posterior slope
    - 6º posterior slope vs. 9º posterior slope

- Combined Misalignment
    - Navigated vs. 20º external rotation, 9º posterior slope
    - Navigated vs. 20º internal rotation, 9º posterior slope

(The term "navigated" describes an implant with 0º of posterior slope with the optimum rotational alignment as calculated by the navigation system.)

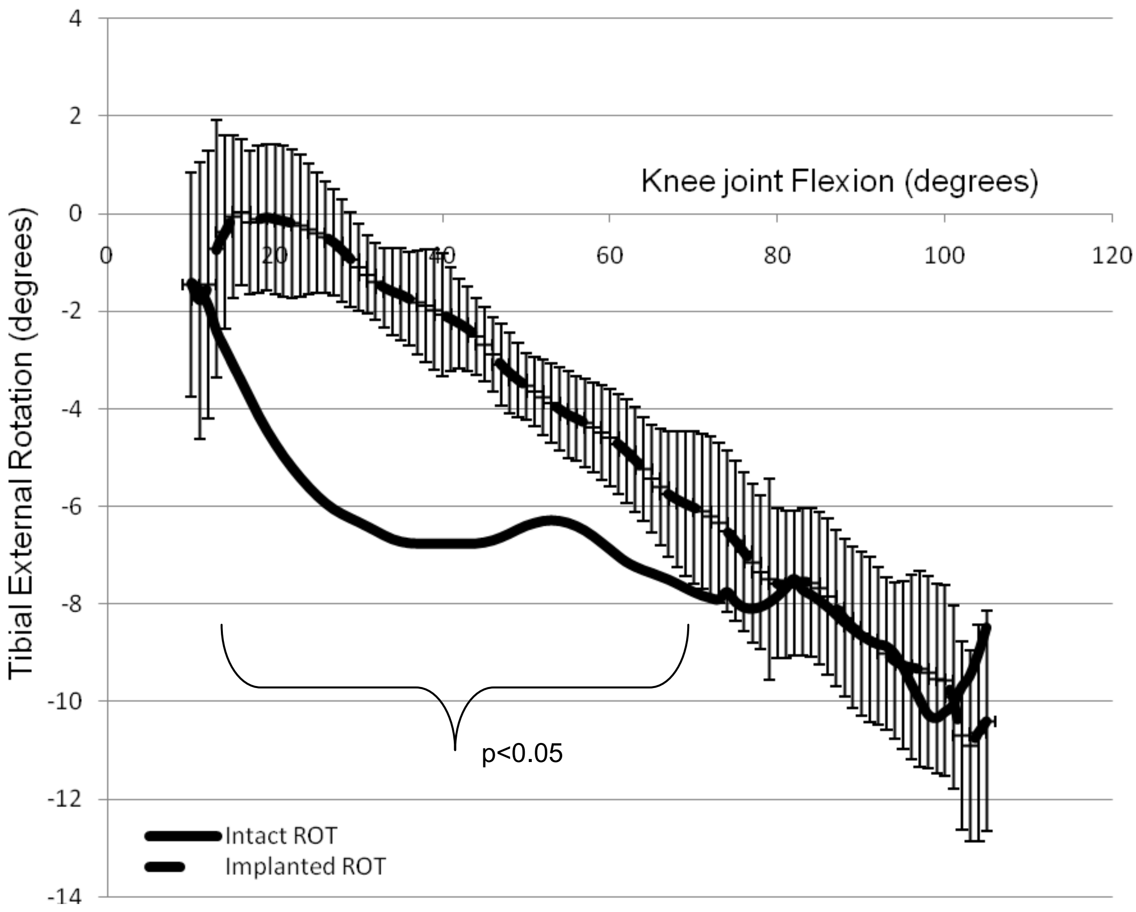

Figure 89: Tibial rotation versus knee joint flexion comparing the neutral rotation pathway between the intact knee and the navigated knee.
[n=8, mean ±95% CI of difference between intact and navigated knees]

Comparison of the mean internal / external rotation pathways of the natural and prosthetic knees (figure 89) demonstrated:

- The screw-home mechanism was abolished by the prosthesis.
- The implant assumed a single axis profile.
- The tibia was in neutral rotation in full extension but rotated into internal rotation as the knee was flexed.
- There was a statistically significant difference of tibial rotation between 15º and 60º of knee flexion ($p<0.05$).

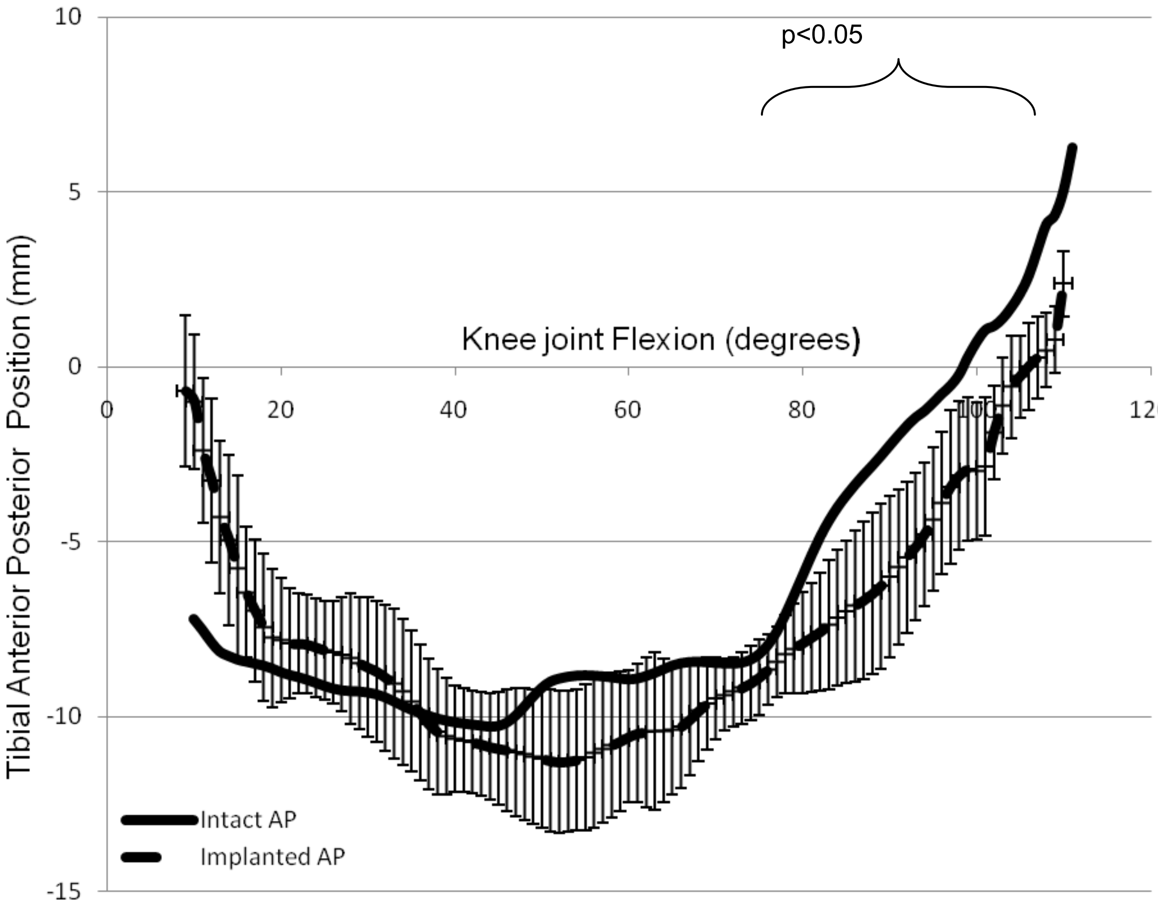

Figure 90: Tibial AP position versus knee joint flexion comparing the neutral AP pathway between the intact knee and the navigated knee.
[n=8, mean ±95% CI of difference between intact and navigated knees]

Comparison of the mean AP neutral pathways of the natural and prosthetic knees (figure 90) demonstrated:

- For both the native and implanted knee, the tibia lay in a slight anterior position in full extension. As the knee was flexed, it moved furthest posteriorly in mid flexion and then stayed in a posterior position as the knee moved into deep flexion.
- The implanted knee was anterior to the native knee in extension but as the knee moved, it adopts a posterior position that was maintained into deep flexion.
- There was a statistically significant difference in the AP position between 80º and 110º of knee flexion ($p<0.05$).

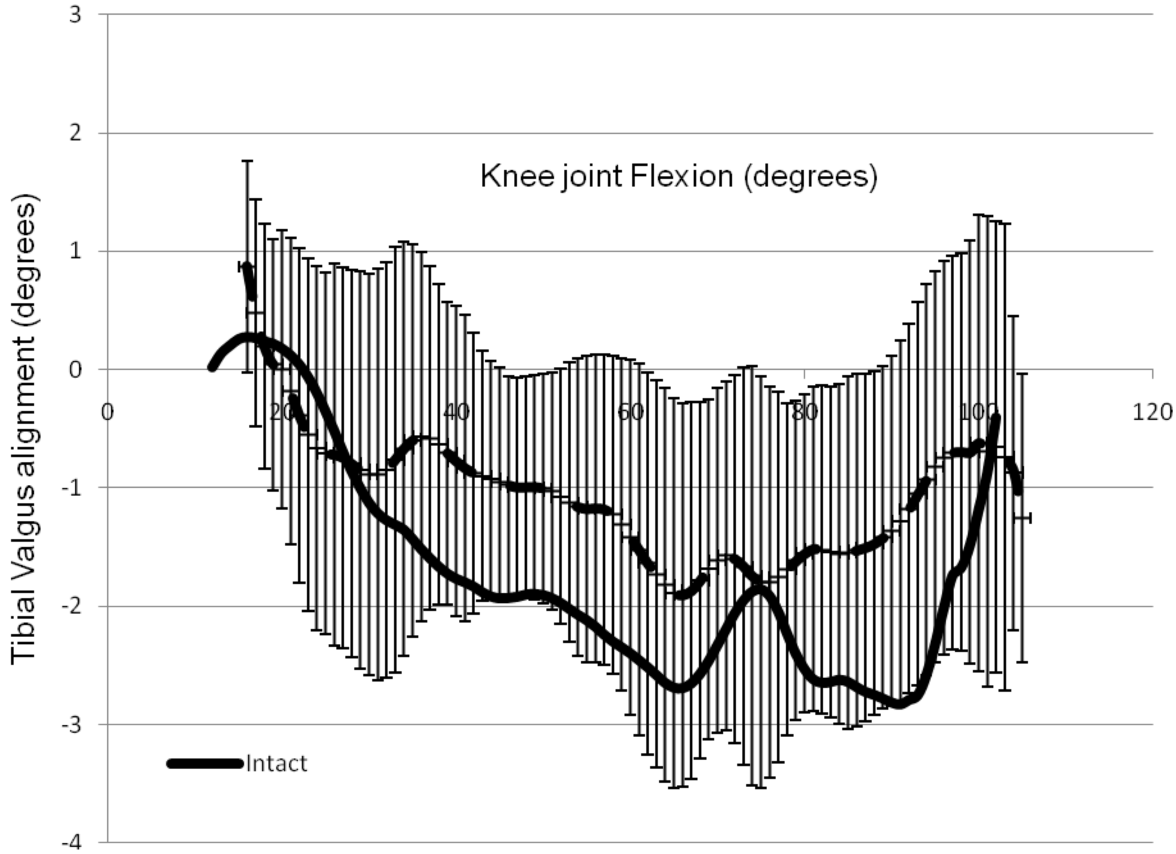

Figure 91: Tibial varus / valgus alignment versus knee joint flexion comparing the neutral varus / valgus pathway between the intact knee and the navigated knee.
[n=8, mean ±95% CI of difference between intact and navigated knees]

Comparison of the mean varus valgus neutral pathways of the natural and prosthetic knees (figure 91) demonstrated:

- In full extension and deep flexion, the implanted knee was in a similar neutral alignment to the native knee.
- As the knee was flexed, both the native knee and the implanted knee moved into varus in mid flexion, with the implanted knee moving less than the native knee.
-

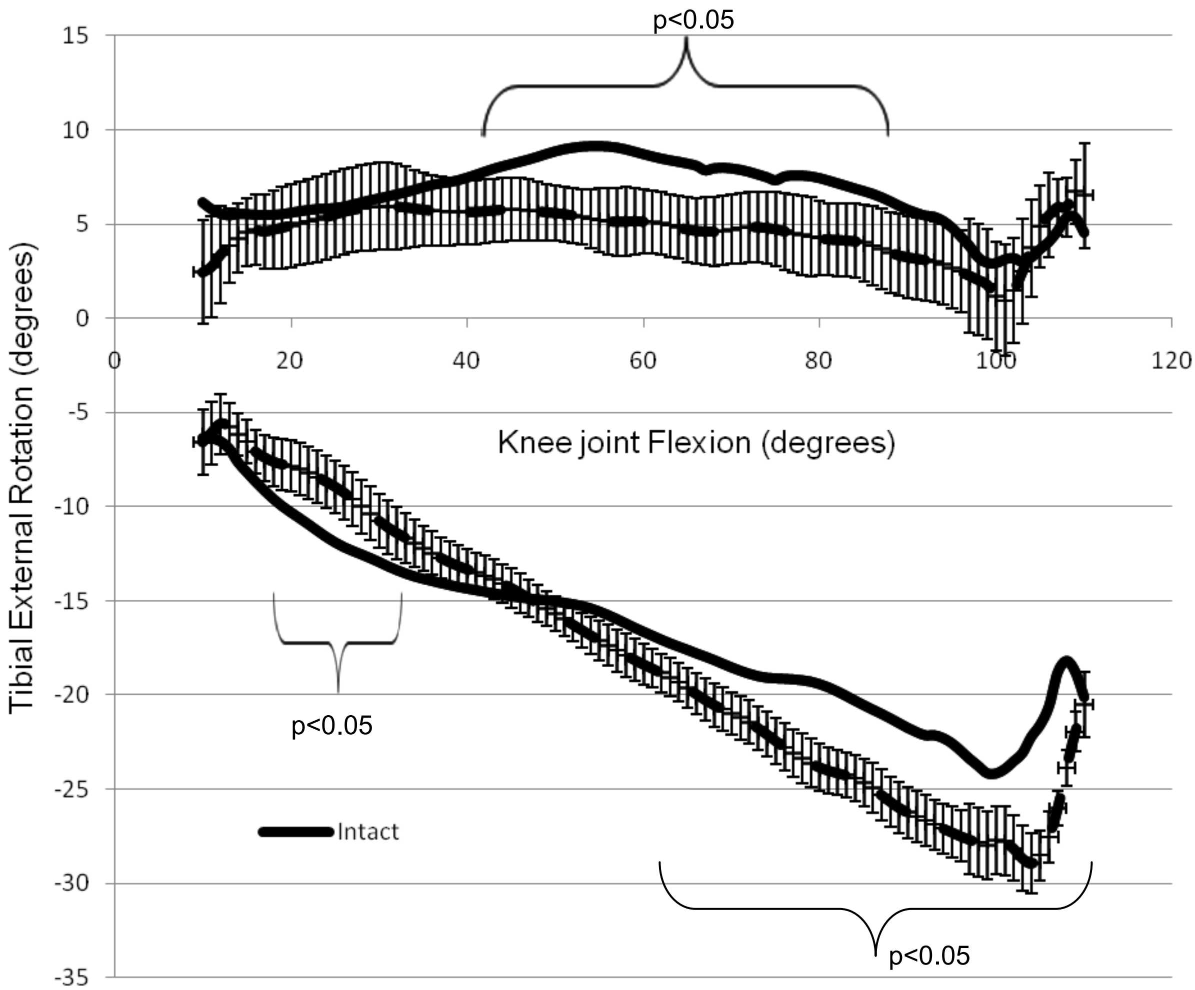

Figure 92: Tibial rotation versus knee joint flexion comparing the rotation envelope of laxity between the intact knee and the navigated knee
[n=8, mean ±95% CI of difference between intact and navigated knees]

Comparison of the mean rotation envelopes of the natural and prosthetic knees (figure 92) demonstrated:

- The screw-home mechanism was abolished by the prosthesis.
- The implant assumed a single axis rotational profile.
- The rotation envelope of the implanted knee allowed significantly greater internal rotation in mid and deep flexion ($p<0.05$).
- There was a statistically significant difference in the external rotation envelopes between 40º and 90º of knee flexion ($p<0.05$) and in the internal rotation envelopes between 20º and 30º of knee flexion & 60º and 110º of knee flexion ($p<0.05$).

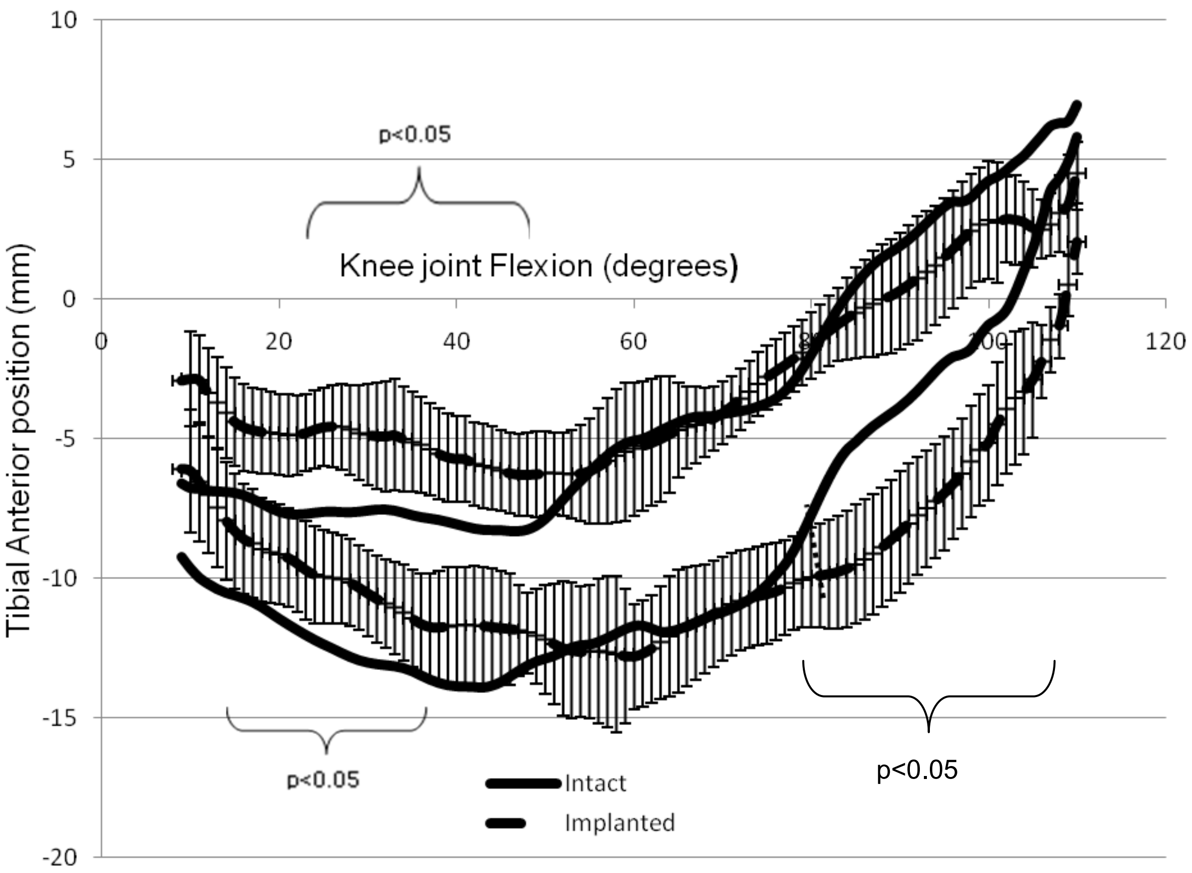

Figure 93: Tibial AP position versus knee joint flexion comparing the AP envelope of laxity between the intact knee and the navigated knee
[n=8, mean ±95% CI of difference between intact and navigated knees]

Comparison of the mean AP envelopes of the natural and prosthetic knees (fig 93) demonstrated:

- There was an anterior translation of the AP envelope of the implanted knee in full extension and early flexion.
- There was a posterior translation of the AP envelope of the implanted knee in deep flexion.
- There was a significant posterior translation in the posterior AP envelope of the implanted knee in deep flexion from 80º to 110º ($p<0.05$).
- There was a statistically significant difference in the anterior and posterior envelopes between 20º and 30º of knee flexion ($p<0.05$).

Figure 94: Tibial varus / valgus alignment versus knee joint flexion comparing the varus / valgus envelope of laxity between the intact knee and the navigated knee.
[n=8, mean ±95% CI of difference between intact and navigated knees]

Comparison of the mean varus / valgus envelopes of the natural and prosthetic knees (figure 94) demonstrated:

- There was no significant difference in the size of the envelopes between the native and implanted knee.
- There was a statistically significant increase in the valgus laxity of the implanted knee in mid and deep flexion compared to the native knee, between 30º and 100º of knee flexion ($p<0.05$).
- There was no significant difference in the varus envelopes between the Implanted and native knee through the full range of flexion

Validation of Results: Intact knee vs. navigated knee

The resultant kinematic graphs of the native and navigated implanted knee demonstrate similar trends to the results of a similar study conducted using the same rig apparatus by *Bull et al* ([28]) from Imperial College London, published in 2008. This similarity in results validates the apparatus, methods, analysis and technique used in this study so far.

Although similar, there are however some subtle differences noted between the results published of *Bull et al* ([28]) and the ones from this study, notably:

- The internal envelope of rotation of the implanted knee in this study started in the neutral position in full extension and early flexion, but translated towards internal rotation in mid and deep flexion by an average of 2º between 60º and 110º of knee flexion ($p<0.05$).

- The external envelope of rotation of the implanted knee started in the neutral position in full extension and early flexion, but similarly moved into an average of 3º of internal rotation (5º max) between 60º and 110º of flexion ($p<0.05$).

- The neutral varus / valgus path of motion and the varus / valgus envelope of laxity of the implanted knee were in neutral in extension, but translated towards valgus beyond the limits of the native knee, as the knee was flexed, average 0.5º (max 1º). The significance of this is questionable as it is just within the recording accuracy of the navigation system.

These minor differences are noted consistently throughout all of the digitised specimens in this study and may be due to a slight variation in the techniques used for the identification of the bony landmarks, digitisation of the specimens and the navigation guided implant positioning and cementing as compared to *Bull et al* ([28]).

Apart from these minor differences, These findings demonstrate that the implanted knee was congruent and balanced throughout the full range of motion with a satisfactory implanted mechanical axis.

Having successfully validated the results obtained from the kinematic analysis of the implanted knee and the intact knee against the published literature ([28]), it is now possible to look at the misalignment kinematic data.

The subsequent figures and explanations will address the component misalignments in the following order:

- Rotational Misalignment only
    - Navigated vs. 10º external rotation
    - Navigated vs. 20º external rotation
    - 10º external rotation vs. 20º external rotation
    - Navigated vs. 10º internal rotation
    - Navigated vs. 20º internal rotation
    - 10º internal rotation vs. 20º internal rotation

- Posterior Slope only
    - Navigated vs. 3º posterior slope
    - Navigated vs. 6º posterior slope
    - 3º posterior slope vs. 6º posterior slope
    - Navigated vs. 9º posterior slope
    - 6º posterior slope vs. 9º posterior slope

- Combined Misalignment
    - Navigated vs. 20º external rotation, 9º posterior slope
    - Navigated vs. 20º internal rotation, 9º posterior slope

The kinematics for all of component positions is examined in the following order:

- Neutral rotation pathway
- Neutral AP pathway
- Neutral varus / valgus pathway
- Rotation envelope of laxity
- AP envelope of laxity
- Varus / valgus envelope of laxity

The term “navigated” describes a tibial tray component implanted with 0º of posterior slope with the optimum rotational alignment as calculated by the navigation system.

All configurations of rotation described in the subsequent graphs were achieved by rotating the navigated tibial tray component around its centre axis in either external or internal rotation as described in the previous methods chapter.

All configurations of posterior slope described in the subsequent graphs were achieved using a standard zero degree insert or custom made sloped polyethylene tibial tray inserts. These inserts were used with the implanted navigated tibial tray component to obtain the required posterior slopes of 0, 3, 6 and 9 degrees, as described in the previous chapter.

Rotational Misalignment only

- Navigated vs. 10º external rotation
- Navigated vs. 20º external rotation
- 10º external rotation vs. 20º external rotation
- Navigated vs. 10º internal rotation
- Navigated vs. 20º internal rotation
- 10º internal rotation vs. 20º internal rotation

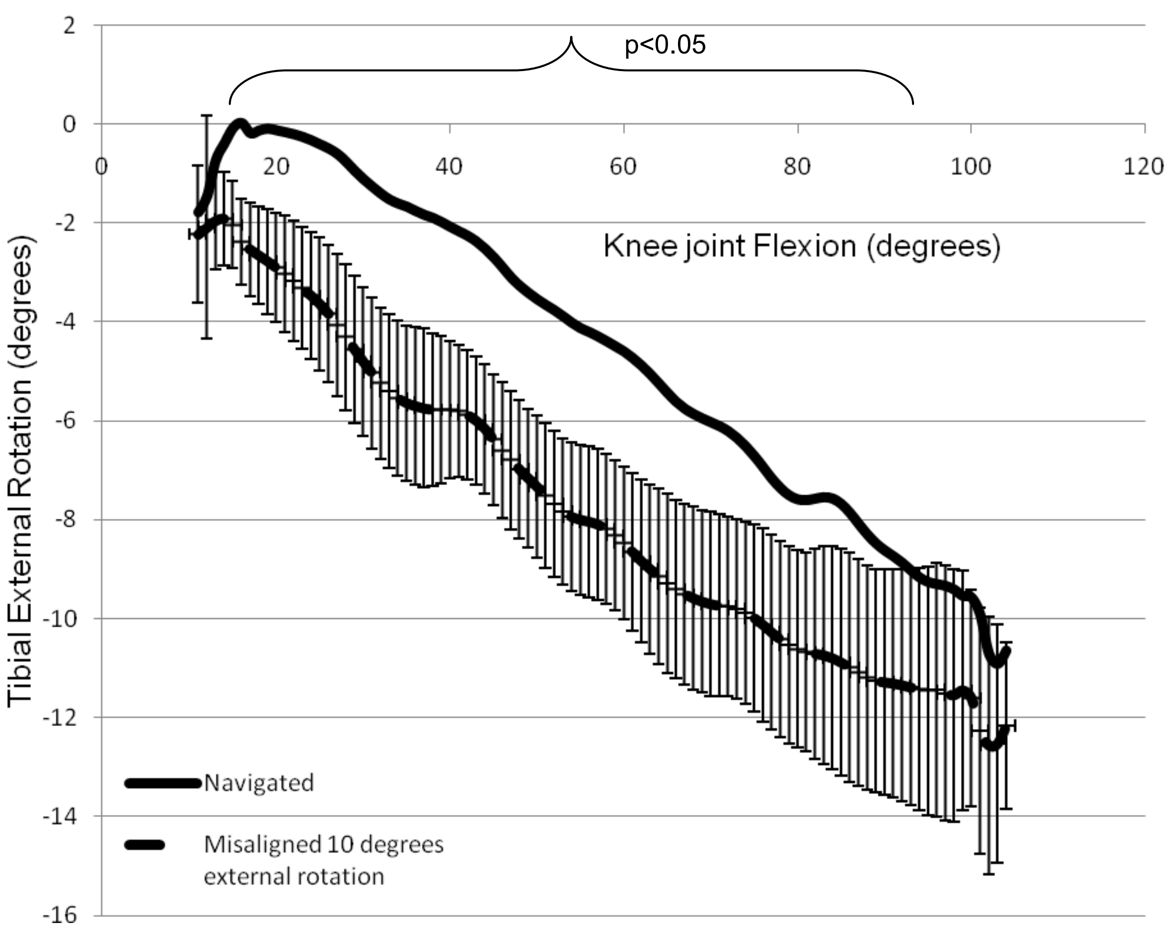

Figure 95: Tibial rotation versus knee joint flexion comparing the neutral rotation pathway between the navigated knee and the misaligned 10° external rotation knee.
[n=8, mean ±95% CI of difference between navigated and misaligned 10° external rotation knees]

Following external rotation of the tibial tray component by 10º (figure 95), there was a statistically significant translation in the neutral rotation pathway of the tibia towards internal rotation by an average of 3º (4º max) throughout the whole range of flexion ($p<0.05$ between 10º and 90º of knee flexion). It is suggested that this internal rotation torque was generated by the femoral condyles as they opposed the incongruent articulation with the dished tibial tray. The remainder of the 6º of expected internal rotation has been overcome by the increasing soft tissue tightness in extension and some presumed component articulation mismatch.

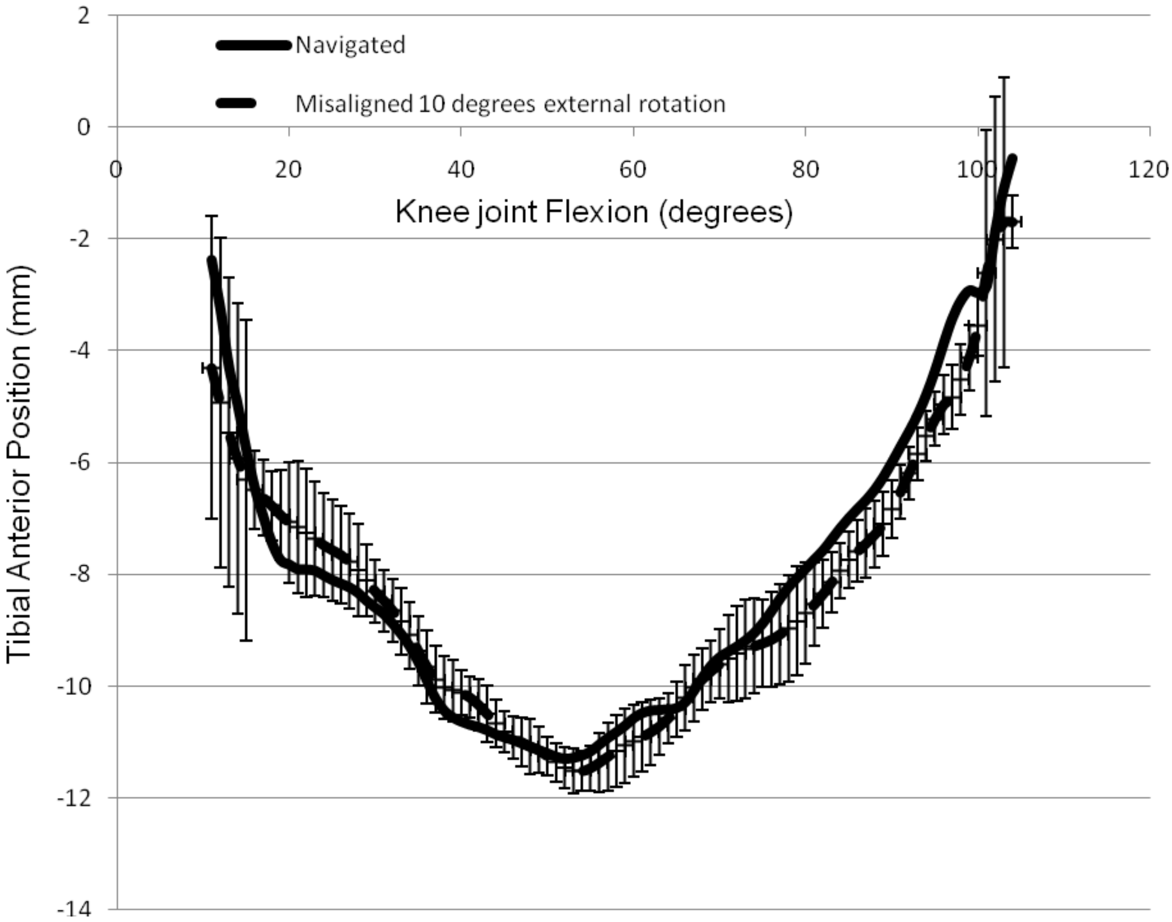

Figure 96: Tibial AP position versus knee joint flexion comparing the neutral AP pathway between the navigated knee and the misaligned 10^{o} external rotation knee.

[n=8, mean ±95% CI of difference between navigated and misaligned 10^{o} external rotation knees]

Following external rotation of the tibial component by 10º (figure 96), there were no significant differences observed in the neutral AP pathway between the navigated and misaligned knee.

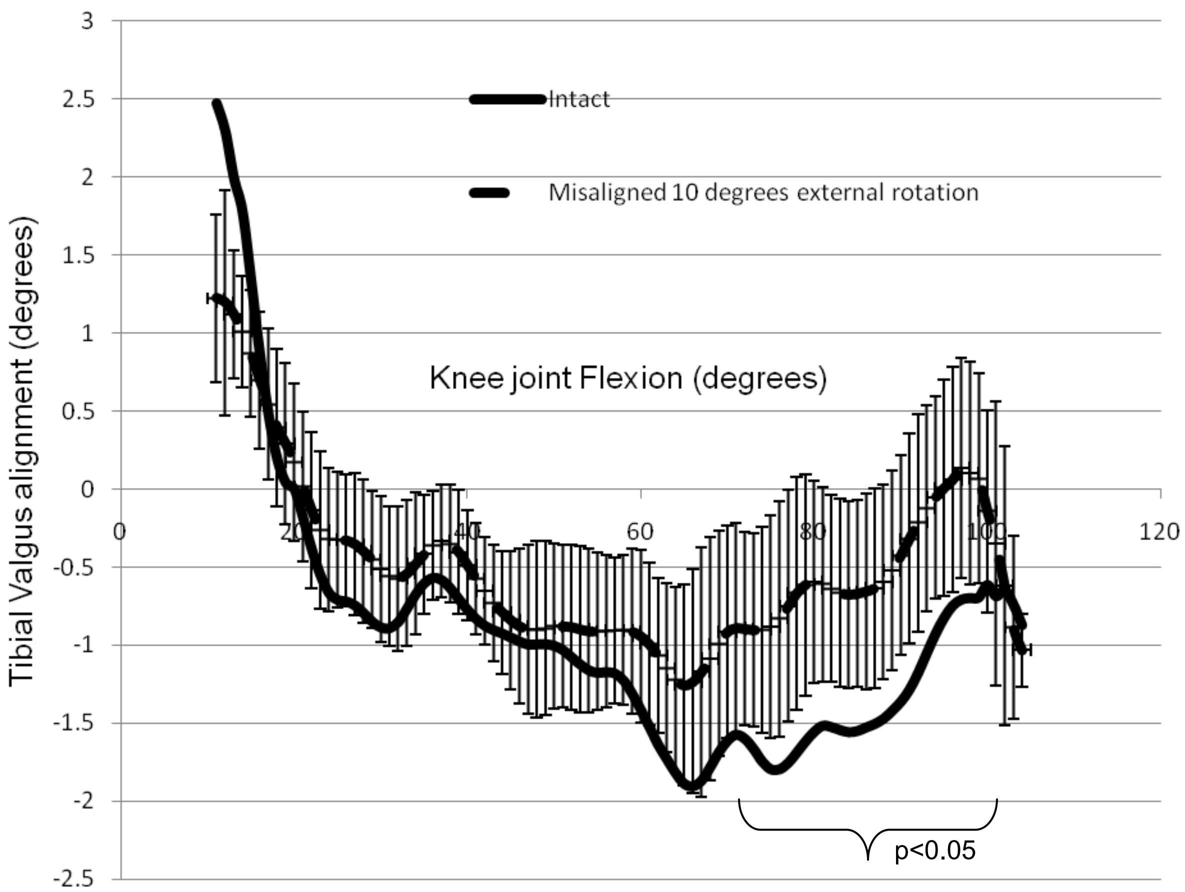

Figure 97: Tibial varus / valgus alignment versus knee joint flexion comparing the neutral varus / valgus pathway between the navigated knee and the misaligned 10º external rotation knee.
[n=8, mean ±95% CI of difference between navigated and misaligned 10º external rotation knees]

Following external rotation of the component by 10º (figure 97), there was an average 1º translation towards valgus. This was statistically significant between 70º and 100º of knee flexion ($p<0.05$). It is suggested that this change may be due to unloading or stretching of the medial compartment that occurs due to the external rotation of the tibial tray, allowing a slight valgus deviation in deep flexion.

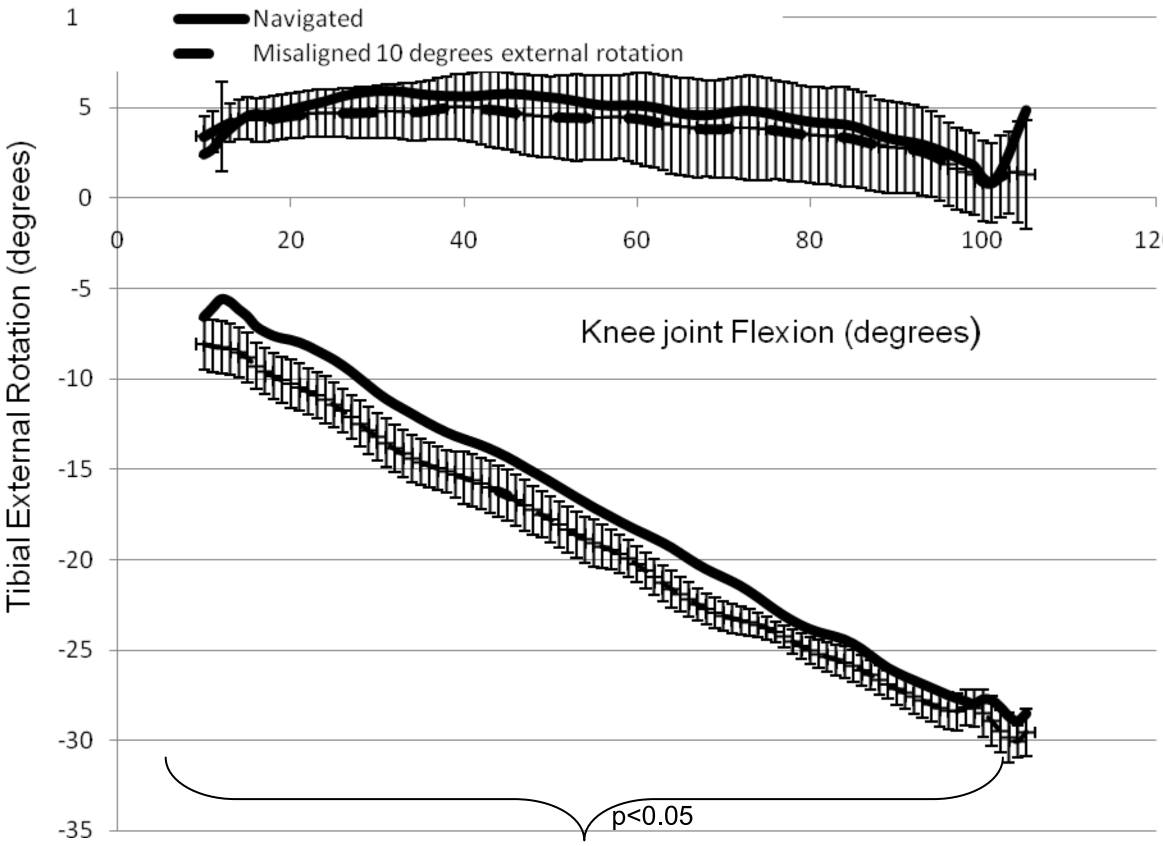

Figure 98: Tibial rotation versus knee joint flexion comparing the rotation envelope of laxity between the navigated knee and the misaligned 10° external rotation knee.

[n=8, mean ±95% CI of difference between navigated and misaligned 10° external rotation knees]

Following 10º of external rotation of the tibial component (figure 98), there was an average 2º translation in the external rotation envelope towards internal rotation, but this change was not statistically significant. There was however, a statistically significant difference in the internal rotation envelope with an average translation of 2º towards internal rotation throughout the whole range of knee flexion ($p<0.05$). It is suggested that despite the 10º of external rotation applied with the misalignment, there is only a 2º tendency towards internal rotation of the tibia. This internal rotation torque provided by the articulation of the femoral condyles against an incongruent tibial tray has been opposed by the soft tissues and some articular conformity compensation.

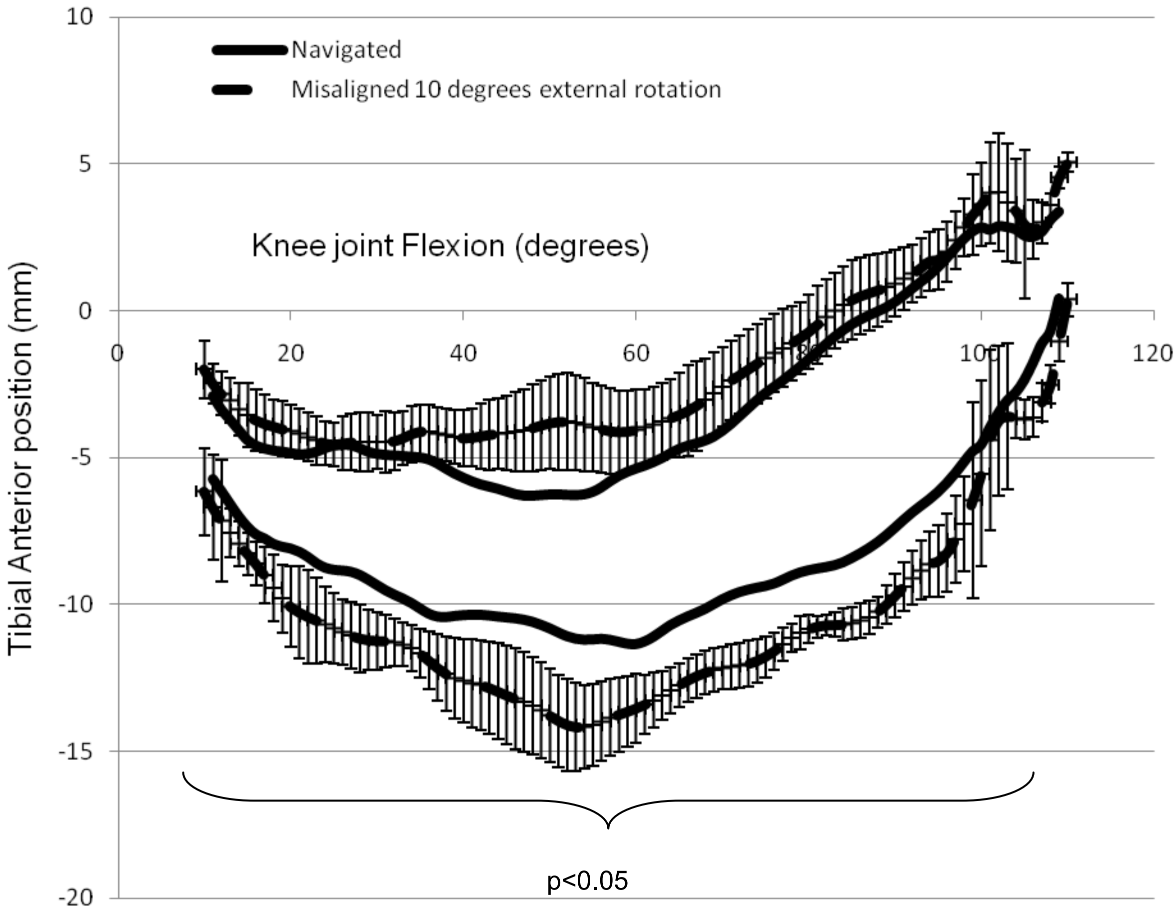

Figure 99: Tibial AP position versus knee flexion comparing the AP envelope of laxity between the navigated knee and the misaligned 10° external rotation knee.

[n=8, mean ±95% CI of difference between navigated and misaligned 10° external rotation knees]

Following 10º of external rotation of the tibial component (figure 99), there was a statistically significant widening of the AP envelope of the knee by an average of 2mm ($p<0.05$), with an average posterior translation of 3mm in the posterior AP envelope throughout the whole range of knee flexion ($p<0.05$). However, the anterior AP envelope was essentially unchanged. It is suggested that the widening of the AP envelope was due to soft tissue stretching or unloading of the anterior soft tissues following the misalignment. There was also a mild posterior thrust generated by the incongruent articulation between the medial femoral condyle and the misaligned tibial tray.

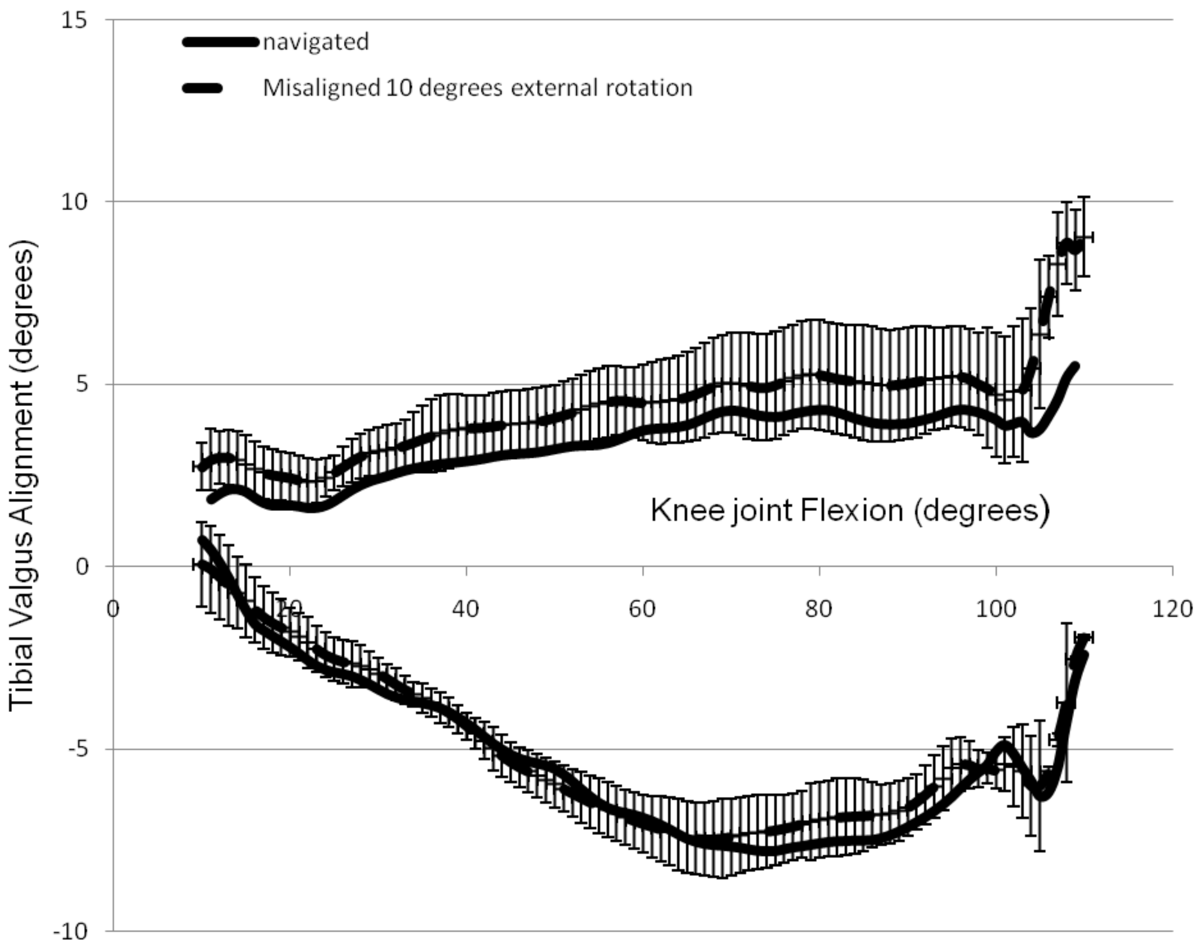

Figure 100: Tibial varus / valgus alignment versus knee joint flexion comparing the varus / valgus envelope of laxity between the navigated knee and the misaligned 10º external rotation knee.

[n=8, mean ±95% CI of difference between intact navigated and misaligned 10º external rotation knees]

Following 10º of external rotation of the tibial component (figure 100), there were no significant differences observed in the varus or valgus envelopes of laxity between the navigated and misaligned knee.

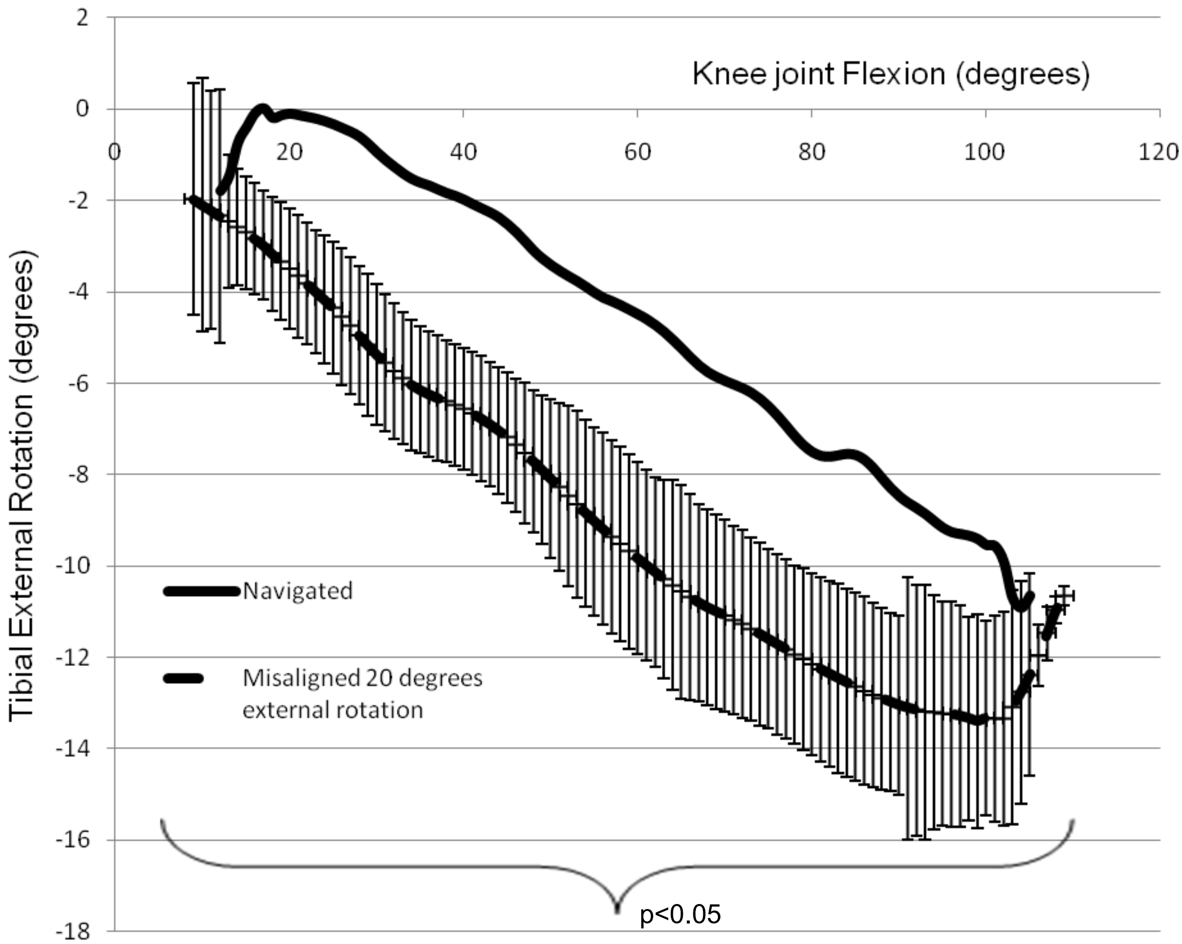

Figure 101: Tibial rotation versus knee joint flexion comparing the neutral rotation pathway between the navigated knee and the misaligned 20^{o} external rotation knee.

[n=8, mean ±95% CI of difference between navigated and misaligned 20^{o} external rotation knees]

Following external rotation of the tibial tray component by 20º (figure 101), there was a statistically significant translation in the neutral rotation pathway towards internal rotation by an average of 5º throughout the whole range of flexion ($p<0.05$). It is suggested that this internal rotation torque was generated by the femoral condyles as they opposed the incongruent articulation with the dished tibial tray. The remainder of the 15º of expected internal rotation has been overcome by the increasing soft tissue tightness in terminal extension, resulting in some presumed component articulation mismatch.

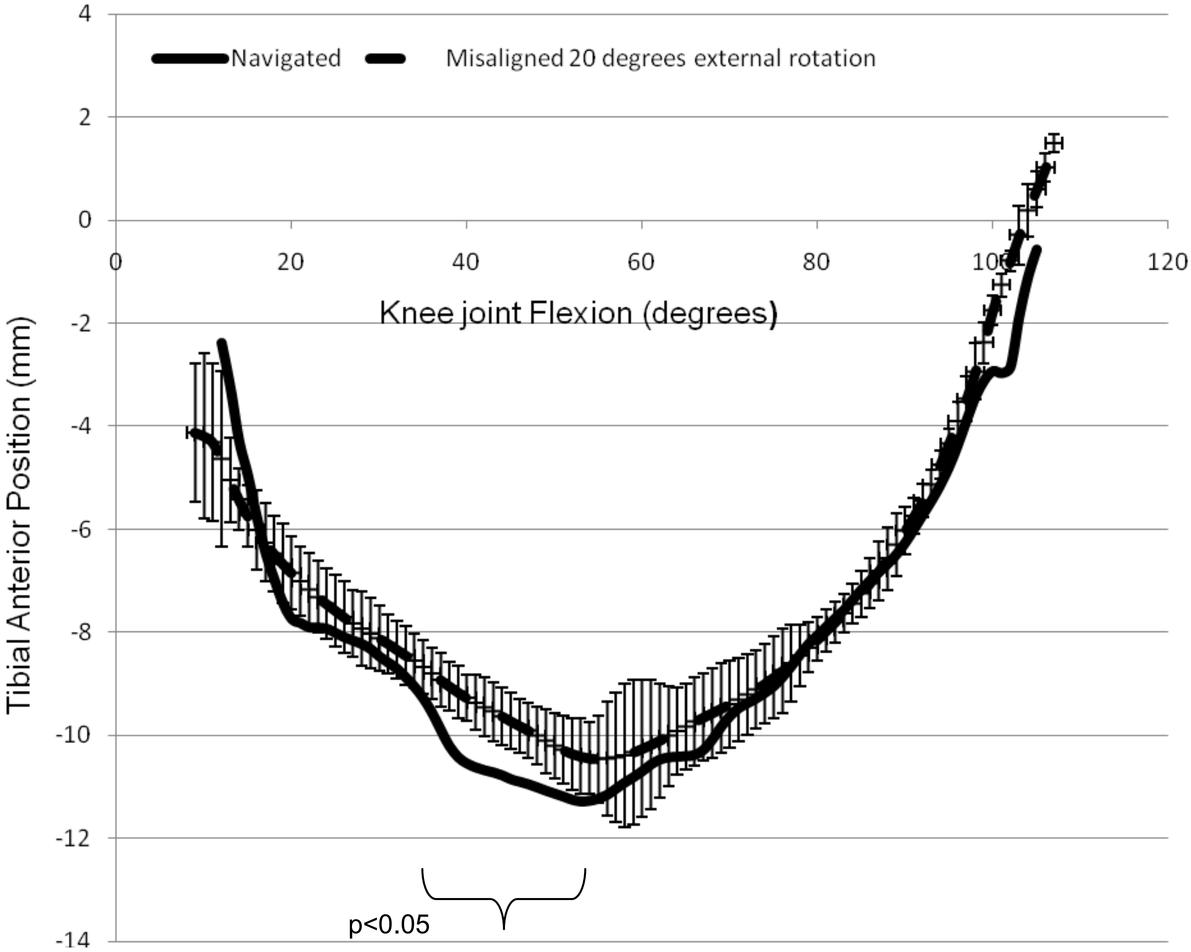

Figure 102: Tibial AP position versus knee joint flexion comparing the neutral AP pathway between the navigated knee and the misaligned 20° external rotation knee.

[n=8, mean ±95% CI of difference between navigated and misaligned 20° external rotation knees]

Following external rotation of the tibial tray component by 20º (figure 102), there was an average 2 mm anterior translation that was significant between 40º and 60º of knee flexion ($p<0.05$). It is suggested, that this anterior translation may be due to the relative anterior translation of the medial side of the tibial insert by the rotation, and component overhang beyond the cut tibial surface, pressing against the soft tissue envelope of the knee. This overhang may alter the tension in the soft tissues resulting in the observed anterior translation in med flexion.

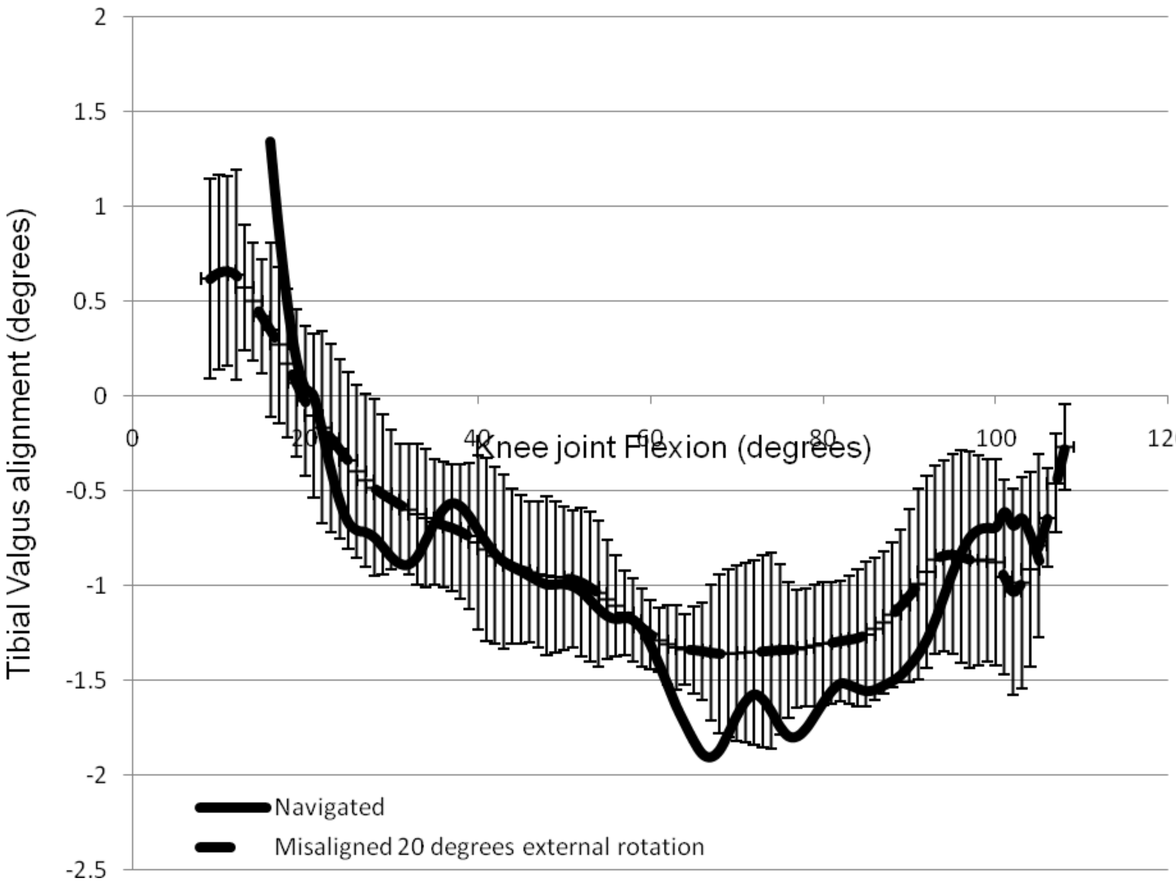

Figure 103: Tibial varus / valgus alignment versus knee joint flexion comparing the neutral varus / valgus pathway between the navigated knee and the misaligned 20^{o} external rotation knee.

[n=8, mean ±95% CI of difference between navigated and misaligned 20^{o} external rotation knees]

Following external rotation of the tibial component by 20º (fig 103), there were no significant differences observed in the neutral varus / valgus pathway between the navigated and misaligned knee.

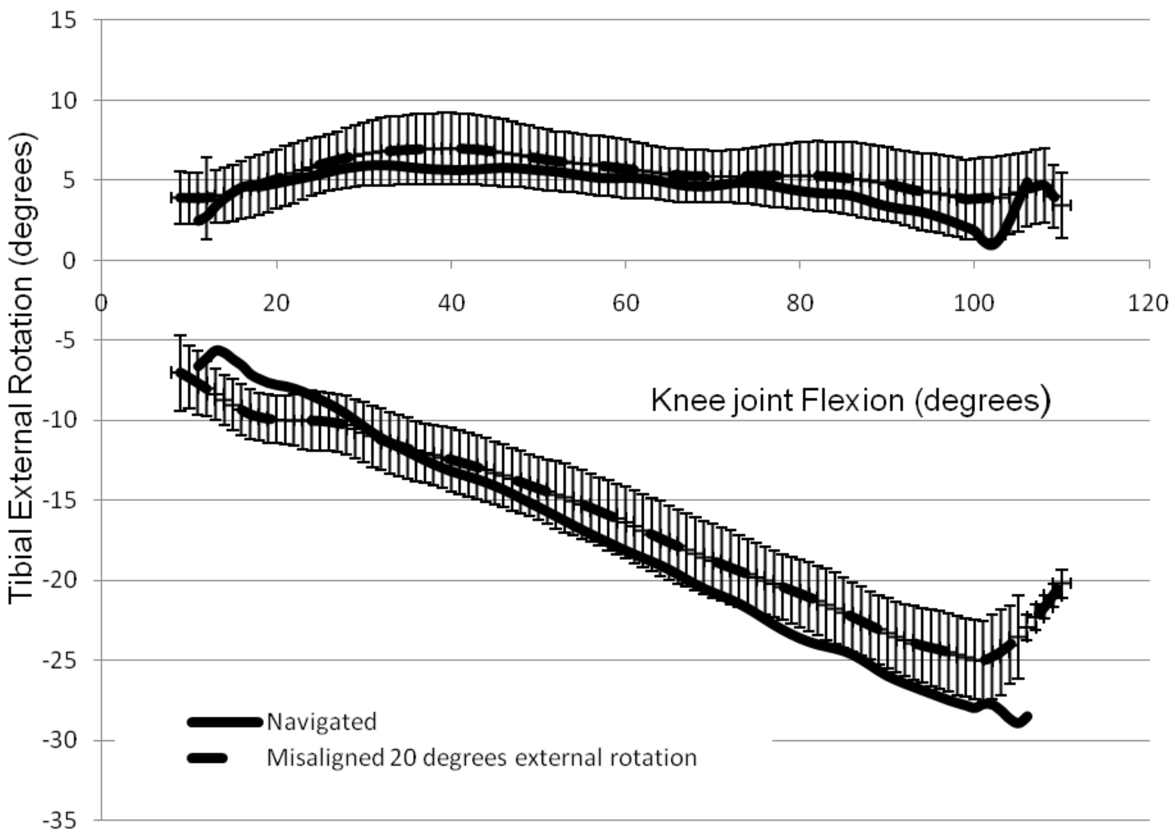

Figure 104: Tibial rotation versus knee joint flexion comparing the rotation envelope of laxity between the navigated knee and the misaligned 20° external rotation knee.

[n=8, mean ±95% CI of difference between navigated and misaligned 20° external rotation knees]

Following 20º of external rotation of the tibial component (figure 104), there was a translation in the whole envelope towards external rotation by an average of 2.5º (4º max), but these findings were not statistically significant. It is suggested that the internal rotation torque was produced by the articulation of the femoral condyles against an incongruent tibial tray, has been opposed by the soft tissues and some articular conformity mismatch compensation.

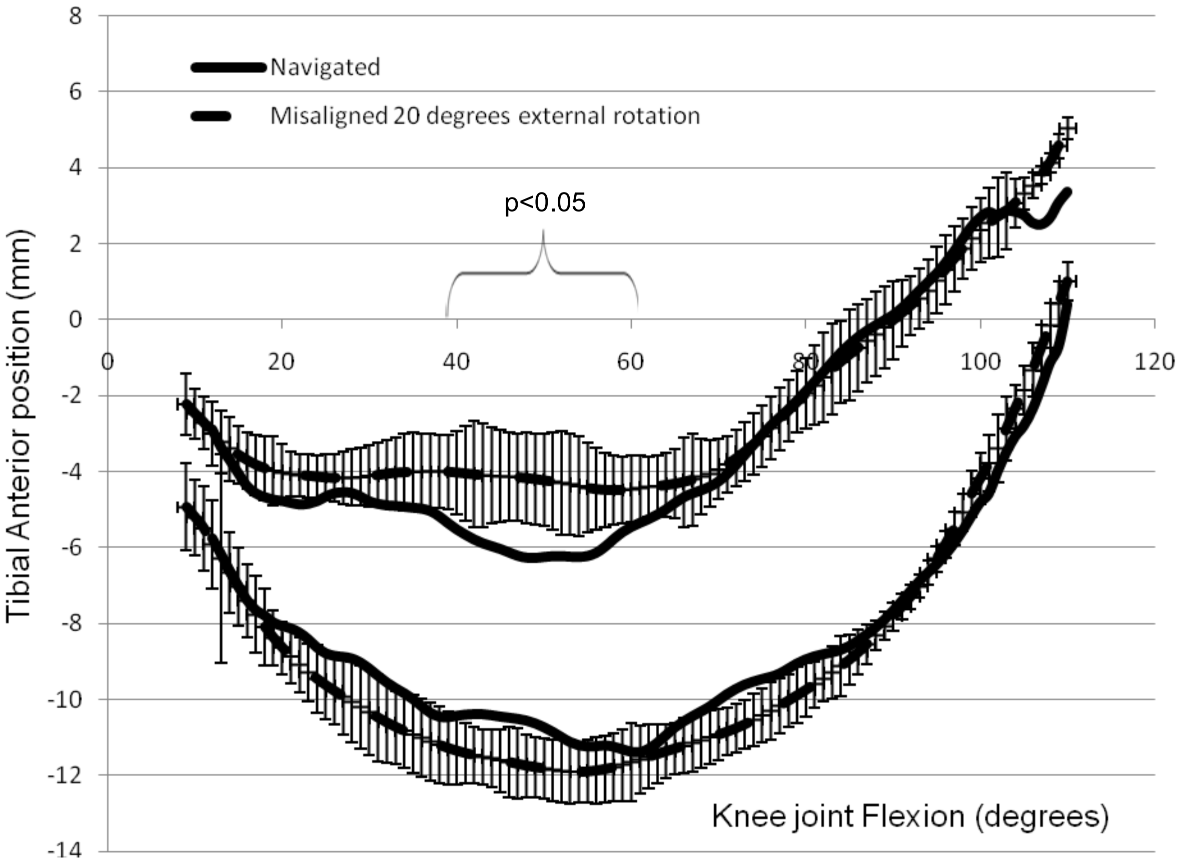

Figure 105: Tibial AP position versus knee joint flexion comparing the AP envelope of laxity between the navigated knee and the misaligned 20° external rotation knee.

[n=8, mean ±95% CI of difference between navigated and misaligned 20° external rotation knees]

Following external rotation of the tibial tray component by 20º (figure 105), there was an average 2 mm anterior translation that was significant in the anterior envelope between 40º and 60º of knee flexion ($p<0.05$). It is suggested, that this anterior translation in the anterior envelope may be due to the relative anterior translation of the medial side of the tibial insert by the rotation, and component overhang beyond the cut tibial surface, pressing against the soft tissue envelope of the knee. This overhang may alter the tension in the soft tissues resulting in the observed anterior translation in med flexion.

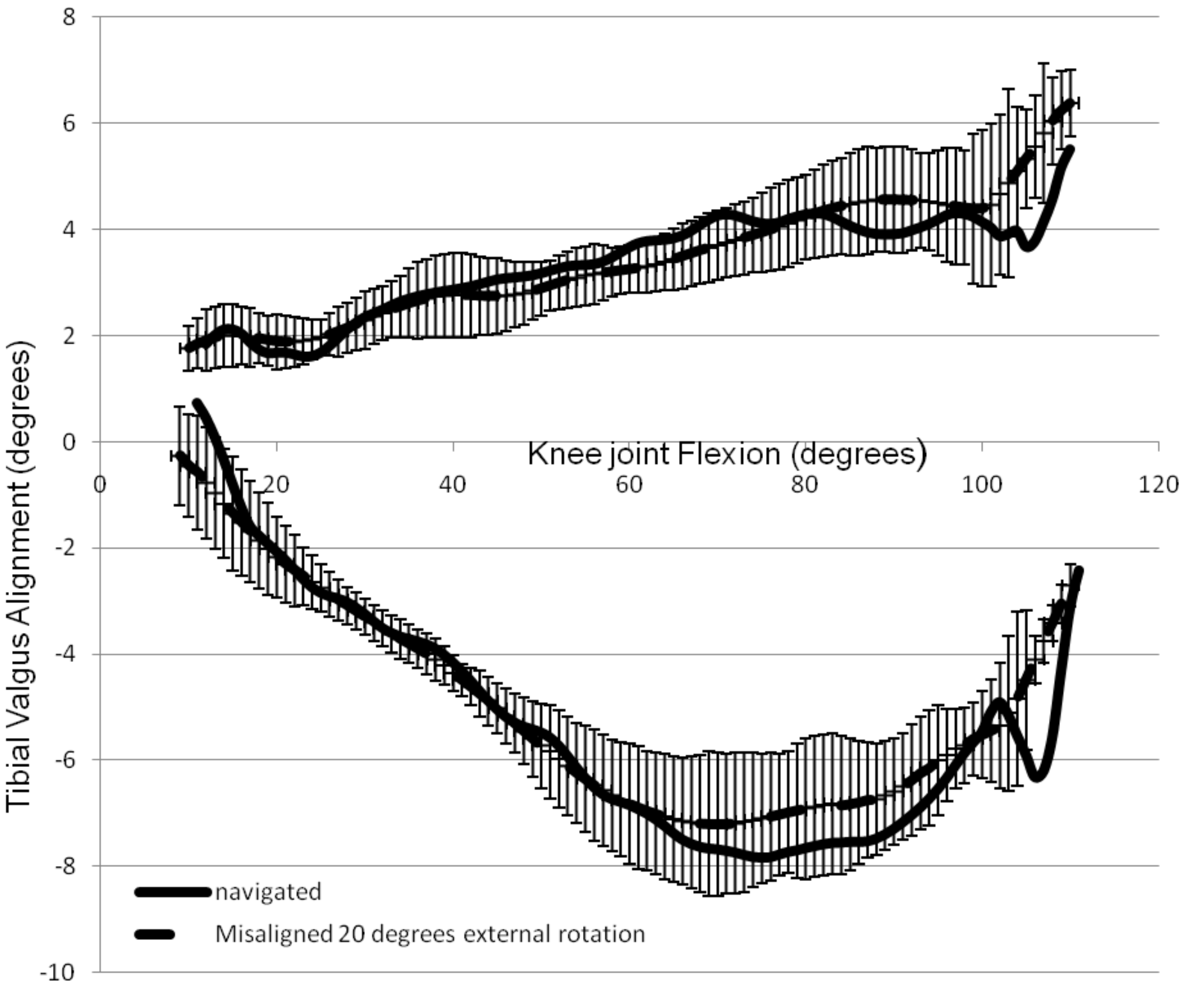

Figure 106: Tibial varus / valgus alignment versus knee joint flexion comparing the varus / valgus envelope of laxity between the navigated knee and the misaligned 20^{o} external rotation knee.

[n=8, mean ±95% CI of difference between navigated and misaligned 20^{o} external rotation knees]

Following 20 º of external rotation of the tibial component (figure 106), there were no significant differences observed in the varus and valgus envelopes between the navigated and misaligned knee.

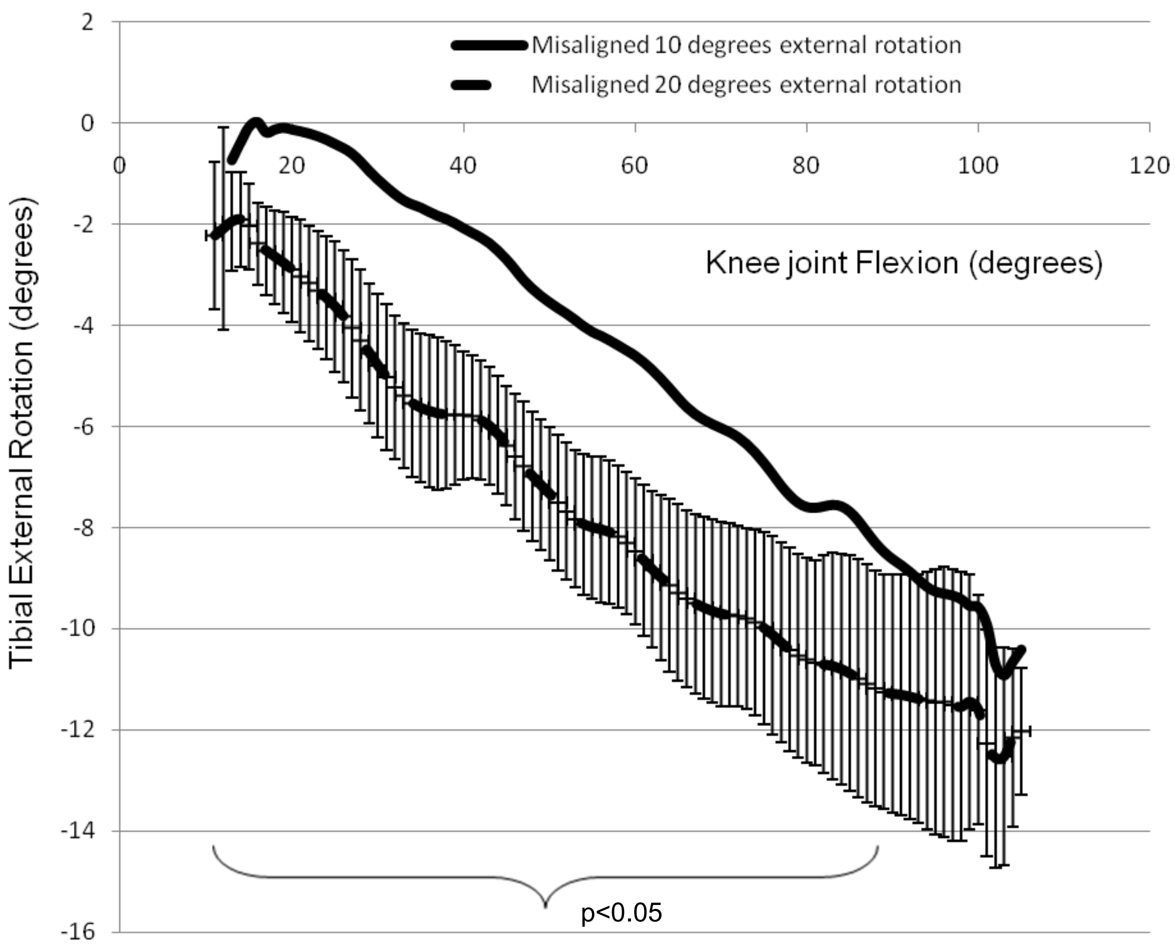

Figure 107: Tibial rotation versus knee joint flexion comparing the neutral rotation pathway between the misaligned 10º external rotation and the 20º external rotation knee.

[n=8, mean ±95% CI of difference between misaligned 10º external rotation and misaligned 20º external rotation knees]

When comparing 10º and 20º of external rotation of the tibial tray component (figure 107), there was a significant average translation of 3º (max 4º) towards internal rotation throughout the full range of movement ($p<0.05$). It is suggested that this further translation towards internal rotation is generated by the femoral condyles as they oppose the incongruent articulation with the dished tibial tray. The remainder of the expected internal rotation has been compensated for by the soft tissues and component articulation.

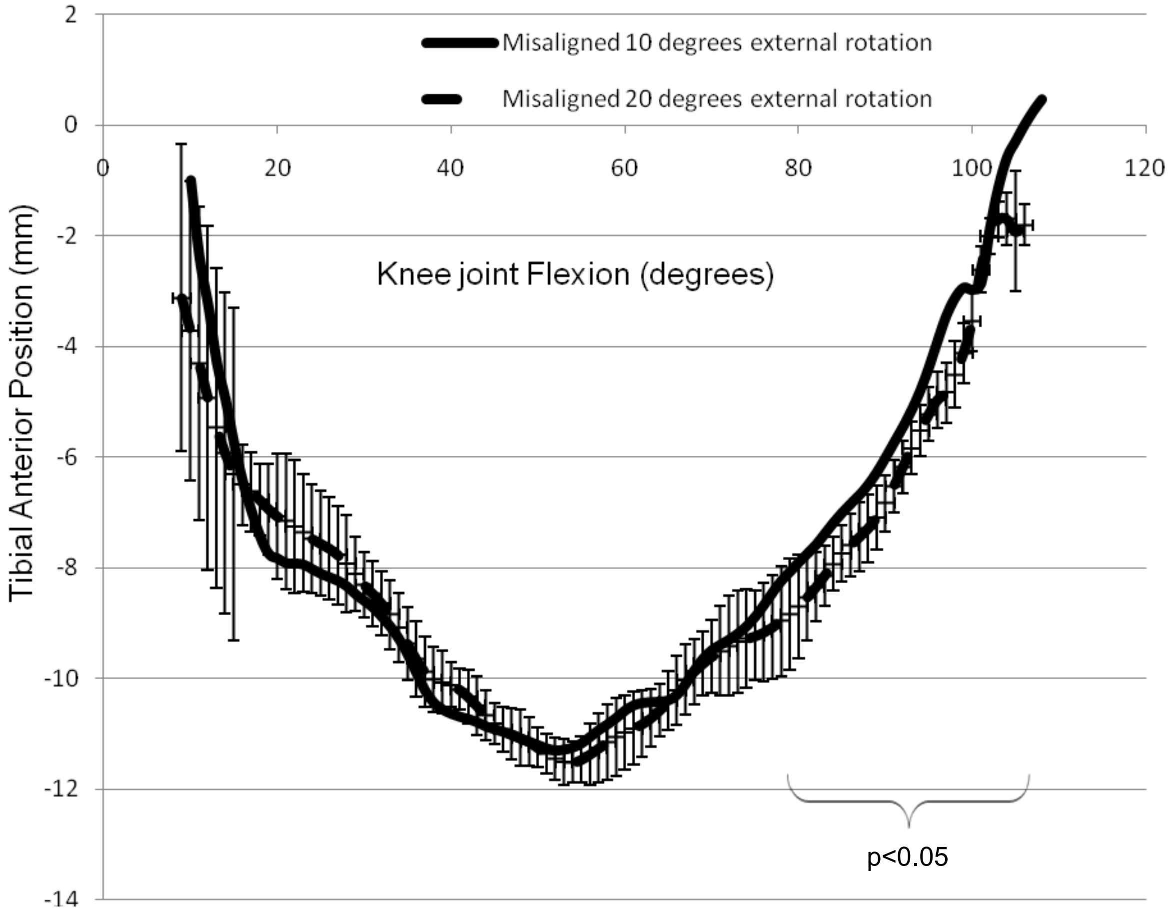

Figure 108: Tibial AP position versus knee joint flexion comparing the neutral AP pathway between the misaligned 10º external rotation and the 20º external rotation knee.
[n=8, mean ±95% CI of difference between misaligned 10º external rotation and misaligned 20º external rotation knees]

When comparing 10º and 20º of external rotation of the tibial tray component (figure 108), there were no significant differences observed in the neutral AP pathway between the misaligned knees.

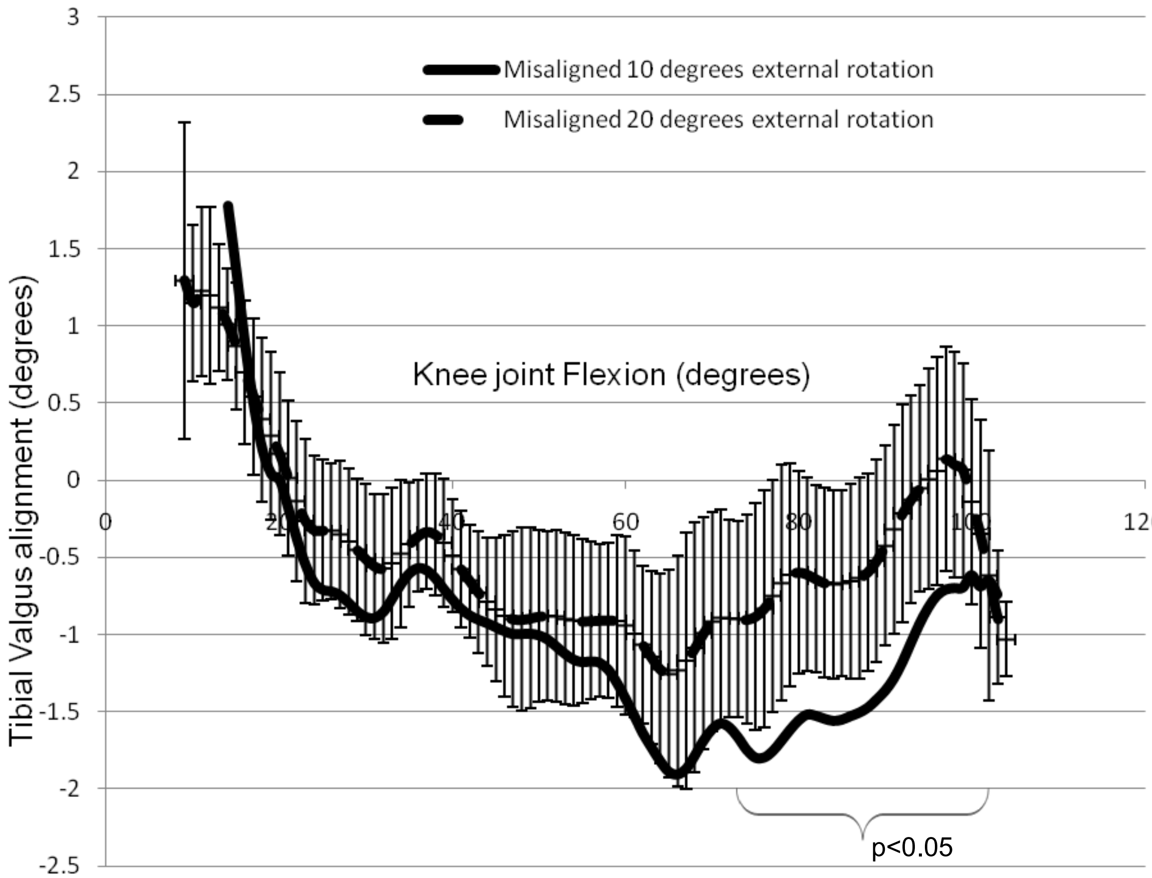

Figure 109: Tibial varus / valgus alignment versus knee joint flexion comparing the neutral varus / valgus pathway between the misaligned 10º external rotation and the 20º external rotation knee. [n=8, mean ±95% CI of difference between misaligned 10º external rotation and misaligned 20º external rotation knees]

When comparing 10º and 20º of external rotation of the tibial tray component (figure 109), there was an average 0.4º translation towards valgus (max 1º) that was statistically significant between 60 and 90º of knee flexion ($p<0.05$).

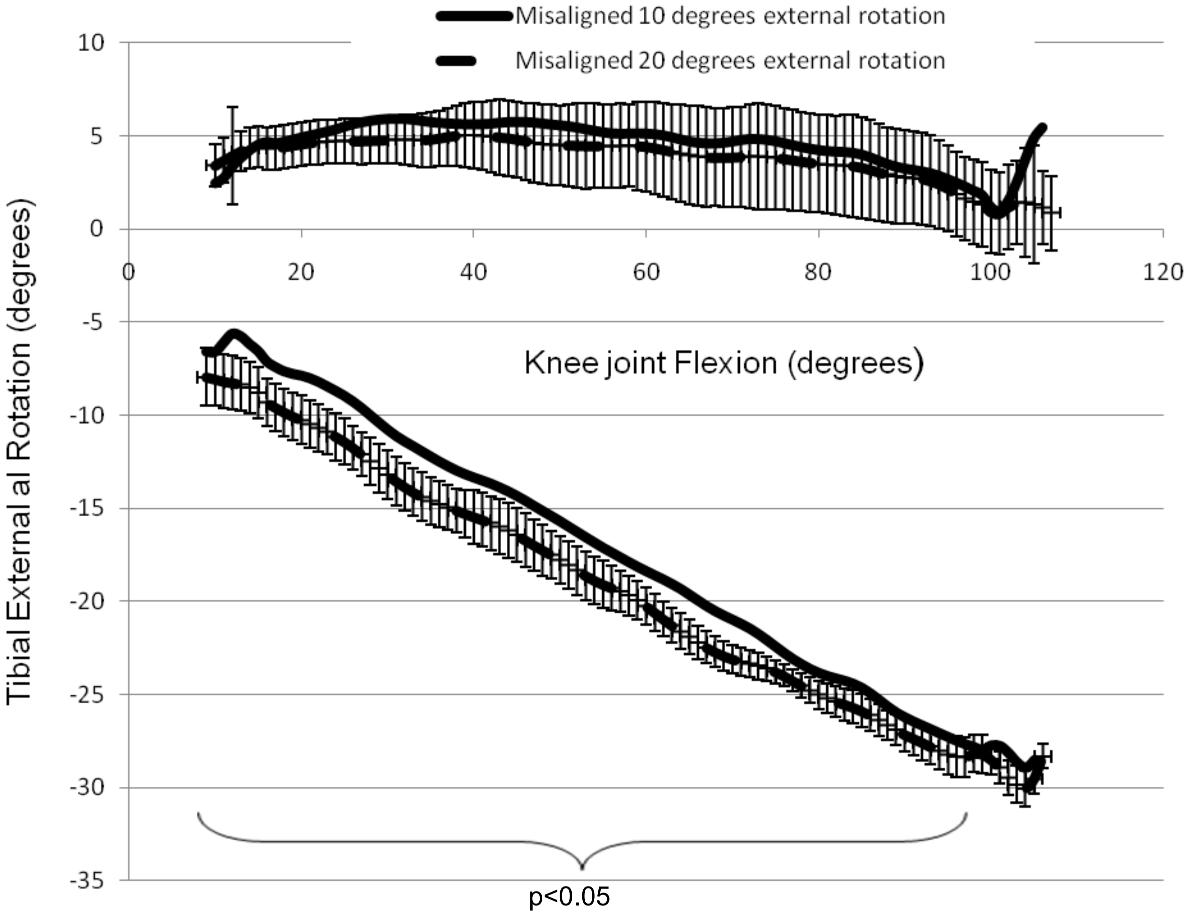

Figure 110: Tibial rotation versus knee joint flexion comparing the rotation envelope of laxity between the misaligned 10º external rotation and the 20º external rotation knee.
[n=8, mean ±95% CI of difference between misaligned 10º external rotation and misaligned 20º external rotation knees]

When comparing 10º and 20º of external rotation of the tibial tray component (figure 110), there was a statistically significant average translation in the envelope of laxity of 2º (3º max) towards internal rotation. In the external rotation envelope, there was an average translation of 1º (max 2º) towards internal rotation, but this translation was not statistically significant. In the internal rotation envelope, there was a statistically significant average translation of 2º (max 3º) towards internal rotation ($p<0.05$). It is suggested that the external rotation torque provided by the articulation of the femoral condyles against an incongruent tibial tray has been opposed by the soft tissues and some articular conformity compensation of the components.

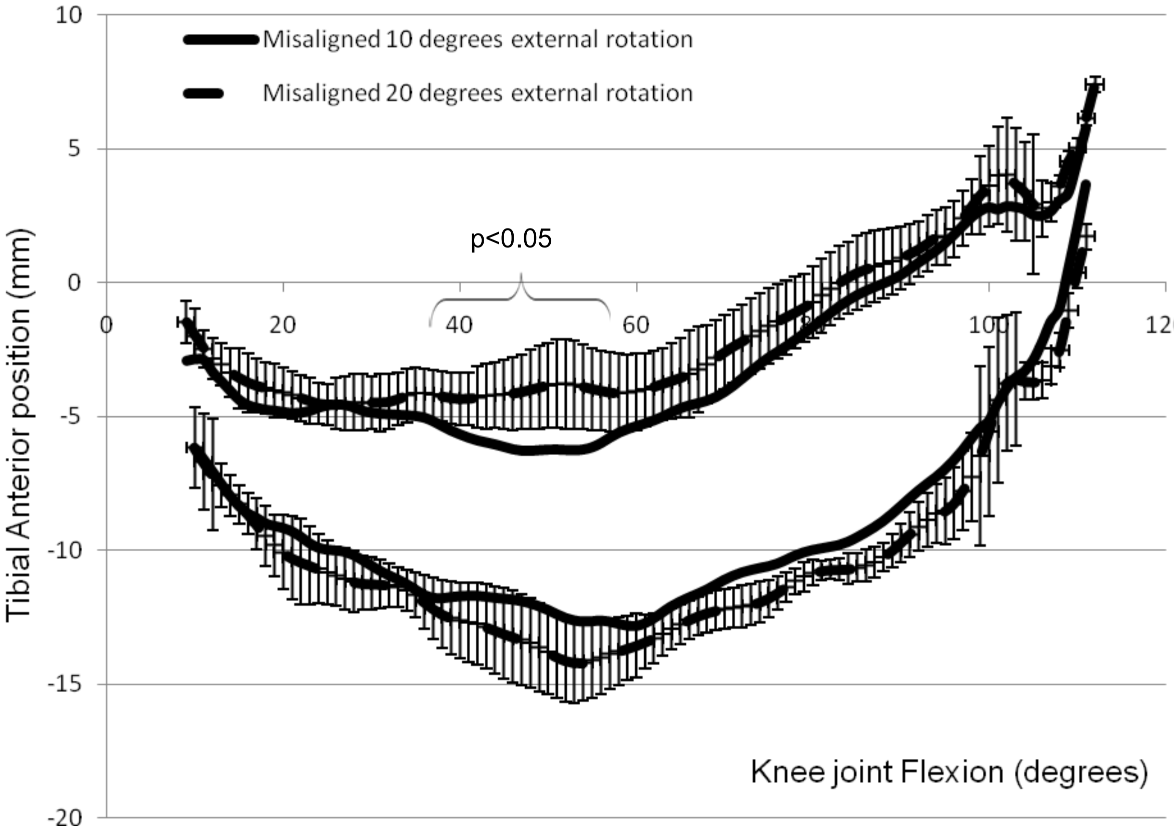

Figure 111: Tibial AP position versus knee joint flexion comparing the AP envelope of laxity between the misaligned 10º external rotation and the 20º external rotation knee.
[n=8, mean ±95% CI of difference between misaligned 10º external rotation and misaligned 20º external rotation knees]

When comparing 10º and 20º of external rotation of the tibial tray component (figure 111), there was an average 2 mm anterior translation that was significant in the anterior envelope between 40º and 60º of knee flexion ($p<0.05$). It is suggested, that this anterior translation in the anterior envelope may be due to the relative anterior translation of the medial side of the tibial insert by the rotation, and component overhang beyond the cut tibial surface, pressing against the soft tissue envelope of the knee. This overhang may alter the tension in the soft tissues resulting in the observed anterior translation in med flexion.

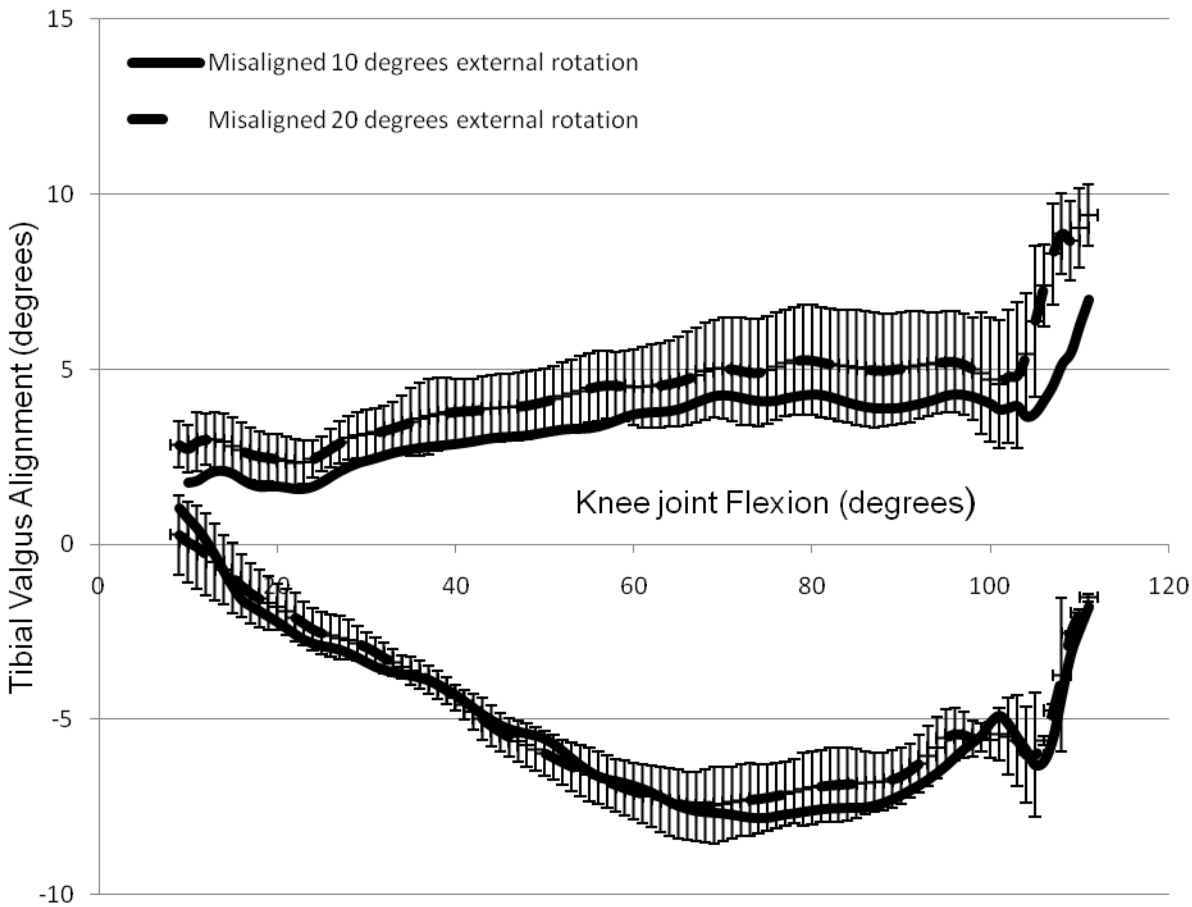

Figure 112**:** Tibial varus / valgus alignment versus knee joint flexion comparing the varus / valgus envelope of laxity between the misaligned 10º external rotation and the 20º external rotation knee.
[n=8, mean ±95% CI of difference between misaligned 10º external rotation and misaligned 20º external rotation knees]

When comparing 10º and 20º of external rotation of the tibial tray component (figure 112), there were no significant differences observed in the varus and valgus envelopes between the misaligned knees.

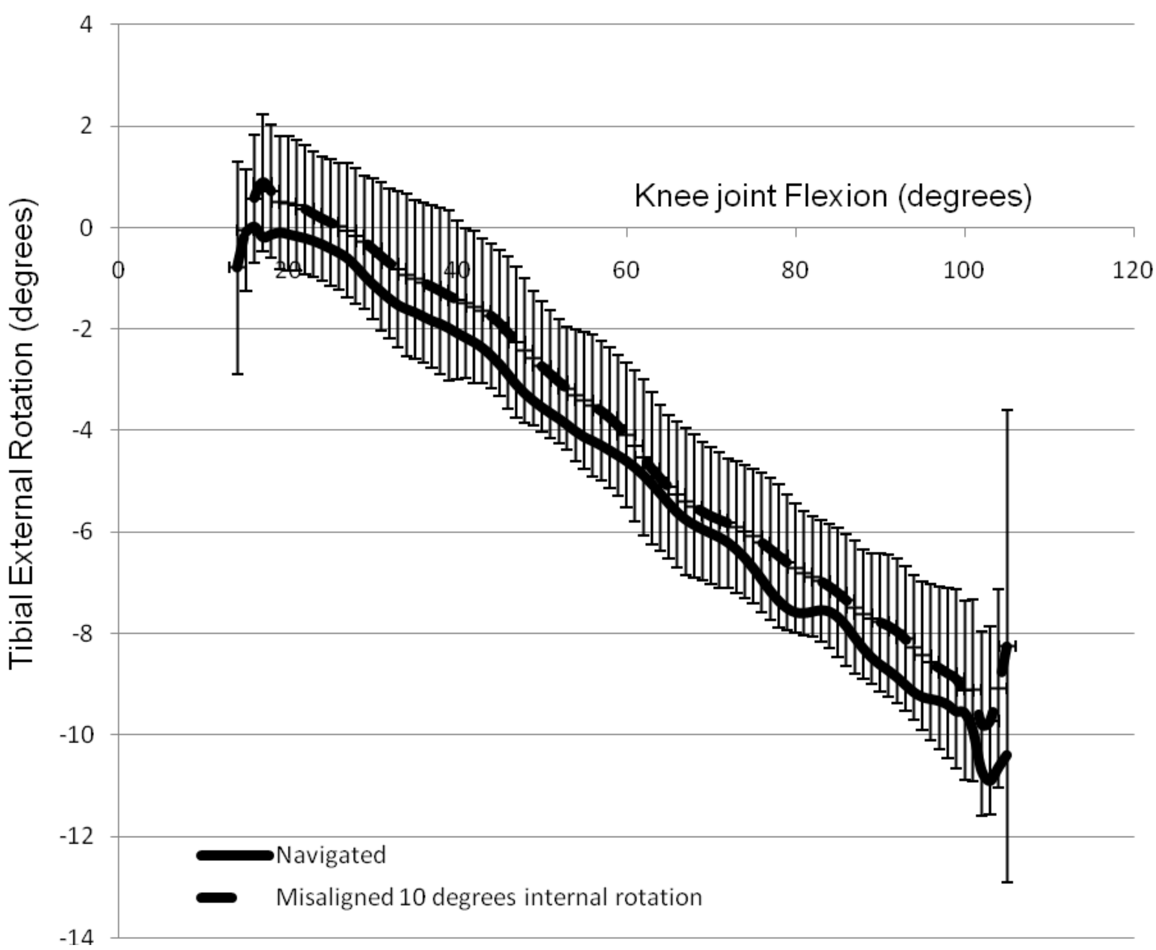

Figure 113: Tibial rotation versus knee joint flexion comparing the neutral rotation pathway between the navigated knee and the misaligned 10° internal rotation knee.

[n=8, mean ±95% CI of difference between navigated and misaligned 10° internal rotation knees]

Following 10° of internal rotation of the tibial component (figure 113), there was an average 1° shift in the neutral path of rotation towards external rotation in the misaligned knee, but this translation was not statistically significant.

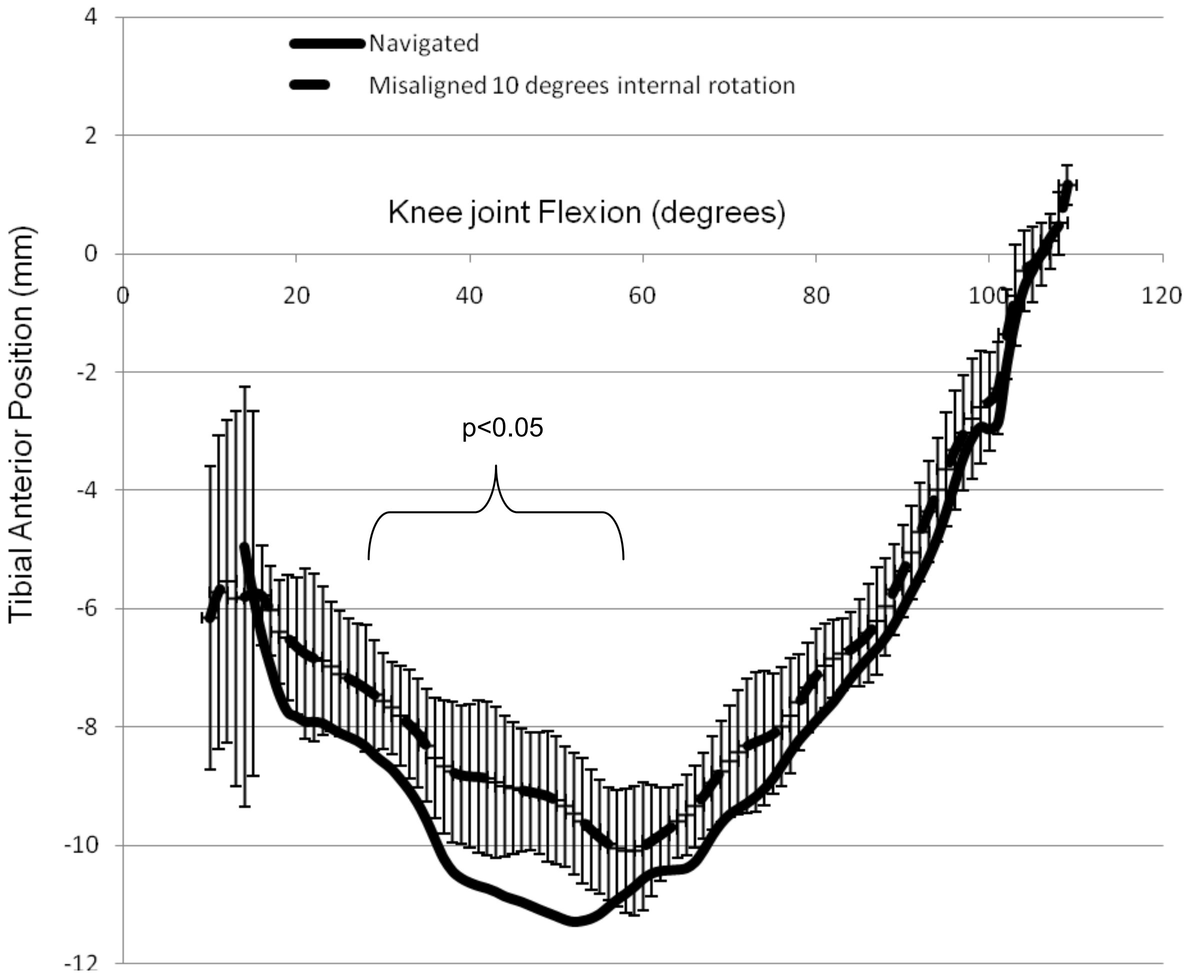

Figure 114: Tibial AP position versus knee joint flexion comparing the neutral AP pathway between the navigated knee and the misaligned 10^{o} internal rotation knee.

[n=8, mean ±95% CI of difference between navigated and misaligned 10^{o} internal rotation knees]

Following internal rotation of the tibial component by 10º (figure 114), there was an average anterior translation in the neutral AP pathway of 2mm (2.5mm max) that was statistically significant between 15º and 100º of knee flexion ($p<0.05$). It is suggested that this anterior translation may be due to the dominant conforming action of the medial femoral condyle in flexion against the incongruent rotated dished tibial insert, resulting in an anterior thrust.

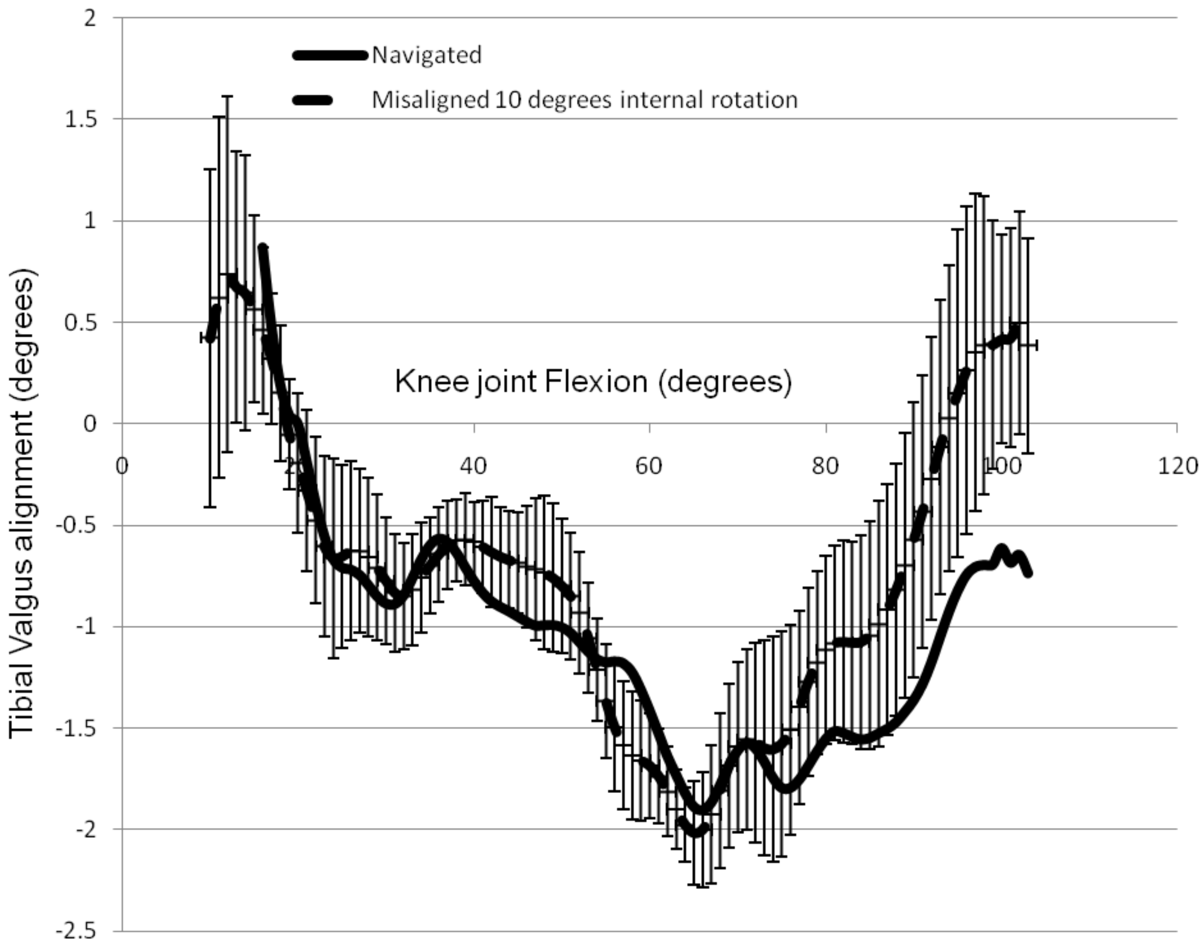

Figure 115: Tibial varus / valgus alignment versus knee joint flexion comparing the neutral varus / valgus pathway between the navigated knee and the misaligned 10º internal rotation knee.
[n=8, mean ±95% CI of difference between navigated and misaligned 10º internal rotation knees]

Following internal rotation of the component by 10º (figure 115), there were no significant differences observed in the neutral varus / valgus path of motion between the navigated and misaligned knees.

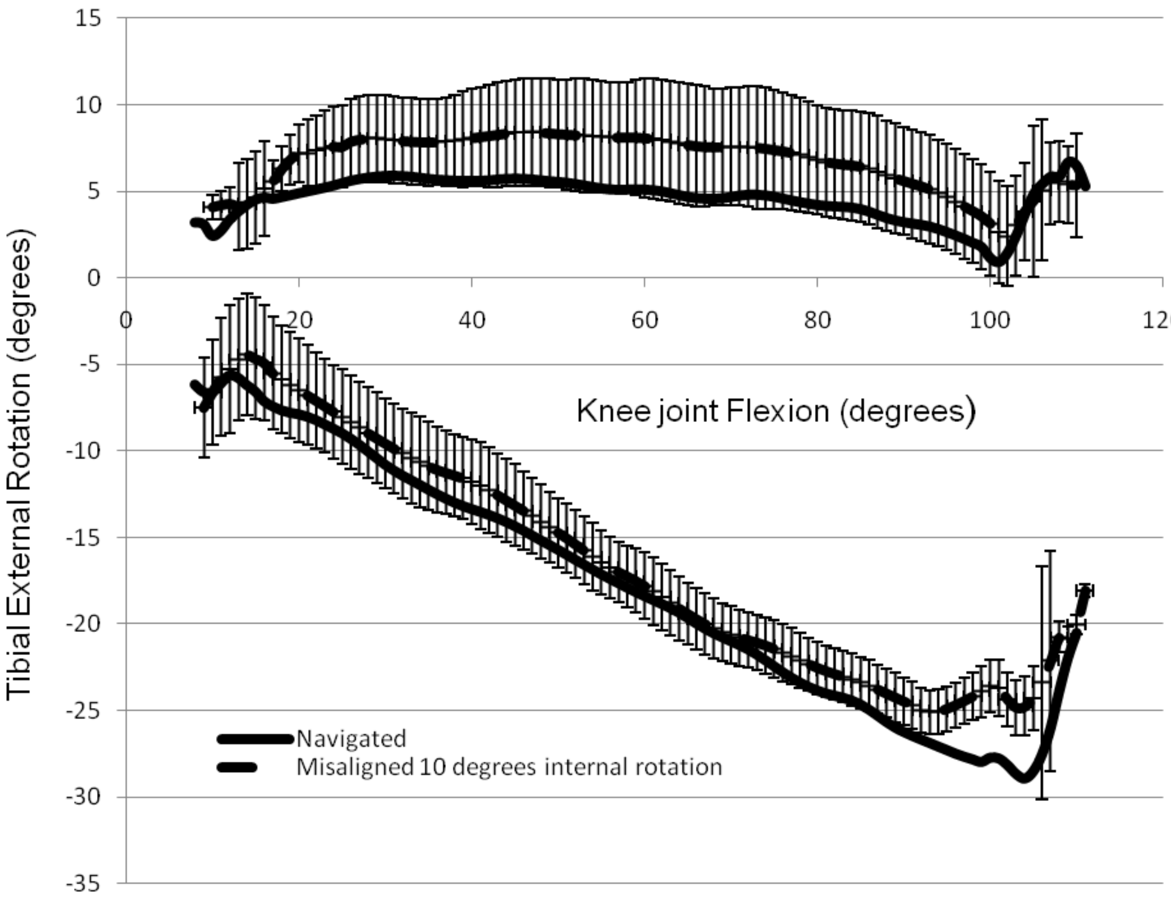

Figure 116: Tibial rotation versus knee joint flexion comparing the rotation envelope of laxity between the navigated knee and the misaligned 10^{o} internal rotation knee.

[n=8, mean ±95% CI of difference between navigated and misaligned 10^{o} internal rotation knees]

Following 10º of internal rotation of the tibial component (figure 116), there was an average 2º translation in the external rotation envelope towards external rotation, but this translation was not statistically significant. There was also a translation in the internal rotation envelope with an average translation of 1º towards internal rotation, but again, this translation was not statistically significant.

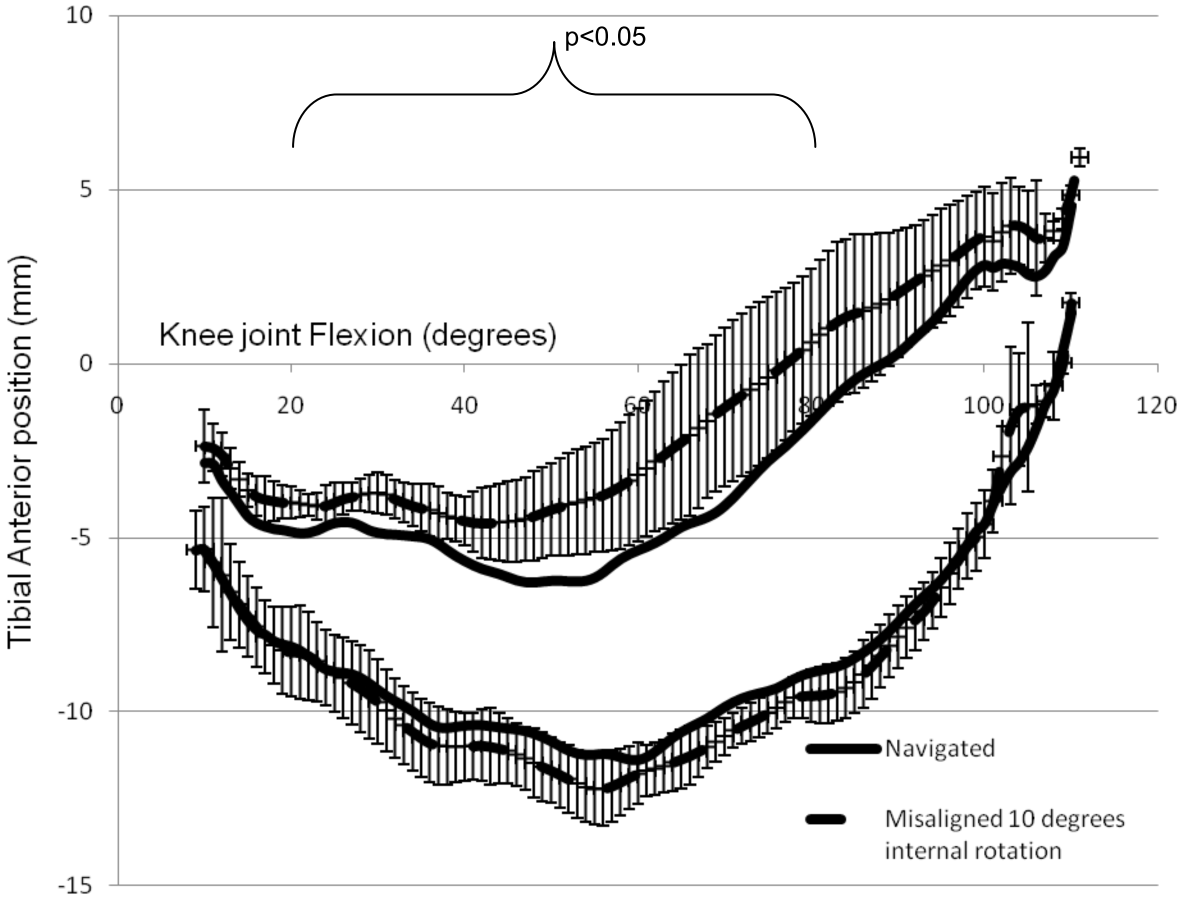

Figure 117: Tibial AP position versus knee joint flexion comparing the AP envelope of laxity between the navigated knee and the misaligned 10° internal rotation knee.

[n=8, mean ±95% CI of difference between navigated and misaligned 10° internal rotation knees]

Following 10º of internal rotation of the tibial component (figure 117), there was a statistically significant widening of the AP envelope of the knee by an average of 2mm ($p<0.05$), with an average anterior translation of 2mm (3mm max) in the anterior AP envelope between 20º and 80º of knee flexion ($p<0.05$). It is suggested that the widening of the AP envelope may be due to soft tissue stretching or unloading of the posterior soft tissues due to the misalignment, with the anterior tibial thrust generated by the incongruent articulation of the medial condyle of the femoral component against the misaligned dished tibial insert.

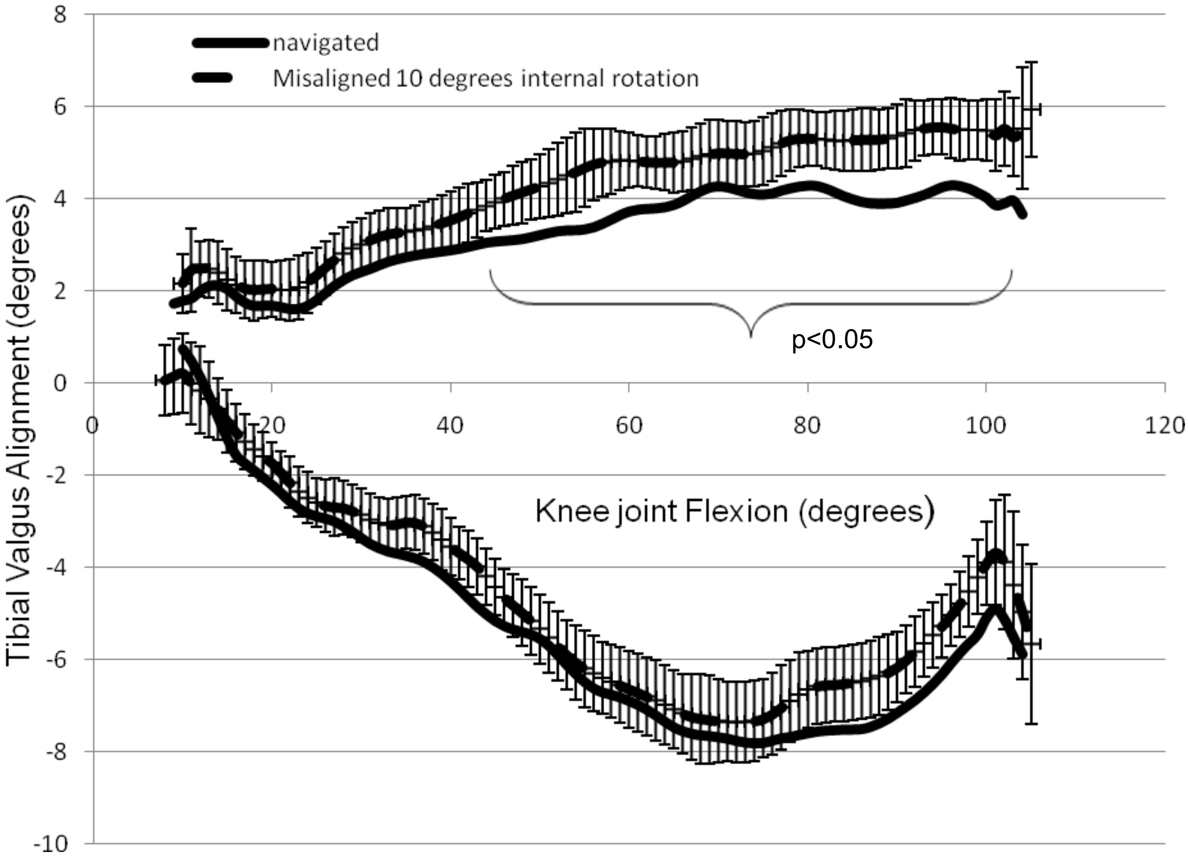

Figure 118: Tibial varus / valgus alignment versus knee joint flexion comparing the varus / valgus envelope of laxity between the navigated knee and the misaligned 10º internal rotation knee. [n=8, mean ±95% CI of difference between navigated and misaligned 10º internal rotation knees]

Following 10º of internal rotation of the tibial component (figure 118), there was an average 1º translation (max 2º) in the envelope of laxity towards valgus. This translation was statistically significant in the valgus envelope ($p<0.05$), but was not statistically significant in the varus envelope. It is suggested that the tibial tray rotation has permitted the minor translation towards valgus by reducing the tension in the soft tissue envelope on the medial side of the knee.

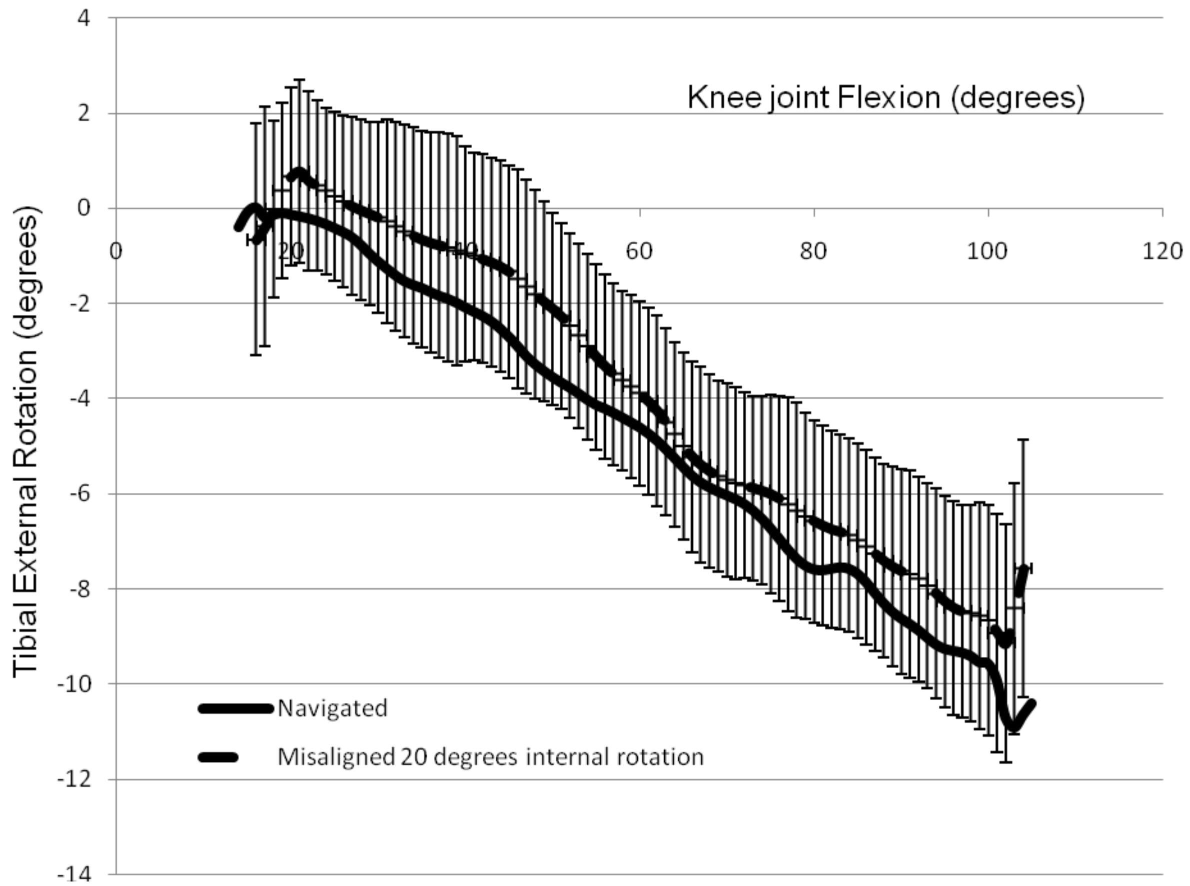

Figure 119: Tibial rotation versus knee joint flexion comparing the neutral rotation pathway between the navigated knee and the misaligned 20º internal rotation knee.

[n=8, mean ±95% CI of difference between navigated and misaligned 20º internal rotation knees]

Following 20º of internal rotation of the tibial component (figure 121), there was an average 1º shift in the neutral path of rotation towards external rotation in the misaligned knee, but this translation was not statistically significant.

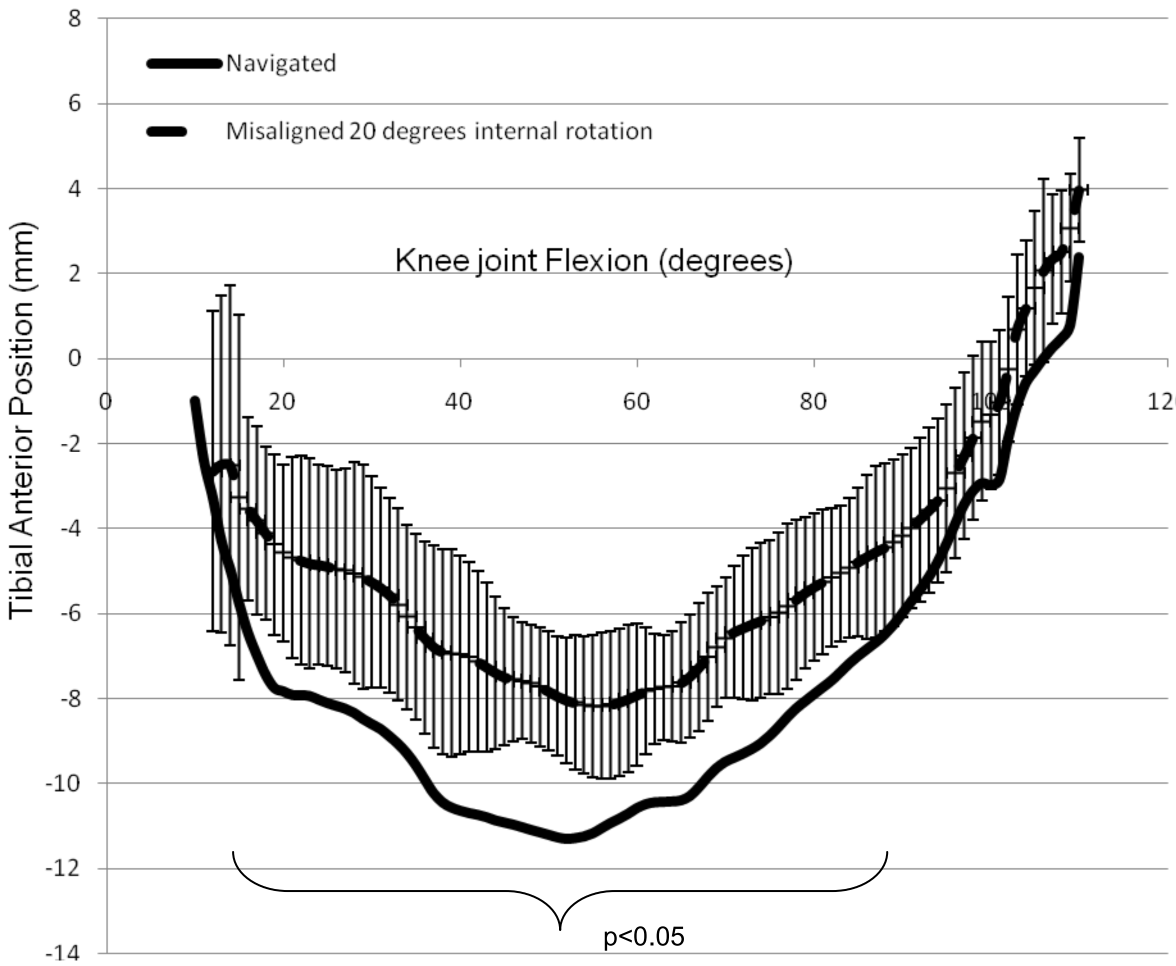

Figure 120: Tibial AP position versus knee joint flexion comparing the neutral AP pathway between the navigated knee and the misaligned 20° internal rotation knee.

[n=8, mean ±95% CI of difference between navigated and misaligned 20° internal rotation knees]

Following internal rotation of the tibial component by 20º (figure 120), there was an average anterior translation in the neutral AP pathway of 2mm (3mm max) that was statistically significant between 15º and 90º of knee flexion ($p<0.05$). It is suggested that this anterior translation is due to a thrust generated by the conforming action of the dominant medial femoral condyle against the incongruent rotated dished tibial insert.

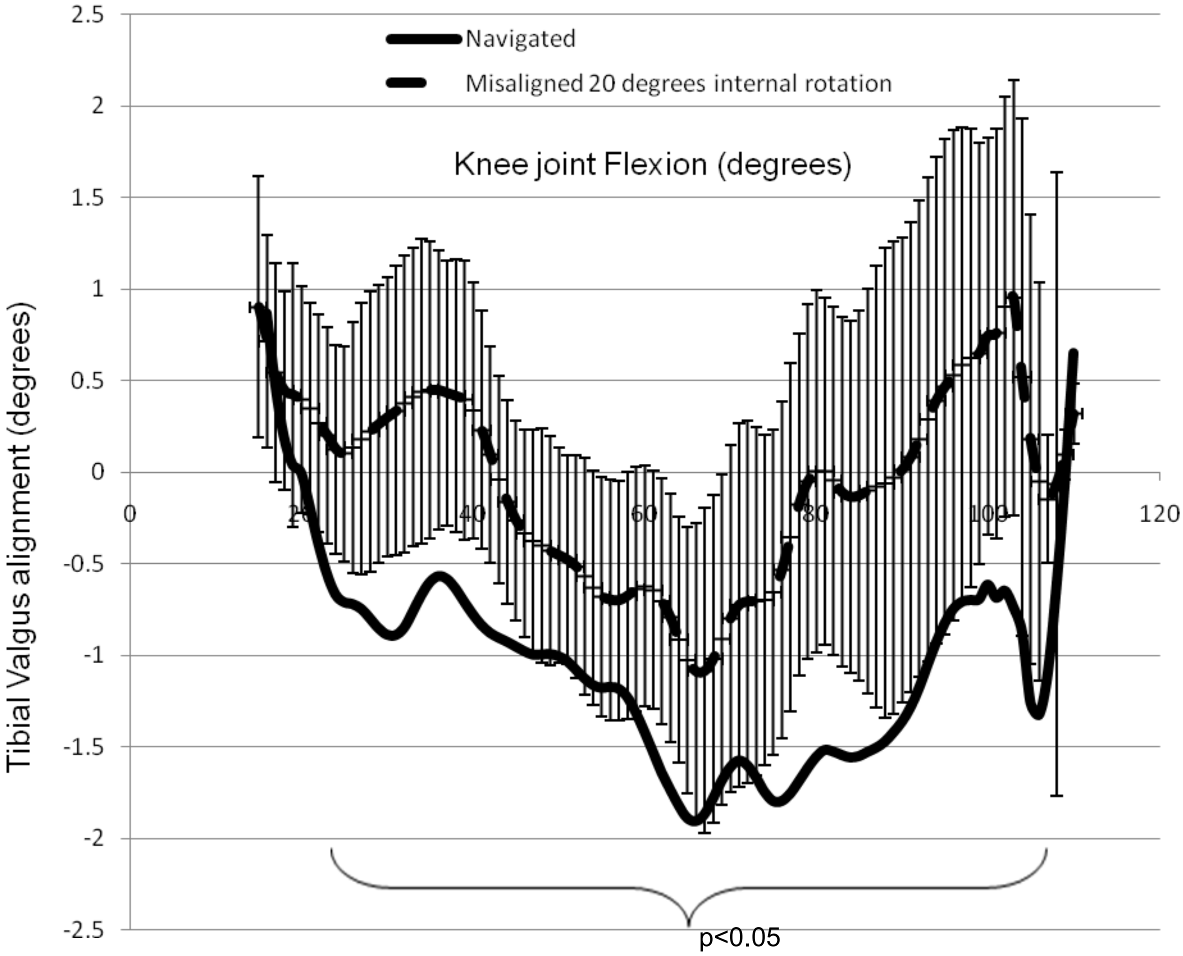

Figure 121: Tibial varus / valgus alignment versus knee joint flexion comparing the neutral varus / valgus pathway between the navigated knee and the misaligned 20° internal rotation knee.

[n=8, mean ±95% CI of difference between navigated and misaligned 20° internal rotation knees]

Following internal rotation of the component by 20º (figure 121), there was a statistically significant average 1º translation towards valgus between 20º and 115º of flexion ($p<0.05$). It is suggested that this change is due to unloading or stretching of the medial compartment that occurs due to the extreme internal rotation of the tibial tray, allowing a valgus deviation in flexion.

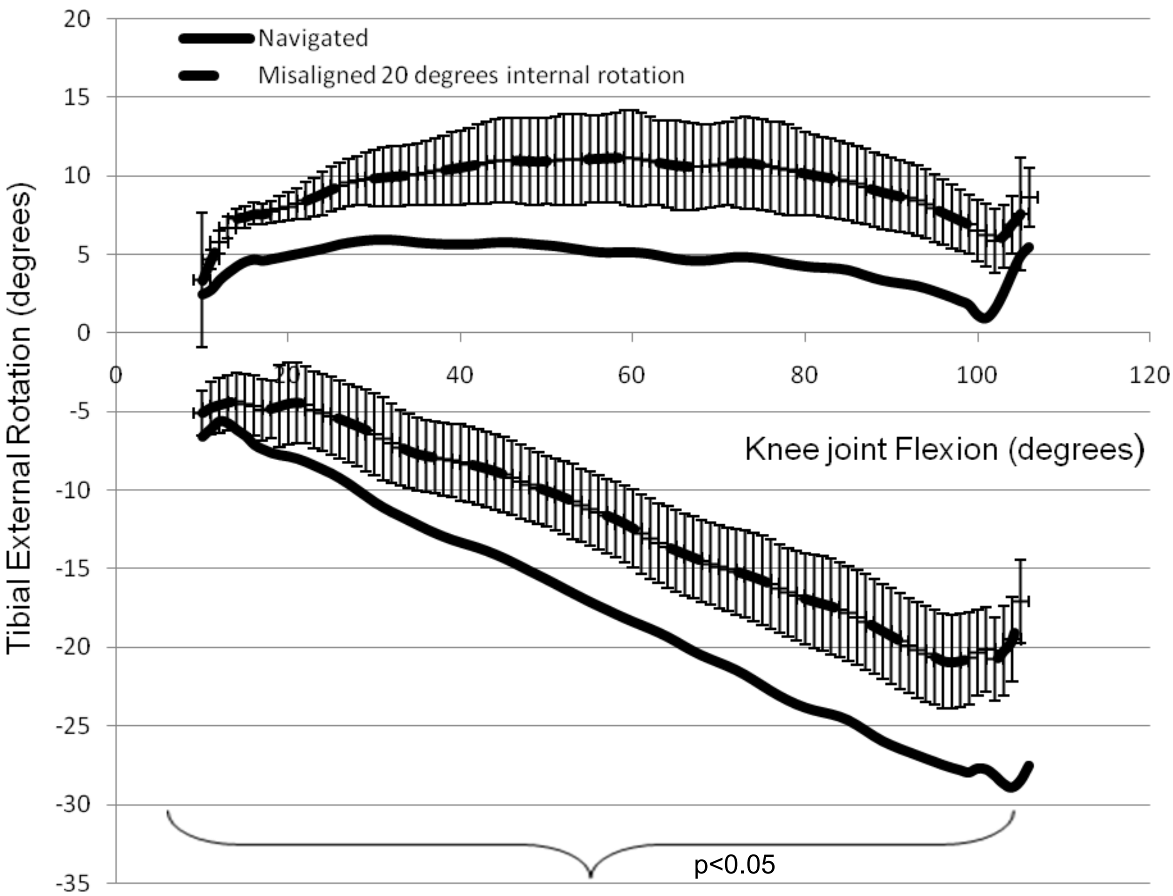

Figure 122: Tibial rotation versus knee joint flexion comparing the rotation envelope of laxity between the navigated knee and the misaligned 20° internal rotation knee.

[n=8, mean ±95% CI of difference between navigated and misaligned 20° internal rotation knees]

Following 20º of internal rotation of the tibial component (figure 122), there was a statistically significant average 5º translation in the rotation envelope (10º max) towards external rotation ($p<0.05$), with an average 4º translation (max 6º) in the external rotation envelope towards external rotation ($p<0.05$). The internal rotation envelope was also translated towards internal rotation by an average of 7º (12º max) ($p<0.05$). It is suggested that despite the 20º of internal rotation applied with the misalignment, there is only an average 5º tendency towards external rotation of the tibia. The external rotation torque is provided by the articulation of the femoral condyles against an incongruent tibial tray and has been opposed by the soft tissues and some articular conformity compensation.

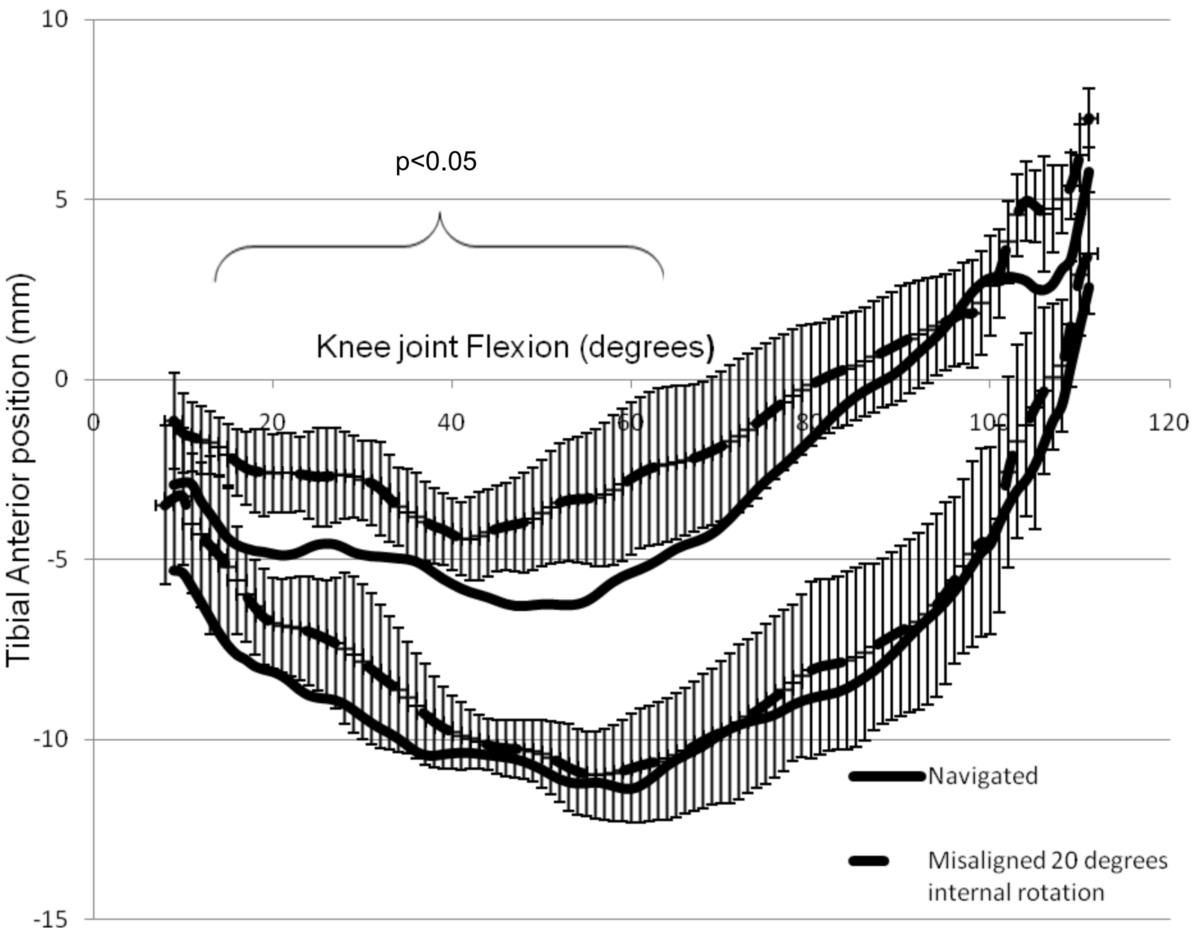

Figure 123: Tibial AP position versus knee joint flexion comparing the AP envelope of laxity between the navigated knee and the misaligned 20° internal rotation knee.

[n=8, mean ±95% CI of difference between navigated and misaligned 20° internal rotation knees]

Following 20º of internal rotation of the tibial component (figure 123), there was a significant anterior translation of the anterior limit of the AP envelope between 20º and 80º of knee flexion ($p<0.05$), but no change in the posterior envelope. It is suggested that the anterior translation of the anterior envelope is due to an anterior thrust generated by the incongruent articulation of the dominant medial condyle of the femoral component against the misaligned dished tibial insert.

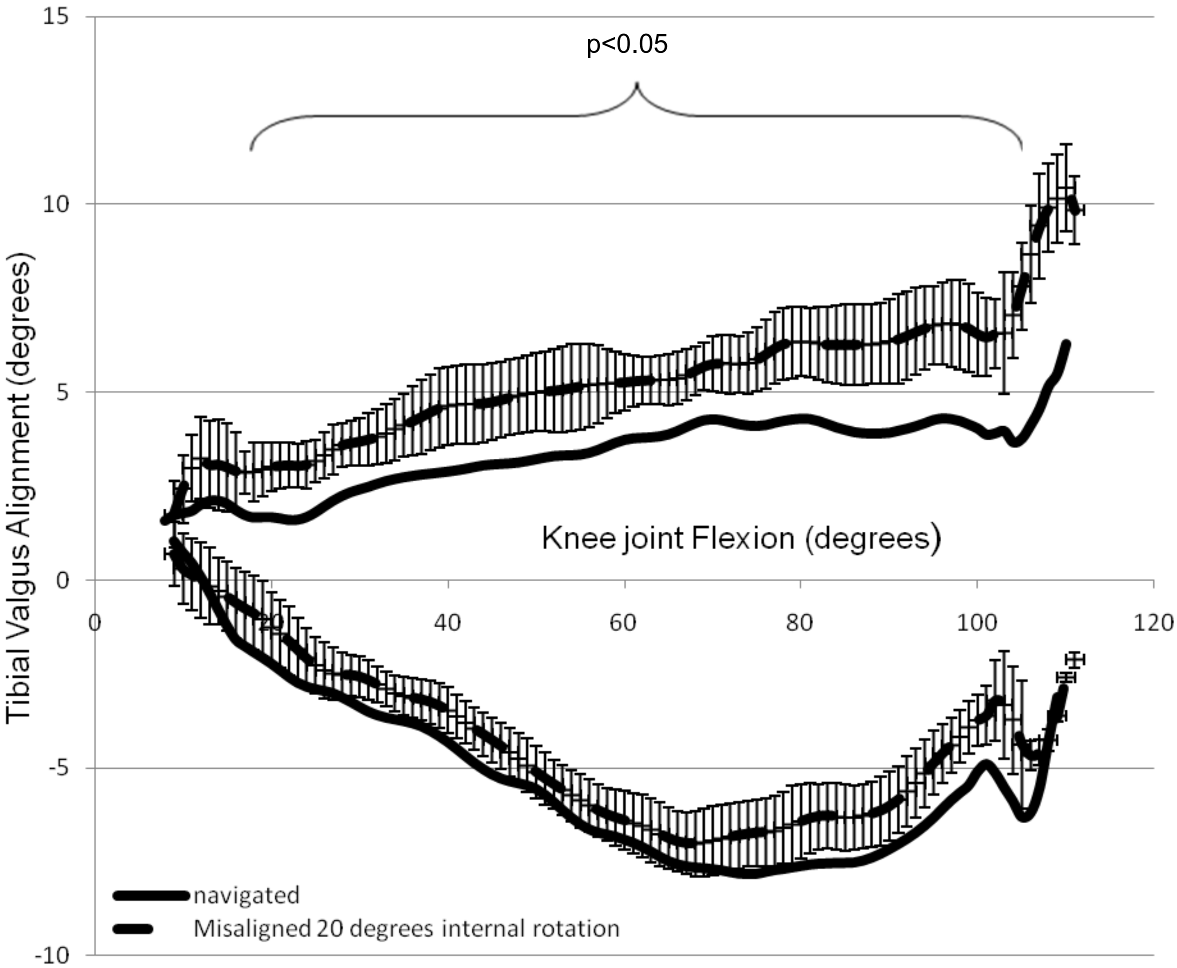

Figure 124: Tibial varus / valgus alignment versus knee joint flexion comparing the varus / valgus envelope of laxity between the navigated knee and the misaligned 20° internal rotation knee.
[n=8, mean ±95% CI of difference between navigated and misaligned 20° internal rotation knees]

Following 20º of internal rotation of the tibial component (figure 124), there was an average 2º translation (max 4º) in the valgus envelope of laxity towards valgus. The varus envelope was unchanged. It is suggested that the tibial tray rotation has permitted the minor translation towards valgus by reducing the tension in the soft tissue envelope on the medial side of the knee, thus allowing further valgus to be achieved.

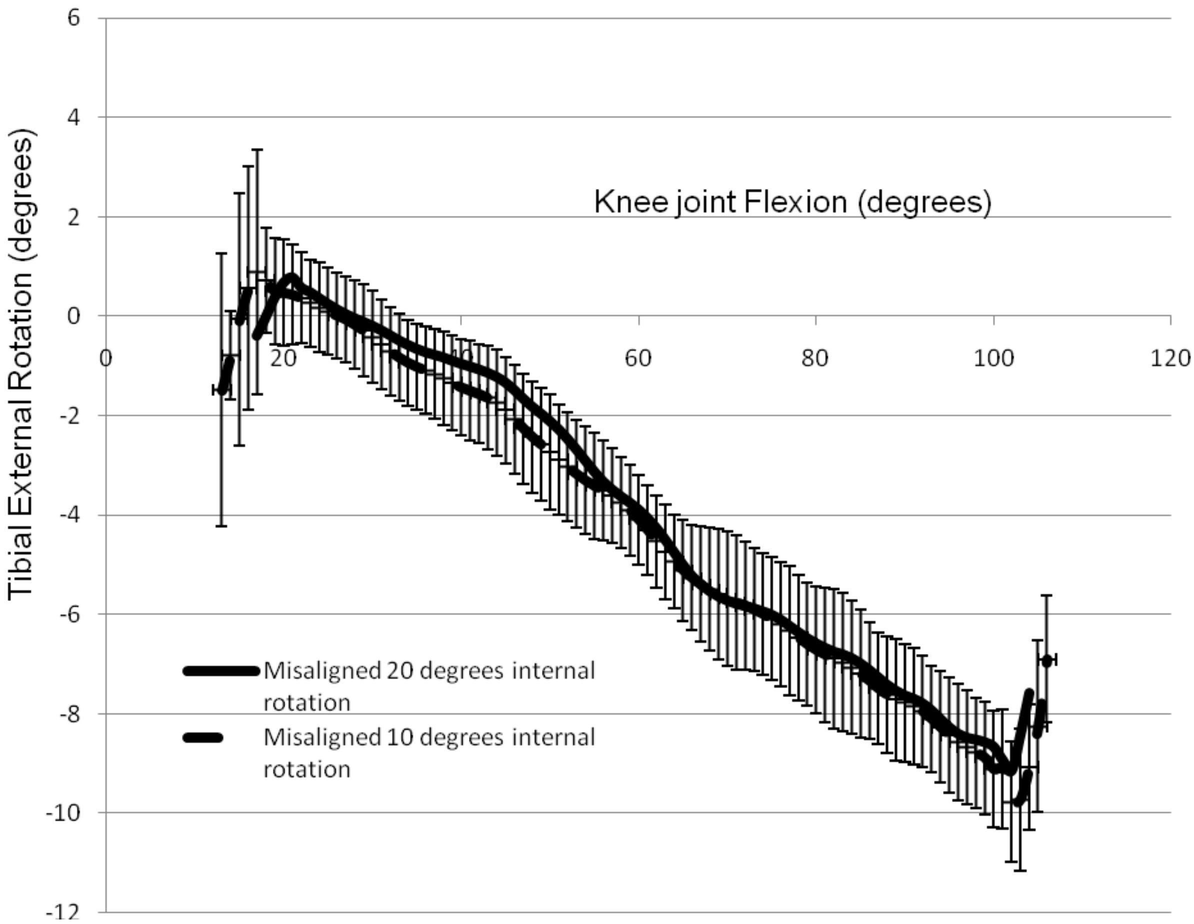

Figure 125: Tibial rotation versus knee joint flexion comparing the neutral rotation pathway between the misaligned 10º internal rotation and the 20º internal rotation knee.
[n=8, mean ±95% CI of difference between misaligned 10º internal rotation and misaligned 20º internal rotation knees]

When comparing 10º and 20º of internal rotation of the tibial tray component (figure 125), there was no difference in the neutral rotation path of motion.

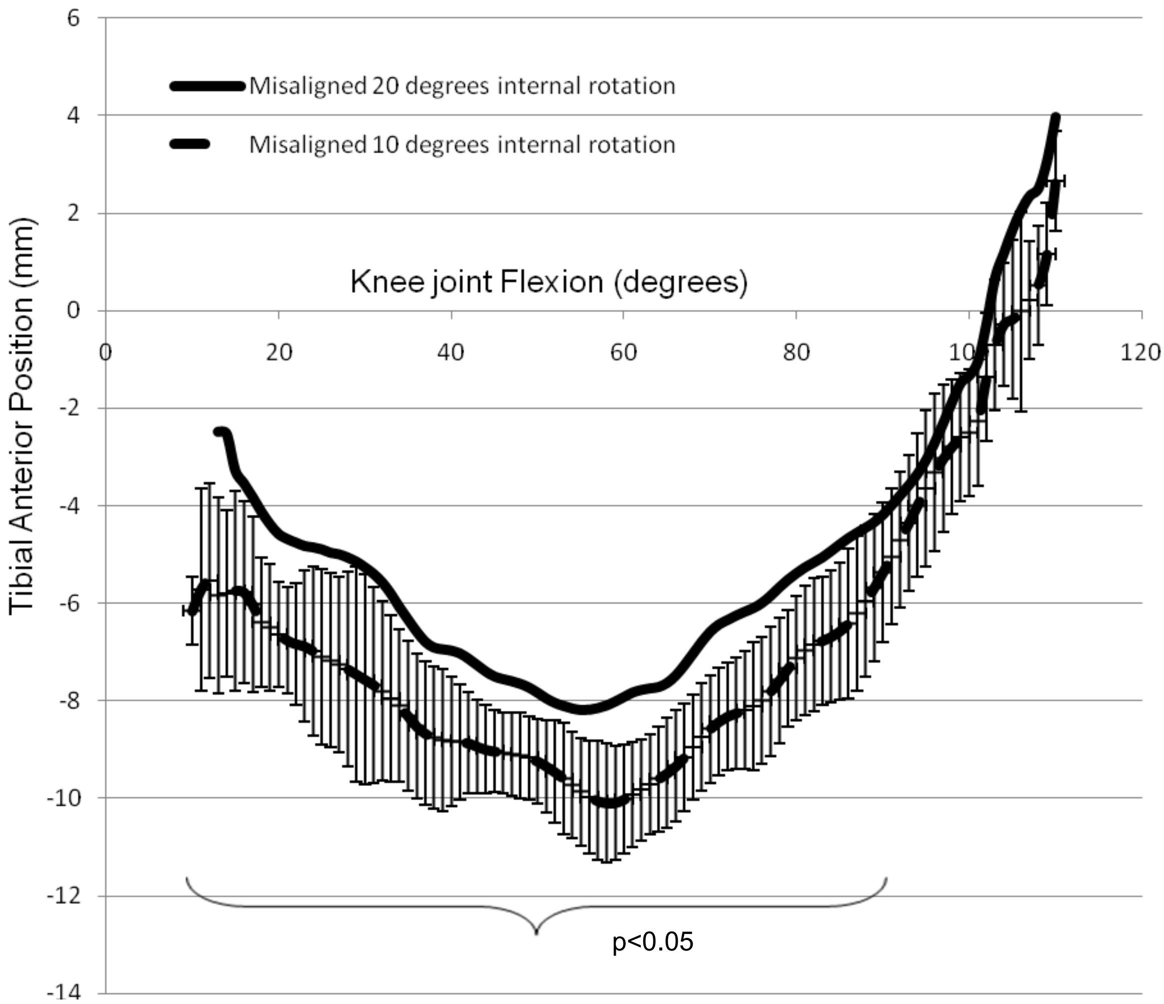

Figure 126: Tibial AP position versus knee joint flexion comparing the neutral AP pathway between the misaligned 10º internal rotation and the 20º internal rotation knee.
[n=8, mean ±95% CI of difference between misaligned 10º internal rotation and misaligned 20º internal rotation knees]

When comparing 10º and 20º of internal rotation of the tibial tray component (figure 126), there was a significant average anterior translation of 2mm (max 3mm) from 15º to 90º of knee flexion ($p<0.05$). It is suggested that this anterior translation is due to the dominant conforming action of the medial femoral condyle against the rotated dished tibial insert producing an anterior thrust.

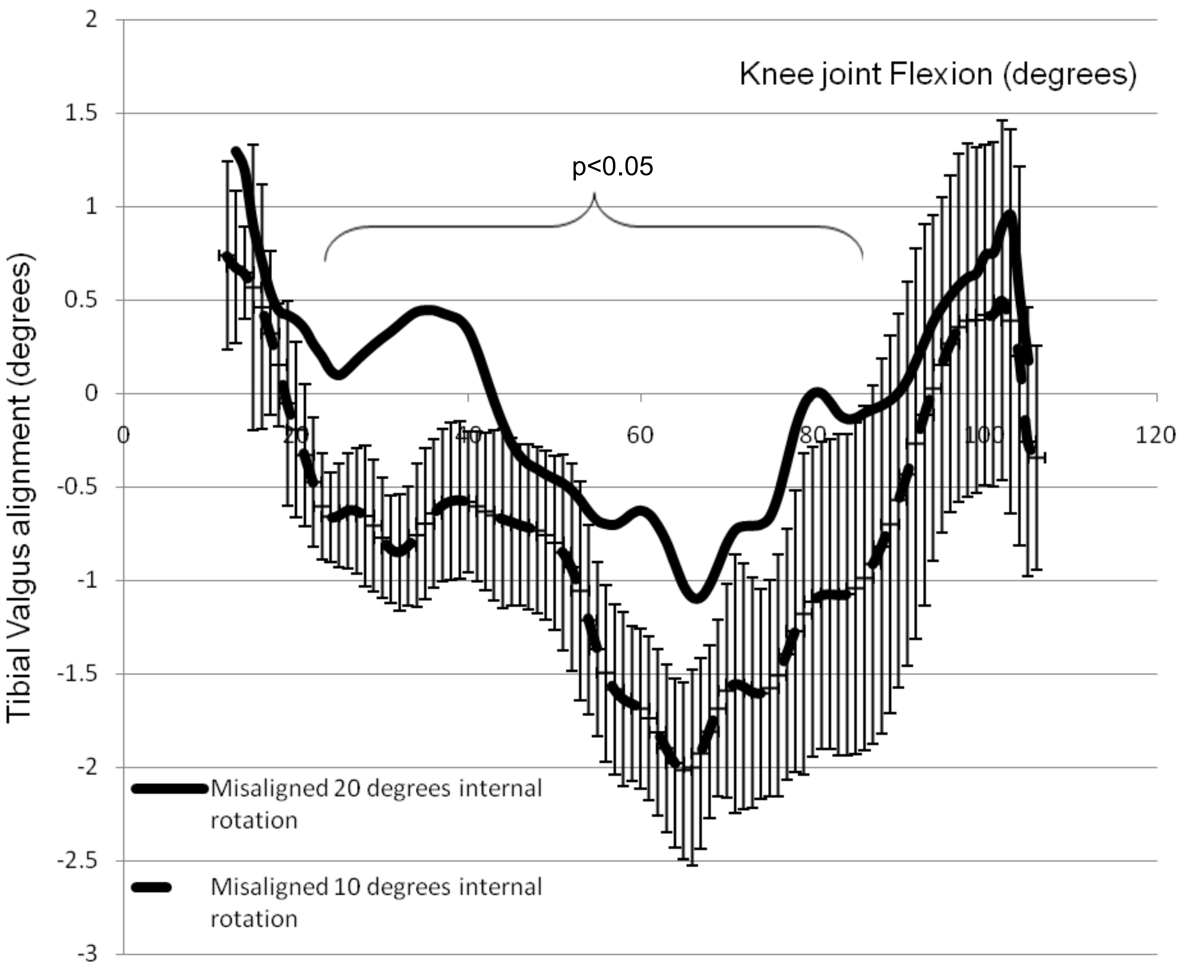

Figure 127**:** Tibial varus / valgus alignment versus knee joint flexion comparing the neutral varus / valgus pathway between the misaligned 10º internal rotation and the 20º internal rotation knee.
[n=8, mean ±95% CI of difference between misaligned 10º internal rotation and misaligned 20º internal rotation knees]

When comparing 10º and 20º of internal rotation of the tibial tray component (figure 127), there was an average 0.5º translation towards valgus (max 1º) that was statistically significant between 20º and 85º of knee flexion ($p<0.05$). It is suggested that this change is due to unloading or stretching of the medial compartment that occurs due to the internal rotation of the tibial tray, allowing a slight valgus deviation in flexion.

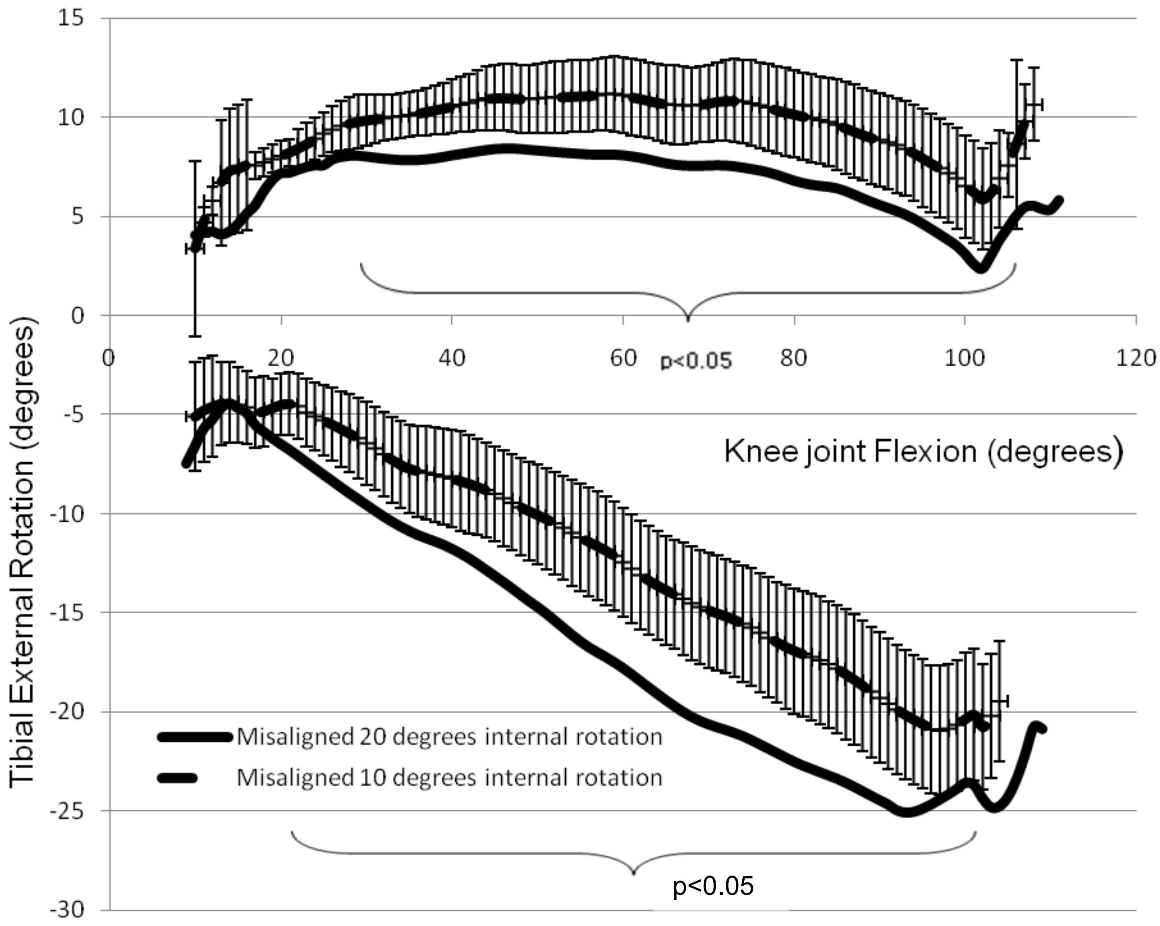

Figure 128: Tibial rotation versus knee joint flexion comparing the rotation envelope of laxity between the misaligned 10º internal rotation and the 20º internal rotation knee.
[n=8, mean ±95% CI of difference between misaligned 10º internal rotation and misaligned 20º internal rotation knees]

When comparing 10º and 20º of internal rotation of the tibial tray component (figure 128), there was a statistically significant average translation in the internal rotation envelope of laxity of 2º (5º max) towards external rotation ($p < 0.05$). There was also a statistically significant average translation of 2º (4º max) towards external rotation ($p<0.05$). It is suggested that the external rotation torque provided by the articulation of the femoral condyles against an incongruent tibial tray has been opposed by the soft tissues and some articular conformity compensation of the components.

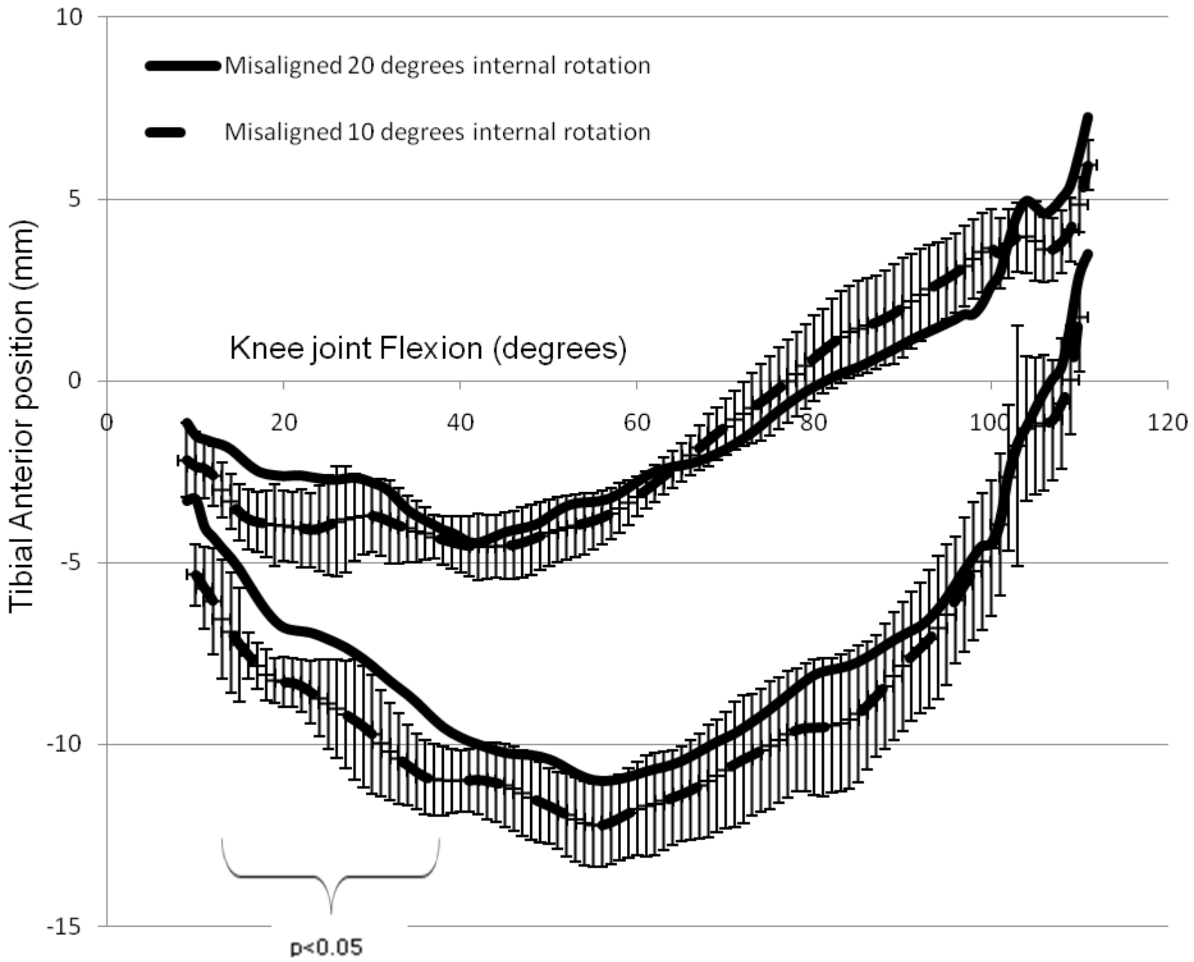

Figure 129: Tibial AP position versus knee joint flexion comparing the AP envelope of laxity between the misaligned 10º internal rotation and the 20º internal rotation knee.
[n=8, mean ±95% CI of difference between misaligned 10º internal rotation and misaligned 20º internal rotation knees]

When comparing 10º and 20 º of internal rotation of the tibial tray component (figure 129), there was an average anterior translation of 2 mm in the posterior envelope between 15 and 40 ($p<0.05$). It is suggested that the AP envelope has already been translated maximally with the 10º internal rotation misalignment, so there is no further translation when the 20º external rotation misalignment is applied.

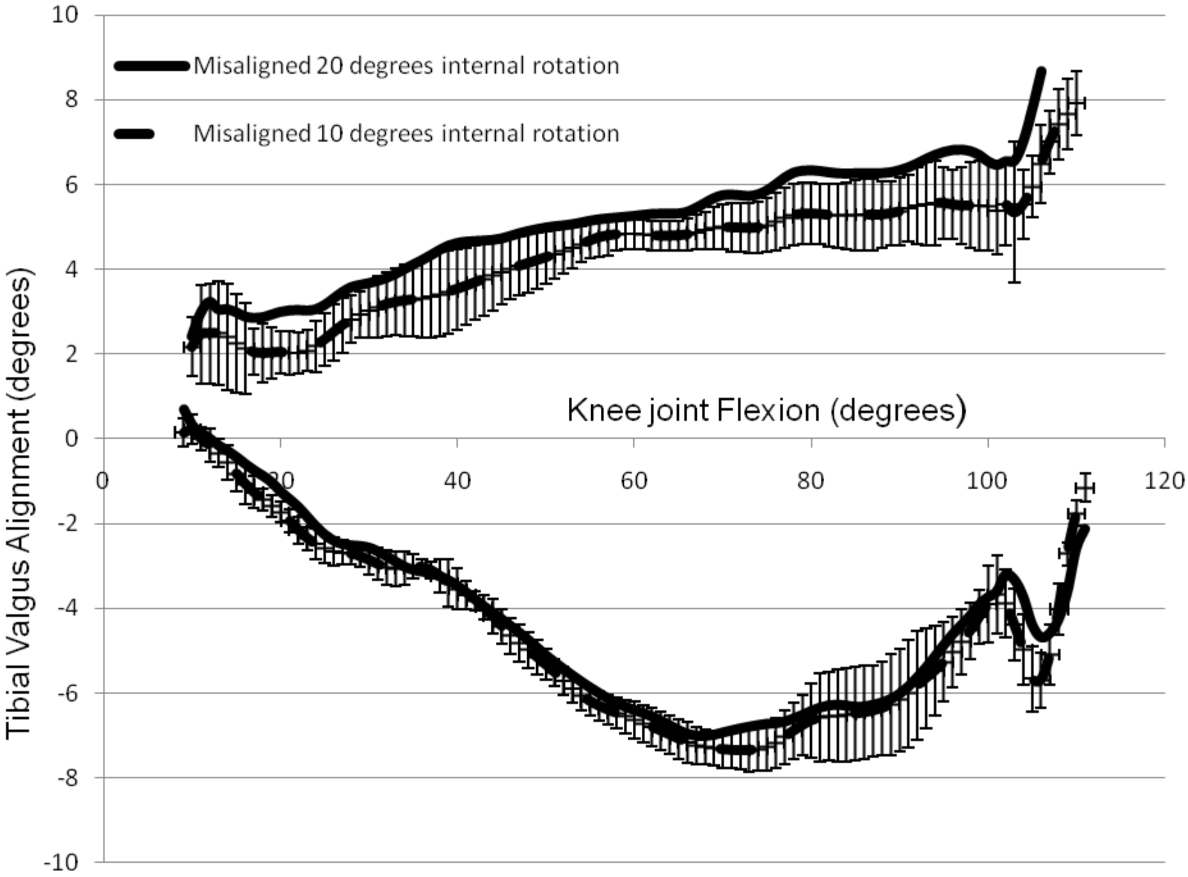

Figure 130: Tibial varus / valgus alignment versus knee joint flexion comparing the varus / valgus envelope of laxity between the misaligned 10º internal rotation and the 20º internal rotation knee. [n=8, mean ±95% CI of difference between misaligned 10º internal rotation and misaligned 20º internal rotation knees]

When comparing 10º and 20º of internal rotation of the tibial tray component (figure 130), there was an average translation of 1º in the valgus envelope of laxity towards valgus, this translation was statistically significant ($p<0.05$). There was no difference between the varus envelopes of laxity.

Posterior Slope only

- Navigated vs. 3º posterior slope
- Navigated vs. 6º posterior slope
- 3º posterior slope vs. 6º posterior slope
- Navigated vs. 9º posterior slope
- 6º posterior slope vs. 9º posterior slope

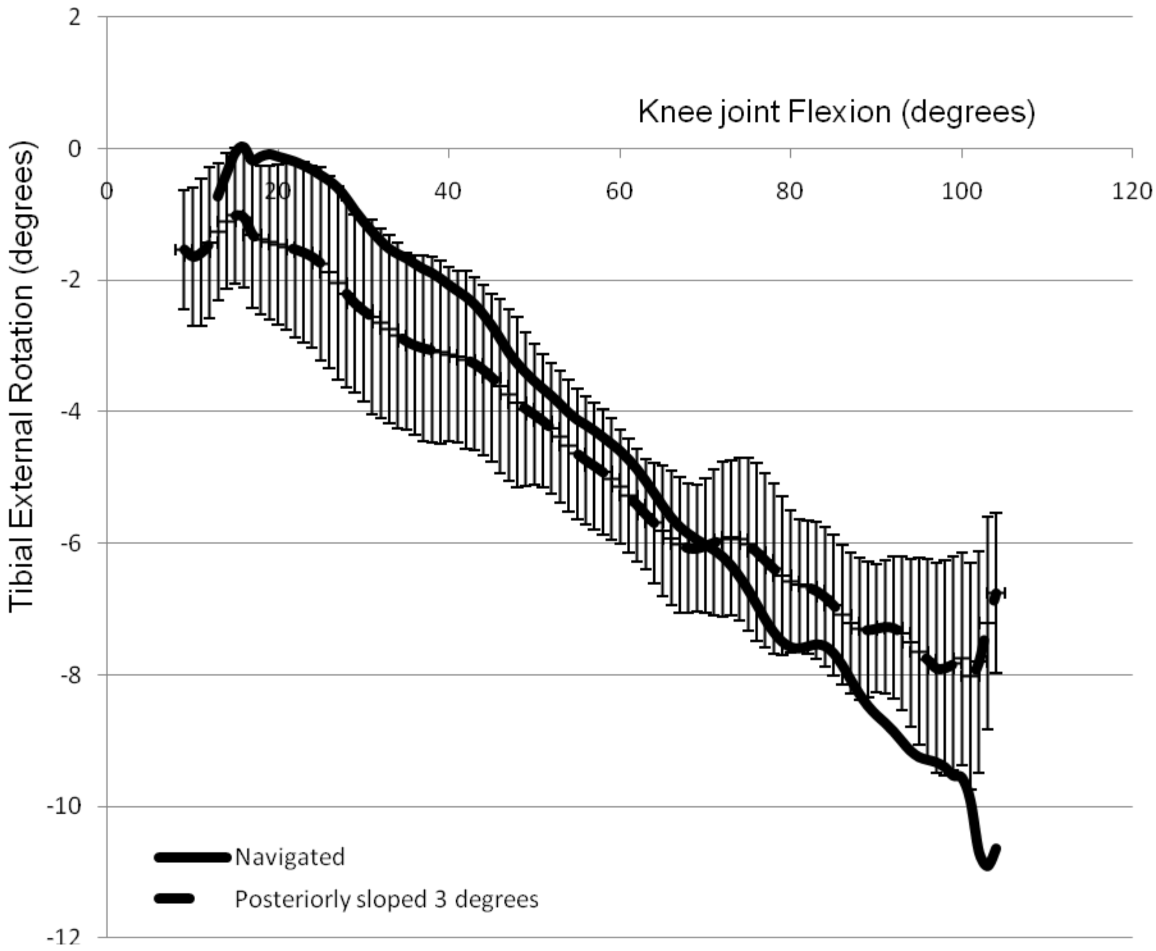

Figure 131: Tibial rotation versus knee joint flexion comparing the neutral rotation pathway between the navigated knee and 3º posterior sloped knee.
[n=8, mean ±95% CI of difference between

Following the addition of 3º of posterior slope (figure 131), there was an observed difference in the neutral rotation pathway with less internal rotation in early flexion and more external rotation in deep flexion compared to the navigated component. However, these observed changes were not statistically significant.

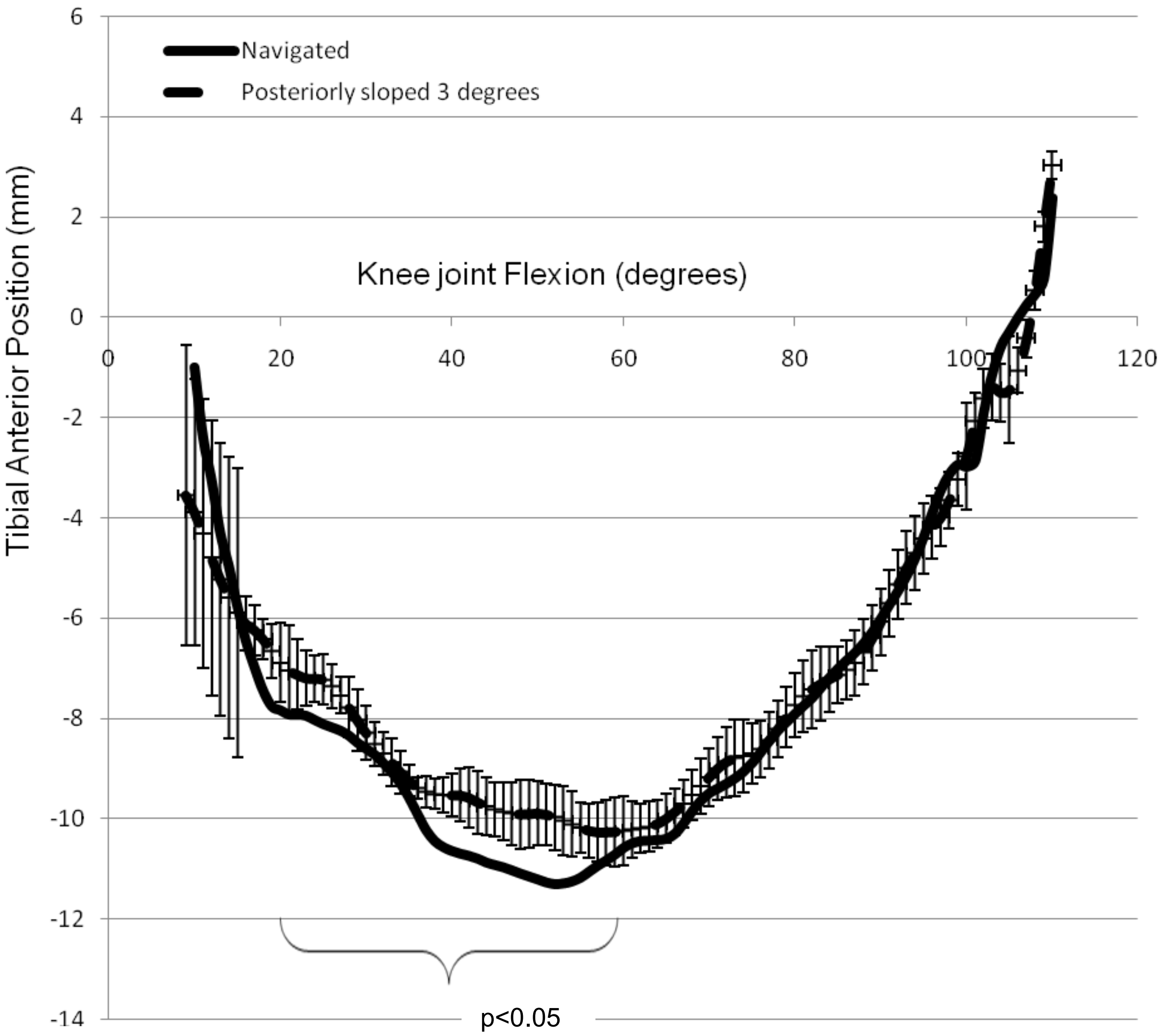

Figure 132: Tibial AP position versus knee joint flexion comparing the neutral AP pathway between the navigated knee and 3º posterior sloped knee.
[n=8, mean ±95% CI of difference between the navigated and 3º posterior sloped knees.

Following the addition of 3º of posterior slope (figure 132), there was an average 1 mm translation (2.5mm max) in the neutral AP pathway towards a more anterior position in mid flexion. These changes were statistically significant between 20º and 60º of knee flexion ($p<0.05$). It is suggested that the posterior slope applied to the tibial tray generated a resultant anterior thrust and reduced the upslope of the polyethylene insert posteriorly. This thrust, along with unloading of the soft tissues and resistance to motion posteriorly allows the anterior translation observed.

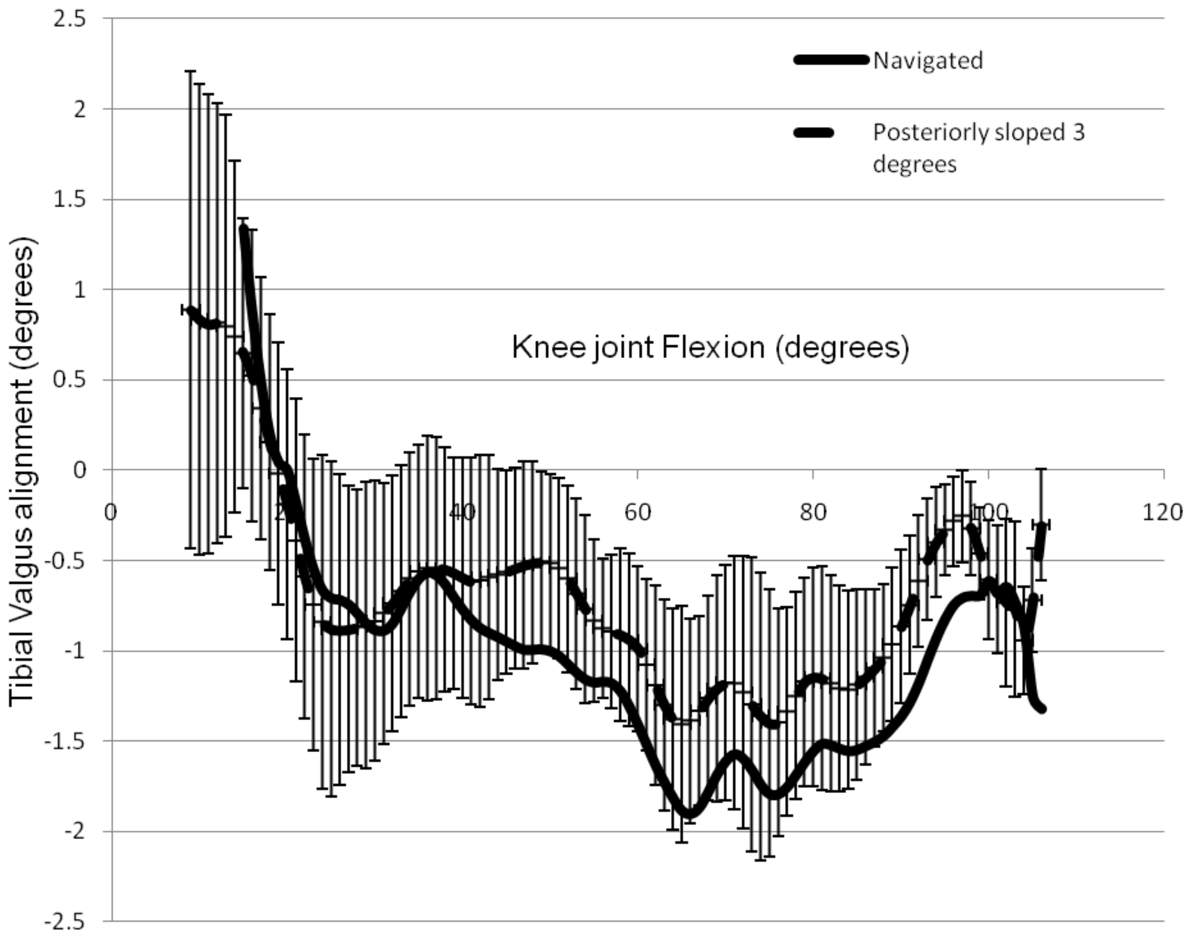

Figure 133: Tibial varus / valgus alignment versus knee joint flexion comparing the neutral varus / valgus pathway between the navigated knee and 3º posterior sloped knee.
[n=8, mean ±95% CI of difference between the navigated and 3º posterior sloped knees.

Following the addition of 3º of posterior slope (figure 133), there was a minor translation in the neutral varus / valgus pathway of the knee towards valgus, but this was not statistically significant.

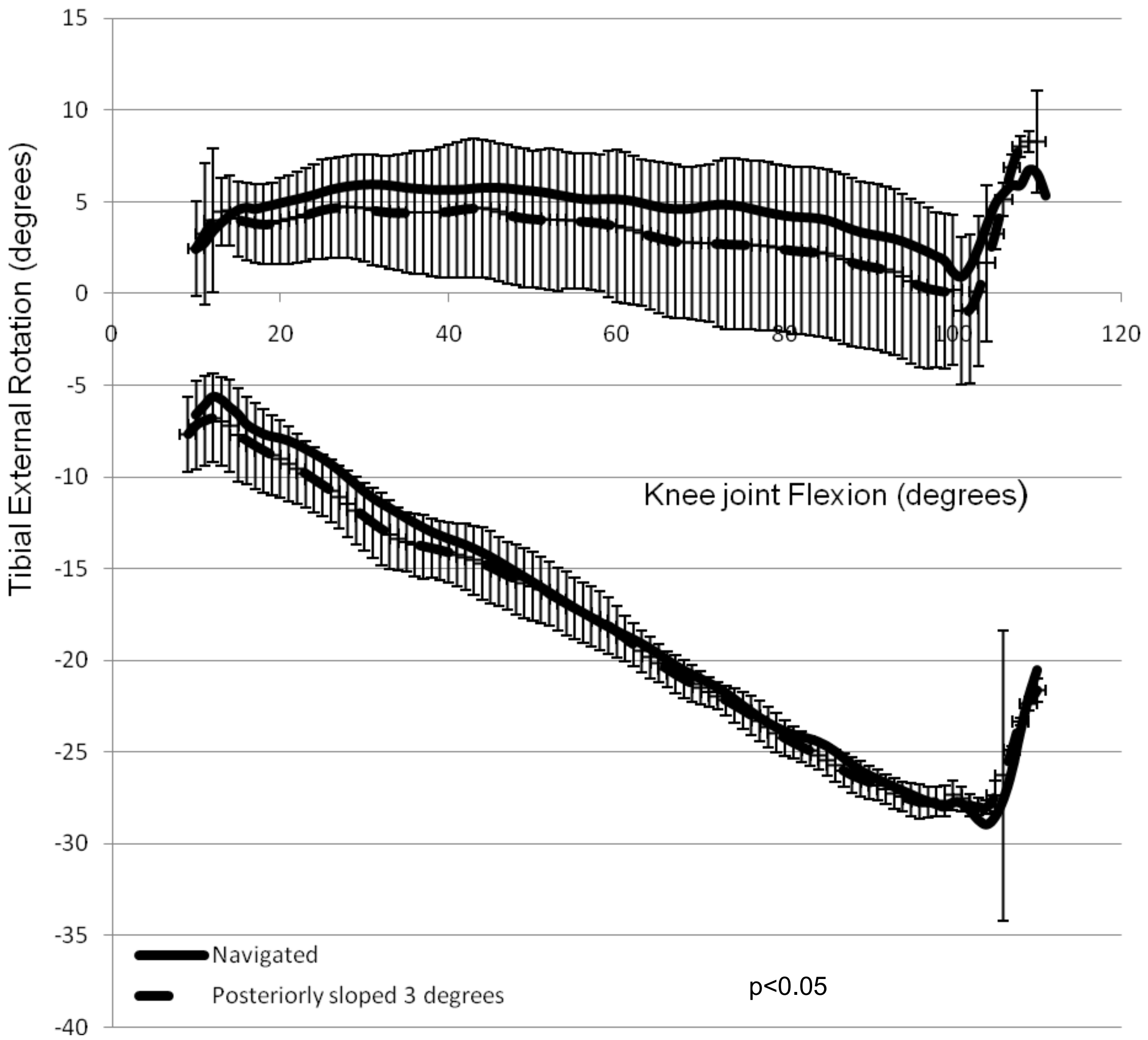

Figure 134: Tibial rotation versus knee joint flexion comparing the rotation envelope of laxity between the navigated knee and 3º posterior sloped knee.
[n=8, mean ±95% CI of difference between the navigated and 3º posterior sloped knees.

Following the addition of 3º of posterior slope (figure 134), there was a minor difference in the internal rotation envelopes, with an average 1º translation towards internal rotation, but this change was not statistically significant.

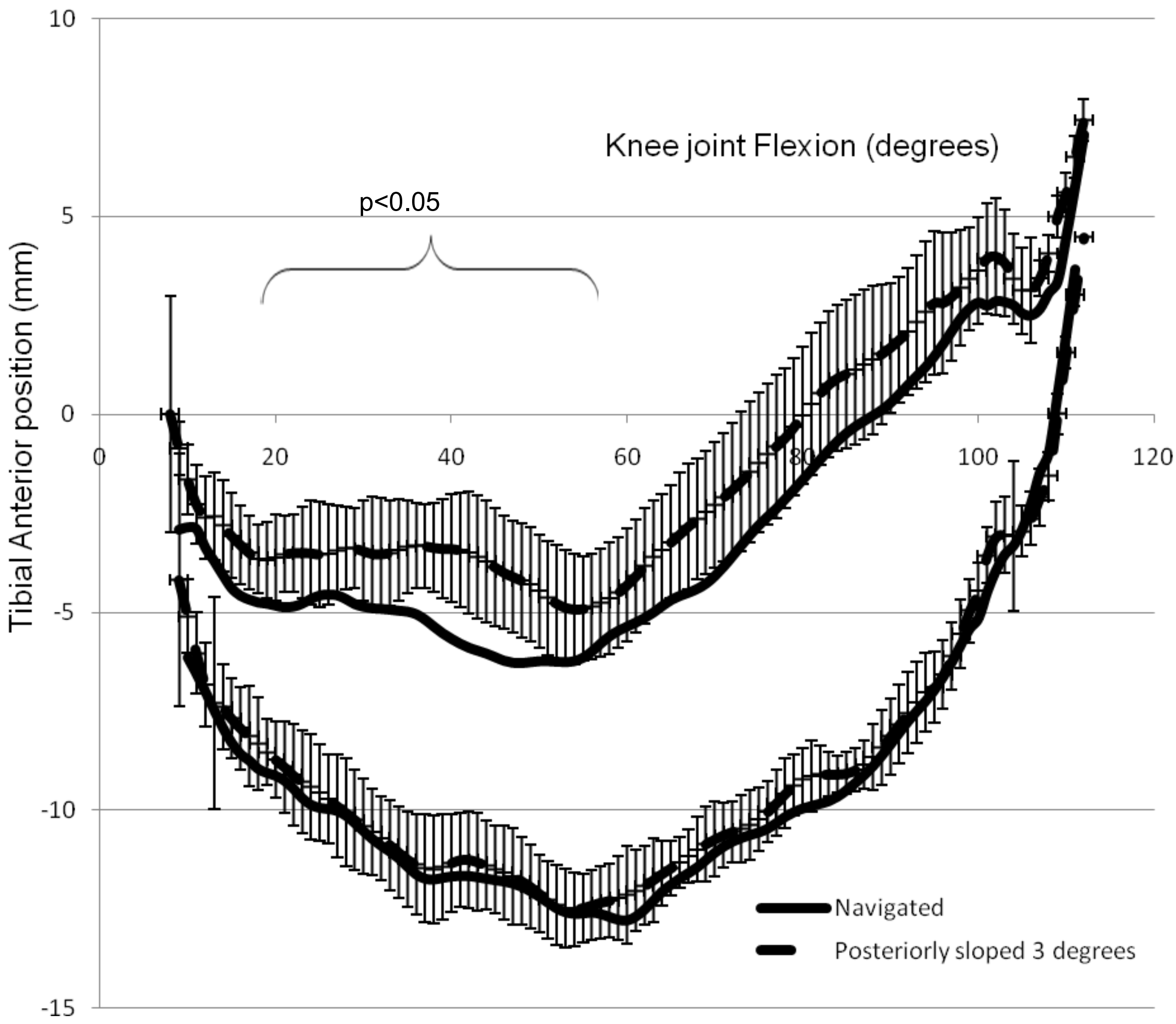

Figure 135: Tibial AP position versus knee joint flexion comparing the AP envelope of laxity between the navigated knee and 3º posterior sloped knee.
[n=8, mean ±95% CI of difference between the navigated and 3º posterior sloped knees.

Following the addition of 3º of posterior slope (figure 135), there was an average anterior 1 mm translation in the anterior limit of the envelope of laxity (max 3mm). This was statistically significant between 15º and 50º of flexion ($p<0.05$). It is suggested that the posterior slope applied to the tibial tray has generated a resultant anterior thrust. This thrust, along with unloading of the soft tissues posteriorly allows the anterior translation observed.

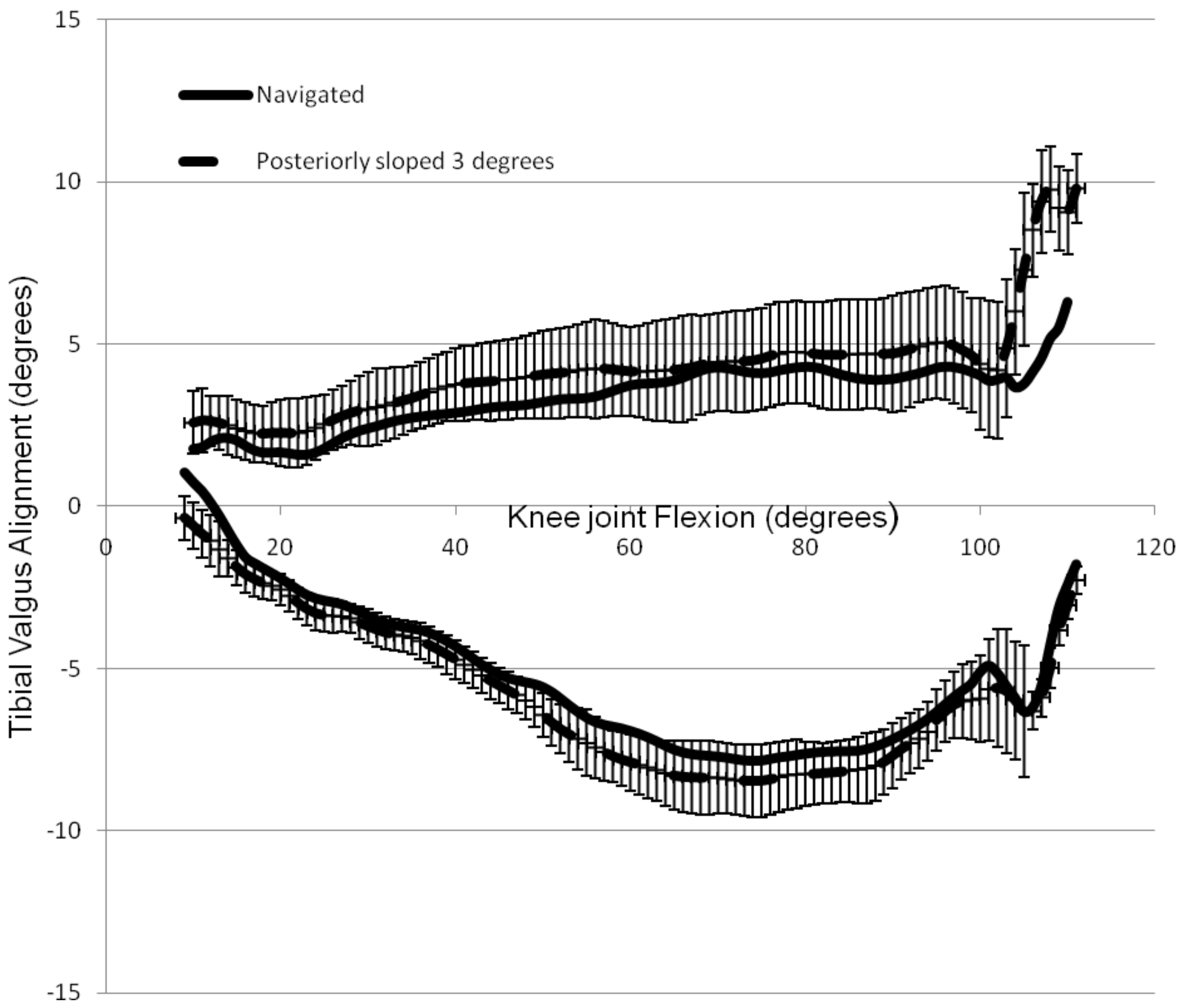

Figure 136: Tibial varus / valgus alignment versus knee joint flexion comparing the varus / valgus envelope of laxity between the navigated knee and 3º posterior sloped knee.
[n=8, mean ±95% CI of difference between the navigated and 3º posterior sloped knees.

Following the addition of 3 º of posterior slope (figure 136), there were no statistically significant differences in the varus or valgus envelopes of laxity.

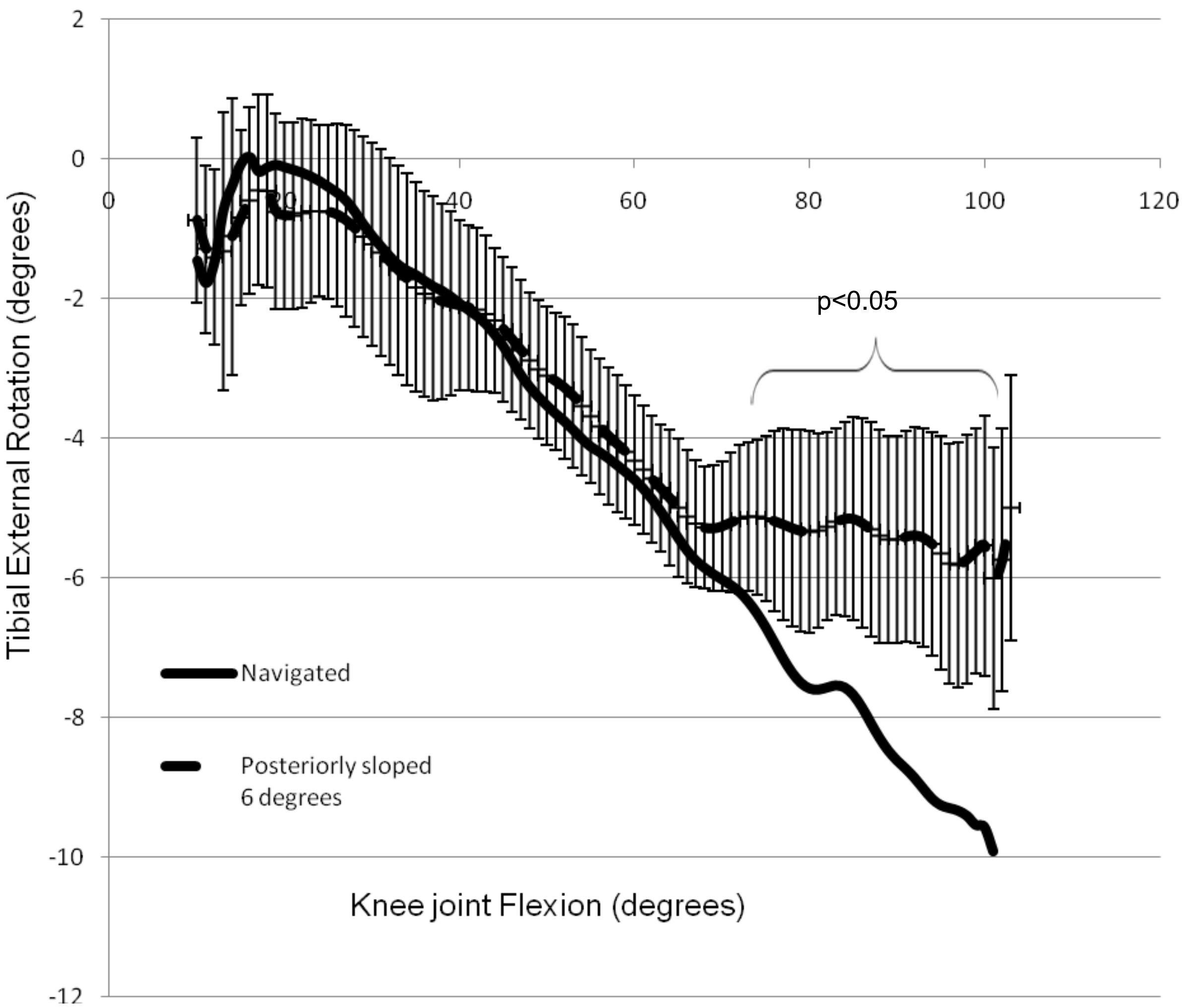

Figure 137: Tibial rotation versus knee joint flexion comparing the neutral rotation pathway between the navigated knee and 6º posterior sloped knee.
[n=8, mean ±95% CI of difference between the navigated and 6º posterior sloped knees.

Following the addition of 6º of posterior slope (figure 137), there was an increasing translation in the neutral rotation pathway towards external rotation in deep flexion, resulting in a neutralisation of the pathway that was statistically significant between 70º and 110º ($p<0.05$). It is suggested that the posterior slope applied to the tibial tray has generated a resultant anterior thrust. This thrust, along with unloading of the soft tissues posteriorly allows the neutralisation of the rotation pathway observed.

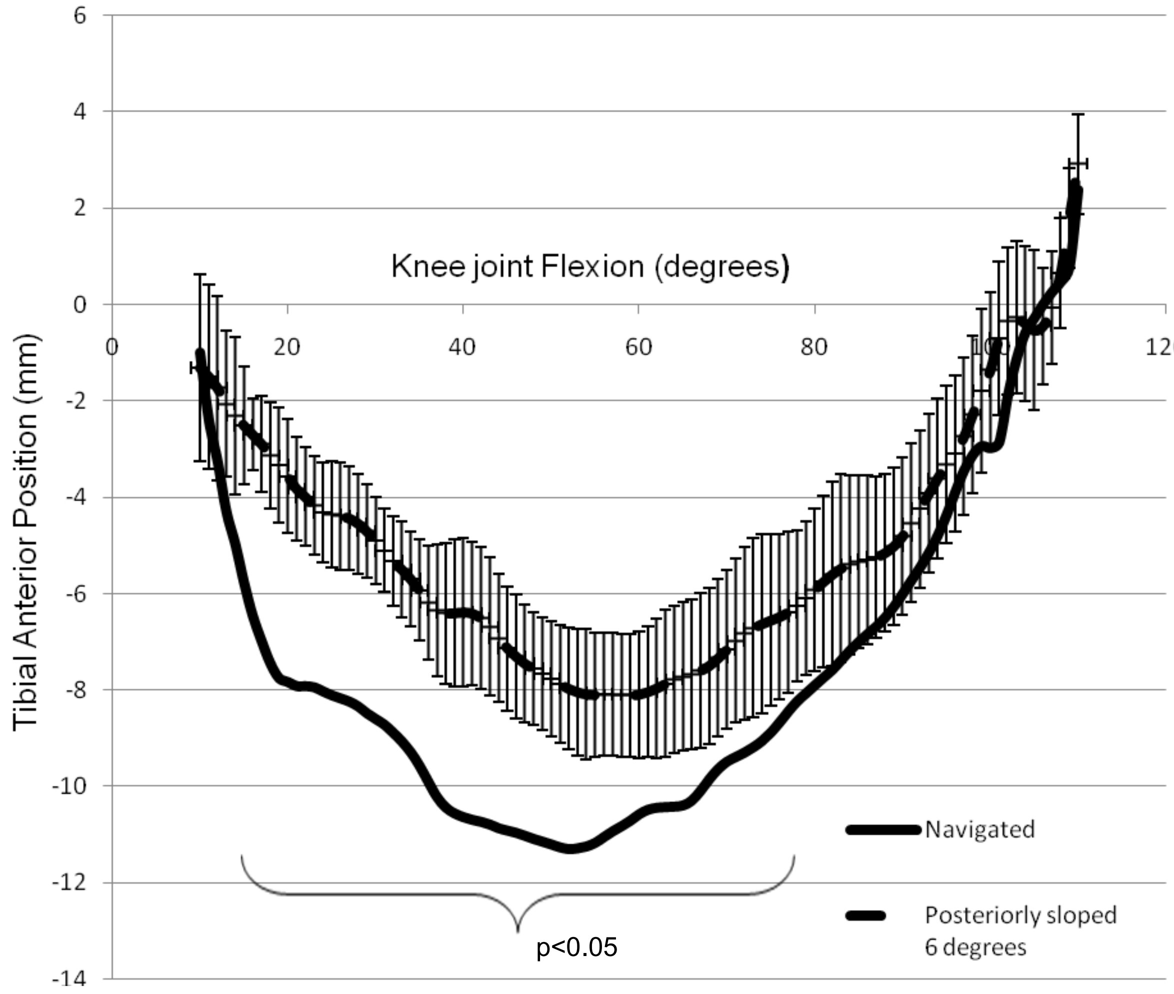

Figure 138: Tibial AP position versus knee joint flexion comparing the neutral AP pathway between the navigated knee and 6º posterior sloped knee.
[n=8, mean ±95% CI of difference between the navigated and 6º posterior sloped knees.

Following the addition of 6º of posterior slope (figure 138), there was a statistically significant average 2mm anterior translation in the neutral AP pathway (max 3.5mm), to a more anterior position between 15º and 80º of knee flexion. It is suggested that the posteriorly slope applied to the tibial tray generated a resultant anterior thrust and reduced the upslope of the polyethylene insert posteriorly. This thrust, along with unloading of the soft tissues and resistance to motion posteriorly allows the anterior translation observed.

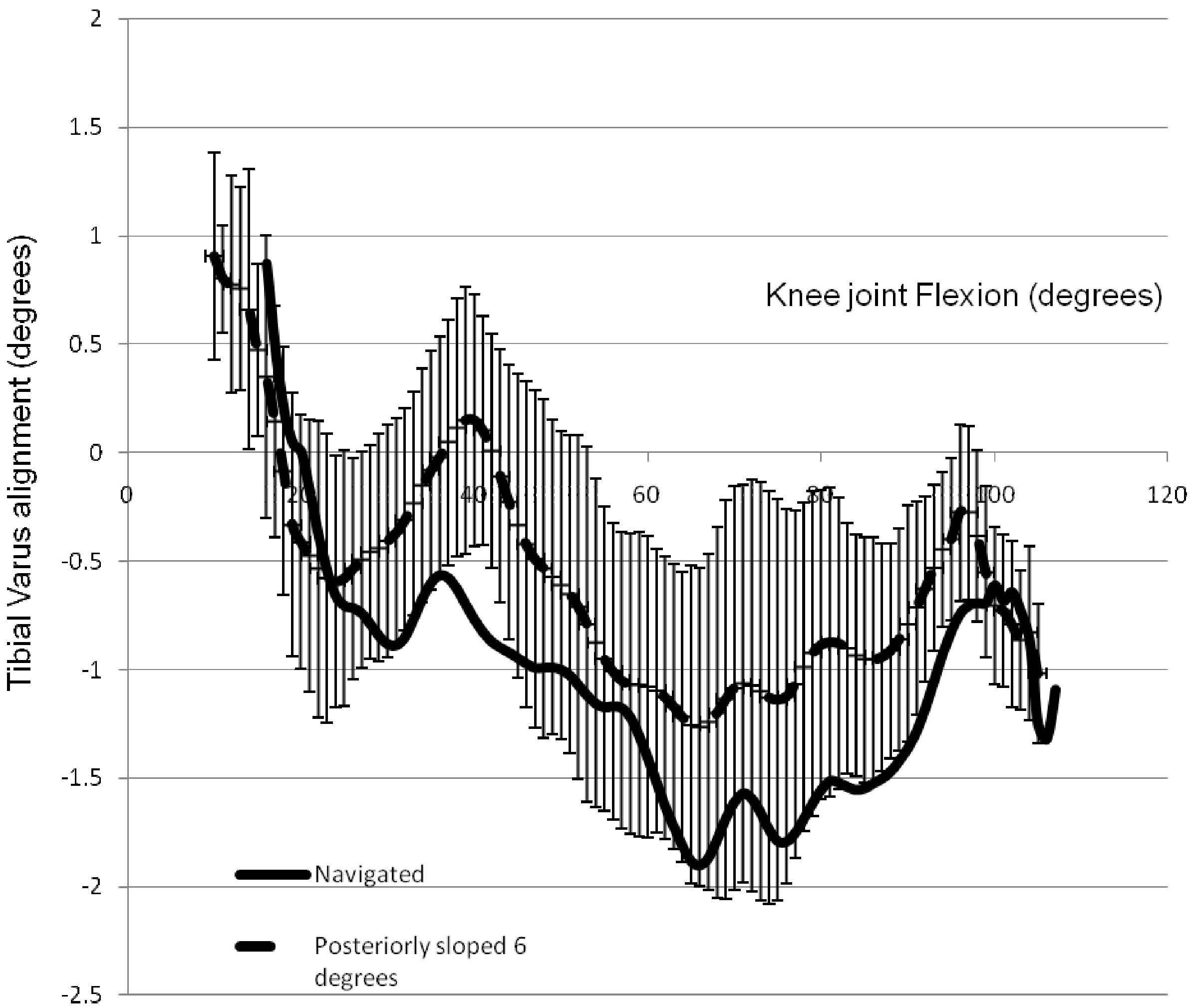

Figure 139: Tibial varus / valgus alignment versus knee joint flexion comparing the neutral varus / valgus pathway between the navigated knee and 6º posterior sloped knee.
[n=8, mean ±95% CI of difference between the navigated and 6º posterior sloped knees.

Following the addition of 6º of posterior slope (figure 139), there was a minor translation in the neutral varus / valgus pathway towards valgus, but this translation was not statistically significant.

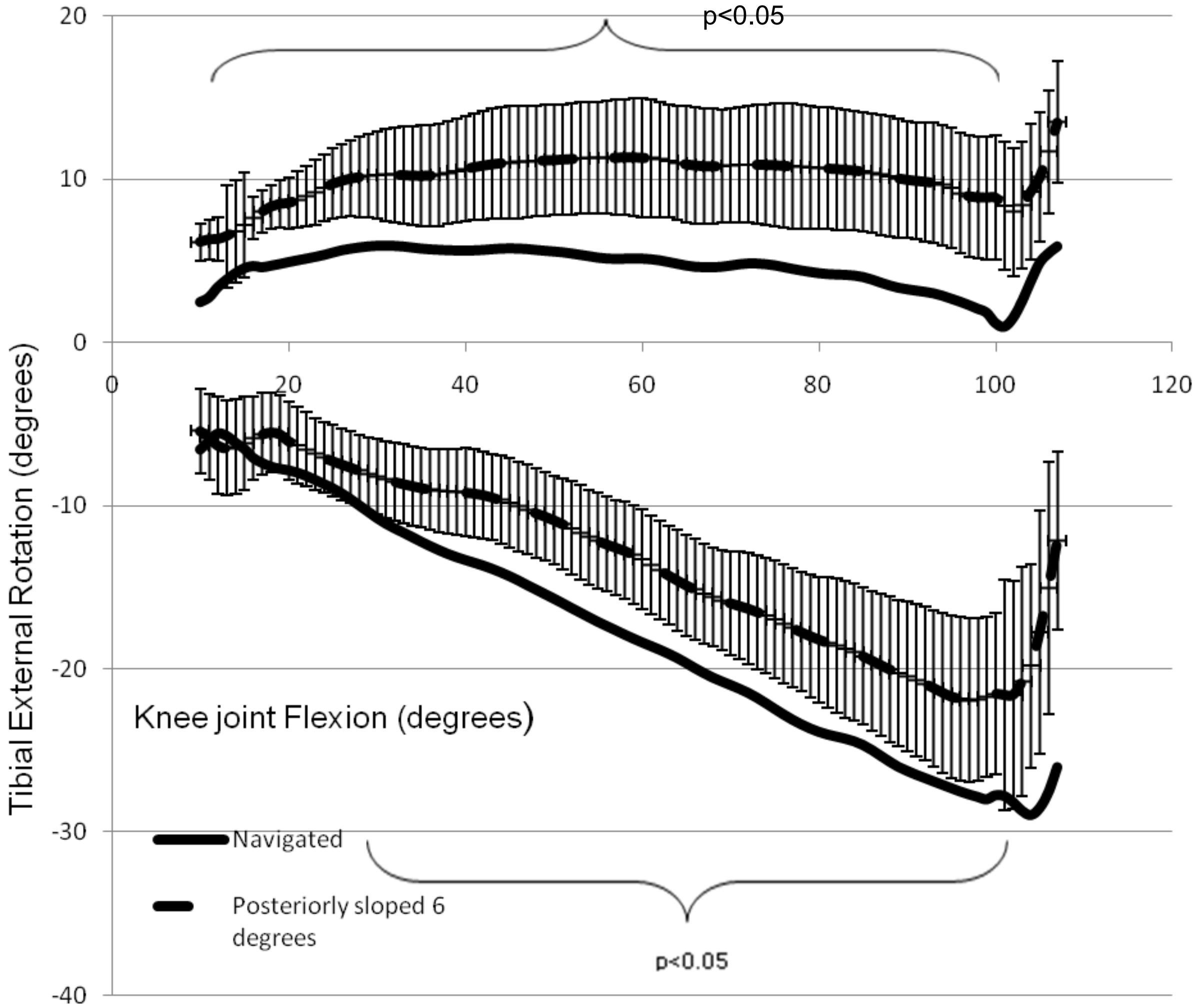

Figure 140: Tibial rotation versus knee joint flexion comparing the rotation envelope of laxity between the navigated knee and 6º posterior sloped knee.
[n=8, mean ±95% CI of difference between the navigated and 6º posterior sloped knees.

Following the addition of 6º of posterior slope (figure 140), there was a significant average translation of 5º (9º max) in the external rotation limit towards external rotation ($p<0.05$) and a significant average translation of 3º (5º max) in the internal rotation limit towards external rotation between 30º and 110º of knee flexion ($p<0.05$). It is suggested, that this translation is due to the extra laxity generated from the posterior slope of the tibial tray.

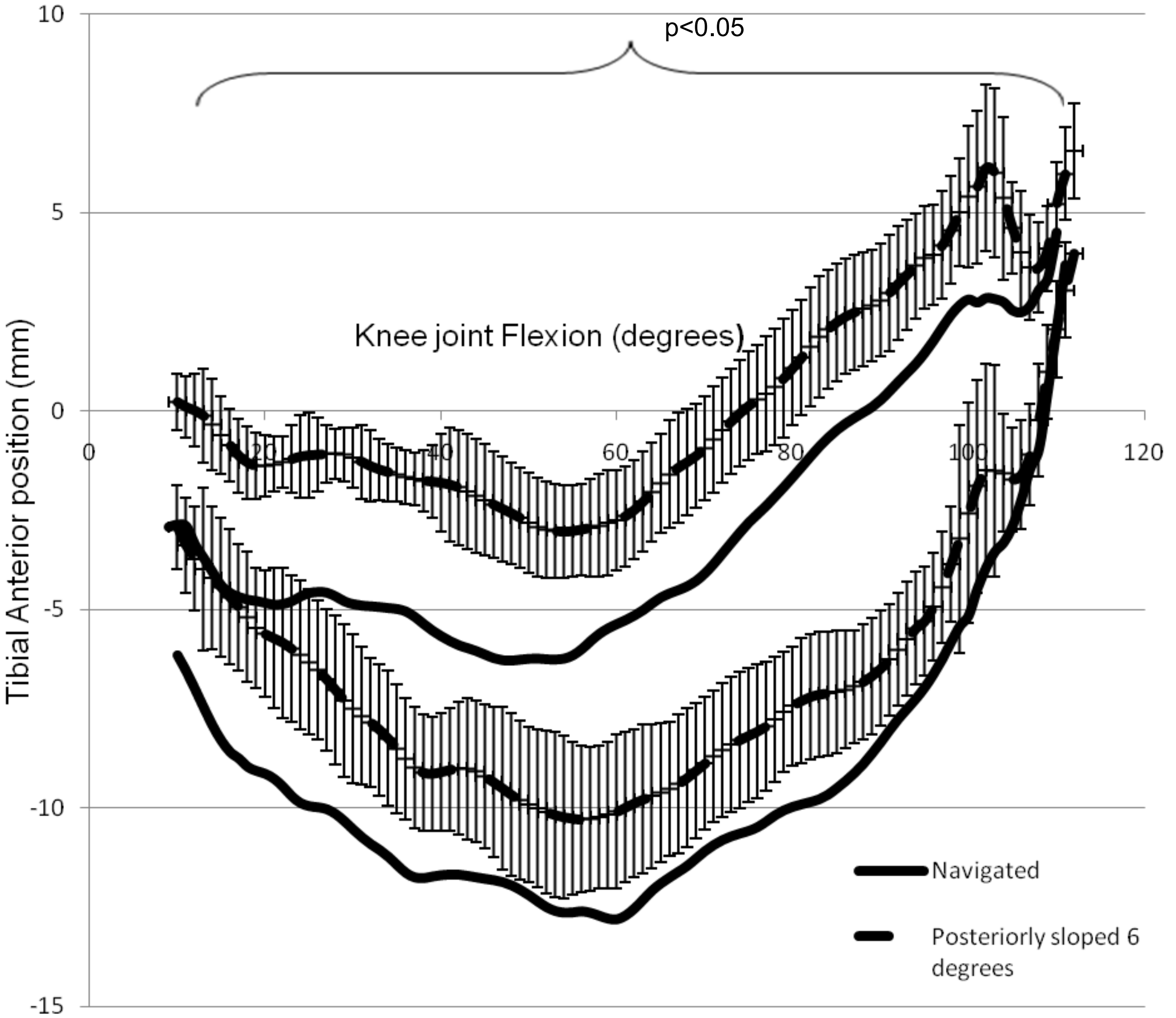

Figure 141: Tibial AP position versus knee joint flexion comparing the AP envelope of laxity between the navigated knee and 6º posterior sloped knee.
[n=8, mean ±95% CI of difference between the navigated and 6º posterior sloped knees.

Following the addition of 6º of posterior slope (figure 141), there were statistically significant, average 2mm translations (max 5mm) in the anterior and posterior limits of the AP envelope of laxity ($p<0.05$). It is suggested that the posteriorly sloped tibial tray generated an anterior thrust and reduced the upslope of the polyethylene insert posteriorly. This thrust, along with unloading of the soft tissues and resistance to motion posteriorly allows the anterior translation observed.

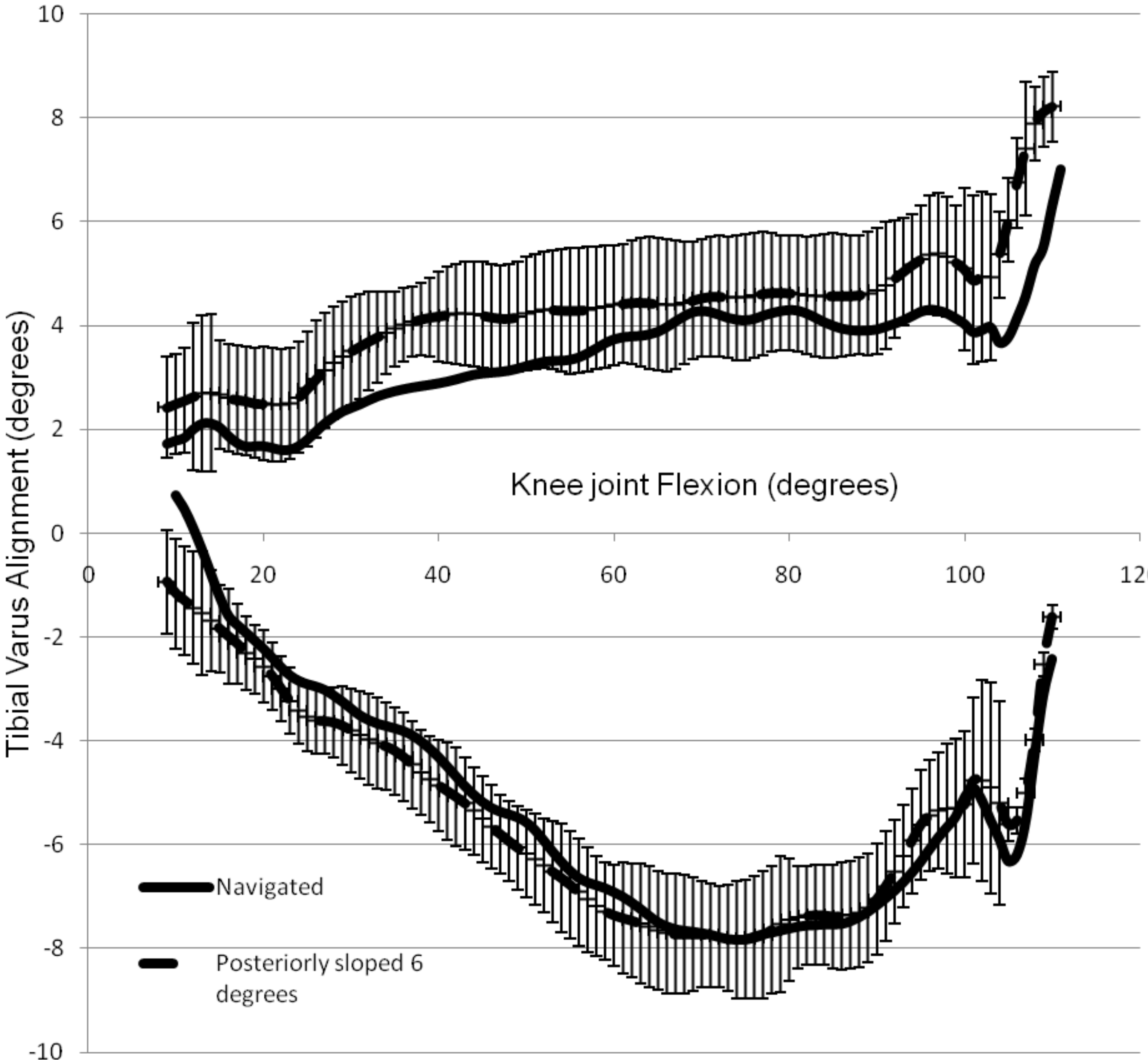

Figure 142: Tibial varus / valgus alignment versus knee joint flexion comparing the varus / valgus envelope of laxity between the navigated knee and 6º posterior sloped knee.
[n=8, mean ±95% CI of difference between the navigated and 6º posterior sloped knees.

Following the addition of 6º of posterior slope (figure 142), there were no significant changes in the varus / valgus envelope of laxity between the navigated and posteriorly sloped knees.

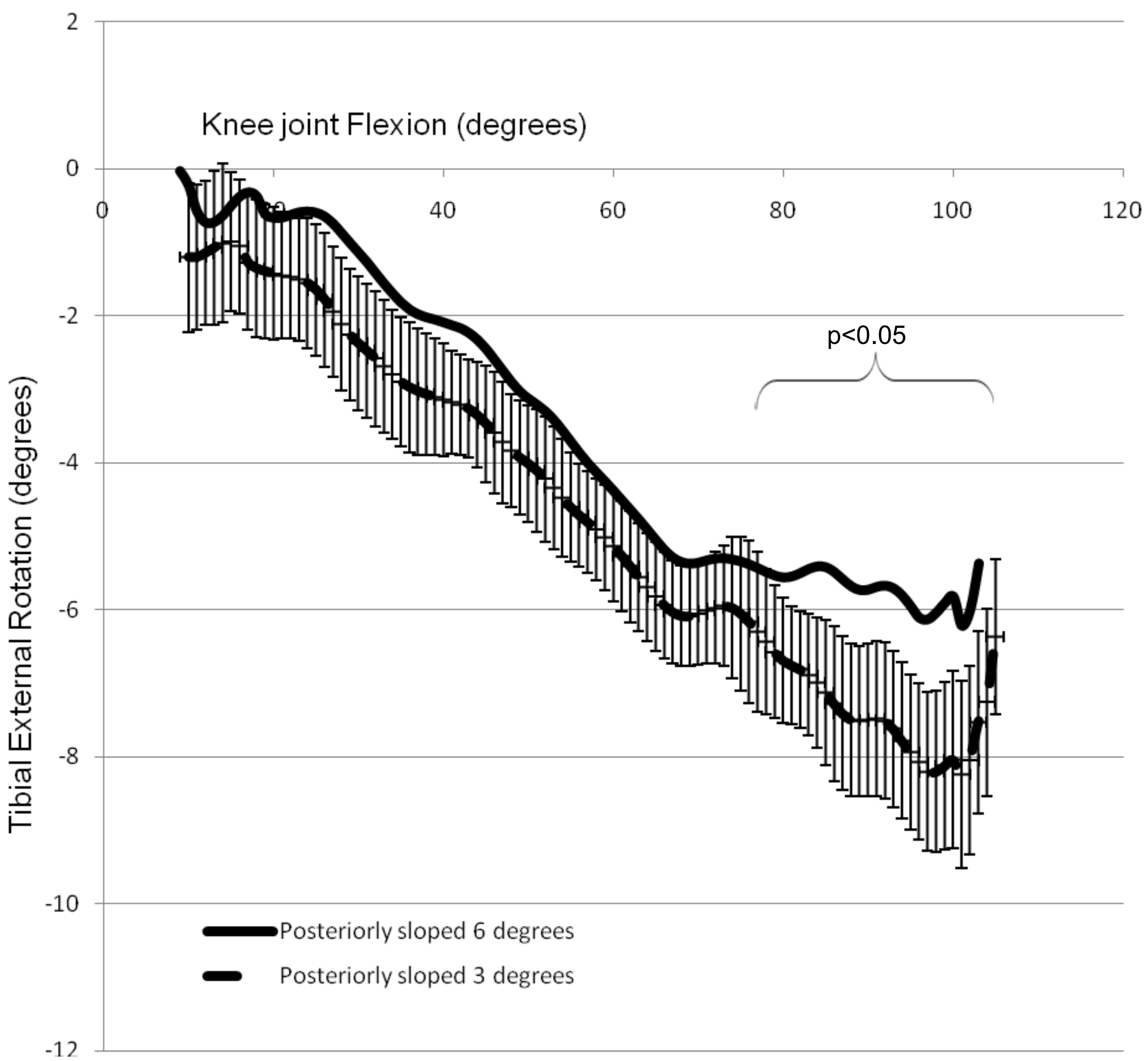

Figure 143: Tibial rotation versus knee joint flexion comparing the neutral rotation pathway between the 3º posterior sloped knee and the 6º posterior sloped knee.
[n=8, mean ±95% CI of difference between the 3º posterior sloped and the 6º posterior sloped knees.

Following the addition of an extra 3º of posterior slope, from 3 to 6º (figure 143), there was an increasing translation in the neutral rotation pathway towards external rotation in deep flexion, resulting in a neutralisation of the pathway that was statistically significant between 80º and 110º ($p<0.05$). It is suggested that the posterior slope applied to the tibial tray has generated a resultant anterior thrust. This thrust, along with unloading of the soft tissues posteriorly allows the neutralisation of the rotation pathway observed.

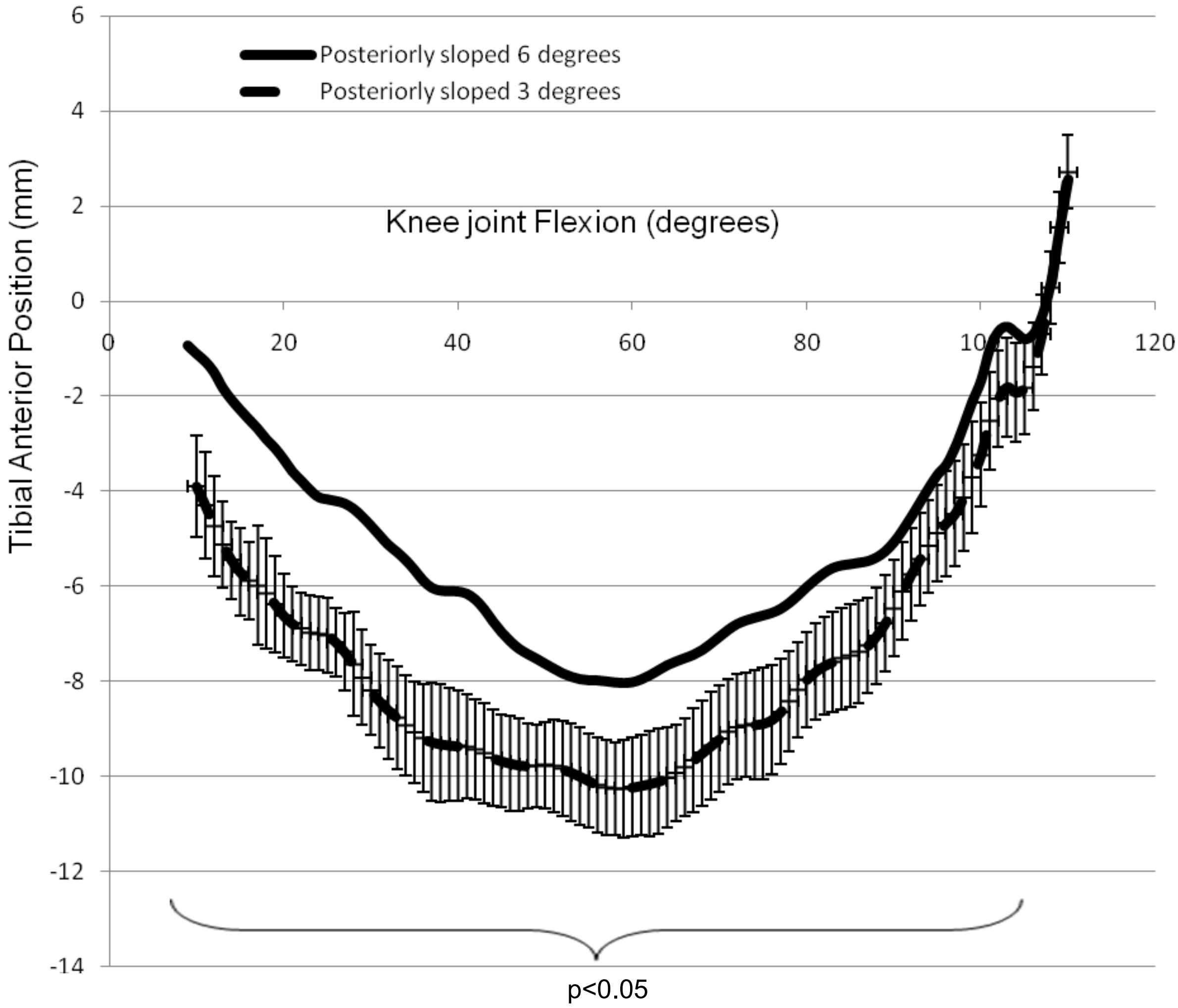

Figure 144: Tibial AP position versus knee joint flexion comparing the neutral AP pathway between 3º posterior sloped knee and the 6º posterior sloped knee.
[n=8, mean ±95% CI of difference between the 3º posterior sloped and the 6º posterior sloped knees.

Following the addition of an extra 3º of posterior slope, from 3º to 6º (figure 144), there was a statistically significant average 1.5 mm anterior translation (2 mm max) in the neutral AP pathway, to a more anterior position, throughout the full range of knee flexion ($p<0.05$). It is suggested that the posterior slope applied to the tibial tray generated a resultant anterior thrust and reduced the upslope of the polyethylene insert posteriorly. This thrust, along with unloading of the soft tissues and resistance to motion posteriorly allows the anterior translation observed.

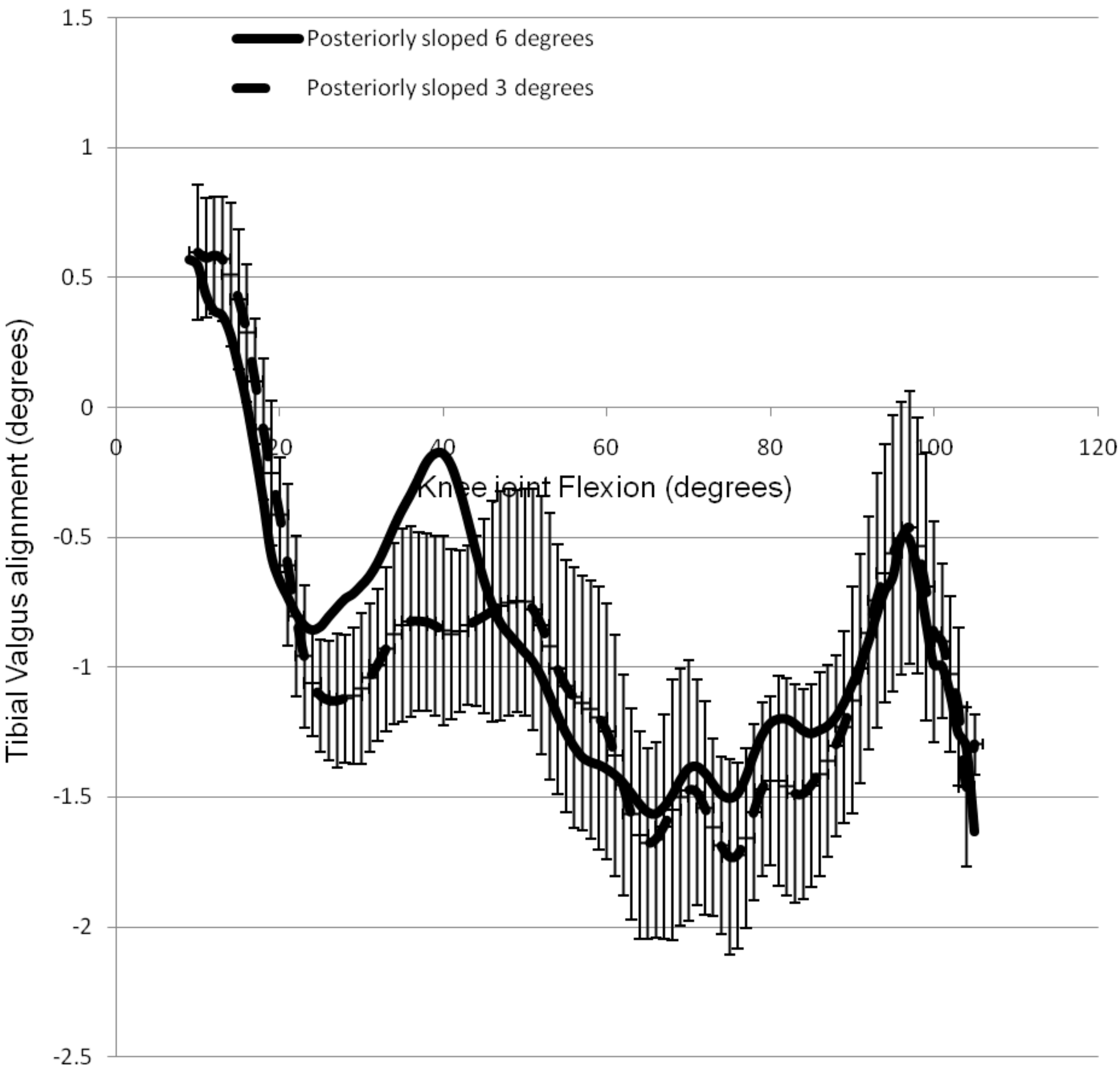

Figure 145: Tibial varus / valgus alignment versus knee joint flexion comparing the neutral varus / valgus pathway between the 3º posterior sloped knee and the 6º posterior sloped knee.
[n=8, mean ±95% CI of difference between the 3º posterior sloped and the 6º posterior sloped knees.

Following the addition of an extra 3º of posterior slope, from 3º to 6º (figure 145), there were no statistically significant changes in the varus-valgus pathway between the knees.

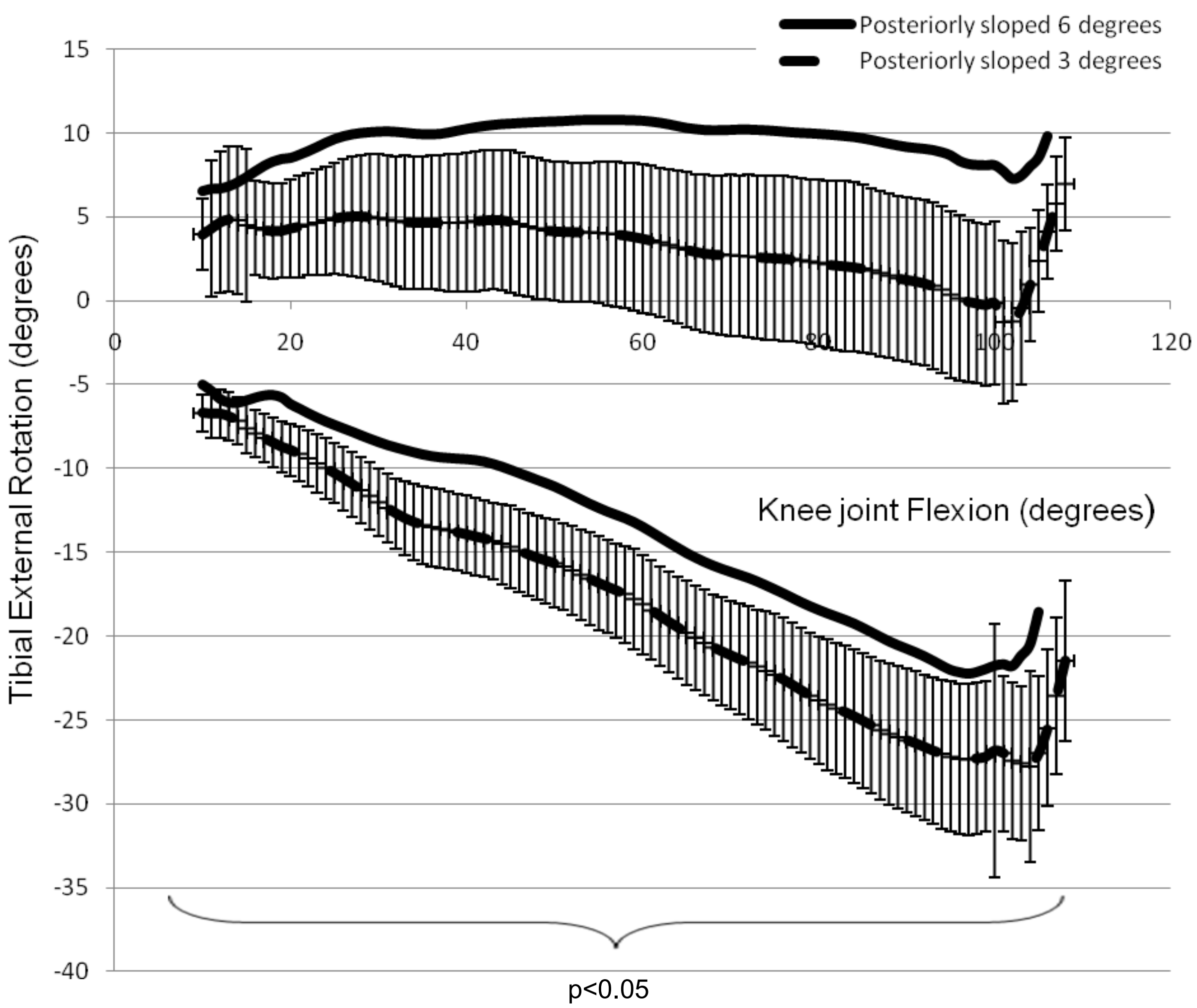

Figure 146: Tibial rotation versus knee joint flexion comparing the rotation envelope of laxity between the 3º posterior sloped knee and the 6º posterior sloped knee.
[n=8, mean ±95% CI of difference between the 3º posterior sloped and the 6º posterior sloped knees.

Following the addition of an extra 3º of posterior slope, from 3º to 6º (figure 146), there was an average 5º translation (9º max) in the external rotation limit of the envelope of laxity with a translation towards external rotation ($p<0.05$). There was also a statistically significant average translation of 4º (7º max) in the internal rotation limit towards external rotation though out the full range of knee flexion ($p<0.05$). Thus overall, the increased slope pushed the envelope of laxity towards internal rotation.

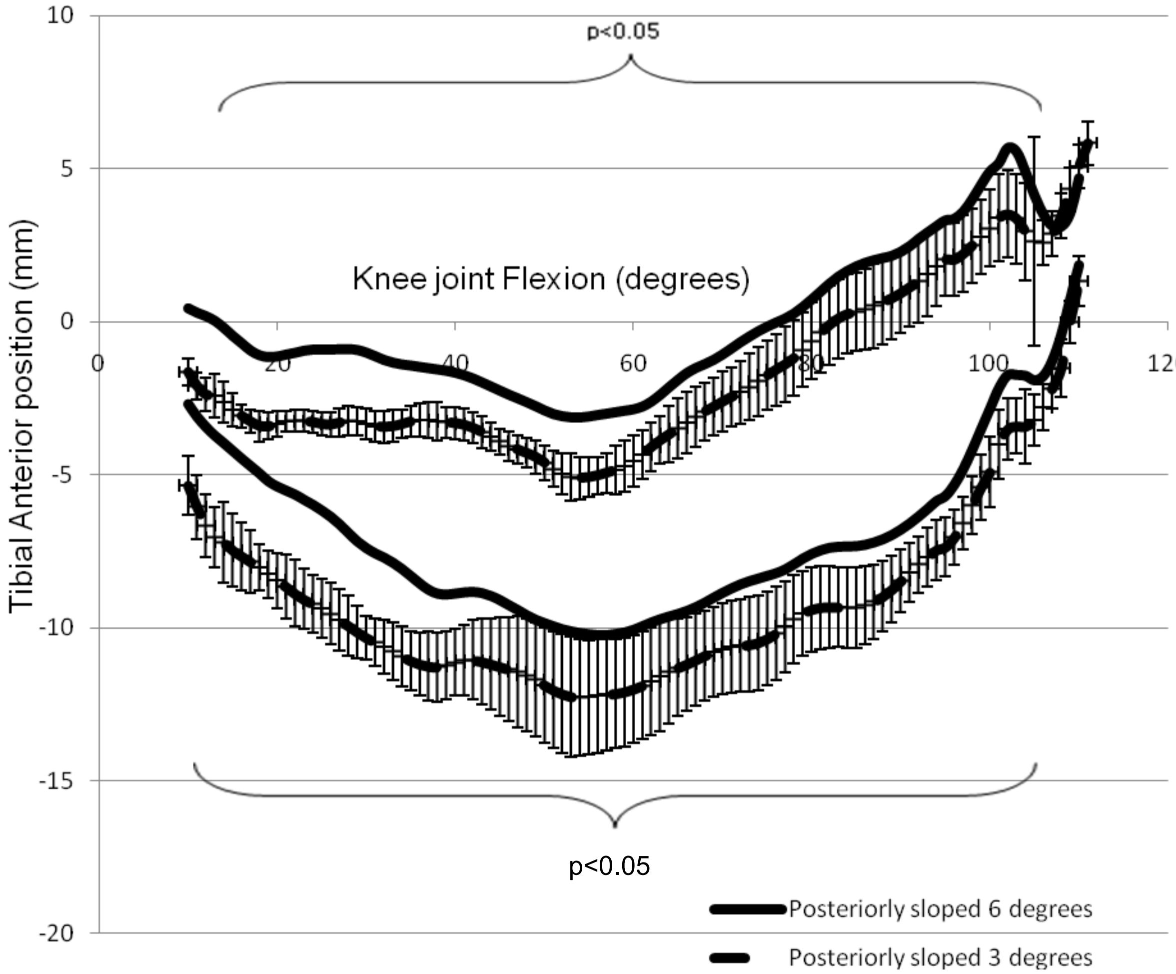

Figure 147: Tibial AP position versus knee joint flexion comparing the AP envelope of laxity between the 3º posterior sloped knee and the 6º posterior sloped knee.
[n=8, mean ±95% CI of difference between the 3º posterior sloped and the 6º posterior sloped knees.

Following the addition of an extra 3º of posterior slope, from 3º to 6º (figure 147), there was a statistically significant average 2mm anterior translation (max 3 mm) in the AP envelope ($p<0.05$). It is suggested that the posterior slope applied to the tibial tray generated a resultant anterior thrust and reduced the upslope of the polyethylene insert posteriorly. This thrust, along with unloading of the soft tissues and resistance to motion posteriorly allows the anterior translation observed.

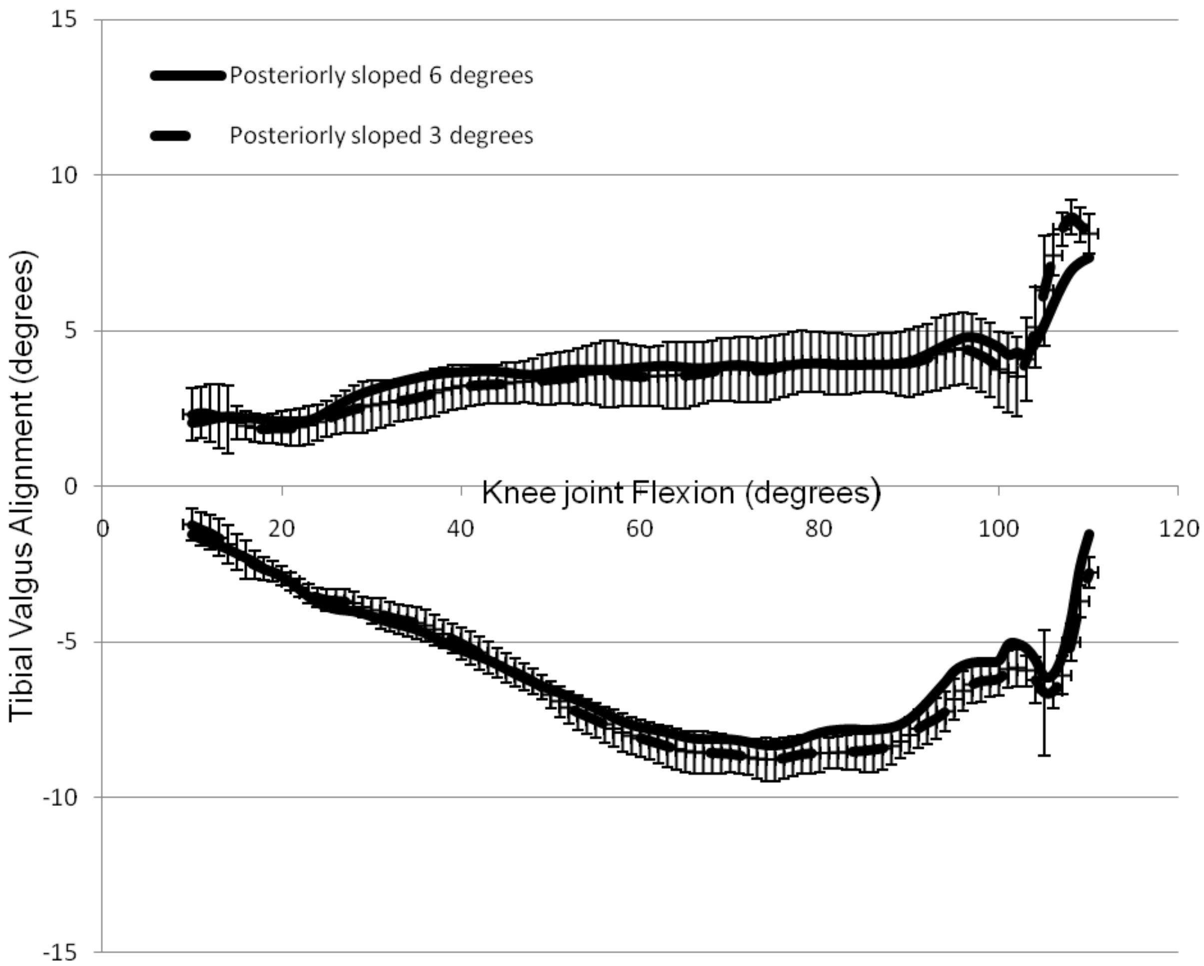

Figure 148: Tibial varus / valgus alignment versus knee joint flexion comparing the varus / valgus envelope of laxity between the 3º posterior sloped knee and the 6º posterior sloped knee.
[n=8, mean ±95% CI of difference between the 3º posterior sloped and the 6º posterior sloped knees.

Following the addition of an extra 3º of posterior slope, from 3º to 6º (figure 148), there were no significant changes in the varus and valgus limits of laxity.

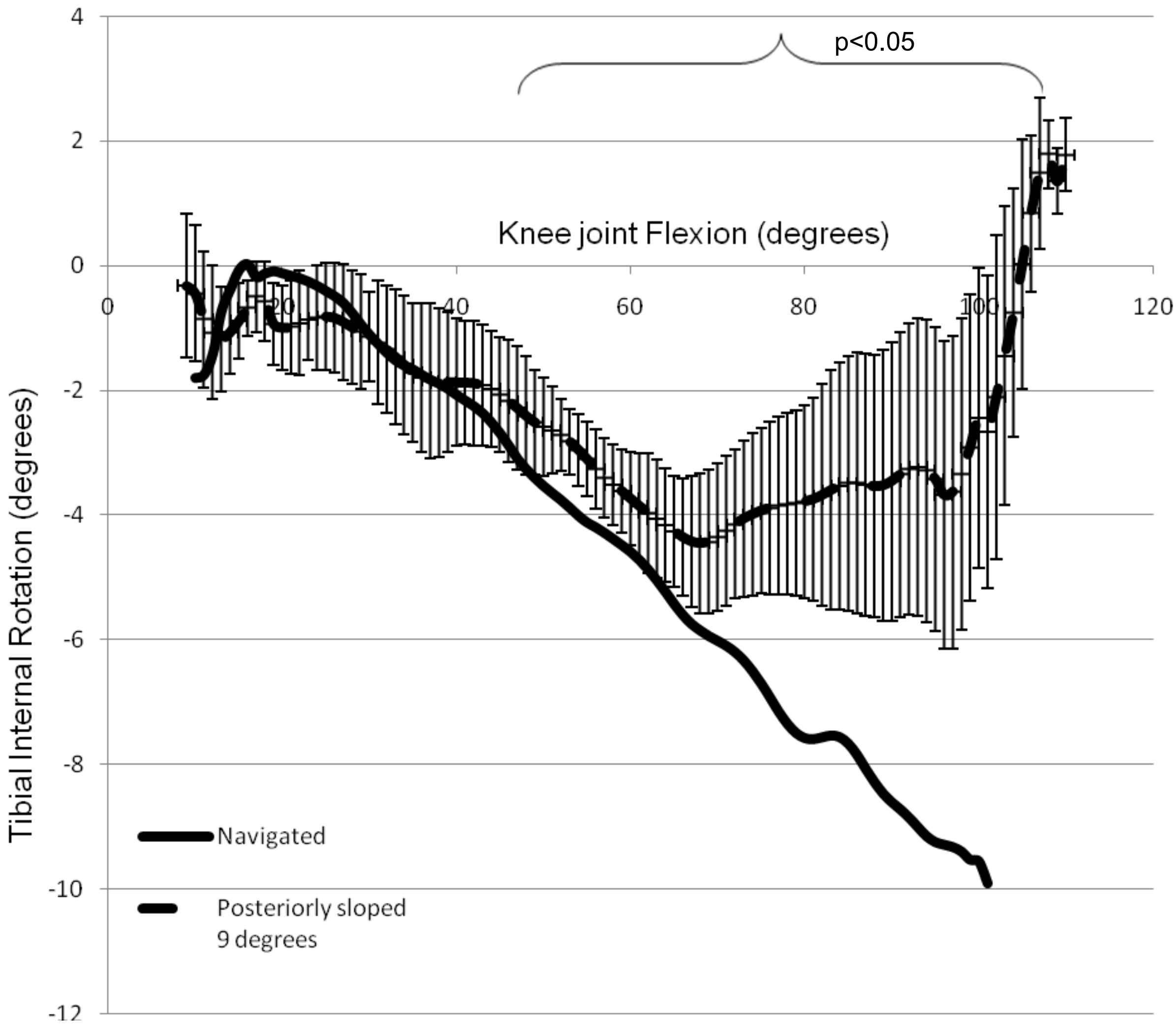

Figure 149: Tibial rotation versus knee joint flexion comparing the neutral rotation pathway between the navigated knee and 9º posterior sloped knee.
[n=8, mean ±95% CI of difference between the navigated and 9º posterior sloped knees.

Following the addition of 9º of posterior slope (figure 149), there was an increasing translation in the neutral rotation pathway towards external rotation in deep flexion, resulting in a neutralisation and reversal of the rotation pathway that was statistically significant between 70º and 110º ($p<0.05$). It is suggested, that the extreme posterior slope applied to the tibial tray has generated a resultant anterior thrust. This thrust, along with unloading of the soft tissues posteriorly allows the neutralisation of the rotation pathway observed.

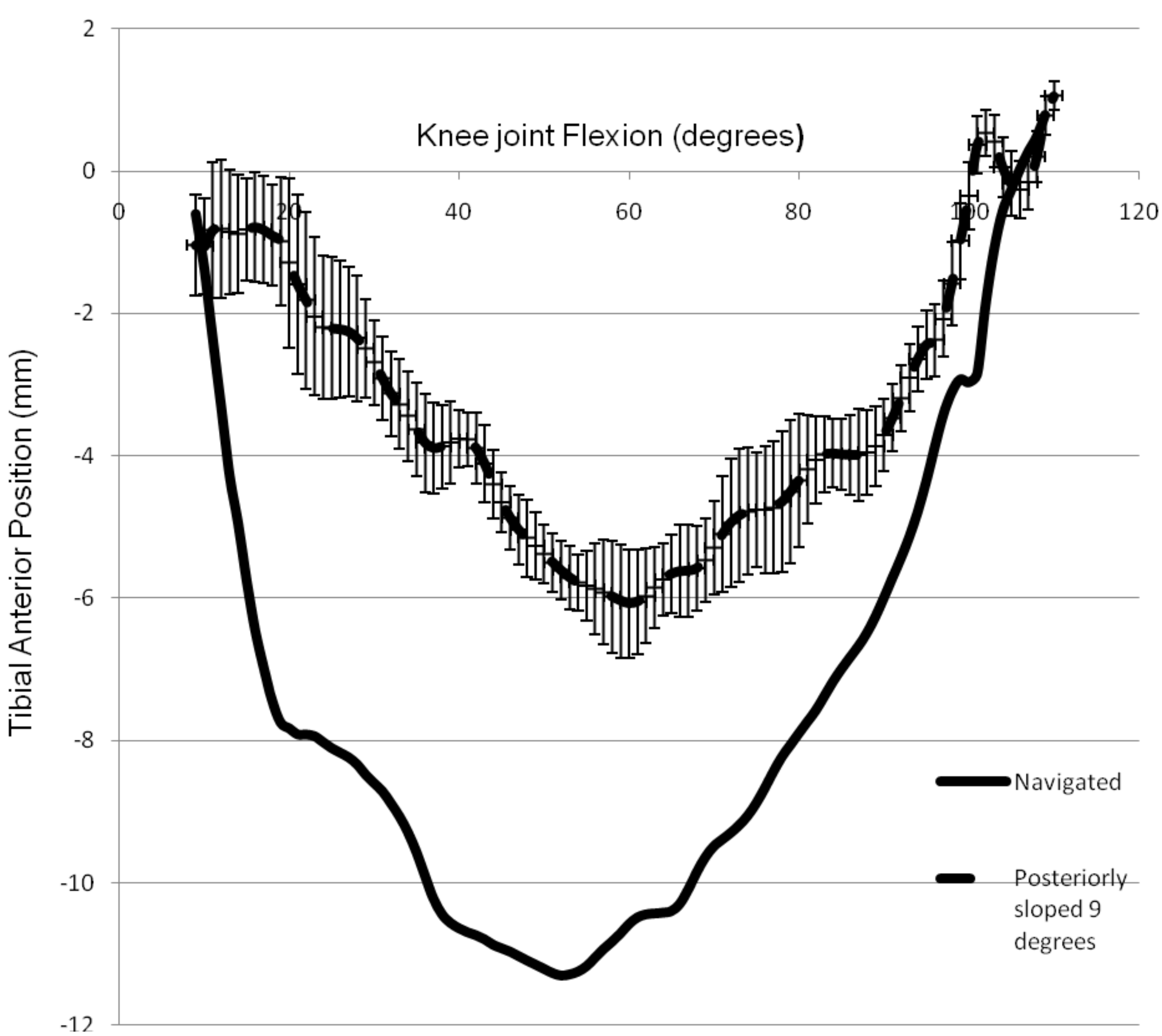

Figure 150: Tibial AP position versus knee joint flexion comparing the neutral AP pathway between the navigated knee and 9º posterior sloped knee.
[n=8, mean ±95% CI of difference between the navigated and 9º posterior sloped knees.

Following the addition of 9º of posterior slope (figure 150), there was a statistically significant average 4mm anterior translation (6mm max) in the neutral AP pathway ($p<0.05$). It is suggested that the extreme posterior slope applied to the tibial tray has generated a resultant anterior thrust, that combined with the reduced upslope of the polyethylene insert posteriorly and the unloading of the soft tissues allows the anterior translation observed.

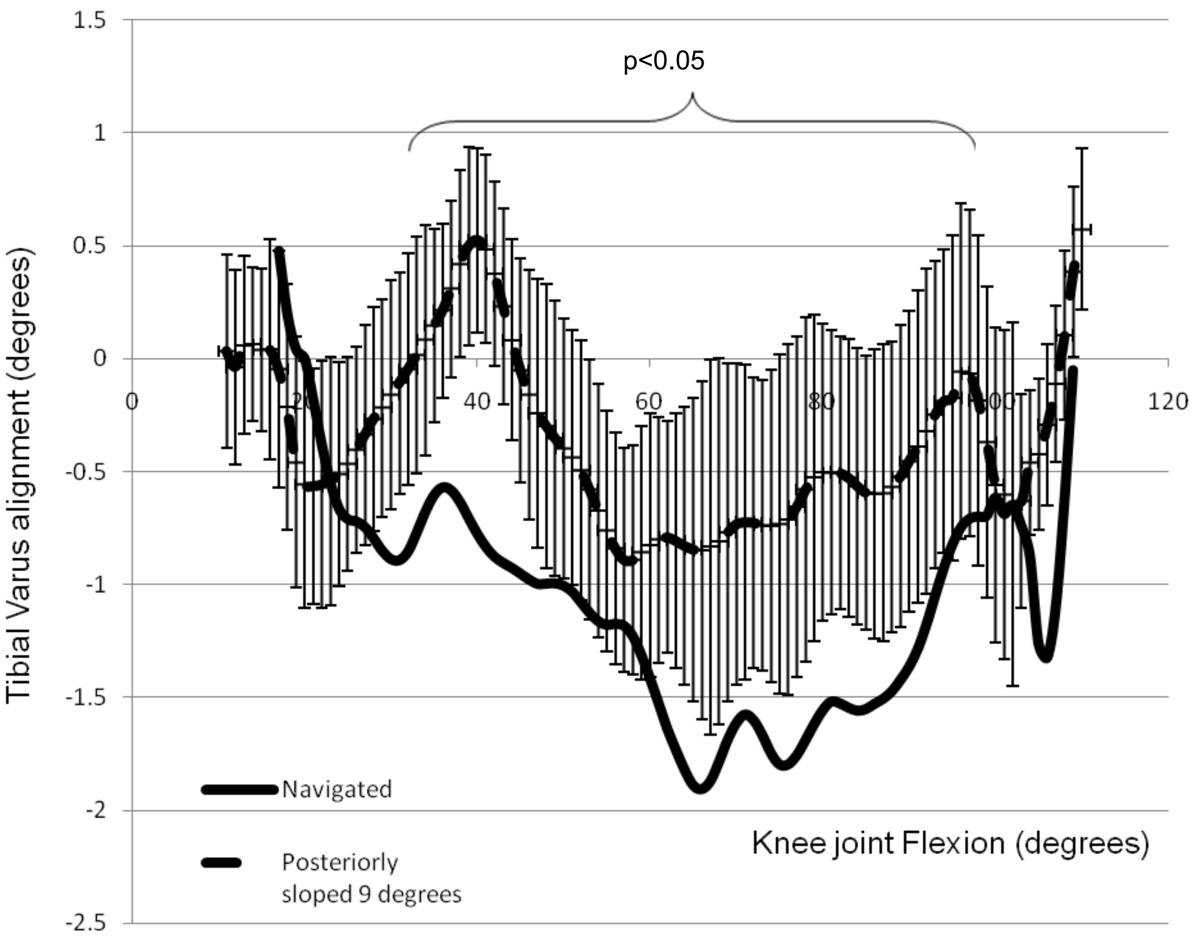

Figure 151: Tibial varus / valgus alignment versus knee joint flexion comparing the neutral varus / valgus pathway between the navigated knee and 9º posterior sloped knee.
[n=8, mean ±95% CI of difference between the navigated and 9º posterior sloped knees.

Following the addition of 9º of posterior slope (figure 151), there was an average 0.5º translation (1º max) in the neutral varus / valgus pathway towards valgus. This translation was statistically significant between 30º and 90º of knee flexion ($p<0.05$). It is suggested that the posterior slope of the tibia may have allowed for some extra knee laxity, resulting in a valgus translation in mid to deep flexion.

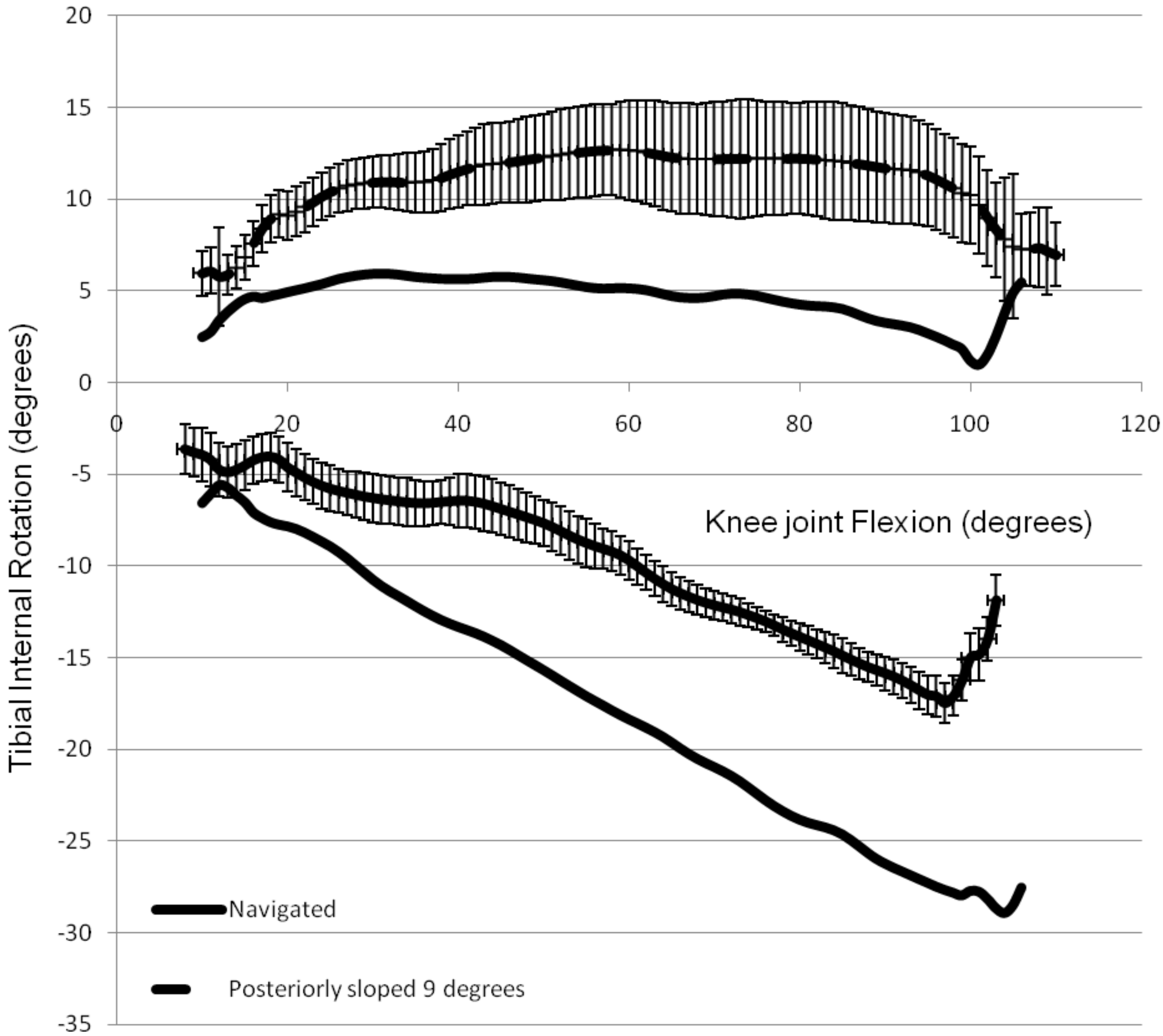

Figure 152: Tibial rotation versus knee joint flexion comparing the rotation envelope of laxity between the navigated knee and 9º posterior sloped knee.
[n=8, mean ±95% CI of difference between the navigated and 9º posterior sloped knees.

Following the addition of 9º of posterior slope (figure 152), there was a statistically significant average 5º translation (8º max) towards external rotation in the external rotation envelope ($p<0.05$). There was also a statistically significant average translation of 7º (10º max) in the internal rotation envelope towards external rotation ($p<0.05$). It is suggested that this translation is due to the extra laxity generated from the extreme posterior slope of the tibial tray.

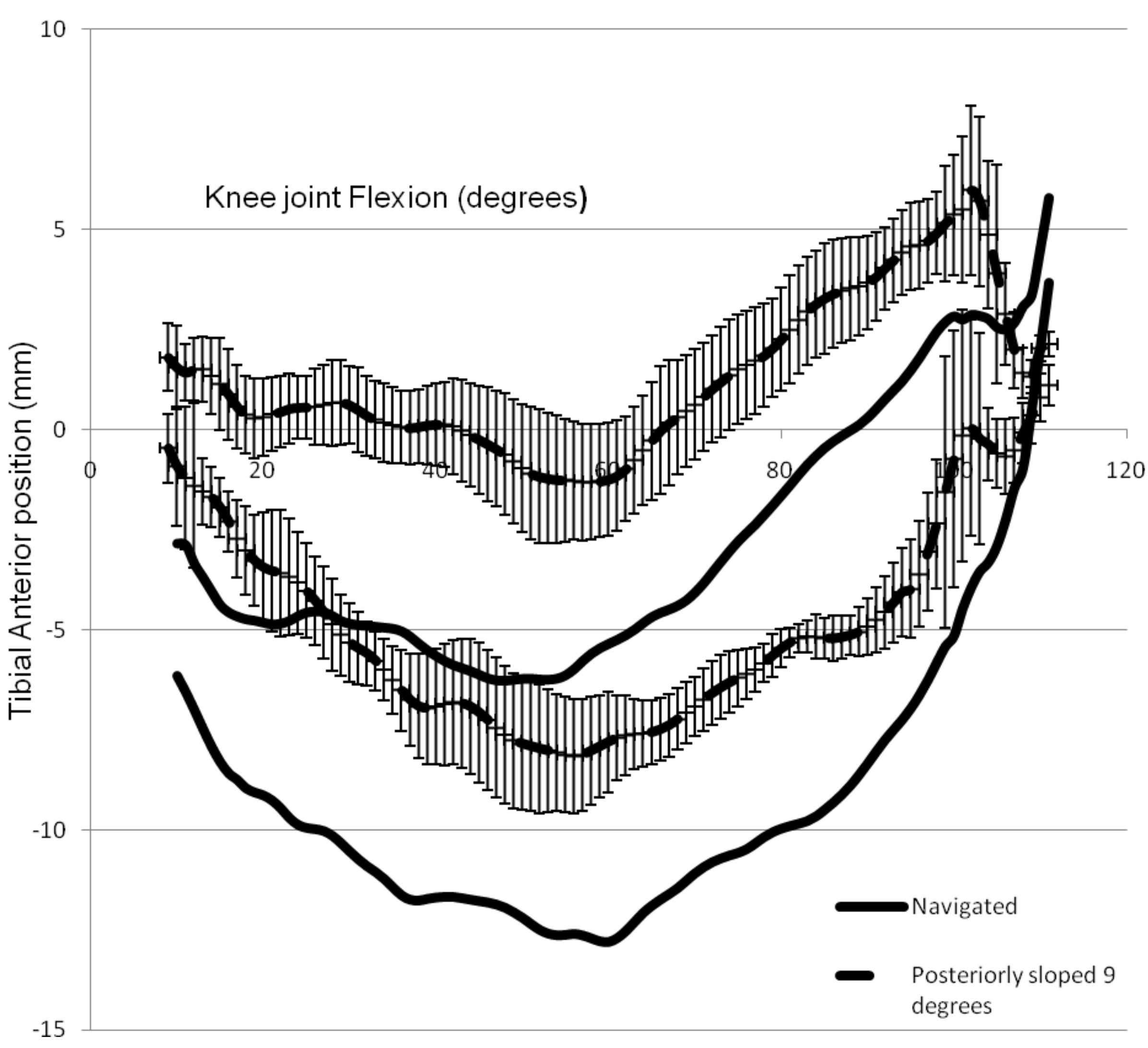

Figure 153: Tibial AP position versus knee joint flexion comparing the AP envelope of laxity between the navigated knee and 9º posterior sloped knee.
[n=8, mean ±95% CI of difference between the navigated and 9º posterior sloped knees.

Following the addition of 9º of posterior slope (figure 153), there was a statistically significant average 4mm translation (max 6mm) in both the anterior and posterior limits of the AP envelope through the whole range of knee flexion ($p<0.05$). It is suggested, that the extreme posterior slope applied to the tibial tray has generated a resultant anterior thrust, that combined with the reduced upslope of the polyethylene insert posteriorly and the unloading of the soft tissues allows the anterior translation observed.

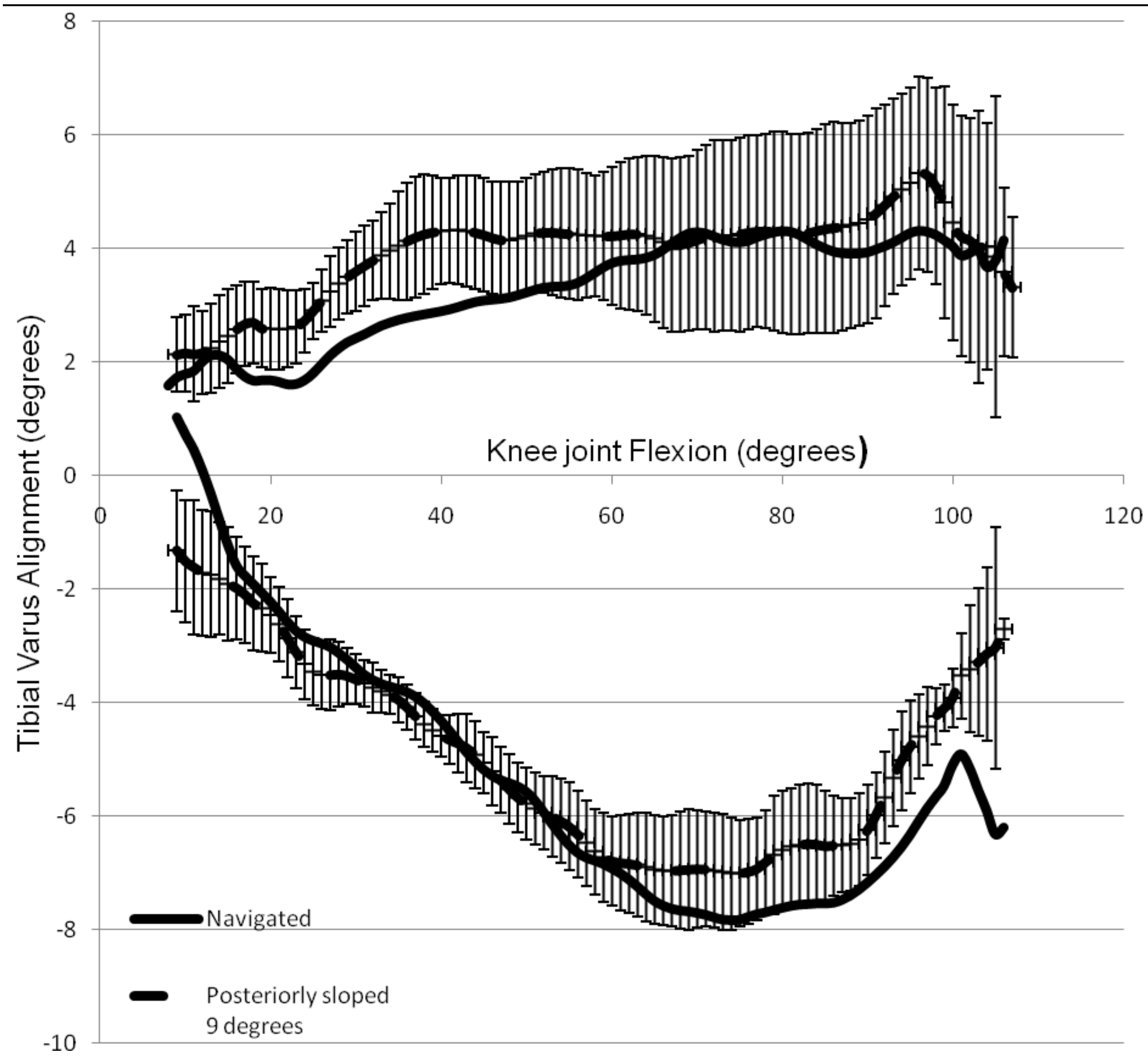

Figure 154: Tibial varus / valgus alignment versus knee joint flexion comparing the varus / valgus envelope of laxity between the navigated knee and 9º posterior sloped knee.
[n=8, mean ±95% CI of difference between the navigated and 9º posterior sloped knees.

Following the addition of 9º of posterior slope (figure 154), there were no significant changes in the varus and valgus limits of the envelope of laxity.

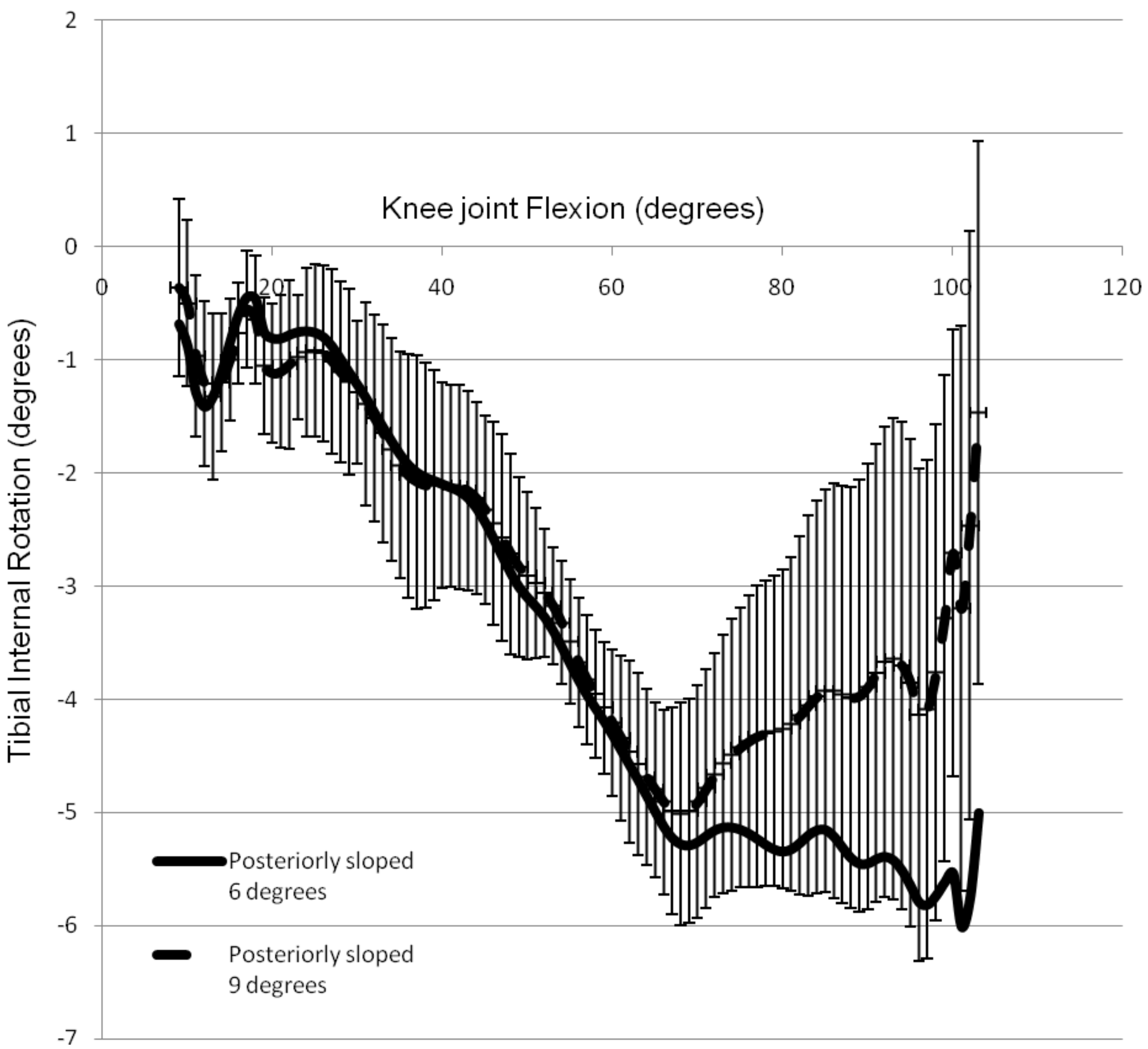

Figure 155: Tibial rotation versus knee joint flexion comparing the neutral rotation pathway between the 6º posterior sloped knee and the 9º posterior sloped knee.
[n=8, mean ±95% CI of difference between the 6º posterior sloped and the 9º posterior sloped knees.

Following the addition of an extra 3º of posterior slope from 6º to 9º (figure 155), there was an average 2º translation (4º max) in the neutral rotation pathway towards external rotation in deep flexion, but this difference was not statistically significant.

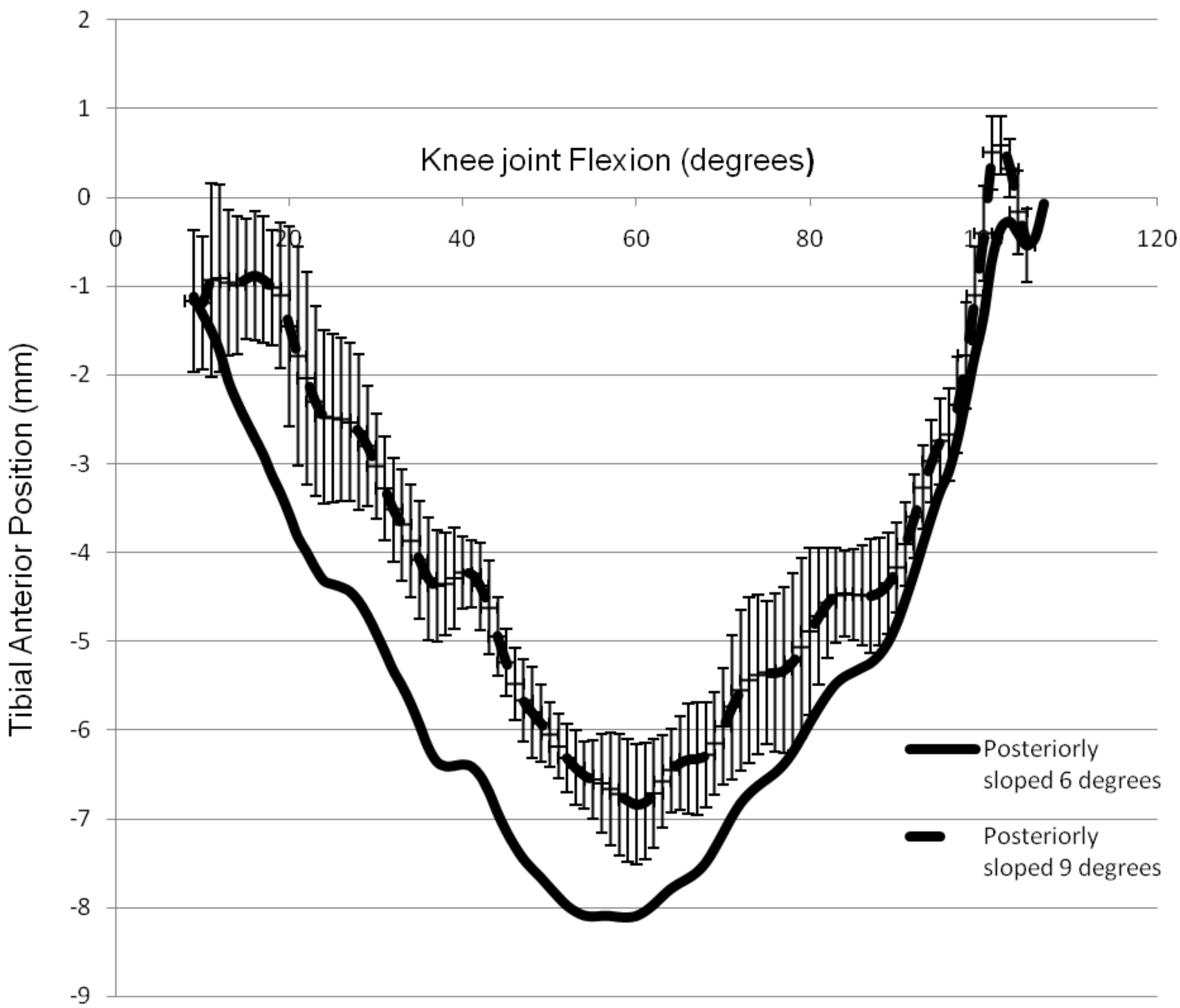

Figure 156**:** Tibial AP position versus knee joint flexion comparing the neutral AP pathway between the 6º posterior sloped knee and the 9º posterior sloped knee.
[n=8, mean ±95% CI of difference between the 6º posterior sloped and the 9º posterior sloped knees.

Following the addition of an extra 3º of posterior slope from 6º to 9º (figure 156), there was a statistically significant average 1.5 mm anterior translation (2.5 mm max) in the neutral AP pathway ($p<0.05$). It is suggested that the increasing posterior slope applied to the tibial tray generated a resultant anterior thrust and reduced the upslope of the polyethylene insert posteriorly. This thrust, along with unloading of the soft tissues and resistance to motion posteriorly allowed the increasing anterior translation observed.

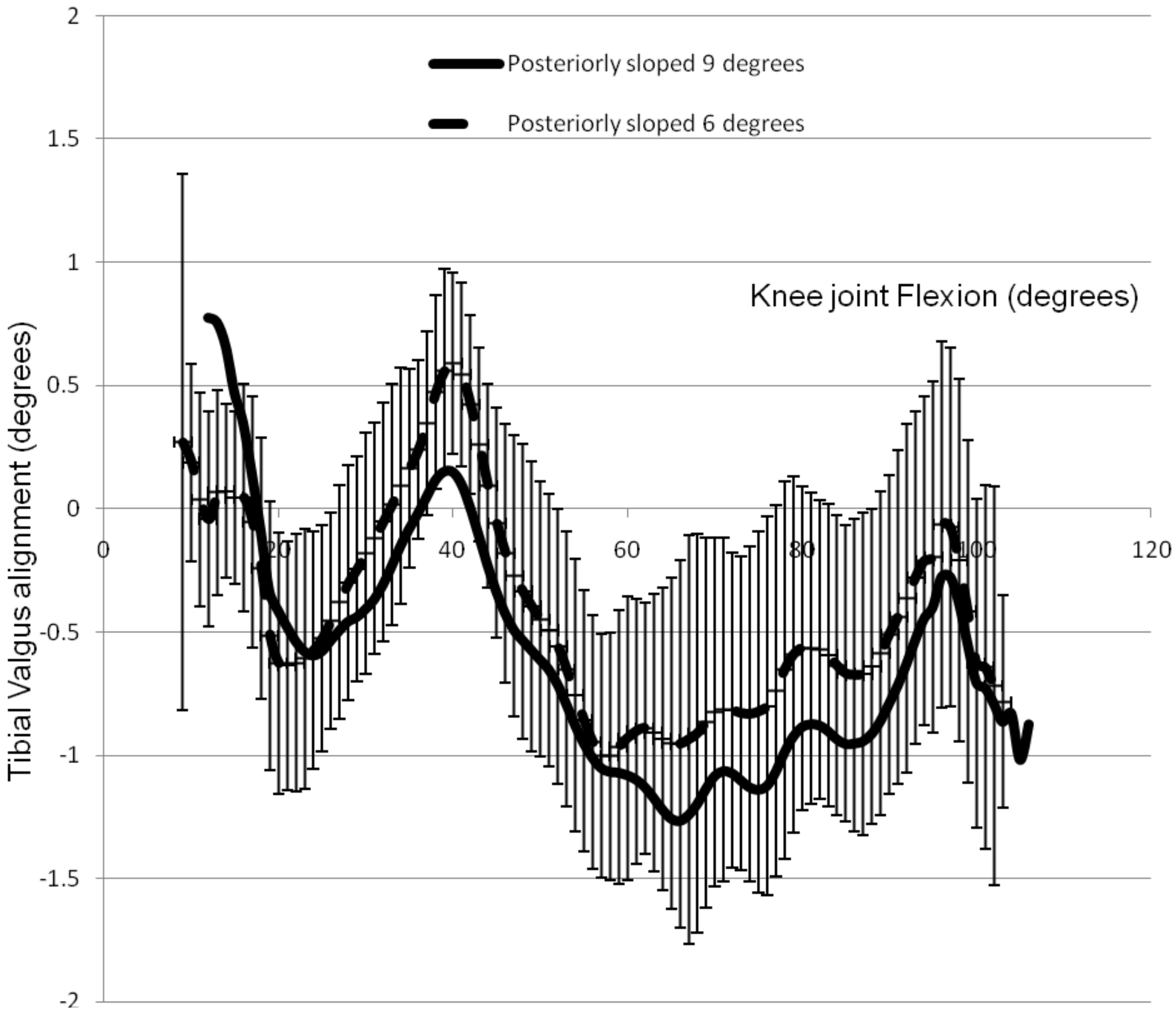

Figure 157: Tibial varus / valgus alignment versus knee joint flexion comparing the neutral varus / valgus pathway between the 6º posterior sloped knee and the 9º posterior sloped knee.
[n=8, mean ±95% CI of difference between the 6º posterior sloped and the 9º posterior sloped knees.

Following the addition of an extra 3º of posterior slope, from 6º to 9º (figure 157), there was no difference in the neutral varus / valgus pathway of the two series.

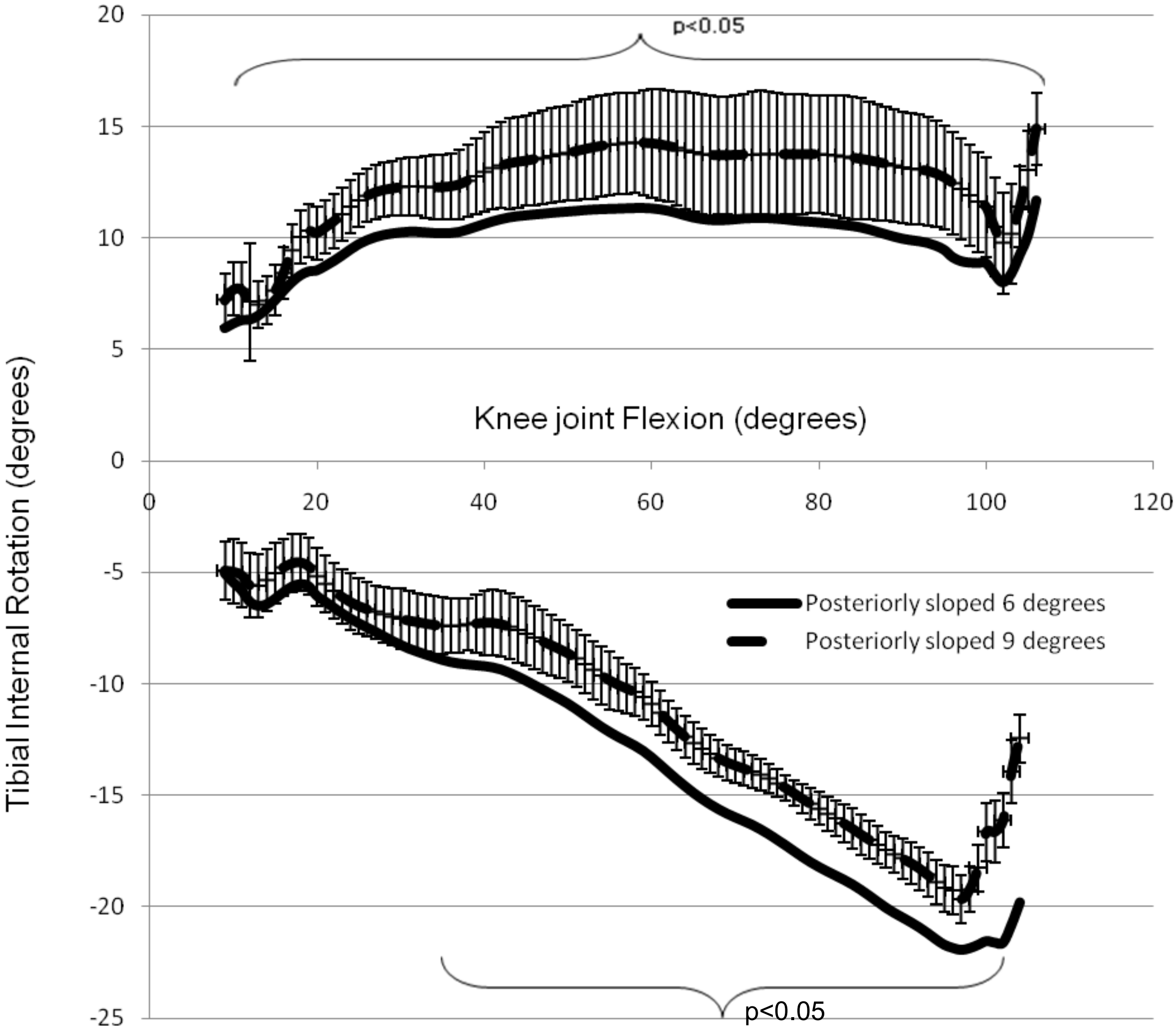

Figure 158: Tibial rotation versus knee joint flexion comparing the rotation envelope of laxity between the 6º posterior sloped knee and the 9º posterior sloped knee.
[n=8, mean ±95% CI of difference between the 6º posterior sloped and the 9º posterior sloped knees.

Following the addition of an extra 3º of posterior slope from 6º to 9º (figure 158), there was a statistically significant average 2.5º translation (4º max) in the external rotation limit of the envelope towards further external rotation throughout the range of knee flexion ($p<0.05$). There was also a statistically significant average translation of 1.5º (3º max) in the internal rotation limit of the envelope towards external rotation though out the full range of knee flexion ($p<0.05$). It is suggested that the rotation limit had already been reached at 6º posterior slope and therefore there was no further movement when compared to 9º.

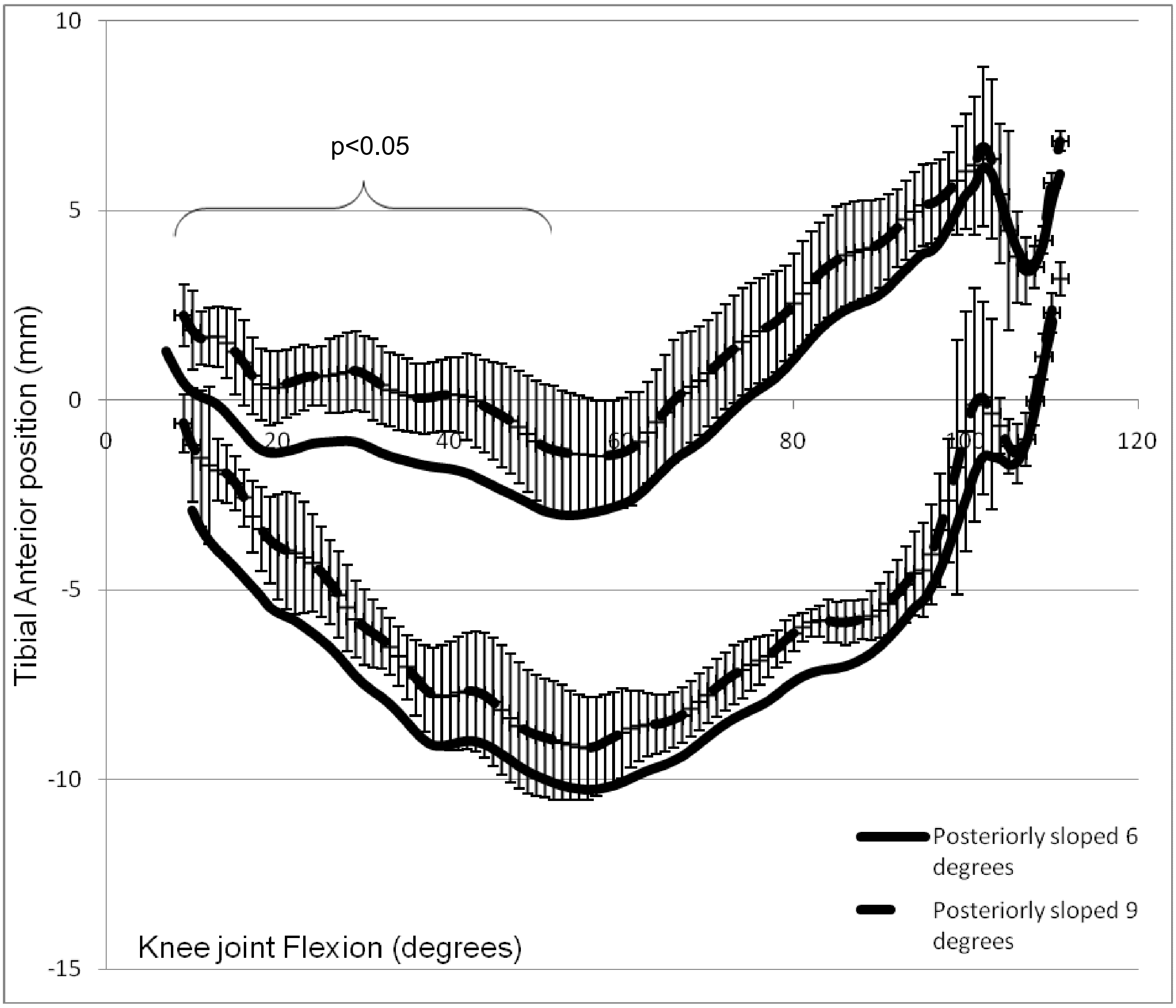

Figure 159: Tibial AP position versus knee joint flexion comparing the AP envelope of laxity between the 6º posterior sloped knee and the 9º posterior sloped knee.

[n=8, mean ±95% CI of difference between the 6º posterior sloped and the 9º posterior sloped knees.

Following the addition of an extra 3º of posterior slope from 6º to 9º (figure 159), there was a statistically significant average 2mm (4mm max) anterior translation of the anterior limit of the AP envelope of laxity between 5º and 50º of knee flexion ($p<0.05$). There was also a statistically significant average 2mm (4mm max) anterior translation of the posterior limit throughout the whole range of knee flexion ($p<0.05$). It is suggested that the 9º posteriorly sloped tibial tray generated more anterior thrust compared to the 6º slope tibial tray. This additional thrust, along with further unloading of the soft tissues posteriorly allowed the extra anterior translation observed.

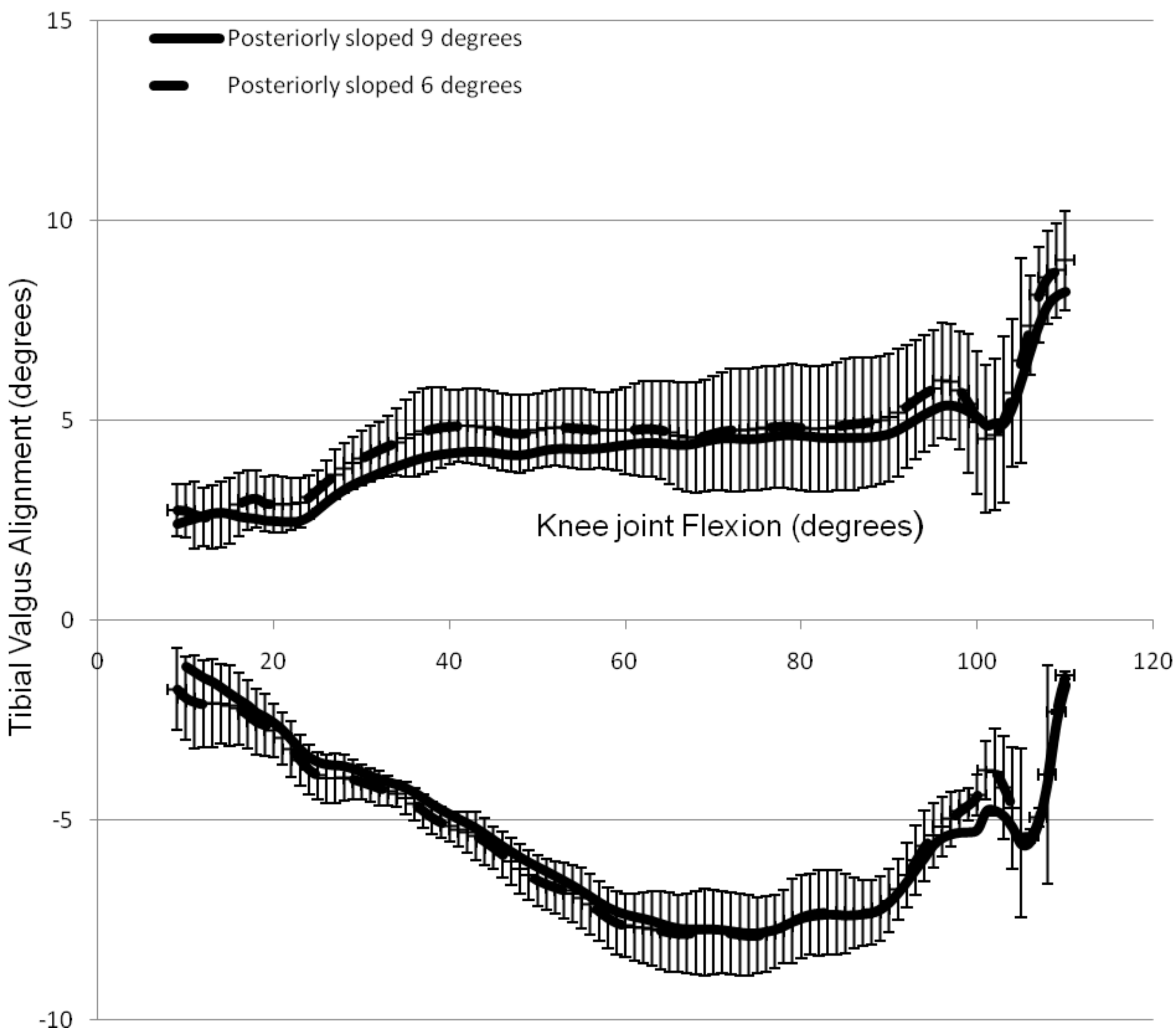

Figure 160: Tibial varus / valgus alignment versus knee joint flexion comparing the varus / valgus envelope of laxity between the 6º posterior sloped knee and the 9º posterior sloped knee.
[n=8, mean ±95% CI of difference between the 6º posterior sloped and the 9º posterior sloped knees.

Following the addition of an extra 3º of posterior slope from 6º to 9º (figure 160), there was no difference in the envelope of varus / valgus laxity.

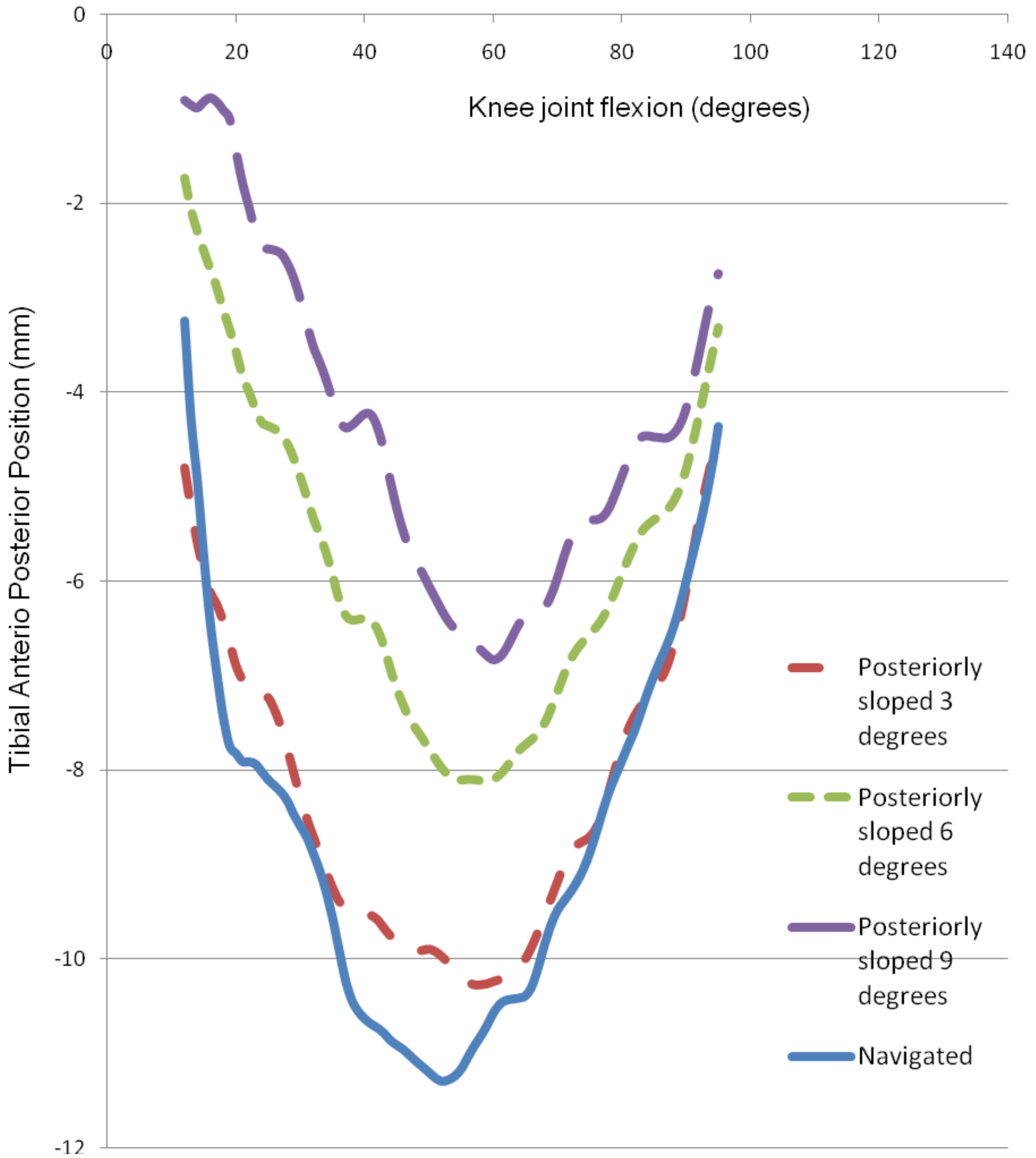

Figure 161: Tibial AP position versus knee joint flexion comparing the neutral AP pathway between the navigated knee component position and the 3,6, and 9 degree posteriorly sloped component positions.
[n=8, mean ±95% CI of difference between navigated and posteriorly sloped implants]

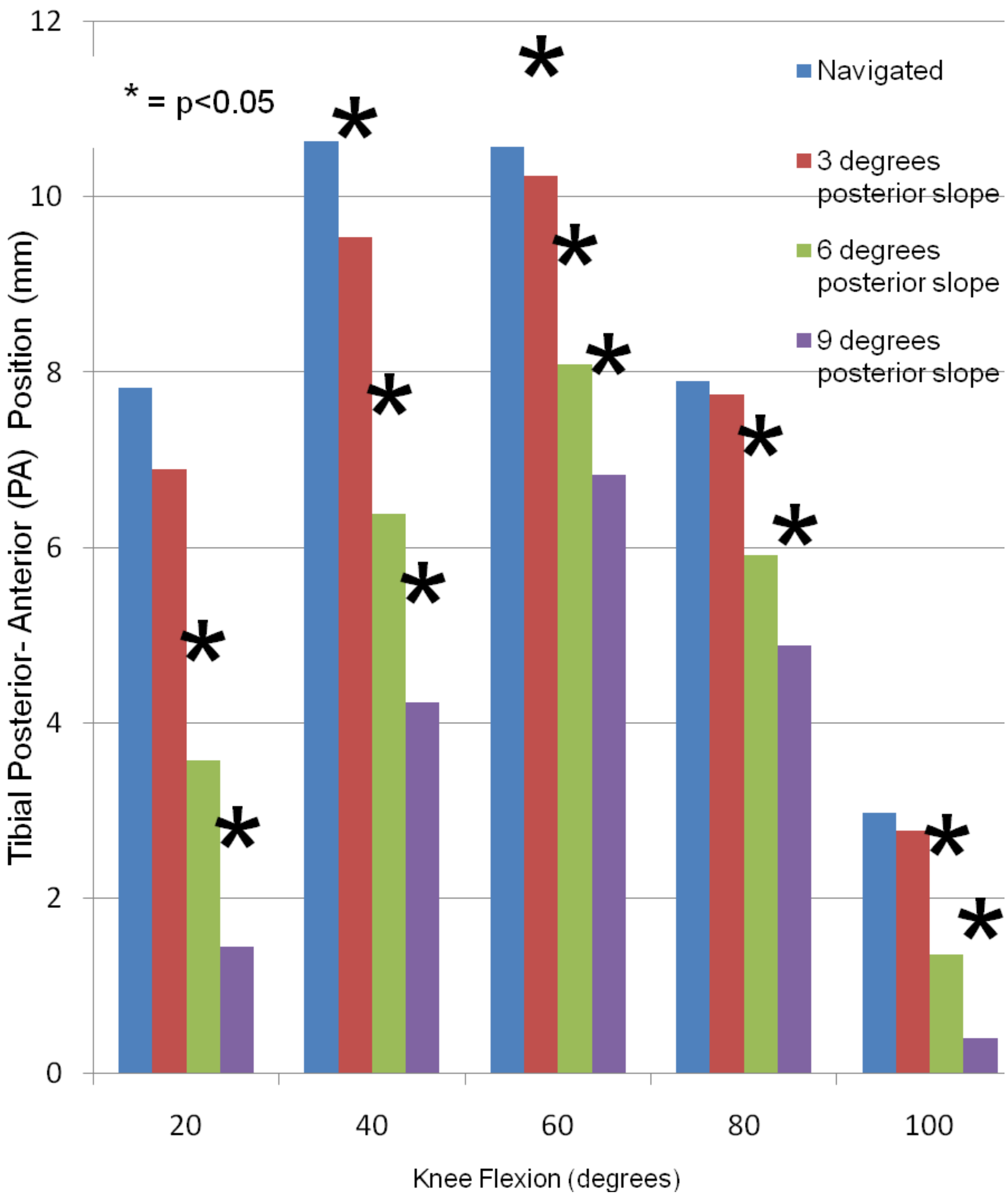

Figure 162: : Tibial AP position versus knee joint flexion comparing the neutral AP pathway between the navigated knee component position and the 3,6, and 9 degree posteriorly sloped component positions.
[n=8, mean ±95% CI of difference between navigated and posteriorly sloped implants]

When comparing all the posteriorly sloped implants to the navigated implants (figure 161 & 162), there was a significant differences in the neutral path of AP motion between the navigated knee and the 3 degree posteriorly sloped component between 40 and 60 degrees of knee flexion ($p<0.05$). There was a significant difference in the neutral path of AP motion between the navigated knee and the 6 and 9 degree posterior sloped implants, as well as between the 3 and 6, and the 6 and 9 degree posteriorly sloped implants ($p<0.05$). It was also noted that as the posterior slope increased from the navigated position of 0º to 9º, there was an incremental translation of the tibia anteriorly ($p<0.05$).

With regard to the rotational pathways and rotational envelope of laxity, there was a statistical significant tendency for the knee to move into to external rotation as the posterior slope was increased ($p<0.05$). As expected, the posterior slope had no impact on the varus / valgus pathway and envelope of laxity of the knee.

It is suggested that the posterior slope applied to the tibial tray generated a resultant anterior thrust and reduced the upslope of the polyethylene insert posteriorly. This thrust, along with unloading of the soft tissues and resistance to motion posteriorly allowed the anterior translation and the increasing internal rotation observed.

Combined Misalignment

- Navigated vs. 20º external rotation, 9º posterior slope
- Navigated vs. 20º internal rotation, 9º posterior slope

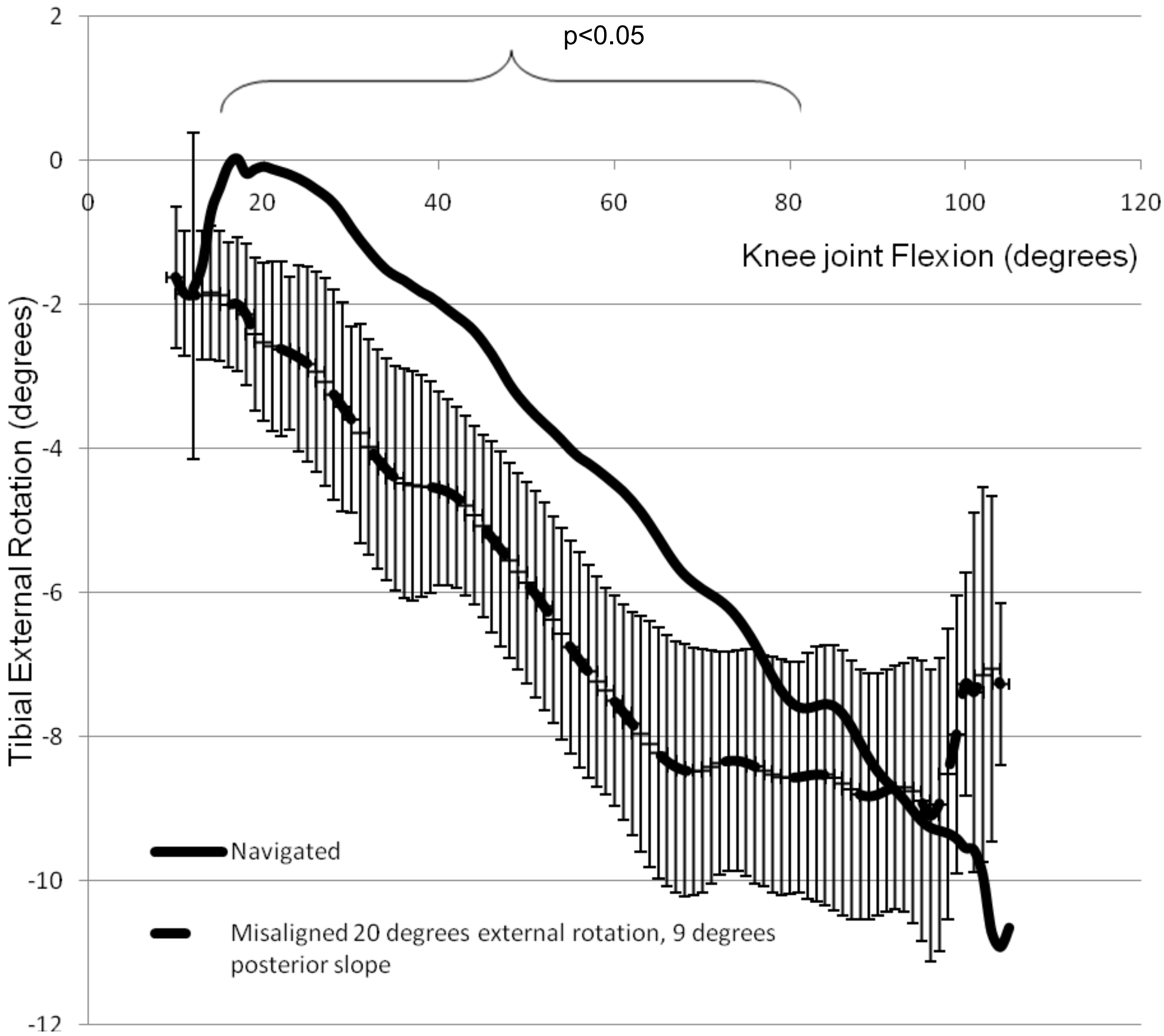

Figure 163: Tibial rotation versus knee joint flexion comparing the neutral rotation pathway between the navigated knee and 20 º externally rotated and 9º posteriorly sloped knee.
[n=7, mean ±95% CI of difference between the navigated and 20 º externally rotated and 9º posteriorly sloped knee.

Following the combined misalignment of 20º external rotation and 9º of posterior slope of the tibial tray component (figure 163), there was a statistically significant average 2º translation (3º max) in the neutral rotation pathway towards external rotation between 20º and 70º of flexion ($p<0.05$). It is suggested that this internal rotation torque was generated by the femoral condyles as they opposed the incongruent articulation with the dished tibial tray. The remainder of the expected internal rotation has been compensated for by the soft tissues and component mal-articulation.

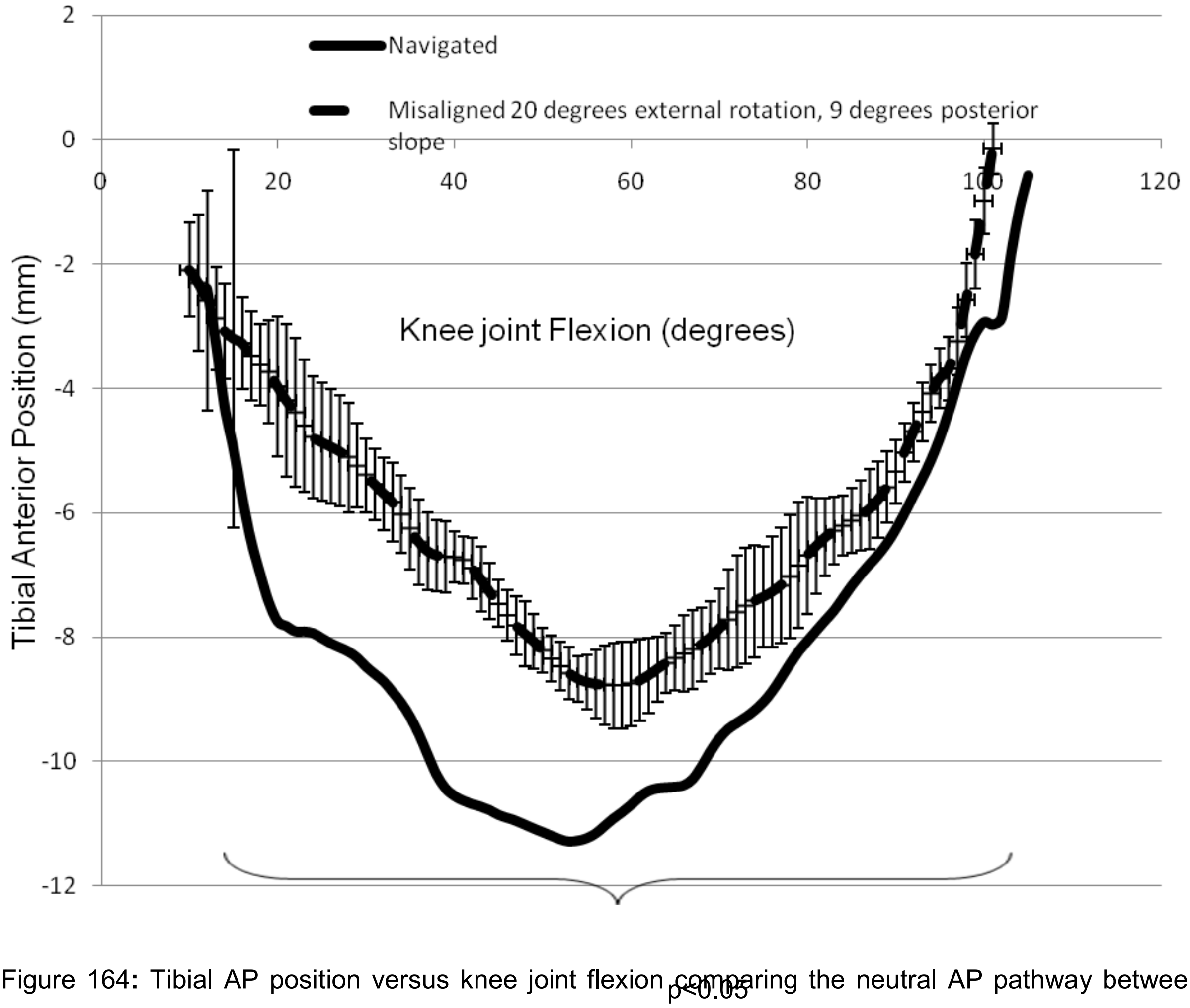

Figure 164: Tibial AP position versus knee joint flexion comparing the neutral AP pathway between the navigated knee and 20 º externally rotated and 9º posteriorly sloped knee.
[n=7, mean ±95% CI of difference between the navigated and 20 º externally rotated and 9º posteriorly sloped knee.

Following the combined misalignment of 20º external rotation and 9º of posterior slope of the tibial tray component (figure 164), there was a significant average 2mm anterior translation (3mm max) in the neutral AP path of motion ($p<0.05$). It is suggested that the posterior slope of the tibial tray generated a resultant anterior thrust. This thrust, along with unloading of the soft tissues posteriorly, caused the anterior translation. However, this translation is small when compared to 9º of posterior slope in isolation. It is suggested that the 20º of external rotation of the tibial tray component has resulted in a rotation of the tibia (against the partially incongruent prosthesis) which has tightened the soft tissues, reducing the knee laxity and dampened down the expected anterior translation.

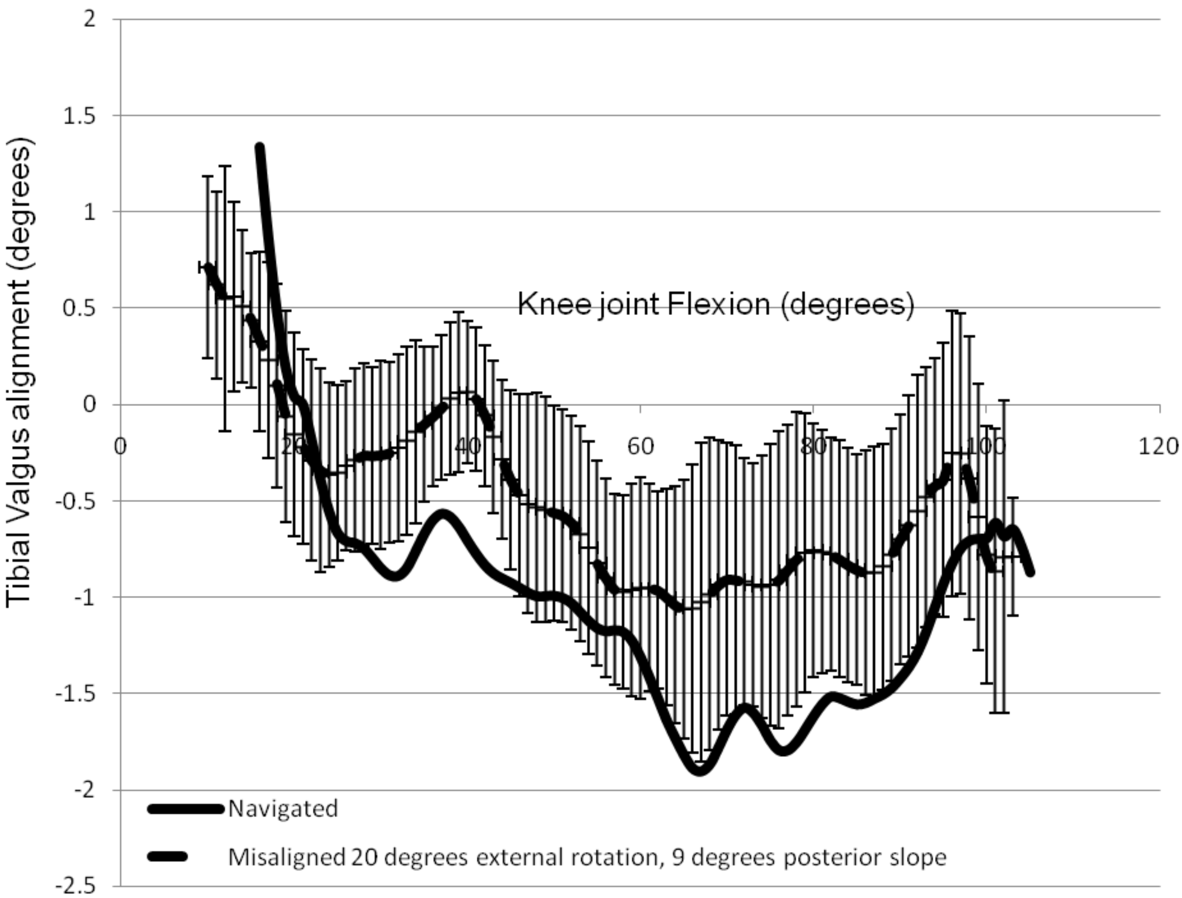

Figure 165: Tibial varus / valgus alignment versus knee joint flexion comparing the neutral varus / valgus pathway between the navigated knee and 20 º externally rotated and 9º posteriorly sloped knee.

[n=7, mean ±95% CI of difference between the navigated and 20 º externally rotated and 9º posteriorly sloped knee.

Following the combined misalignment of 20º external rotation and 9º of posterior slope of the tibial tray component (figure 165), there were no significant observed difference in the neutral varus / valgus pathway between the navigated and misaligned knees.

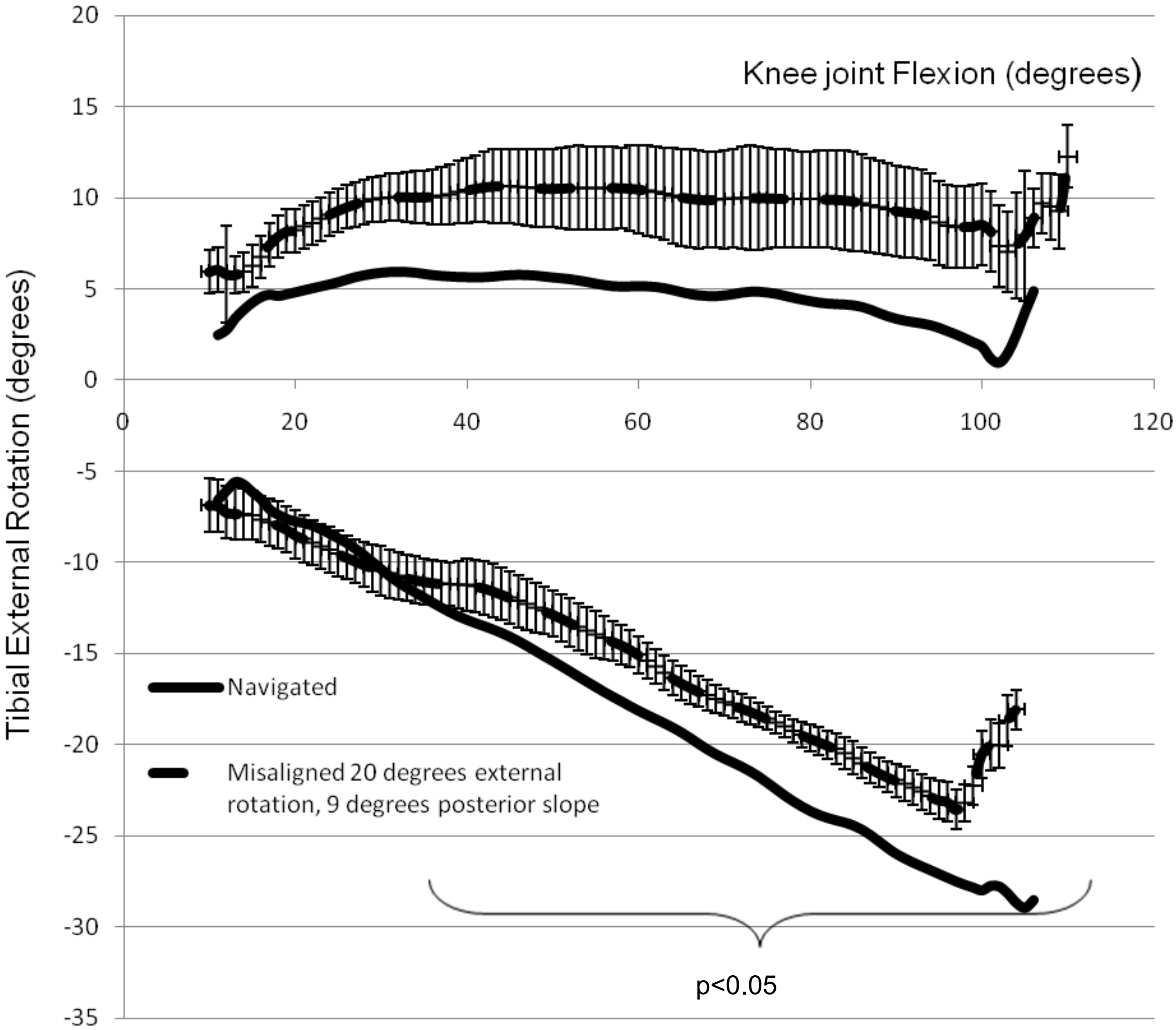

Figure 166: Tibial rotation versus knee joint flexion comparing the rotation envelope of laxity between the navigated knee and 20 ° externally rotated and 9º posteriorly sloped knee.
[n=7, mean ±95% CI of difference between the navigated and 20 ° externally rotated and 9º posteriorly sloped knee.

Following the combined misalignment of 20º external rotation and 9º of posterior slope of the tibial tray component (figure 166), there was an average 4º translation (5º max) towards external rotation in the external rotation envelope ($p<0.05$). There was also a statistically significant average translation of 1.5º (3º max) in the internal rotation limit towards external rotation between 30º and 110º of knee flexion ($p<0.05$). It is suggested, that this translation is due to the extra laxity generated by the posterior slope combined with an external rotation torque generated by the incongruent articulation of the dished tibial tray and the condyles of the femoral prosthesis.

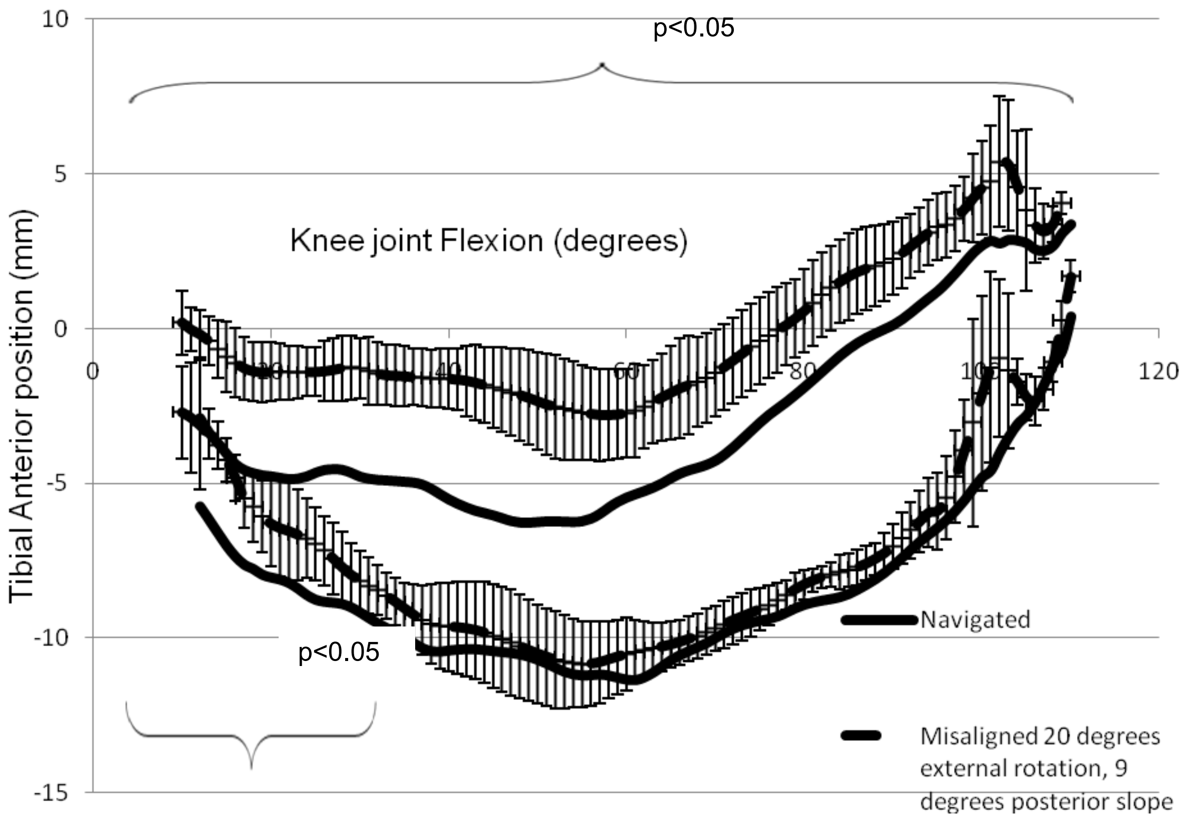

Figure 167: Tibial AP position versus knee joint flexion comparing the AP envelope of laxity between the navigated knee and 20 º externally rotated and 9º posteriorly sloped knee.
[n=7, mean ±95% CI of difference between the navigated and 20 º externally rotated and 9º posteriorly sloped knee.

Following the combined misalignment of 20º external rotation and 9º of posterior slope of the tibial tray component (figure 167), there was significant widening of the envelope of laxity ($p<0.05$), with a significant average 4mm (6mm max) anterior translation in the anterior envelope ($p<0.05$). There was also a significant average 1 mm (1.5 mm max) anterior translation in the posterior envelope between 5º and 40º of knee flexion ($p<0.05$). It is suggested that the posterior slope generated a resultant anterior thrust, which along with unloading of the soft tissues posteriorly, allowed the anterior translation. However, the translation was small when compared to that observed with 9º of posterior slope alone. This can be explained by the 20º of external rotation, which has resulted in a rotation of the tibia (against the partially incongruent prosthesis), tightened the soft tissues and reducing the available laxity, dampening down the expected anterior translation.

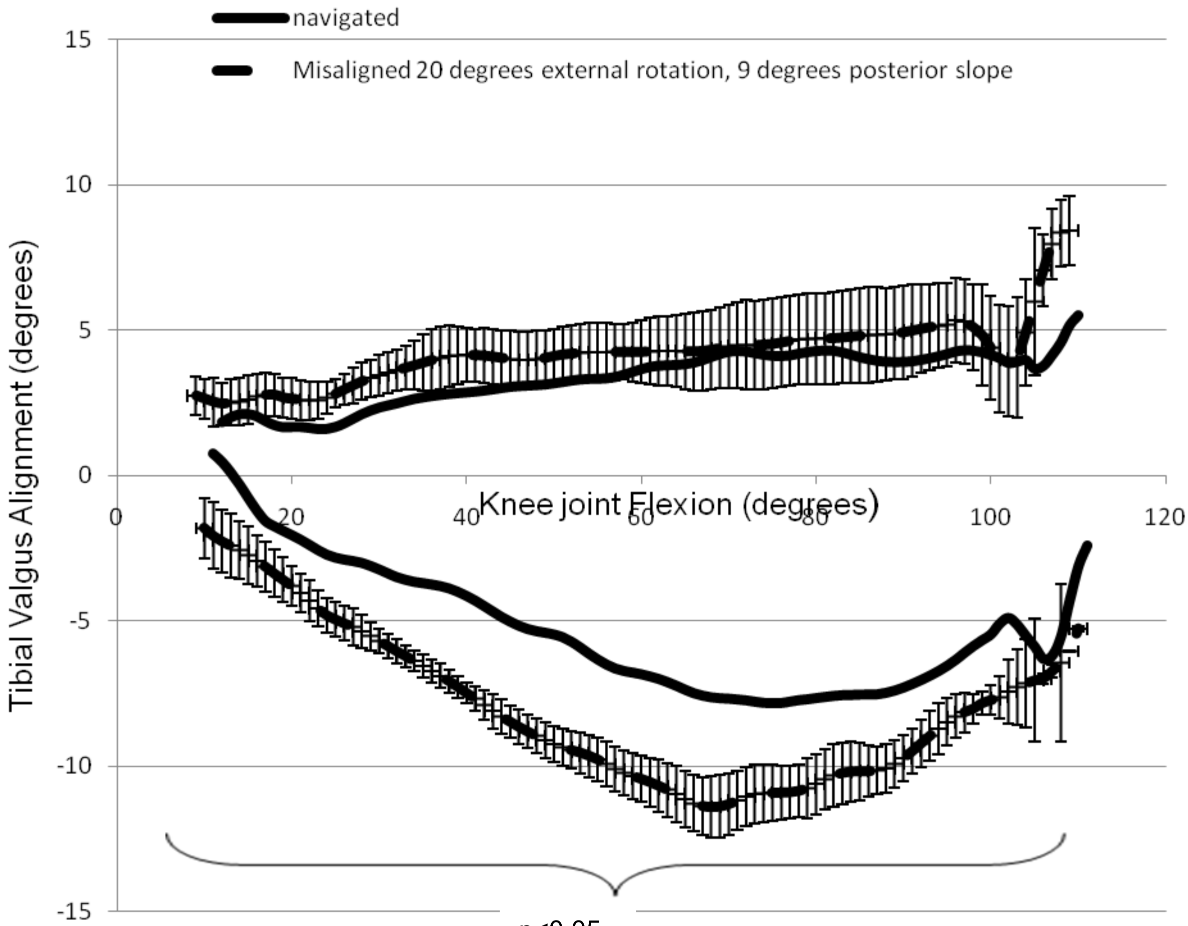

Figure 168: Tibial varus / valgus alignment versus knee joint flexion comparing the varus / valgus envelope of laxity between the navigated knee and 20 ° externally rotated and 9º posteriorly sloped knee.

[n=7, mean ±95% CI of difference between the navigated and 20 ° externally rotated and 9º posteriorly sloped knee.

Following the combined misalignment of 20º external rotation and 9º of posterior slope of the tibial tray component (figure 168), there was a statistically significant widening of the envelope of laxity ($p<0.05$), with an average 3º translation (4º max) in the varus envelope of laxity towards varus. It is suggested that extra laxity generated by the posterior slope combined with an anterior and rotated tibial tray has resulted in the observed varus.

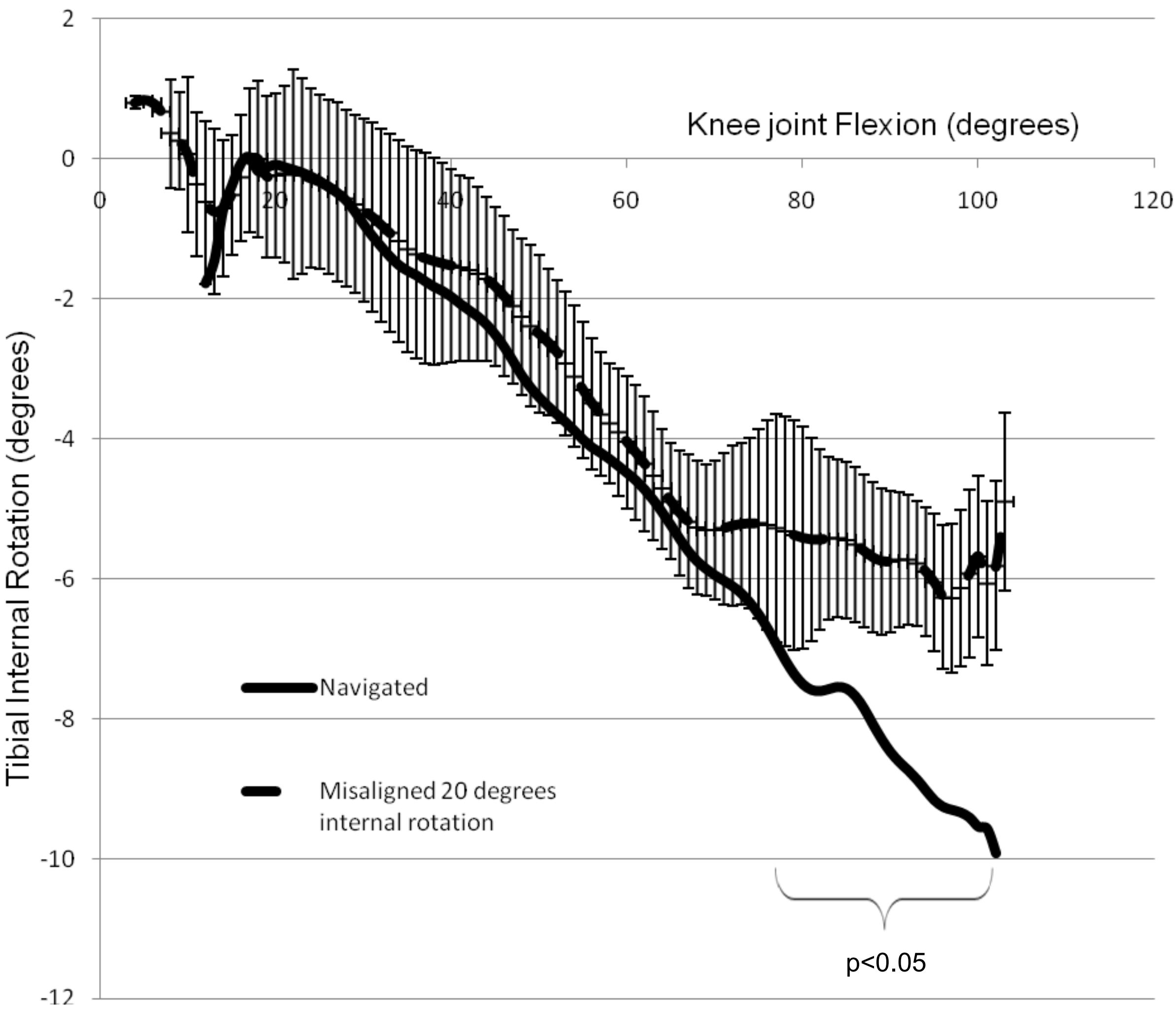

Figure 169: Tibial rotation versus knee joint flexion comparing the neutral rotation pathway between the navigated knee and 20 º internally rotated and 9º posteriorly sloped knee.
[n=7, mean ±95% CI of difference between the navigated and 20 º internally rotated and 9º posteriorly sloped knee.

Following the combined misalignment of 20º internal rotation and 9º of posterior slope to the tibial tray component (figure 169), there was an average 2º (4º max) translation in the neutral rotation pathway towards external rotation between 80º and 110º of flexion ($p<0.05$). It is suggested that this external rotation torque was generated by the femoral condyles as they opposed the incongruent articulation with the dished tibial tray. The remainder of the expected external rotation has been compensated for by the soft tissues and component articulation.

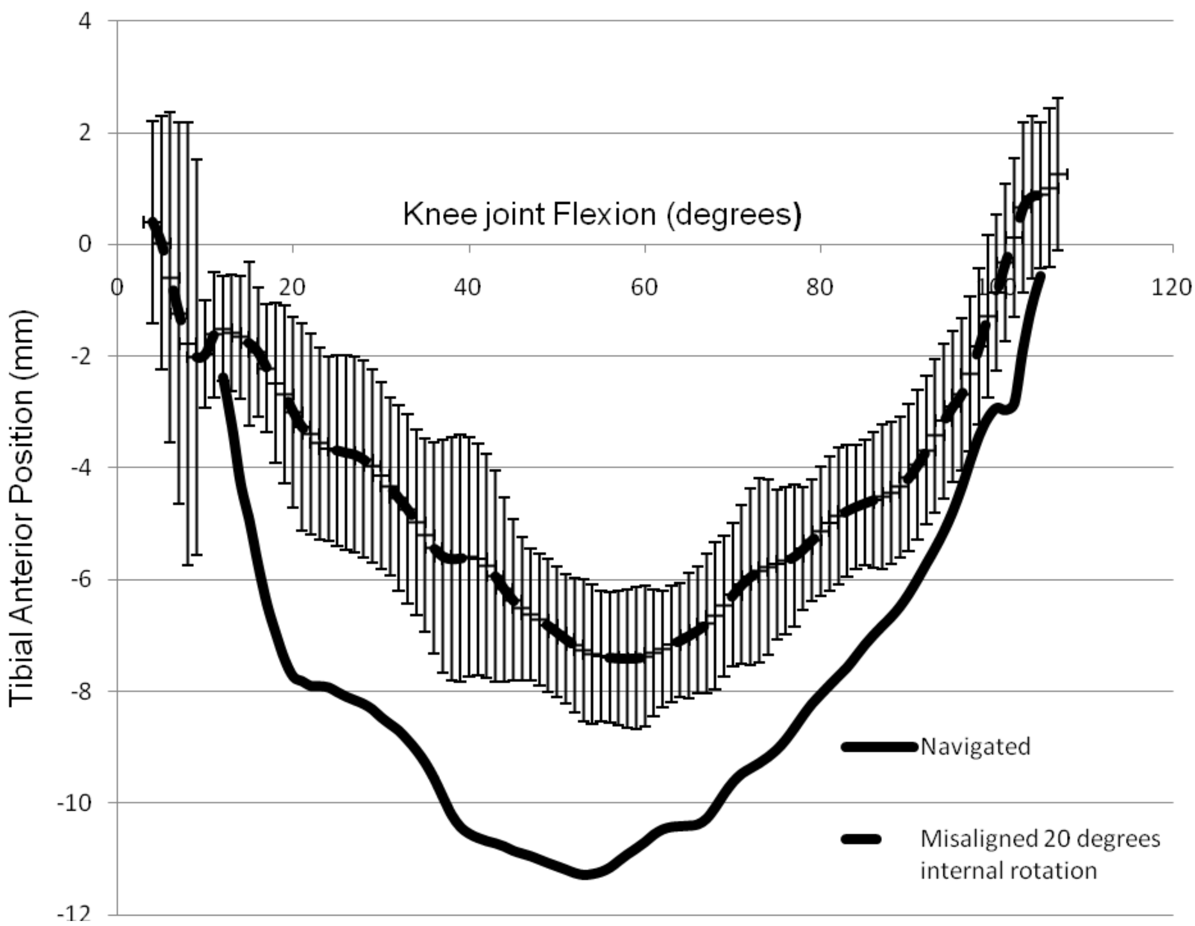

Figure 170: Tibial AP position versus knee joint flexion comparing the neutral AP pathway between the navigated knee and 20 º internally rotated and 9º posteriorly sloped knee.
[n=7, mean ±95% CI of difference between the navigated and 20 º internally rotated and 9º posteriorly sloped knee.

Following the combined misalignment of 20º internal rotation and 9º of posterior slope to the tibial tray component (figure 170), there was a statistically significant average 4 mm anterior translation (6 mm max) in the neutral AP path of motion ($p<0.05$). It is suggested that the posterior slope of the tibial tray generated a resultant anterior thrust. This thrust, along with unloading of the soft tissues posteriorly, caused the anterior translation. However, this translation is small when compared to 9º of posterior slope in isolation. It is suggested that the 20º of internal rotation of the tibial tray component has resulted in a rotation of the tibia (against the partially incongruent prosthesis) which has tightened the soft tissues, reducing the knee laxity and dampened down the expected anterior translation.

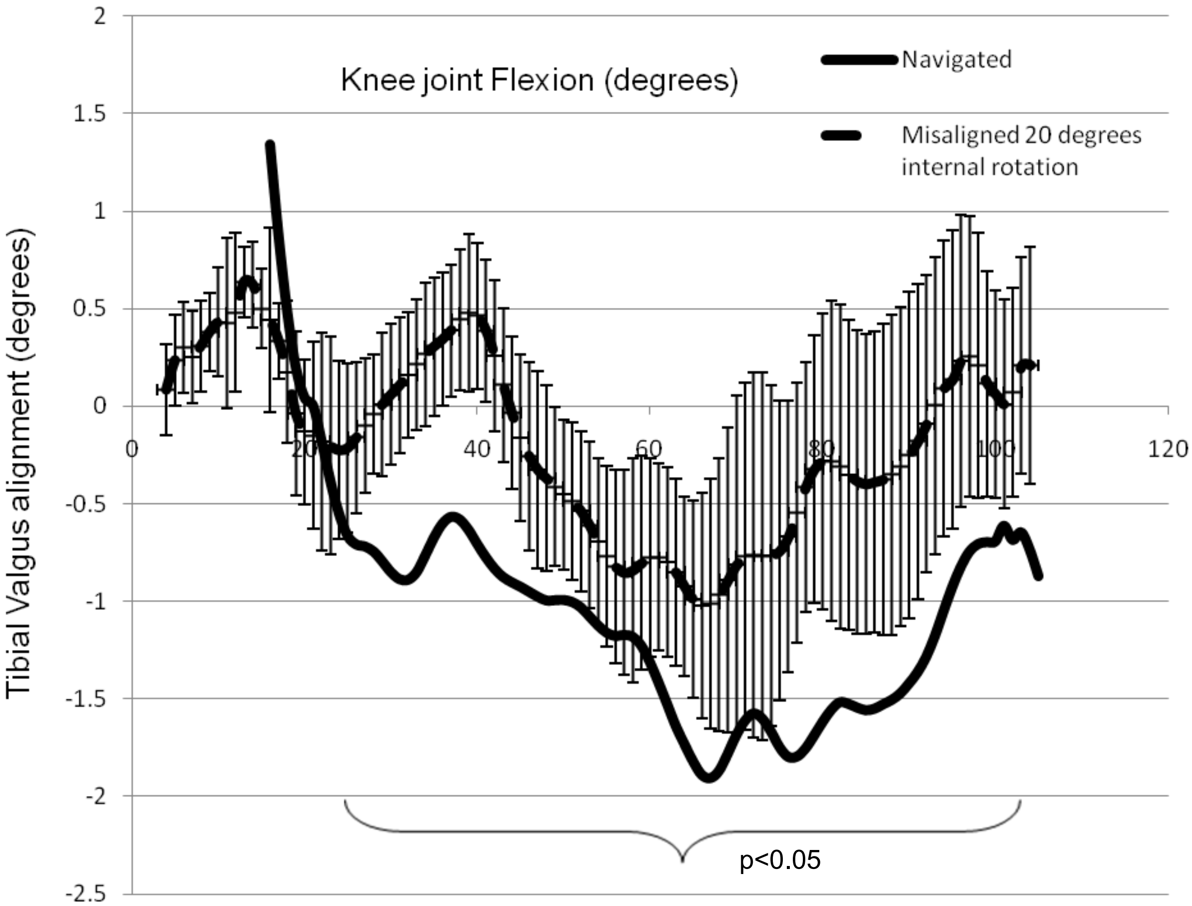

Figure 171: Tibial varus / valgus alignment versus knee joint flexion comparing the neutral varus / valgus pathway between the navigated knee and 20 º internally rotated and 9º posteriorly sloped knee. [n=7, mean ±95% CI of difference between the navigated and 20 º internally rotated and 9º posteriorly sloped knee.

Following the combined misalignment of 20º internal rotation and 9º of posterior slope of the tibial tray component (figure 171), there was a statistically significant average 0.5º translation (1.5º max) in the neutral varus / valgus pathway towards valgus. This translation was statistically significant between 20º and 110º of knee flexion ($p<0.05$). It is suggested that extra laxity generated by the posterior slope combined with an anterior and rotated tibial tray has resulted in a component articulation that has translated the knee into valgus.

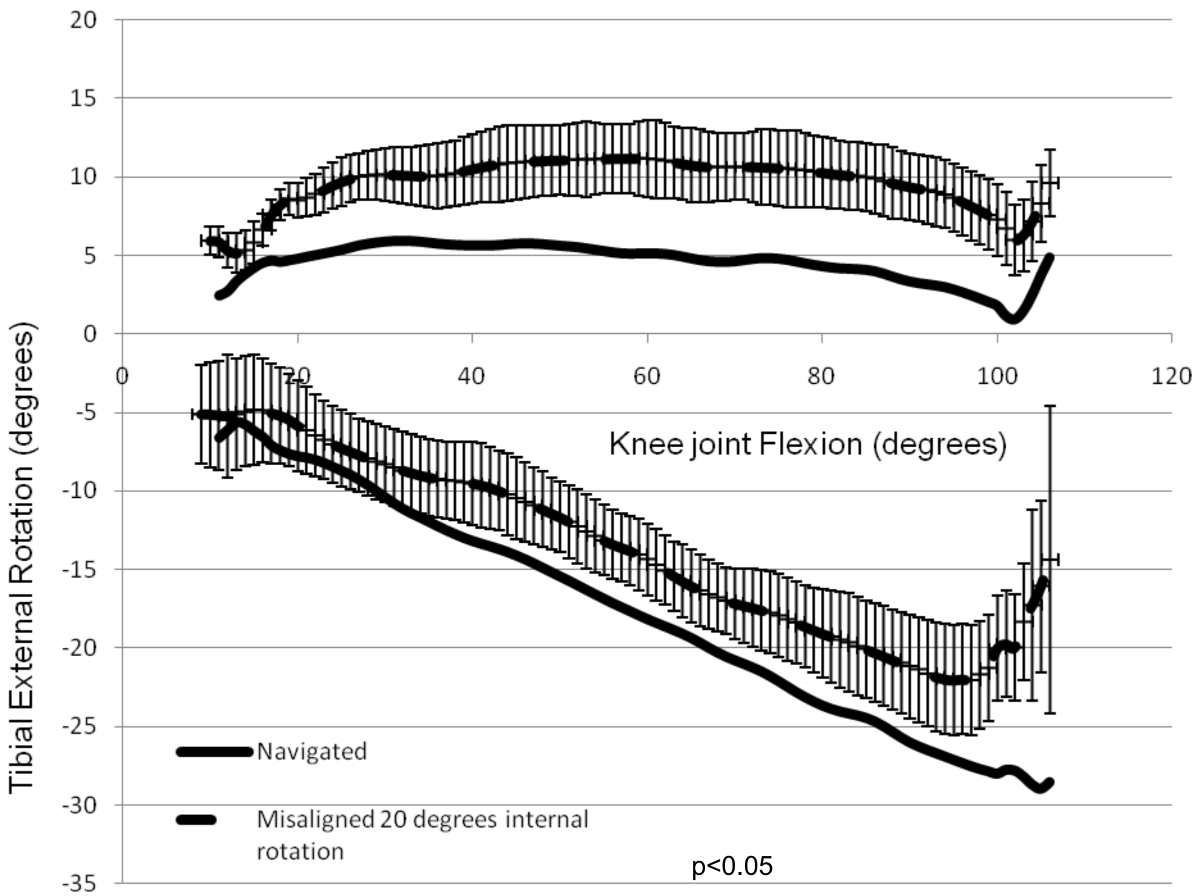

Figure 172: Tibial rotation versus knee joint flexion comparing the rotation envelope of laxity between the navigated knee and 20 º internally rotated and 9º posteriorly sloped knee.
[n=7, mean ±95% CI of difference between the navigated and 20 º internally rotated and 9º posteriorly sloped knee.

Following the combined misalignment of 20º internal rotation and 9º of posterior slope of the tibial tray component (figure 172), there was an average 3º (max 5º) translation in the external rotation limit of the envelope of laxity towards external rotation ($p<0.05$). There was also a statistically significant average translation of 2º (4º max) in the internal rotation limit towards external rotation between 25 º and 110 º of knee flexion ($p<0.05$).

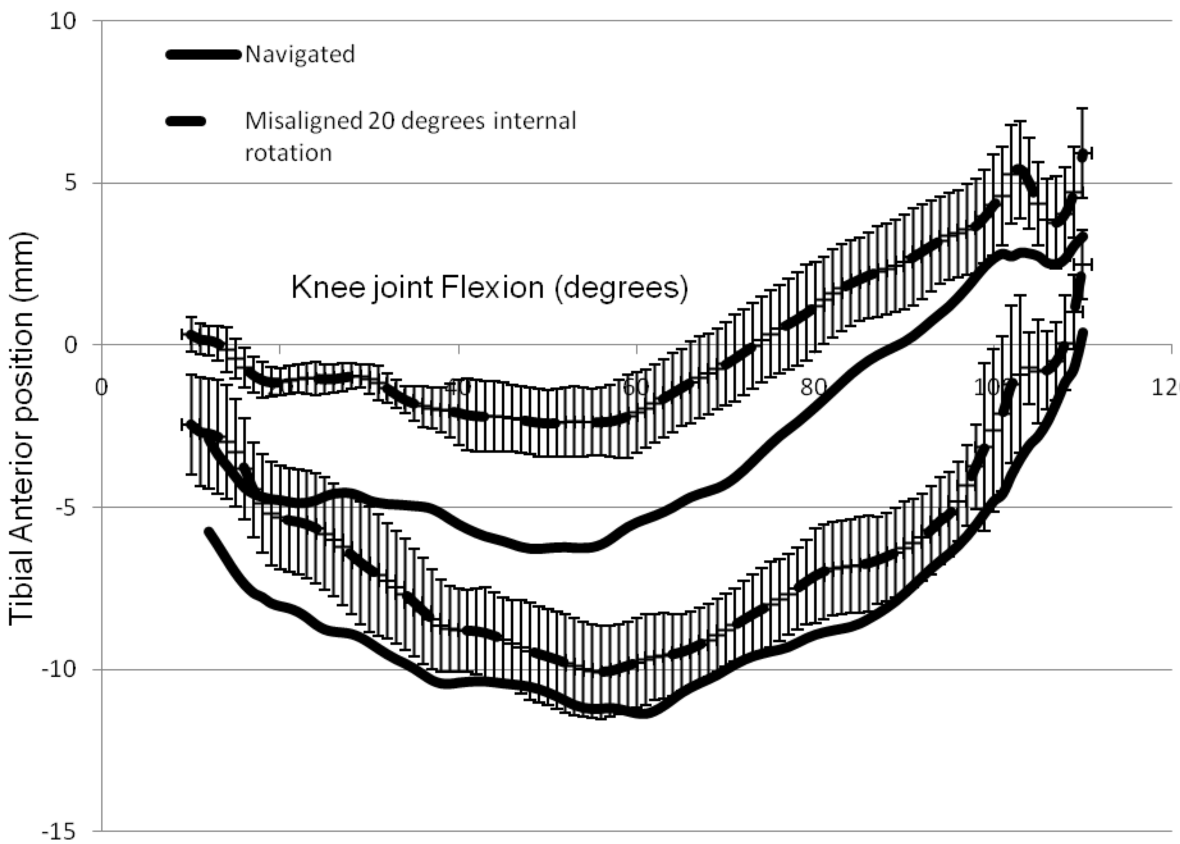

Figure 173: Tibial AP position versus knee joint flexion comparing the AP envelope of laxity between the navigated knee and 20 º internally rotated and 9º posteriorly sloped knee.
[n=7, mean ±95% CI of difference between the navigated and 20 º internally rotated and 9º posteriorly sloped knee.

Following the combined misalignment of 20º internal rotation and 9º of posterior slope of the tibial tray component (figure 173), there was a significant widening of the envelope of laxity ($p<0.05$). There was also a significant average 3.5mm (5mm max) anterior translation in the anterior envelope ($p<0.05$), and an average 2mm (3mm max) anterior translation in the posterior envelope of laxity ($p<0.05$). It is suggested that the posterior slope applied to the tibial tray generated a resultant anterior thrust. This thrust, along with unloading of the soft tissues posteriorly allowed the anterior translation observed. However, this translation is small when compared to 9º of posterior slope in isolation. It is suggested that the 20º of internal rotation of the tibial tray component has resulted in a rotation of the tibia (against the partially incongruent prosthesis) which has tightened the soft tissues, reducing the knee laxity and dampened down the expected anterior translation.

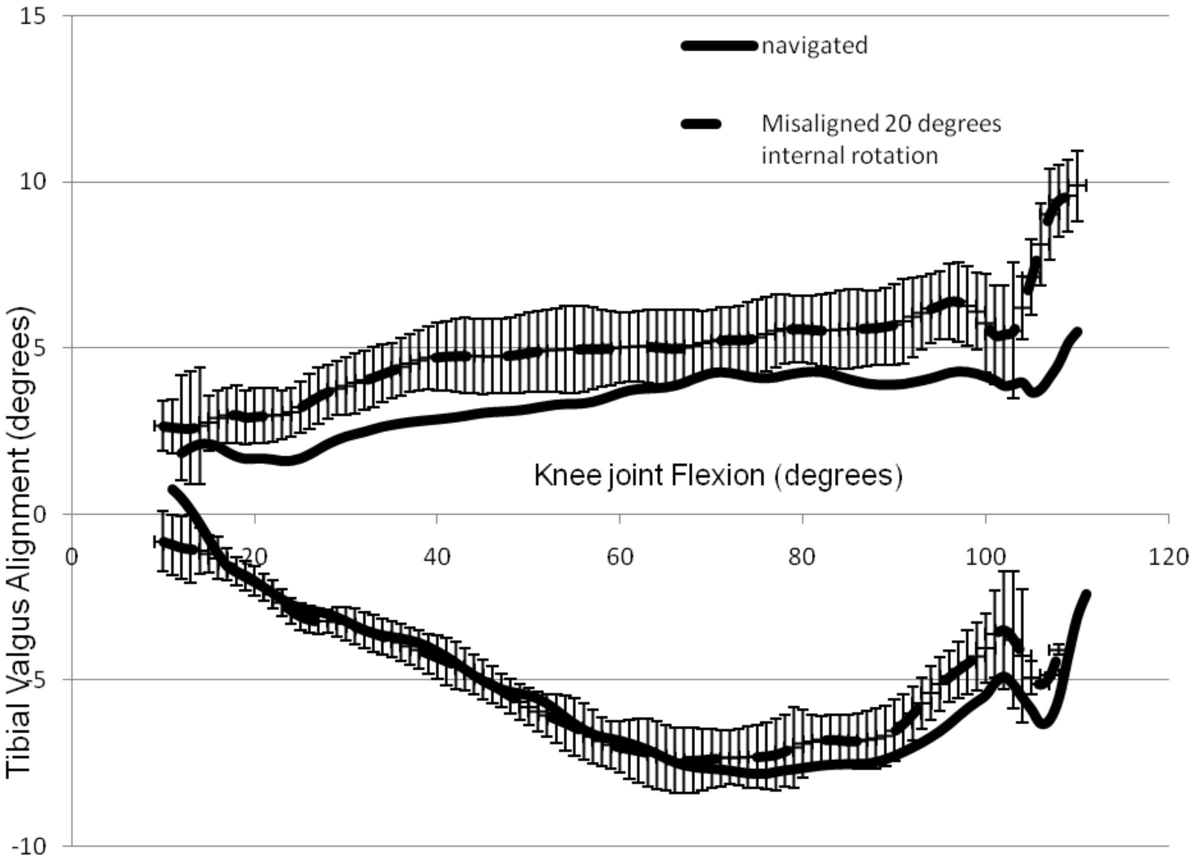

Figure 174: Tibial varus / valgus alignment versus knee joint flexion comparing the varus / valgus envelope of laxity between the navigated knee and 20 º internally rotated and 9º posteriorly sloped knee.

[n=7, mean ±95% CI of difference between the navigated and 20 º internally rotated and 9º posteriorly sloped knee.

Following the combined misalignment of 20º internal rotation and 9º of posterior slope of the tibial tray component (figure 174), there was also a statistically significant average 1º translation (3º max) in the valgus envelope of laxity towards valgus. There was no observed difference in the varus envelope between the series. It is suggested that the extra laxity generated by the posterior slope combined with a rotated tibial tray has resulted in the observed extra valgus.

Interpretation of Results Data

Having determined the effects of the implantation procedure on the kinematics of the knee joint, it may now be possible to explain the observed deviations in kinematics following the misalignment protocols, through forces generated by the resulting incongruent articulations.

To aid the explanation of this principle, several anatomical life size digital models were created using postoperative digital radiographs and images from scanned implants.

For the rotational misalignments, an accurate model of the tibial surface with its important soft tissue attachments was created using an anatomical human tibia saw bone specimen ([3;7]). This underwent a 0º resection of the tibial plateau performed 10 mm below the joint surface as per the experimental and normal surgical protocols. A best fit size 7 Scorpio standard tibial tray (dimensions 46 mm x 71 mm ([130;131])) and standard CR insert were selected, along with a matching size 7 standard Scorpio CR femoral component. This was scanned in 60º of flexion to determine the articulating surface of the femoral condyles (60º was chosen as the midpoint of the flexion / extension range and because a majority of the kinematic translations could be observed at 60º of knee flexion in this series). The selected implants and tibial cut surface were then scanned using a high definition scanner to acquire life size images, with dimensions checked against the known component specifications ([130;131]) (figures 175,176,177, 178).

Figure 175: Scanned life size image of a Scorpio size 7 CR standard tibial tray.

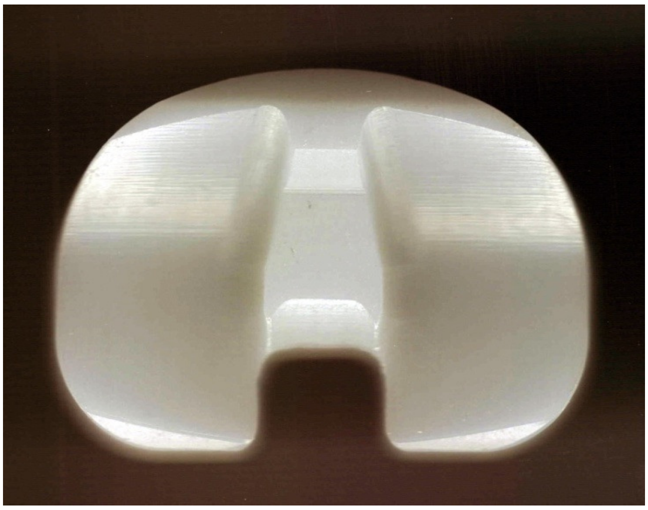

Figure 176: Scanned life size images of a Scorpio size 7 standard polyethylene tibial insert.

Figure 177: Scanned life size image of the tibial cut surface of an anatomical Sawbones([7]) model of the human tibia following a 10 mm 0 degree resection as per the experimental and normal surgical protocols.

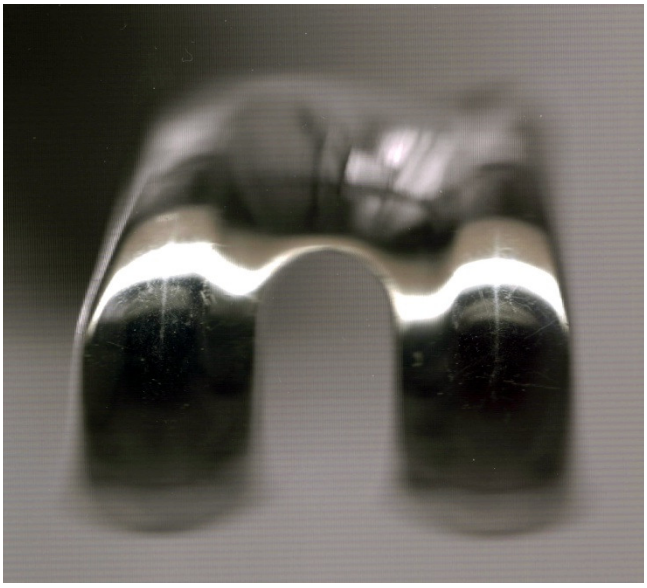

Figure 178: Scanned life size image of a Scorpio size 7 CR standard femoral component in 60º of flexion

These correctly sized images were then digitally locked to prevent accidental resizing and processed using edge identification software to create life size outlines of the tibial cut surface, tibial tray, tibial inserts and the articulation of the femoral condyles in 60º of flexion (figures 179, 180, 181).

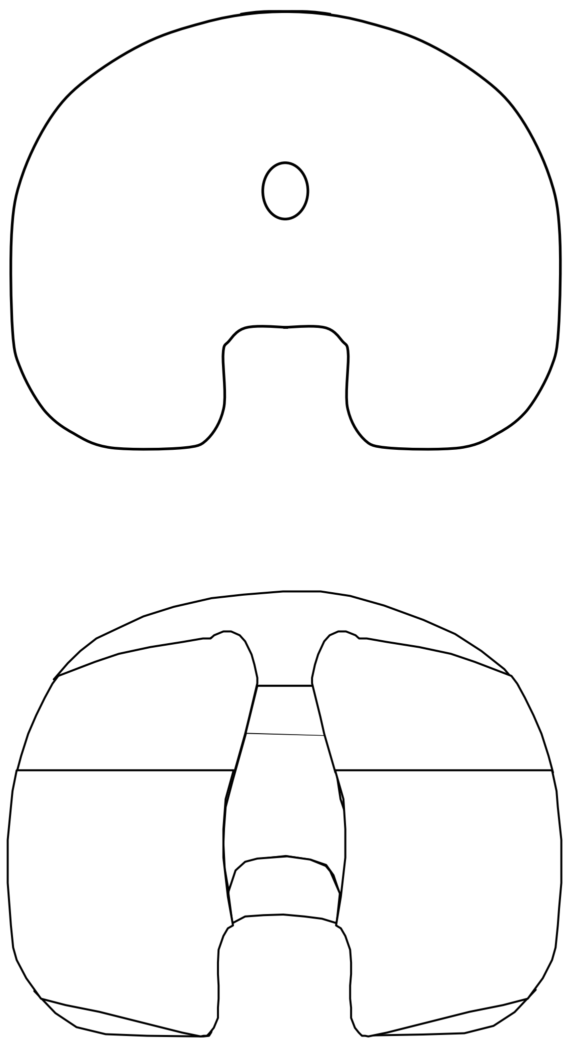

Figure 179: Digital life size images of a Scorpio size 7 CR tibial tray and a Scorpio size 7 CR polyethylene tibial insert following analysis and processing with edge detection software.

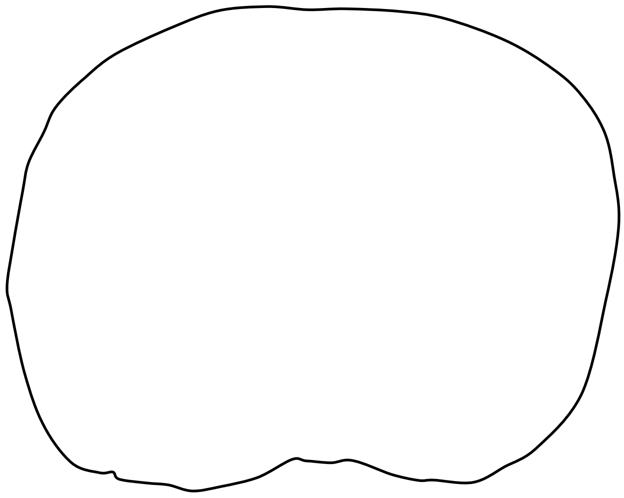

Figure 180: Digital life size image of the tibial cut surface of an anatomical Sawbones ([3;7]) model of the human tibia following a 10 mm 0 degree resection as per the experimental and normal surgical protocols following processing with edge detection software.

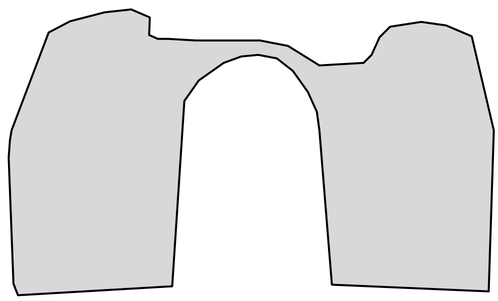

Figure 181: Shaded digital life size image of a Scorpio size 7 CR standard femoral component in 60º of flexion following processing with edge detection software.

The tibial cut surface was then shaded and a cross sectional atlas of anatomy ([24]) used to place anatomical markers denoting the position of the collateral ligaments and other significant soft tissue landmarks. The front of the tibia was also marked with an arrow that corresponded to the anatomical AP axis of the knee in line with the PCL attachment and extrapolated ankle centre (figure 182). The outline images of the tibial tray insert were also shaded to graphically represent the height and slopes of the different sections of the insert. The centre of rotation of the implant used in the kinematic experiments, taken from the tibial tray outline, was also marked to ensure rotation about the same axis (figure 183).

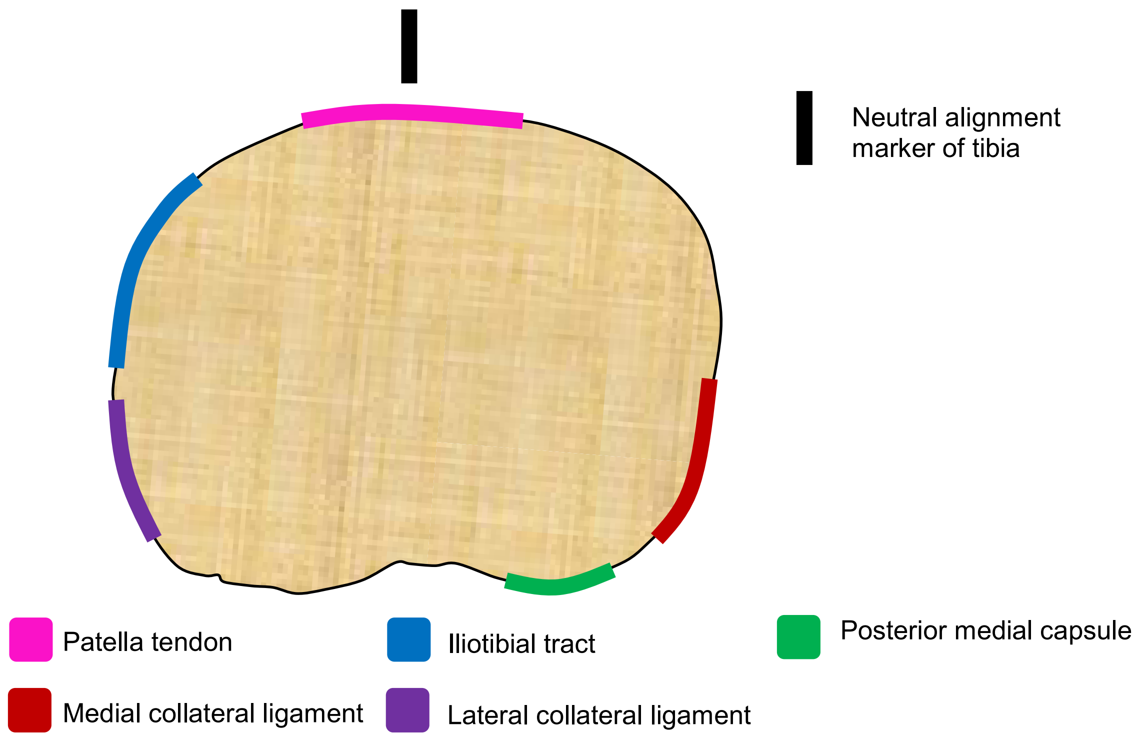

Figure 182: Shaded and marked digital life size image of the edge detected tibial cut surface of an anatomical Sawbones ([3;7]) model of the human tibia following a 10 mm 0 degree resection as per the experimental and normal surgical protocols.

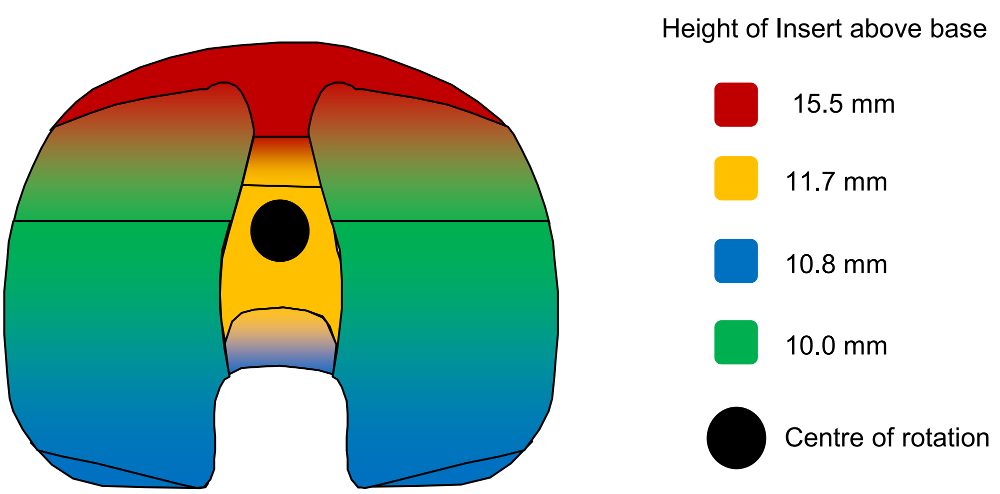

Figure 183: Shaded digital life size images of a 10mm Scorpio size 7 CR tibial tray and a Scorpio size 7 CR polyethylene tibial insert following processing with edge detection software and subsequent colour shading. The shading has been applied to demonstrates the relative total height of the different areas of the component above the metal tibial baseplate.

For the posteriorly sloped misalignments, the surface scanned tibial insert and tibial resection images were used in combination with scanned radiographs.

Following fully informed consent of the patient involved, AP and lateral radiographs of a successful implanted size 7 Scorpio CR TKR with 0 degree tibial slope were selected (figures 184, 185). They were then scanned using a high definition scanner and the images resized to life size, using the known dimensions of the tibial tray insert and femoral component ([130;131]). These correctly sized images were then reduced to 70% and locked digitally to prevent accidental resizing, and then processed using edge detection software to create 70% life size outlines of the tibia, femur, patella and the TKR implants in the coronal and sagittal planes (figures 186, 187).

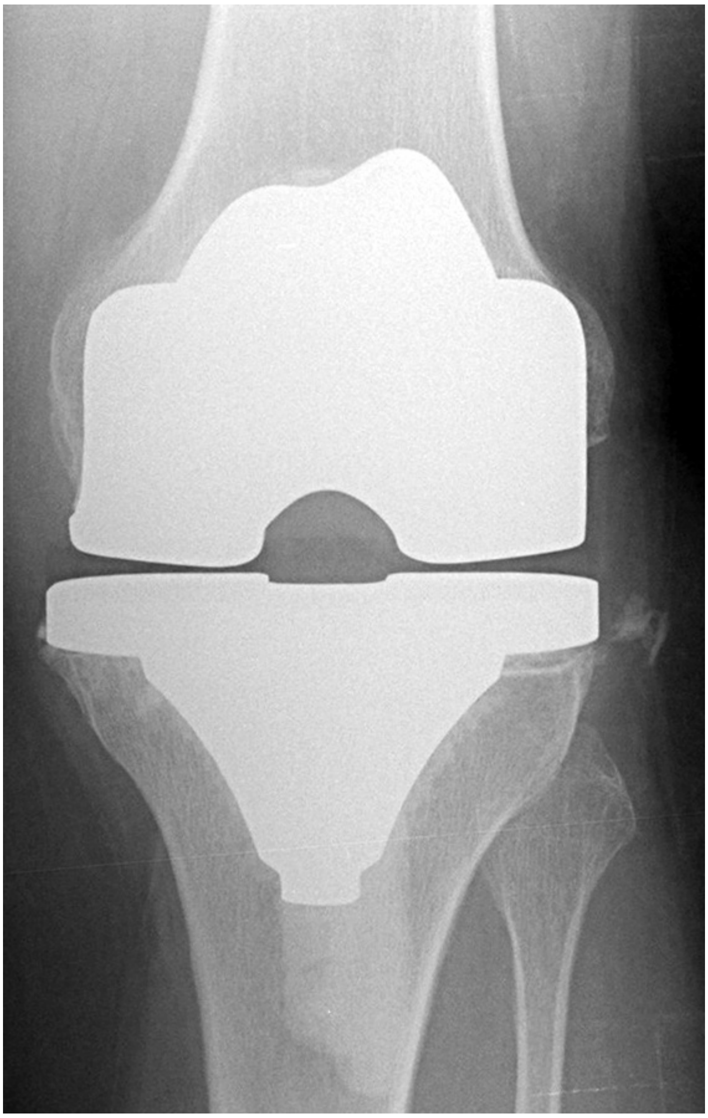

Figure 184: Scanned life size image of AP radiograph of a successfully implanted size 7 Scorpio CR TKR with 0 degree tibial slope using the known dimensions of the tibial tray insert and femoral component ([130;131])

Figure 185: Scanned life size image of lateral radiograph of a successful implanted size 7 Scorpio CR TKR with 0 degree tibial slope using the known dimensions of the tibial tray insert and femoral component ([130;131]).

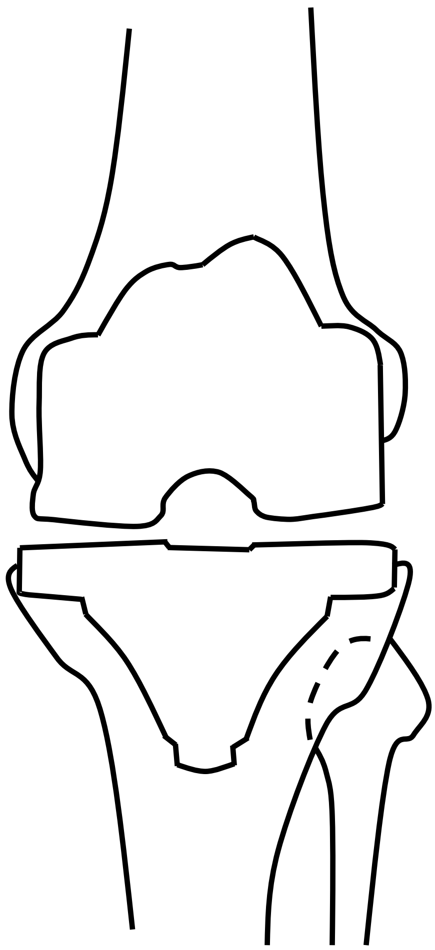

Figure 186: Digital 70% of life size image of AP radiograph of a successful implanted size 7 Scorpio CR TKR with 0 degree tibial slope processed with edge detection software.

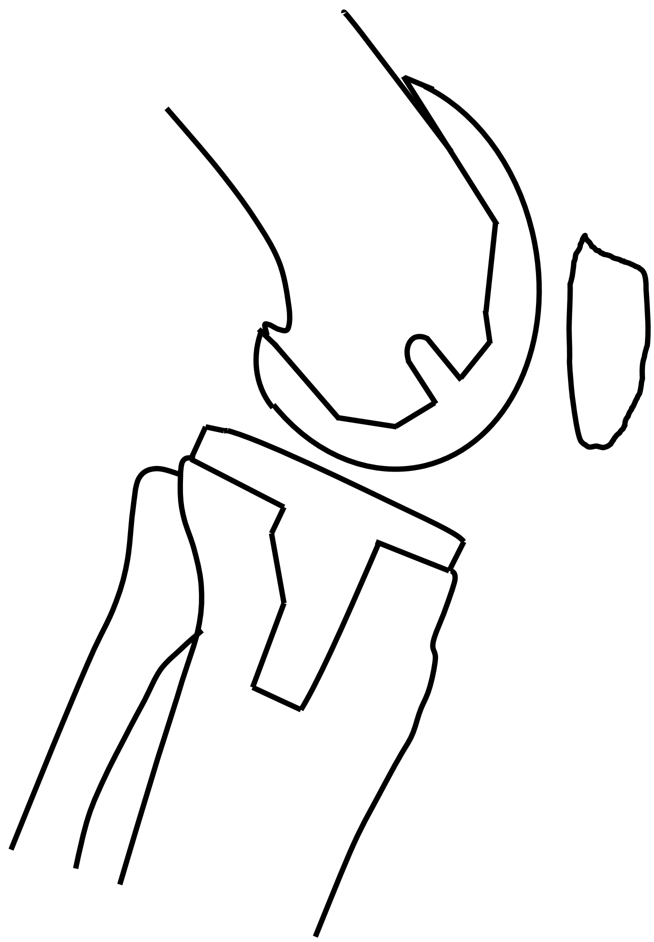

Figure 187: Digital 70% of life size image of lateral radiograph of a successful implanted size 7 Scorpio CR TKR with 0 degree tibial slope processed with edge detection software.

For the rotational misalignment figures, all images are compared to the life size navigated image (figure 188) that has been reconstituted as a best fit profile on the digitally scanned 10 mm resected tibial plafond as discussed previously in this chapter.

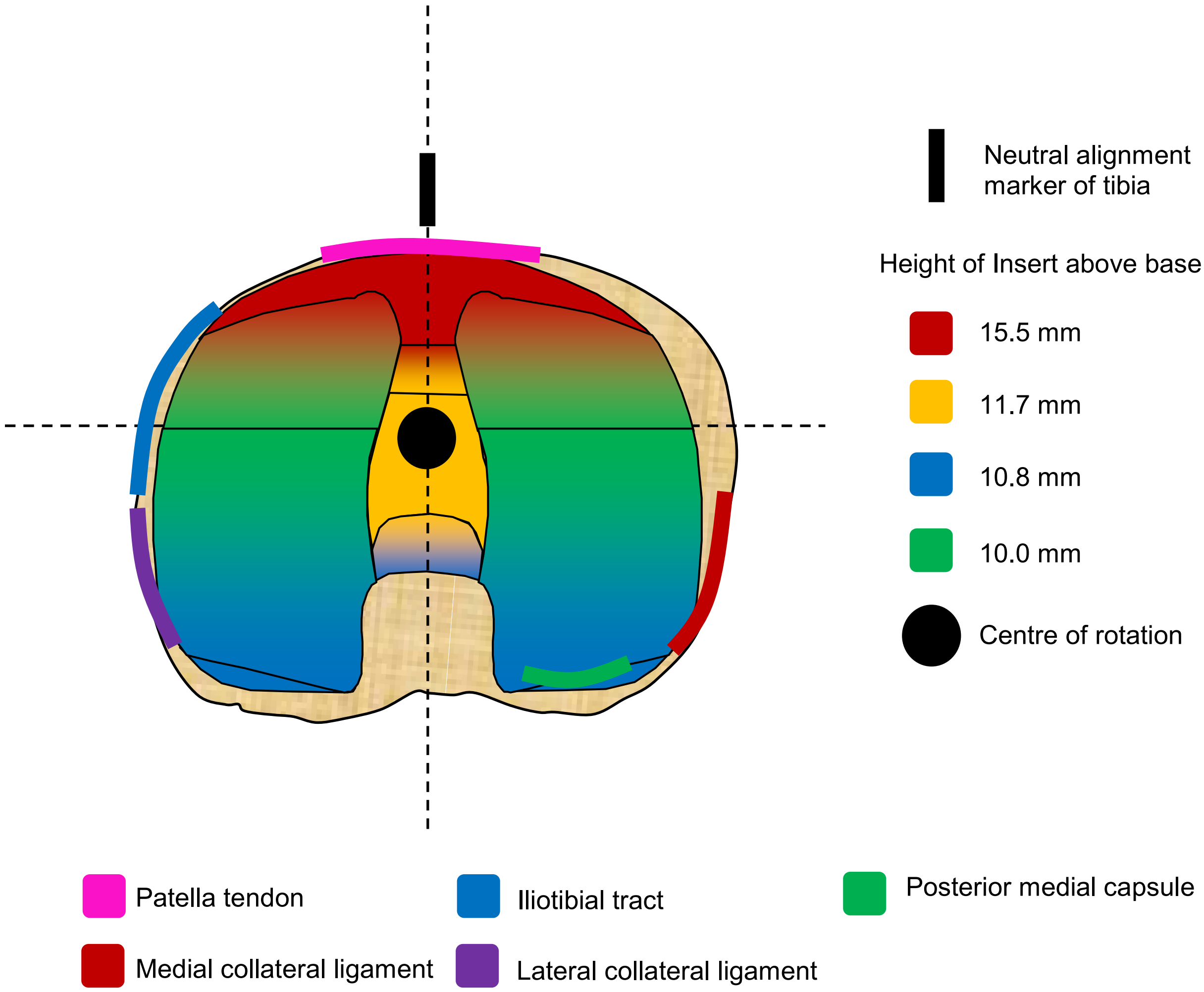

Figure 188: Diagram of a navigated implant profile created using life size images of the cut tibial surface and the scanned and shaded size 7 Scorpio CR tibial tray insert.

For the posterior slope misalignment figures, all images used are constituted from the 70% life size scanned (for better fit on A4 paper) AP and lateral radiographs of a successfully implanted size 7 Scorpio CR TKR (figures 188, 190). Drawings of the tibial trays, that maintain the same joint line height, have been added to demonstrate the effect of the posterior slope on the tibial position. The forces described as acting across the sloped tibial insert surface are made with reference to a standardised force diagram of an object at rest on a slope (figure 189).

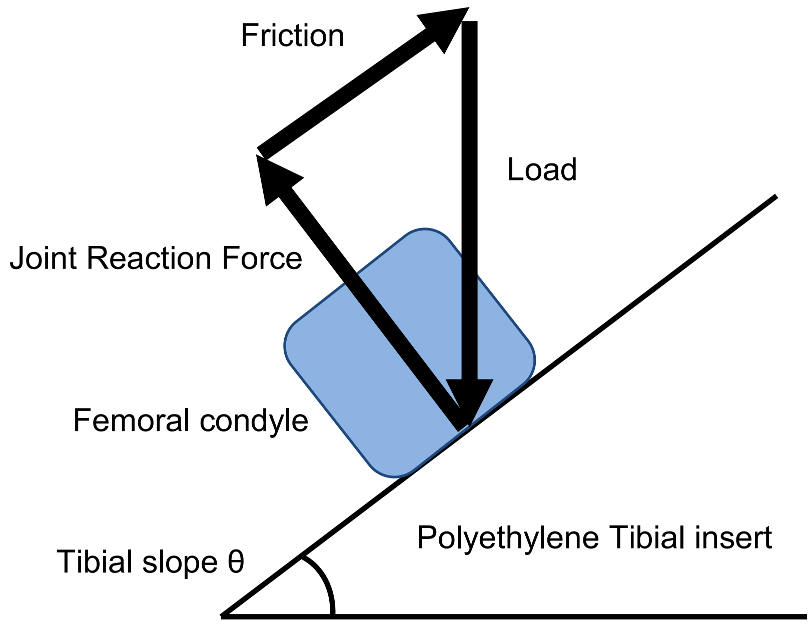

Coefficient of friction of TKR = μ = 0.03 - 0.10 in joint replacements ([40])
Limiting frictional force = Joint Reaction Force . μ
Joint reaction force = Load . Cos θ

Therefore maximum tibial slope before slippage occurs = Tan^{-1} . 0.03 - 0.10 = 1.7^{o} - 5.7^{o}

Figure 189: Simplified diagram of forces acting across a sloped polyethylene tibial insert. When the knee is loaded, the low coefficient of friction of the bearing may allow the femoral component to slide down the tibial insert, resulting in an anterior translation of the tibia.

DISCUSSION

Measuring and quantifying knee kinematics following TKR has always been a challenging task. This is in part due to the large variety of implants commercially available (each with their own specific design features), the variation in surgical technique for implantation between surgeons and implants, and other patient specific factors such as variations in bony anatomy, in the extent and severity of arthritic disease in the joint, and the extent of soft tissue involvement or compromise by the arthritic disease process.

The introduction of computer navigation systems has helped to standardise some aspects of surgical technique relative to the anatomical bony landmarks of the knee in a repeatable fashion, and can measure subsequent changes in kinematics by ±0.5 mm or ±0.5º angulation. However, they are unable to accurately interpret and quantify the behaviour of the soft tissue envelope of the knee. It is therefore incredibly difficult to determine the influence of a specific implant and its component design features on subsequent knee kinematics, even with the aid of computer navigation, in clinical use.

Implant choice, surgical technique and component positioning play crucial roles in the mechanics and function of the prosthetically replaced knee. Incompatibilities of alignment, joint loading or implant geometry will produce abnormal knee kinematics. This may manifest clinically through subjective dissatisfaction or mechanically through abnormal joint contact forces that may ultimately result in early implant failure due to loosening or wear ([142;149]). If implants can be designed that better replicate normal knee kinematics, then this may improve the patients' satisfaction, performance and longevity of the implants.

Intact Knee versus Navigated Knee Kinematics

This study reports kinematic data specific to one type of prosthesis, the Scorpio cruciate retaining (CR) total knee replacement system manufactured by the Stryker Corporation, from a position navigated and implanted by a single surgeon. This chosen implant is a single constant radius design with equally sized femoral condyles (figure 190) and a compartment symmetrical fixed dished tibial tray (figure 191). It was therefore expected when comparing the kinematics of the navigated knee and the intact knee that the navigated knee would assume a fixed axis profile with similar results as demonstrated by *Bull et al ([28])*.

Figure 190: The front view of a flexed Stryker Scorpio cruciate retaining femoral component, demonstrating symmetry of the femoral condyles.

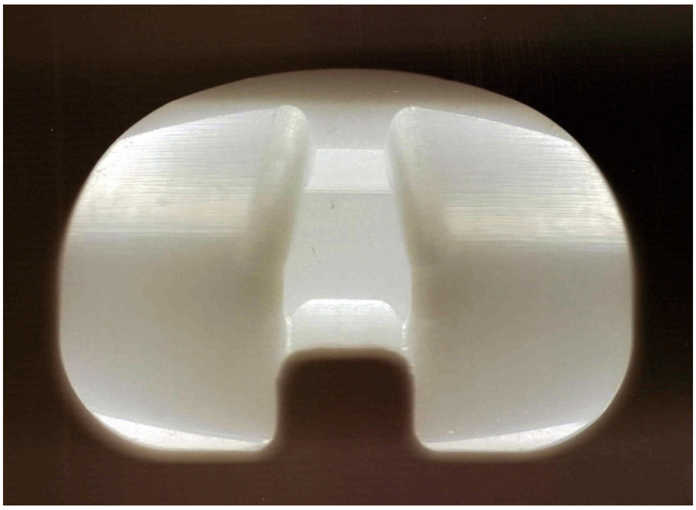

Figure 191: A Stryker Scorpio cruciate retaining fixed bearing polyethylene tibial tray component, demonstrating symmetrically dished medial and lateral compartments.

It was also expected that the screw-home mechanism would be absent from the navigated knee kinematics. This mechanism of coupled rotation between the tibia and femur that occurs automatically between full extension (0^o) and 20^o of knee flexion is attributed to the function of the ACL in the presence of the asymmetry of the medial and lateral condyles. Because the implant used in this study does not preserve the ACL and has symmetrical femoral condyles and tibial compartments, it did not induce this motion pattern. However, previous work has been published that describes a limited screw-home mechanism following TKR ([128;129]) and *Ishii et al* ([58]) reported a screw-home motion in their series of posterior cruciate substituting TKR subjects under certain weight bearing conditions and motions.

It was also thought that loss of the ACL would lead to increased anterior translation of the tibia in this series, but this was not the case with the tibias of the navigated knees assuming a more posterior position between 50º to 110º of knee flexion than the intact knees ($p<0.05$). This sliding anterior translation of the femur in flexion is paradoxical, and represents a loss of the normal femoral roll-back mechanism. This mechanism is a complex function of the PCL that results in movement of the femoral condyles relative to the tibial plateau, which resulting in translation of the tibio-femoral contact point posteriorly as the knee is flexed. This finding is consistent with other published series that also describe this anterior femoral translation at mid to deep flexion in posterior cruciate substituting knees ([38;80;132]). The loss of PCL function is not due to an intrinsic failure of the PCL, but can be explained by an anterior tibial thrust that is generated from the articulation of the femoral condyles against the sloping posterior aspect of the dished tibial tray insert as the knee is flexed. This anterior tibial thrust effectively results in a slack PCL throughout flexion and prevents the femoral roll-back mechanism.

As has been discussed in the previous chapter, the navigated knees had tendency to move towards an average valgus alignment of 0.5º (1º max) in the neutral path of motion (although this translation was not statistically significant and within the detection error limit for the navigation system), with a tendency towards increased internal rotation laxity in knee flexion. These changes were consistent for all the specimens and may be due to a variation in the technique used for the identification of the bony landmarks, digitisation of the specimens and the navigation guided implant positioning and cementing as compared to *Bull et al ([28]).* Minor variations in the varus / valgus envelopes in particular may reflect the rotational position of the implanted femoral component, a direct result of the surgeon's judgement both when digitising the femur and when selecting the trans-epicondylar axis to determine the cut for the femoral condyles. When comparing the varus / valgus neutral path and envelope of laxity between navigated and intact knees, there were minor 0.5º average translations in the neutral path of motion towards a valgus alignment in deep flexion (max 1º). However, these minor translations may be accounted for by some extra laxity that has been generated following the opening of the knee, the component implantation and excision of the ACL and again, were not statistically significant and were within the detection error limit for the navigation system.

As predicted, the neutral path of motion in tibial internal-external rotation was similar for the navigated knee as for the intact knee, with the exception of the tibial external rotation when the knee approached full extension, generated by the screw home mechanism in the intact series. The pattern of an increased envelope of rotational laxity in deep flexion that narrowed as the knee was extended (from approximately

110º of flexion to approximately 40º of knee flexion) was observed in the native and navigated series, although there was significantly more internal rotation laxity observed in deep flexion in the navigated series ($p<0.05$). This extra internal rotation laxity may also be accounted for by some extra generalised laxity of the knee following the arthrotomy, excision of the ACL and the implantation of the prosthesis.

The observed differences in the neutral paths of motion and envelopes of laxity between the intact and navigated knees, apart from the influence of the surgery on the soft tissues during implantation, may be attributed to the geometry of the implants. It is still unknown if the "navigated" or datum position chosen for implant placement by the computer guidance system in this series will reproduce the best physiological kinematics in vivo, or that reproduction of native knee kinematics in a prosthetic knee will improve the satisfaction, performance and longevity of the implants.

Excluding any influence due to the soft tissues of the knee, the observed differences in the neutral paths of motion and envelopes of laxity between the intact and navigated knees may be solely attributed to the geometry and position of the implants.

Misalignment kinematics

Rotational misalignment in isolation

For the rotational misalignment figures, all images are compared to the life size navigated image (figure 192) that has been reconstituted as a best fit profile on the digitally scanned 10 mm resected tibial plafond as discussed previously in this chapter.

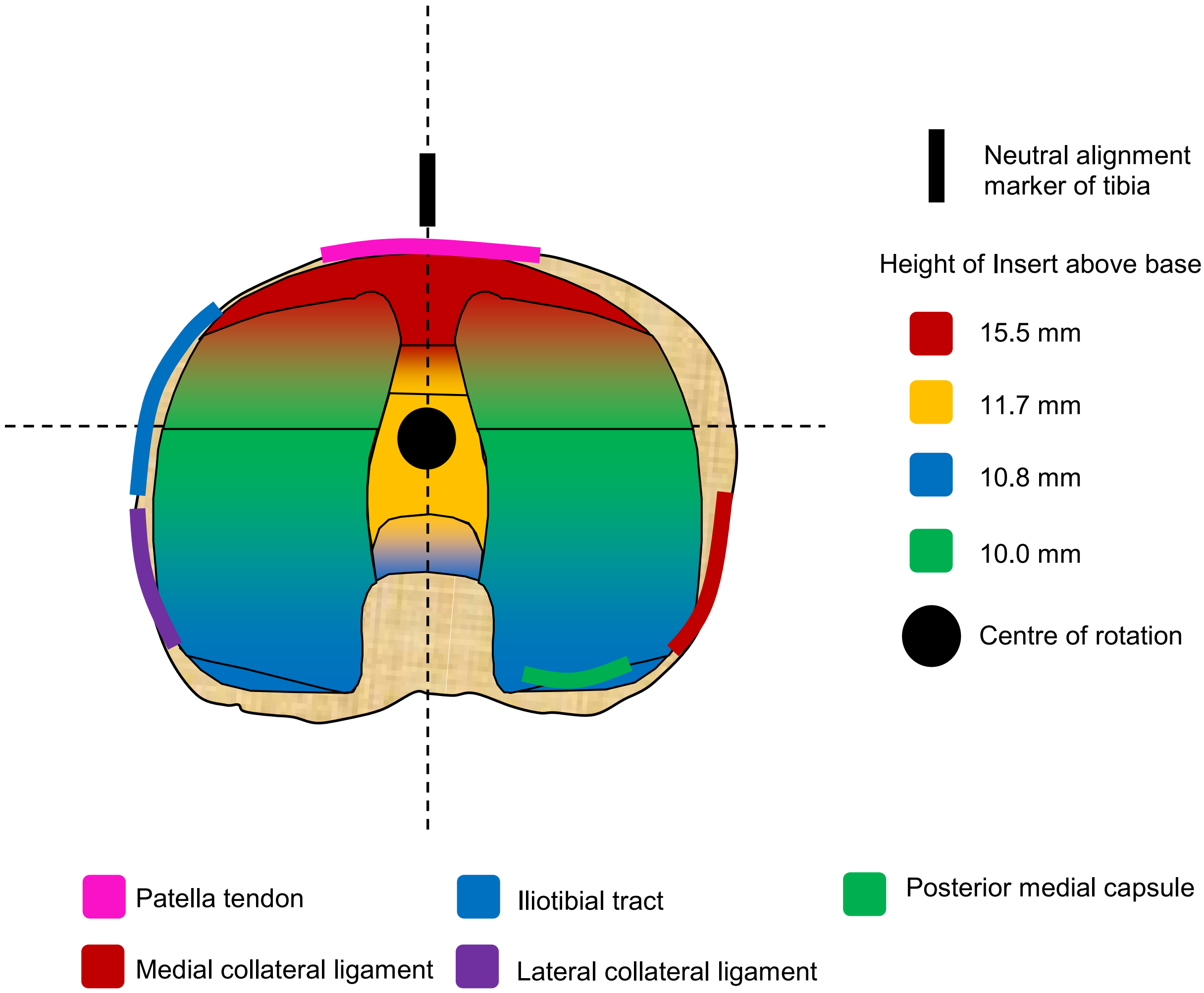

Figure 192: Diagram of a navigated implant profile created using life size images of the cut tibial surface and the scanned and shaded size 7 Scorpio CR tibial tray insert.

10º external rotation of the tibial tray insert:

When compared with the navigated insert (figure 192), there was significant internal rotation of the neutral path of rotation throughout the full range of knee flexion (0.05). There was also statistically significant posterior displacement ($p<0.05$) and valgus angulation of the knee in deep flexion ($p<0.05$) in the respective neutral paths. The statistically significant translations in the internal rotational envelope of laxity towards internal rotation ($p<0.05$) and a posterior translation in the anterior envelope of laxity throughout the full range of knee flexion ($p<0.05$) reflect alterations of soft tissue tensions resulting from the repositioning of the implant.

These changes may be explained by the incongruent articulation of the femoral condyles against the rotated tibial tray component. Following the 10º external rotation misalignment, there is no observed significant overhang of the prosthesis. However, the rotated dished tibial insert is no longer congruent with the overlying condyles of the femoral component at two points, the sloped anterior lateral aspect of the insert and the medial posterior aspect of the insert (figure 193). As the knee is flexed, the postero-medial incongruence dominates, generating an internal rotation torque and a posterior thrust that are applied to the tibia. This causes the tibia to rotate internally and to move backwards during knee flexion (figure 194).

The reason why the postero-medial incongruence dominates is not fully understood. However, it is suggested that due to the asymmetric shape of the dish on the tibial insert in the sagittal plane, an external rotation of 10º may result in a more significant incongruence on the postero-medial side compared to the antero-lateral side of the insert. In addition, the surgical dissection for implantation along with resection of the ACL may result in greater soft tissue restraints on the medial side of the knee. As the knee is loaded and flexed, these restraints may result in a greater compressive force in the medial side compared to the lateral side, resulting in the dominance of the medial compartment incongruence observed.

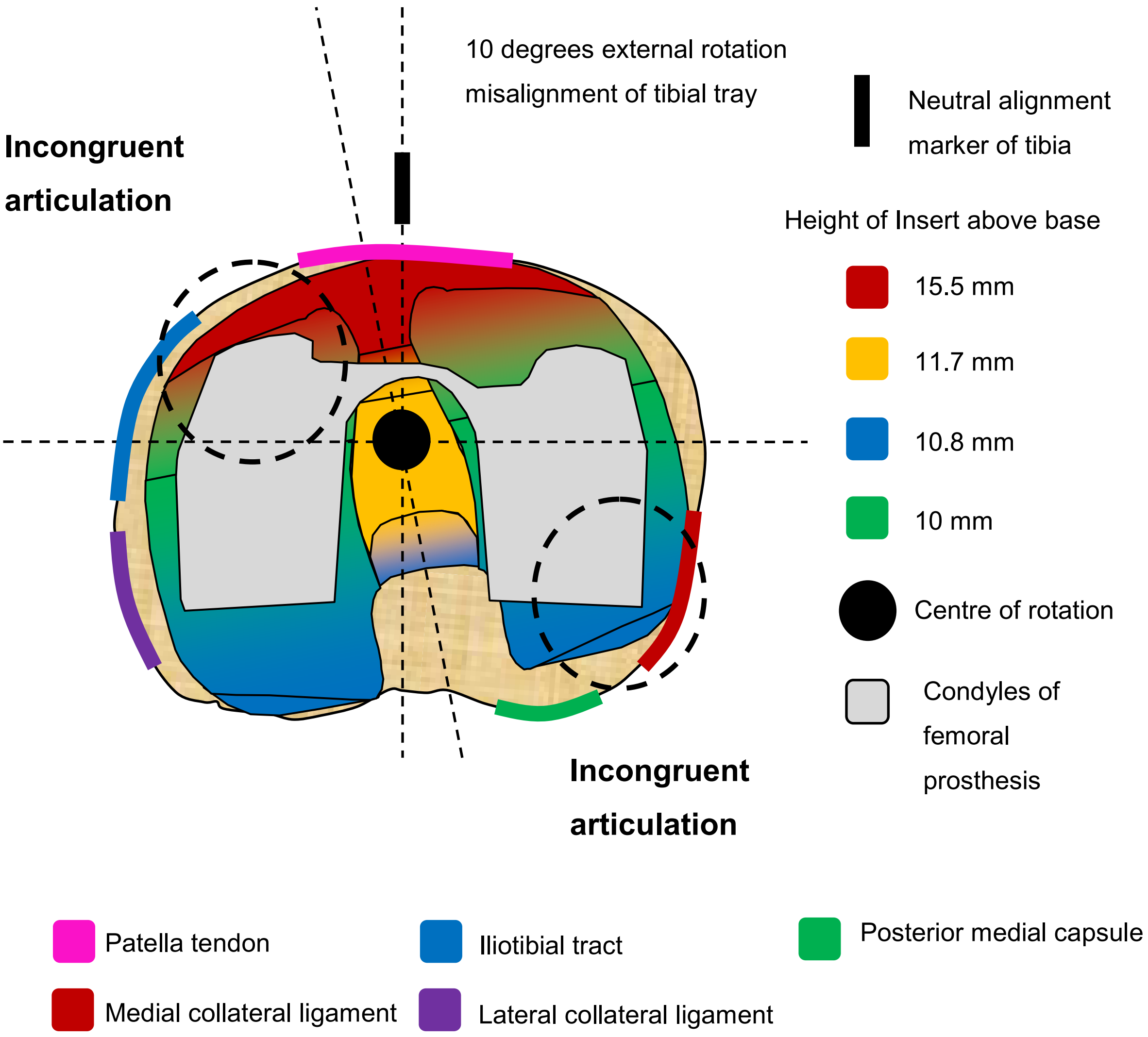

Figure 193: Diagram of a life size image of a 10º externally rotated misaligned tibial tray component rotated about its central axis, demonstrating no significant overhang of the tibial tray. There are however, incongruent articulations between the antero-lateral and postero-medial aspects of the tibial insert and the condyles of the femoral component before the knee is loaded and flexed.

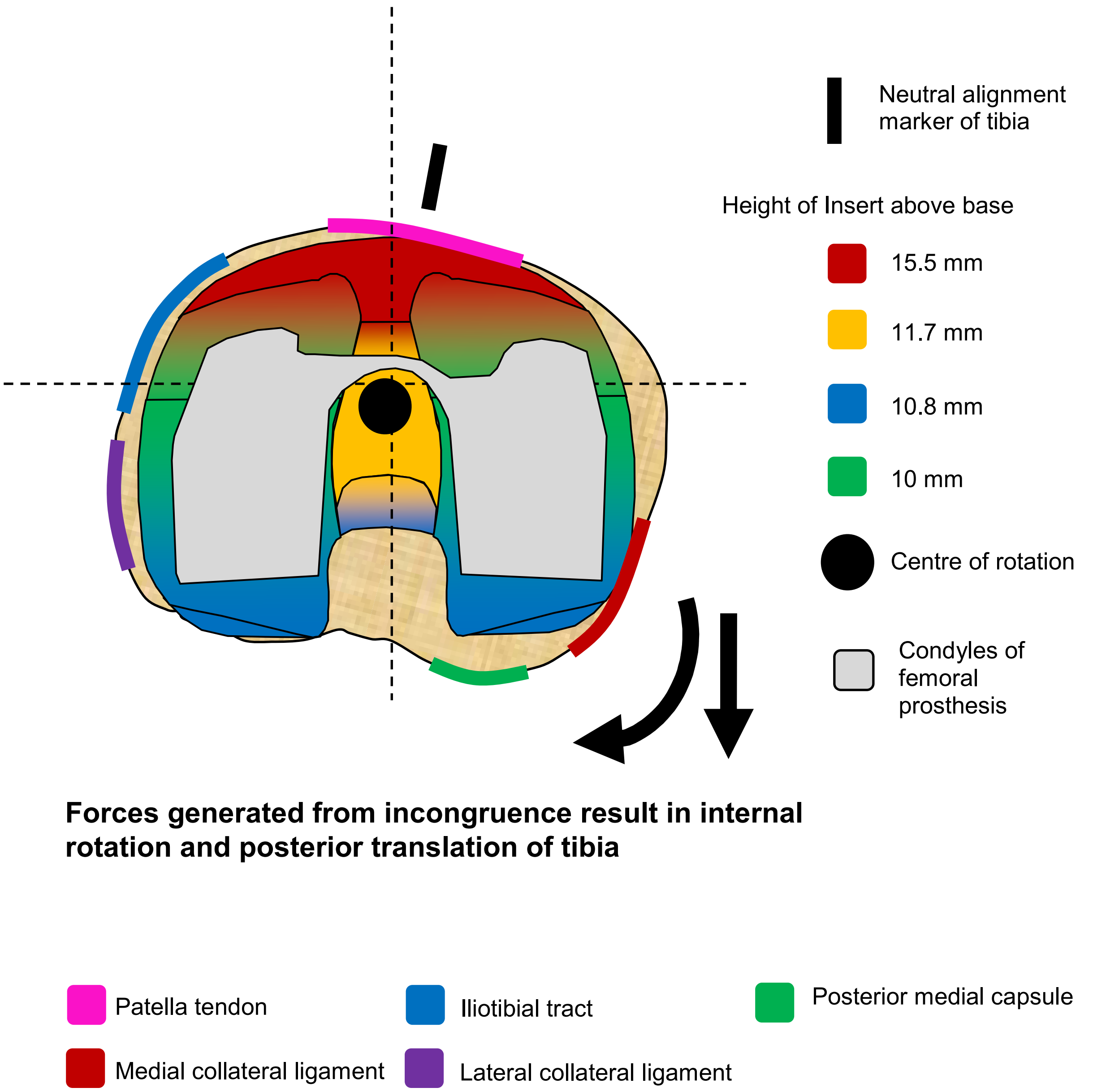

Figure 194: Diagram of a life size image of a 10º externally rotated misaligned and axially loaded tibial tray component rotated about its central axis, demonstrating the resultant internal rotation torque and posterior translation of the tibia when the knee is loaded and flexed.

20º external rotation of the tibial tray insert:

When compared with the navigated insert (figure 192), there was significant internal rotation (of greater magnitude compared with 10º external rotation of the tibial insert) of the neutral path of rotation throughout the full range of knee flexion (0.05). There was also a statistically significant anterior translation in the neutral AP pathway (of greater magnitude compared with10º external rotation of the tibial insert) between 20º and 65º of knee flexion ($p<0.05$). These displacements of the tibia were also evident as statistically significant translations in the internal rotation envelope of laxity towards internal rotation between 50º and 115º of knee flexion ($p<0.05$) and an anterior translation in the anterior AP envelope of laxity between 5º and 65º of knee flexion ($p<0.05$).

These changes may be explained by the incongruent articulation of the femoral condyles against the rotated tibial tray component. Following the extreme 20º external rotation misalignment, there was significant overhang of the prosthesis medially in the region of the medial collateral ligament (MCL) and anteriorly in the region of the patellar tendon. The rotated tibial tray pressing against the MCL, in particular, may alter the tension in the soft tissue envelope and result in further degradation of kinematics. In addition, the severely rotated dished tibial insert is no longer congruent with the overlying condyles of the femoral component, particularly at the sloped antero-lateral aspect of the insert (figure 195). As the knee is flexed, the significant antero-lateral incongruence results in the generation of an internal rotation torque and an anterior thrust that are applied to the tibia. This causes the tibia to rotate internally and to move forwards during knee flexion (figure 196).

The reason for the dominance of the antero-lateral incongruence rather than the postero-medial incongruence is not fully understood; however, it is suggested that at this extreme 20º rotation, the incongruence on the steeper antero-lateral side of the tibial insert, combined with soft tissue interaction at the MCL by the tibial tray, result in an anterior translation of the tibia rather than a posterior translation as was observed in the 10º external rotation series. A further suggestion is that at 20º external rotation, the medial condyle of the femoral component overhangs and articulates with the steeply sloped edge of the cruciate recess in the tibial insert, resulting in a further anterior thrust being applied to the tibia as the knee is flexed.

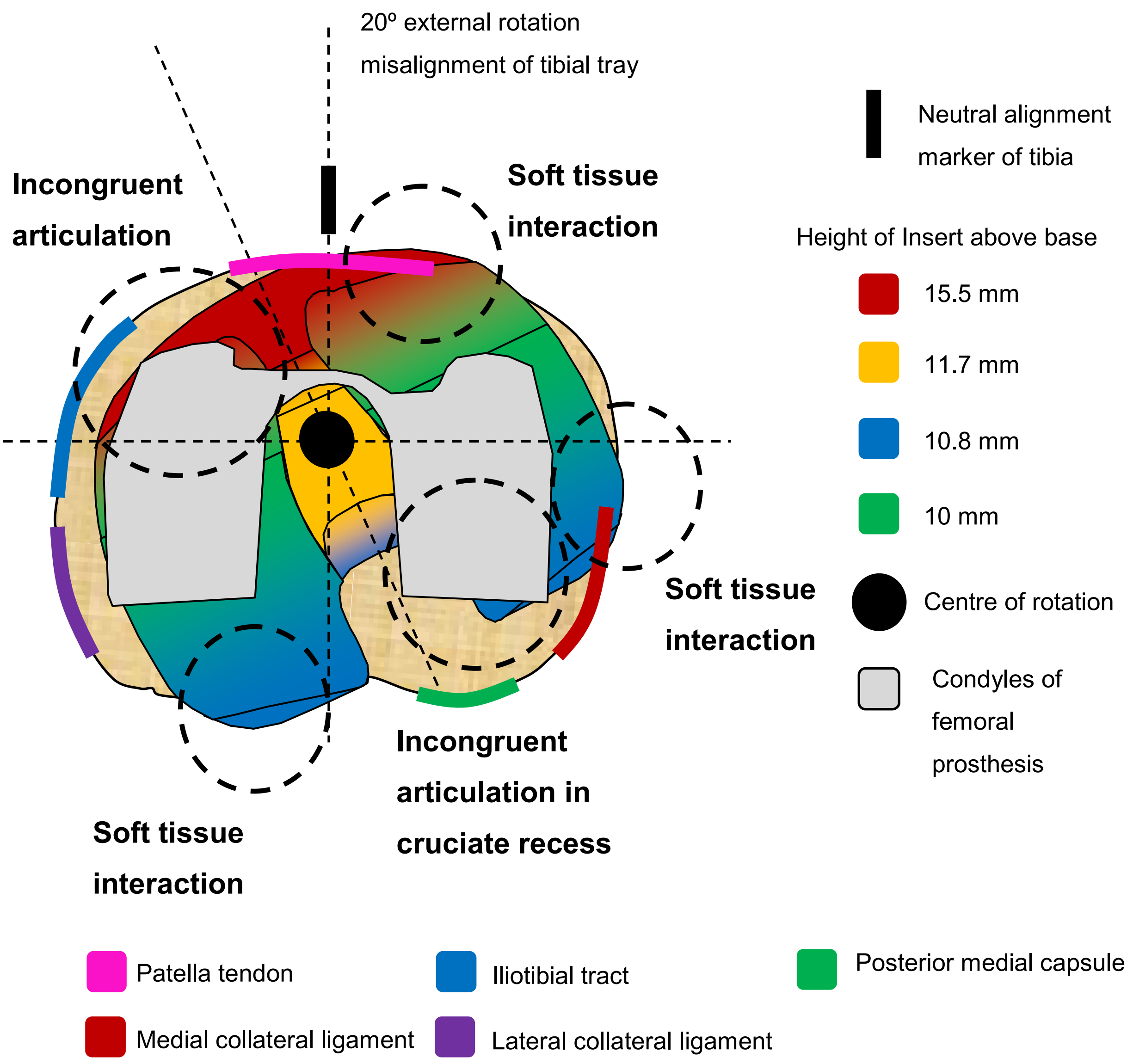

Figure 195: Diagram of a life size image of a 20º externally rotated misaligned tibial tray component rotated about its central axis, demonstrating incongruent articulations between the antero-lateral aspect of the tibial insert and the lateral condyle of the femoral component, as well as between the postero-medial aspect of the tibial insert, the cruciate recess and the medial condyle of the femoral component. Note also the soft tissue interactions in the region of the MCL, patella tendon and posterior joint capsule before the knee is loaded and flexed.

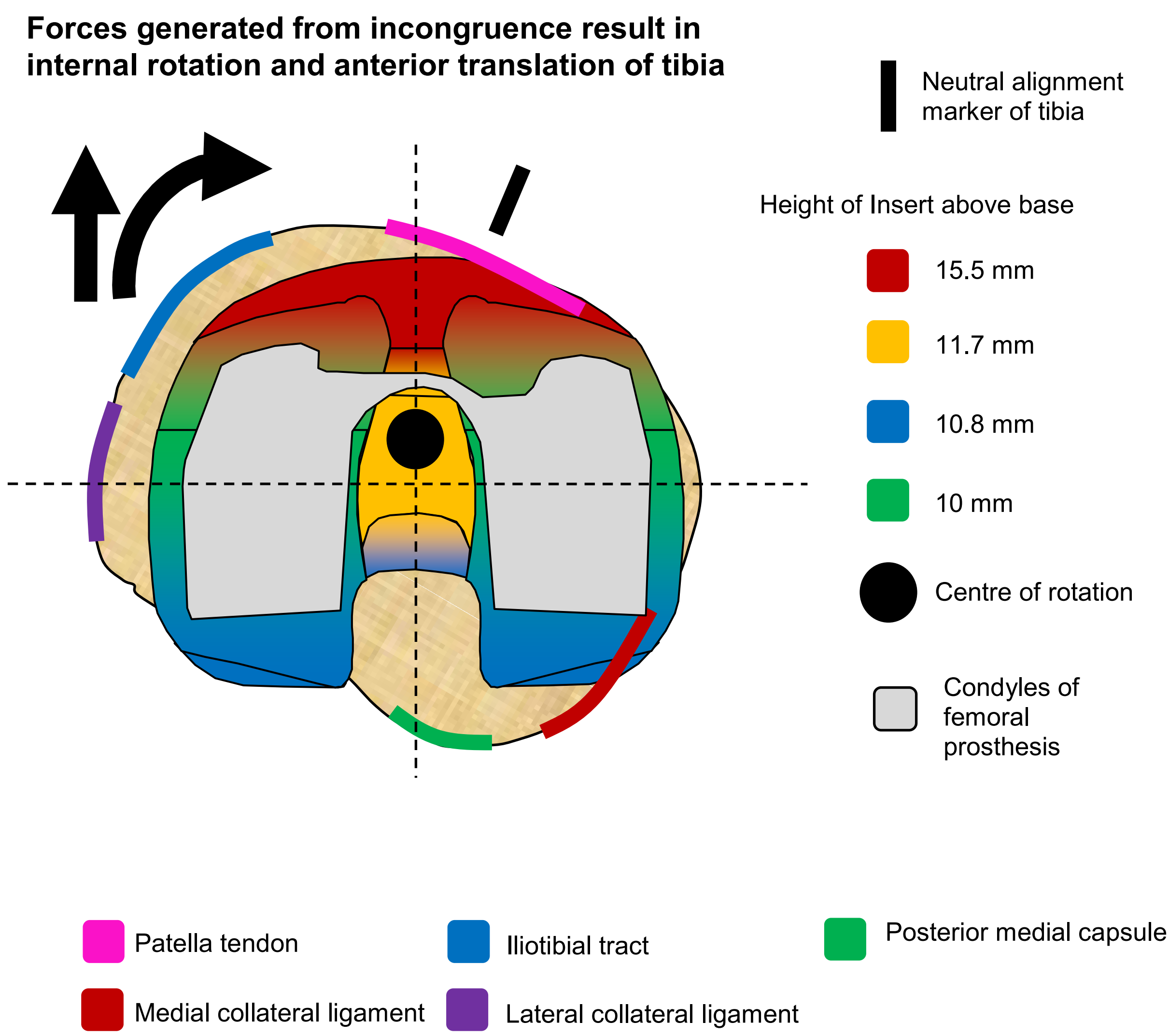

Figure 196: Diagram of a life size image of a 20º externally rotated misaligned and axially loaded tibial tray component rotated about its central axis, demonstrating the resultant internal rotation and anterior translation of the tibia when the knee is loaded and flexed. There is also ongoing soft tissue interaction in the region of the MCL and patella tendon.

10º internal rotation of the tibial tray insert:

When compared with the navigated insert (figure 192), there was external rotation of the neutral path of movement throughout the full range of knee flexion, but this was not statistically significant. There was, however, a statistically significant anterior displacement in the neutral AP pathway throughout the full range of knee flexion ($p<0.05$) and a statistically significant translation of the neutral varus / valgus pathway towards valgus in deep flexion ($p<0.05$). These forces applied to the tibia were also evident as statistically significant translations in the internal rotation, anterior AP and varus envelopes of laxity towards external rotation ($p<0.05$) throughout the full range of knee motion, an anterior translation throughout the full range of knee flexion ($p<0.05$) towards valgus between 30º and 115º of knee flexion ($p<0.05$).

These changes may be explained by the incongruent articulation of the femoral condyles against the rotated tibial tray component. Following the 10º internal rotation misalignment, there is no observed significant overhang of the prosthesis. However, the rotated dished tibial insert is no longer congruent with the overlying condyles of the femoral component, particularly at the sloped antero-medial aspect of the insert (figure 197). As the knee is flexed, an external rotation torque and anterior thrust are generated and applied to the tibia. This causes the tibia to rotate externally and to move forwards during knee flexion (figure 198).

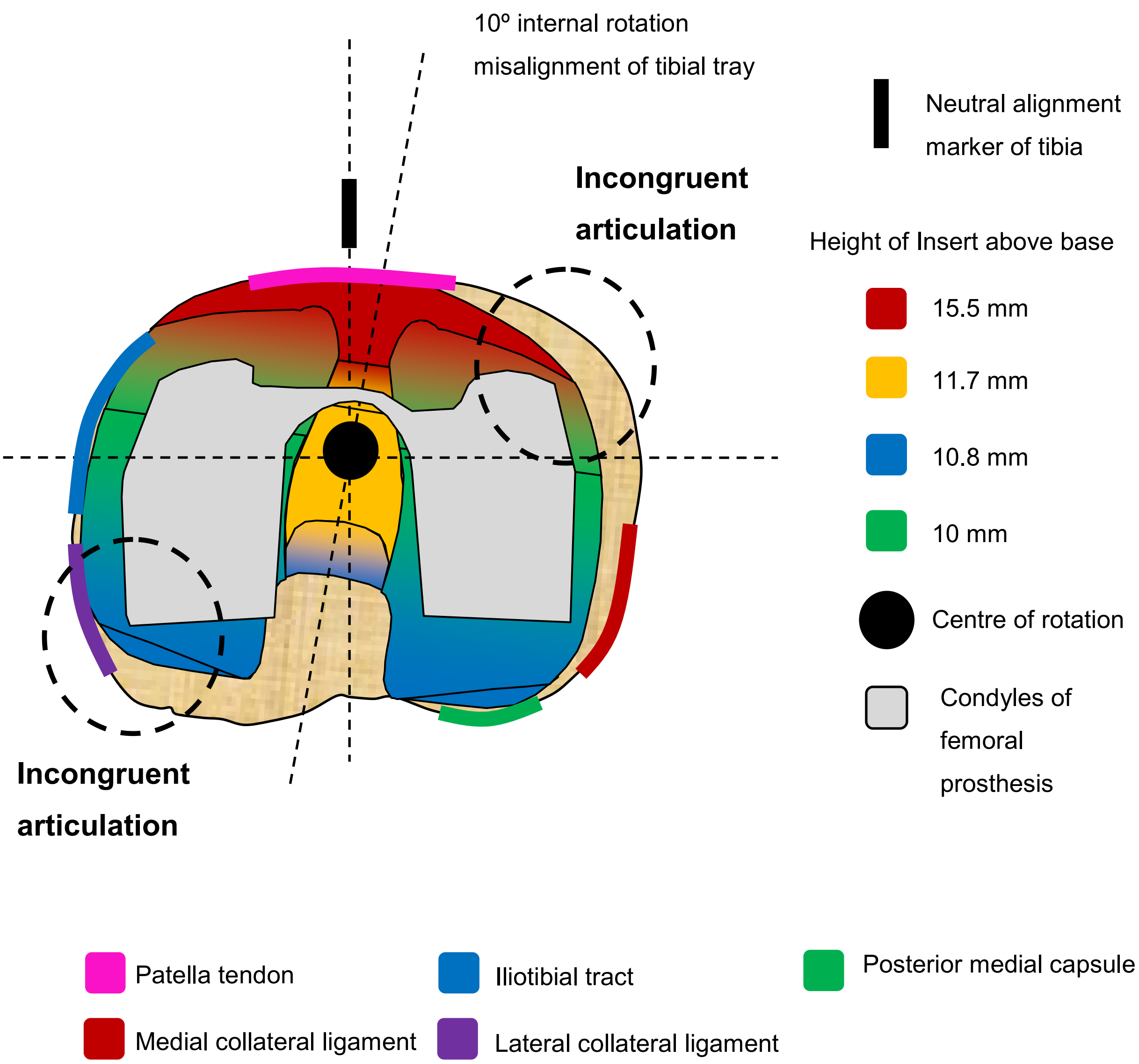

Figure 197: Diagram of a life size image of a 10º internally rotated misaligned tibial tray component rotated about its central axis, demonstrating no significant overhang of the tibial tray. There are however, incongruent articulations between the antero-medial and postero-lateral aspects of the tibial insert and the condyles of the femoral component before the knee is loaded and flexed.

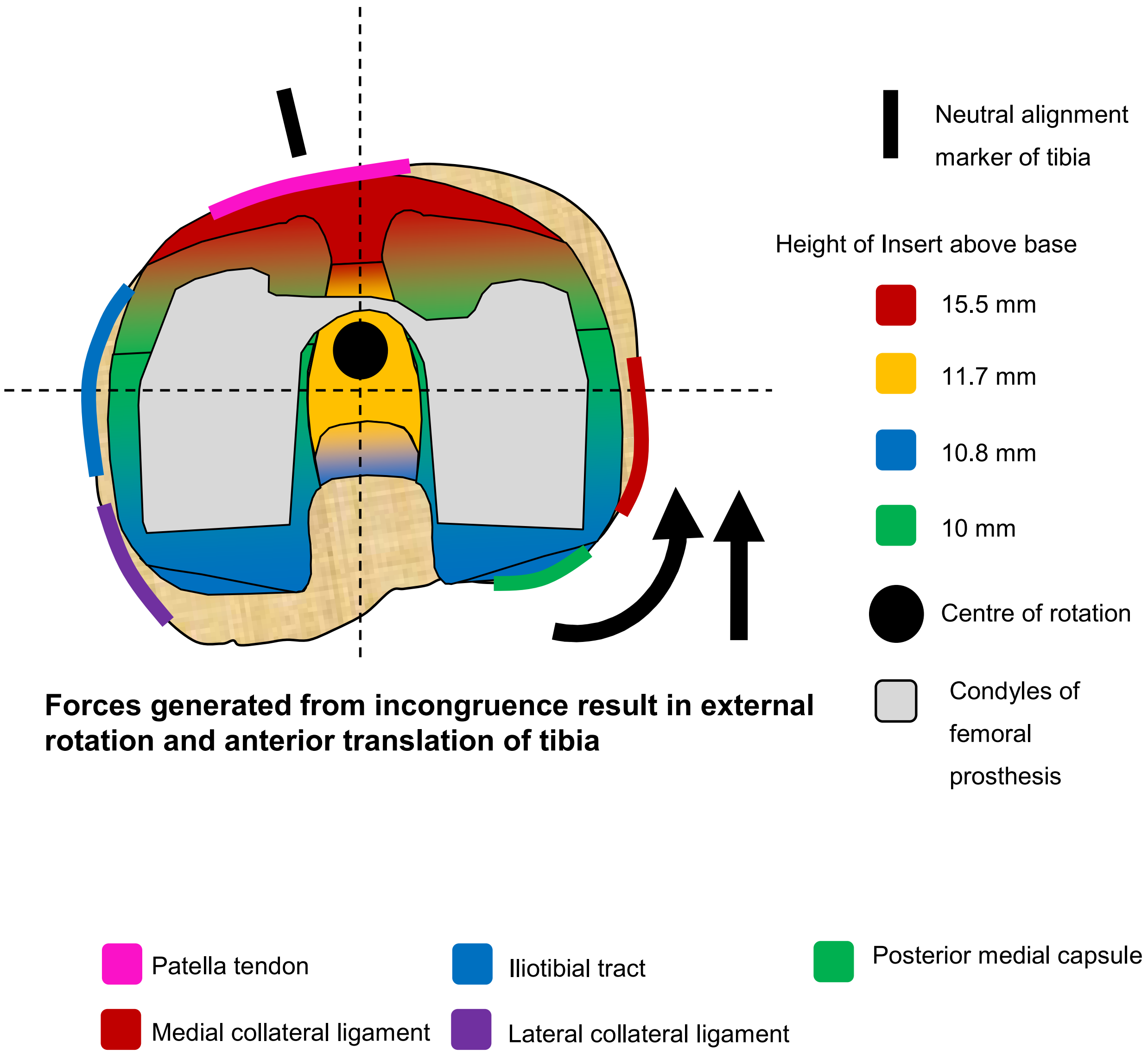

Figure 198: Diagram of a life size image of a 10º externally rotated misaligned tibial tray component rotated about its central axis, demonstrating the resultant internal rotation and posterior translation of the tibia when the knee is loaded and flexed.

20º internal rotation of the tibial tray insert:

When compared with the navigated insert (figure 192), there was internal rotation of the neutral path of movement throughout the full range of knee flexion, but this was not statistically significant. There was however, a statistically significant anterior displacement ($p<0.05$) (of greater magnitude compared with 10º internal rotation of the tibial insert) in the neutral AP pathway throughout the full range of knee flexion. There was also a significant translation in the neutral varus / valgus pathway towards valgus between 20º and 115º of knee flexion ($p<0.05$). The forces applied to the tibia were also evident as statistically significant translations in the internal rotation envelope of laxity towards external rotation throughout the full range of knee flexion ($p<0.05$), anterior translations in the anterior AP envelope between 5º and 90º of knee flexion and in the posterior AP envelope between 5º and 40º of knee flexion and also in the varus envelope of laxity towards valgus between 10º and 115º of knee flexion ($p<0.05$).

These translations may be explained by the incongruent articulation of the femoral condyles against the rotated tibial tray component. Following the extreme 20º internal rotation misalignment, there is significant overhang of the prosthesis laterally in the region of the lateral collateral ligament (LCL) and iliotibial band, anteriorly in the region of the patella tendon and posteriorly in the region of the Posterior medial capsule. The rotated tibial tray pressing against the LCL and iliotibial tract, in particular, may alter the tension in the soft tissue envelope and result in further degradation of kinematics. In addition, the severely rotated dished tibial insert is no longer congruent with the overlying condyles of the femoral component at the sloped antero-medial aspect of the tibial insert and postero-laterally at the cruciate recess (figure 199). It is suggested that as the knee is flexed, the incongruent articulations at the antero-medial and the postero-lateral (cruciate recess) region result in the generation of an external rotation torque and an anterior thrust that are applied to the tibia. This causes the tibia to rotate externally and to move forwards during knee flexion (figure 200).

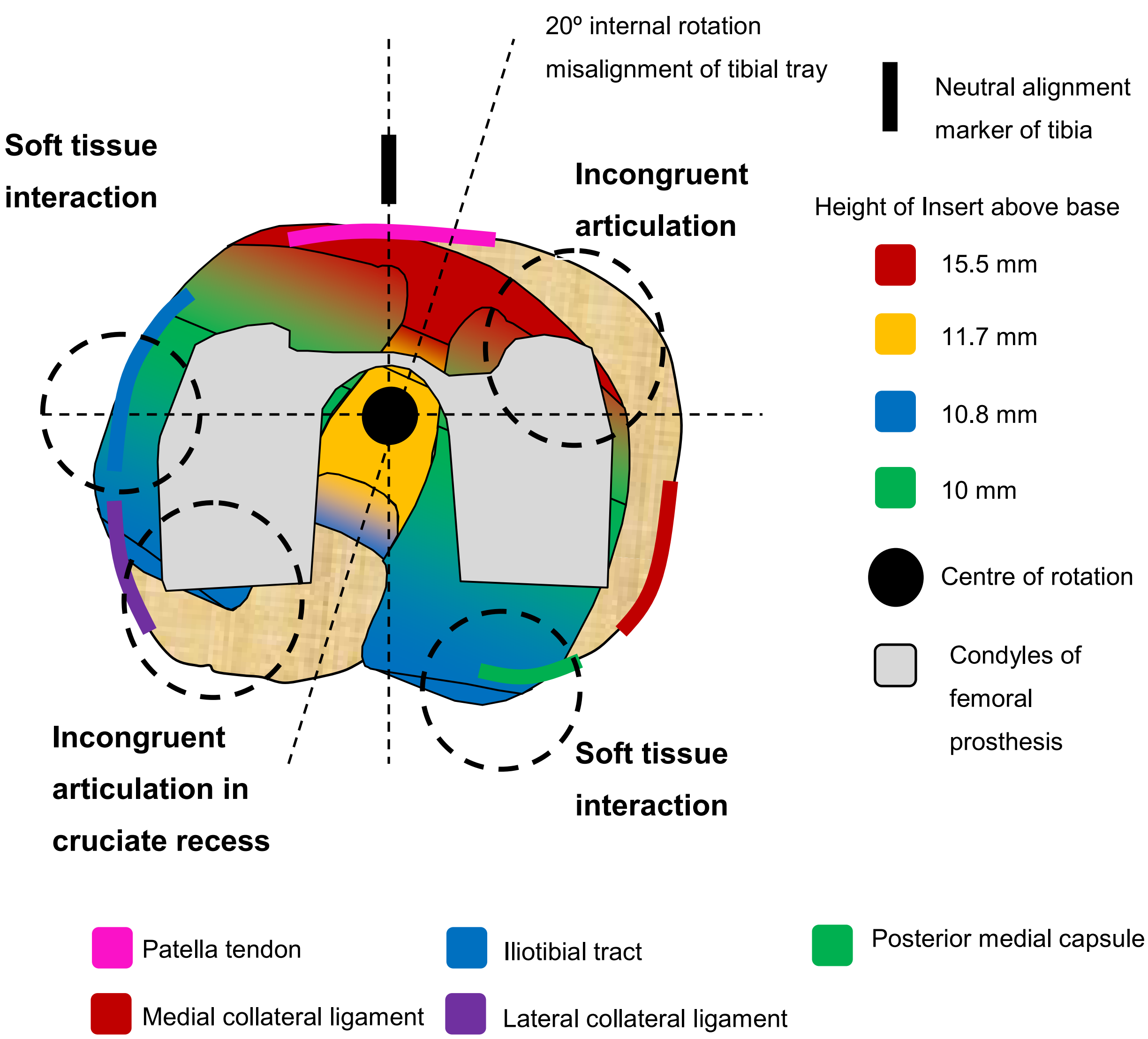

Figure 199: Diagram of a life size image of a 20º internally rotated misaligned tibial tray component rotated about its central axis, demonstrating incongruent articulation between the antero-medial aspect of the tibial insert and the medial condyle of the femoral component, as well as between the postero-lateral aspect of the tibial insert, the cruciate recess and the lateral condyle of the femoral component. Note also the soft tissue interaction in the region of the LCL, iliotibial tract, patella tendon and Posterior medial capsule before the knee is loaded and flexed.

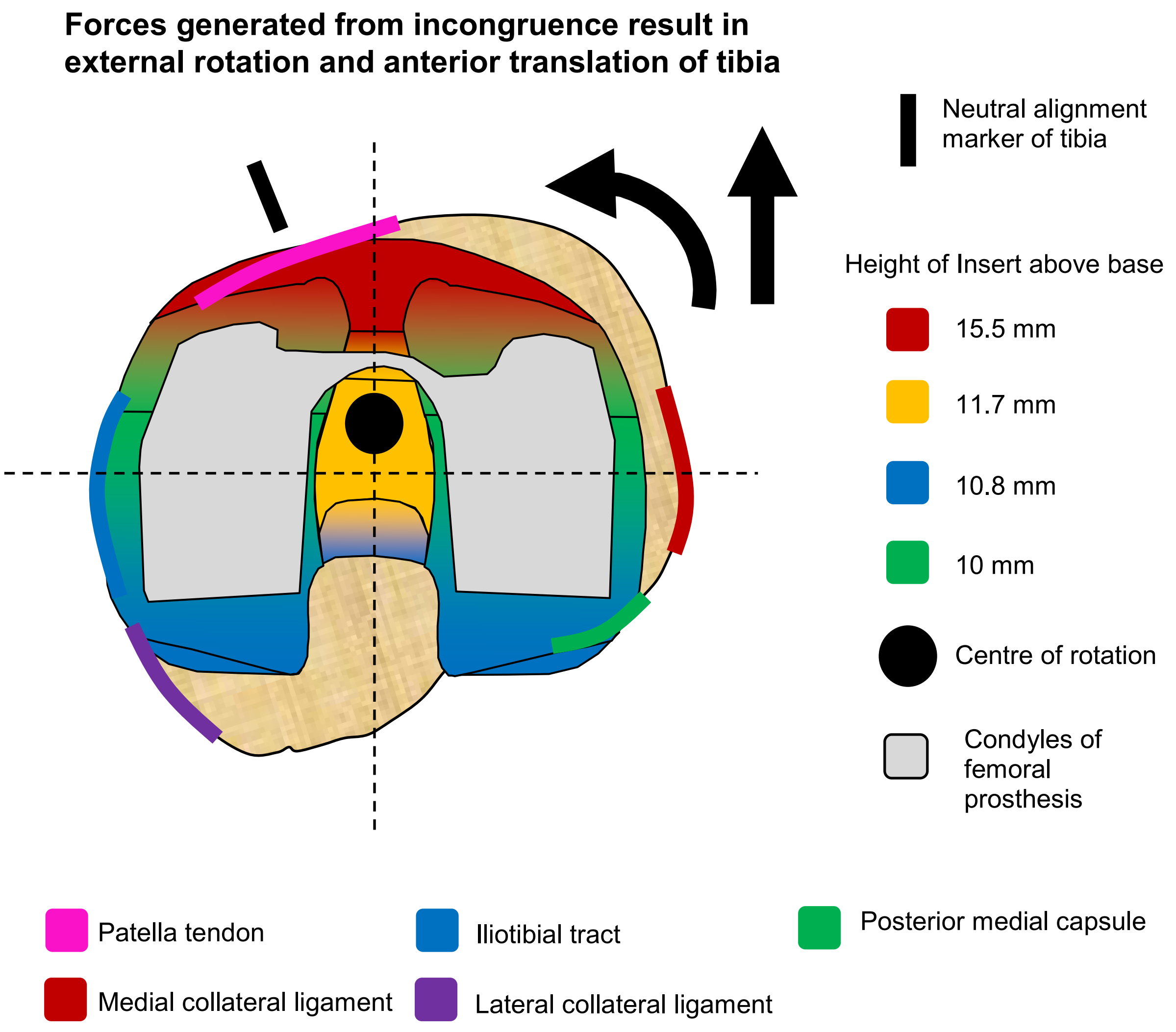

Figure 200: Diagram of a life size image of a 20° internally rotated misaligned tibial tray component rotated about its central axis, demonstrating the resultant external rotation and anterior translation of the tibia when the knee is loaded and flexed. There is also ongoing soft tissue interaction in the region of the LCL, iliotibial tract, patella tendon and Posterior medial capsule.

Posterior slope misalignment of the tibial tray insert in isolation:

For the posterior slope misalignment figures, all images used are constituted from the 70% life size scanned (for better fit on A4 paper) AP and lateral radiographs of a successfully implanted size 7 Scorpio CR TKR (figures 186, 187). Drawings of the tibial trays, that maintain the same joint line height, have been added to demonstrate the effect of the posterior slope on the tibial position.

3 degrees posterior slope of the tibial tray in isolation

When compared with the navigated insert, there was a statistically significant anterior displacement in the neutral AP pathway between 20º and 60º of knee flexion ($p<0.05$), and anterior translation of the anterior limit of AP laxity between 20º and 60º 20 of knee flexion ($p<0.05$). These forces applied to the tibia were also evident as a statistically significant change in the internal rotation envelope towards further internal rotation between 80º and 110º of knee flexion ($p<0.05$).

These changes may be explained by an alteration in the resultant force applied across the tibial joint surface due to the posterior slope, resulting in the generation of an anterior thrust applied to the tibia. This force, combined with an unloading of the posterior soft tissue structures and joint capsule of the knee, resulted in some extra laxity that allowed the anterior translation, internal rotation and valgus alignment observed.

6 degrees posterior slope of the tibial tray in isolation

When compared with the navigated insert, there was a statistically significant anterior displacement in the neutral AP pathway between 10º and 90º of knee flexion ($p<0.05$), and a neutralisation of the neutral rotation pathway between 70º and 110º of flexion ($p<0.05$). The forces applied to the tibia were also evident as statistically significant rotations in the internal and external rotation envelope towards external rotation throughout the whole range of knee flexion ($p<0.05$), and an anterior translation in the anterior AP envelope of laxity throughout the full range of knee flexion ($p<0.05$). There was a tendency for the knee to move into a valgus position both in the neutral pathway and then limits of the envelope of laxity. However, these translations were not statistically significant.

These changes may be explained by the posterior slope, resulting in an anterior thrust applied to the tibia, as before, this force combined with an unloading of the posterior soft tissue structures and joint capsule of the knee result in some extra laxity that allowed the anterior translation, internal rotation and valgus alignment observed.

The translations noted with 6º of posterior slope were also noted to be of statistically significant greater magnitude in the AP neutral path of motion ($p<0.05$), internal and external rotation envelopes of laxity ($p<0.05$) and in the anterior ($p<0.05$) and posterior ($p<0.05$) envelopes of laxity when compared with the 3º posteriorly sloped insert. This suggests that increasing posterior slope is directly related to the knee laxity that has allowed the subsequent tibial translations and rotations observed.

9 degrees posterior slope of the tibial tray in isolation

When compared with the navigated insert (figures 201, 202), there were statistically significant changes in the neutral pathways towards internal rotation between 80º and 110º of knee flexion ($p<0.05$), to an anterior position throughout the full range of movement ($p<0.05$) and towards valgus between 30º and 90º of knee flexion ($p<0.05$). The forces applied to the tibia were also evident as statistically significant changes in the internal and external rotation envelopes towards external rotation throughout the full range of movement ($p<0.05$) and an anterior translation in the anterior ($p<0.05$) and posterior ($p<0.05$) AP envelopes throughout the full range of knee flexion. The envelopes of varus and valgus laxity were unchanged between the series.

The translations noted with 9º of posterior slope were also noted to be of significant greater magnitude in the AP neutral path of motion (although not statistically significant), the internal ($p<0.05$) and external ($p<0.05$) rotation envelopes of laxity and in the anterior ($p<0.05$) and posterior ($p<0.05$) envelopes of laxity when compared with the 6º posteriorly sloped insert. This supports the previous suggestion made when comparing the 3º and 6º posteriorly sloped inserts, that increasing posterior slope is directly related to the knee laxity that has allowed the subsequent tibial translations and rotations observed.

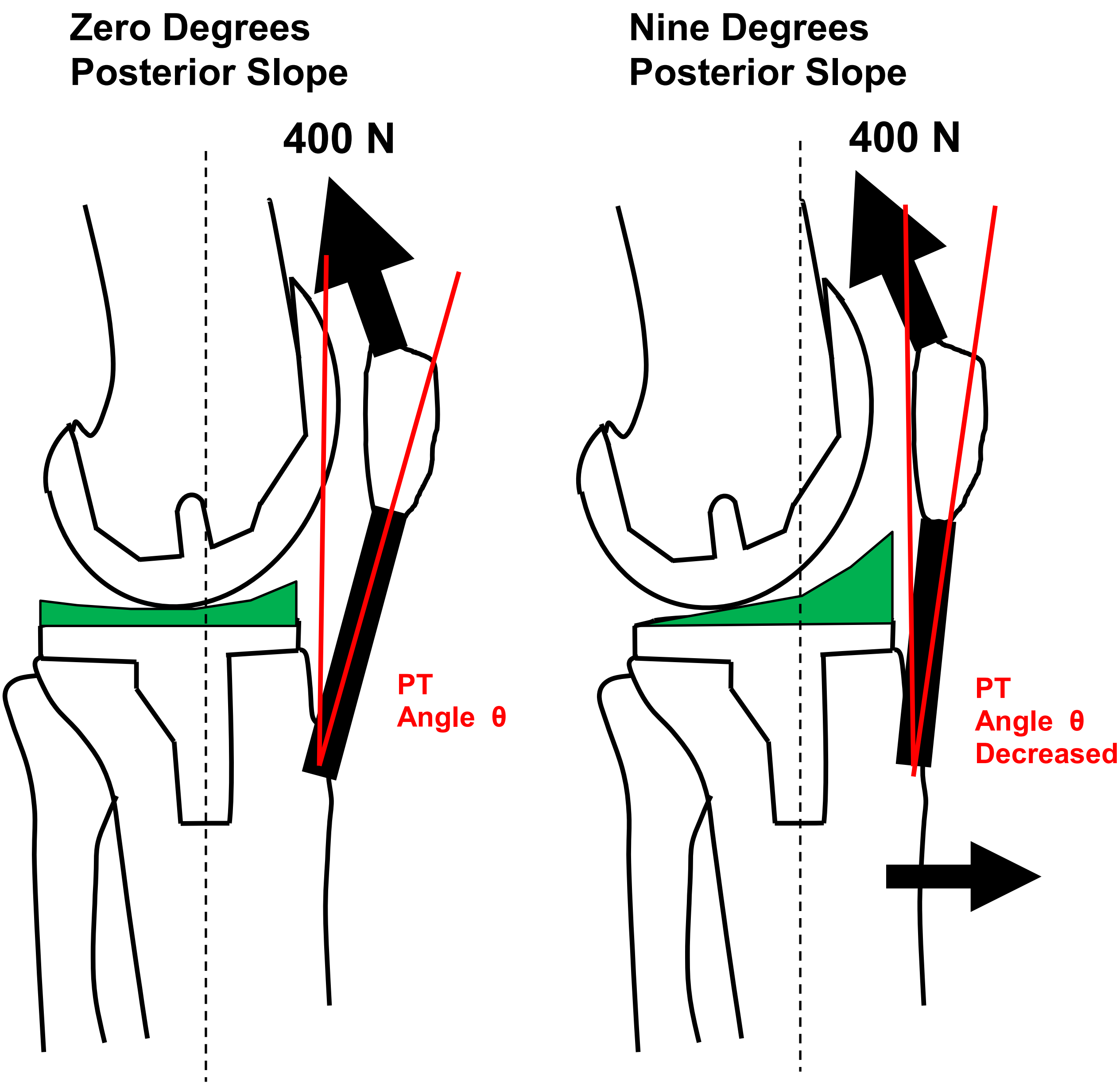

Figure 201: Diagrams of 70% life size 7 Scorpio CR TKRs, the left with a standard un-sloped tibial insert and the right with a 9º posteriorly sloped tibial tray insert. The posterior slope of the insert on the right unloads the posterior structures of the knee resulting in greater AP laxity. The resultant force of the femoral condyles against the sloped polyethylene insert results in a resultant thrust that causes the tibia to sublux anteriorly in the presence of the extra AP laxity. This decreases the patella tendon angle θ, decreasing the anterior moment of the simulated quadriceps force (400N . Sin PT Angle θ). However, the net effect is still the observed anterior translation of the tibia.

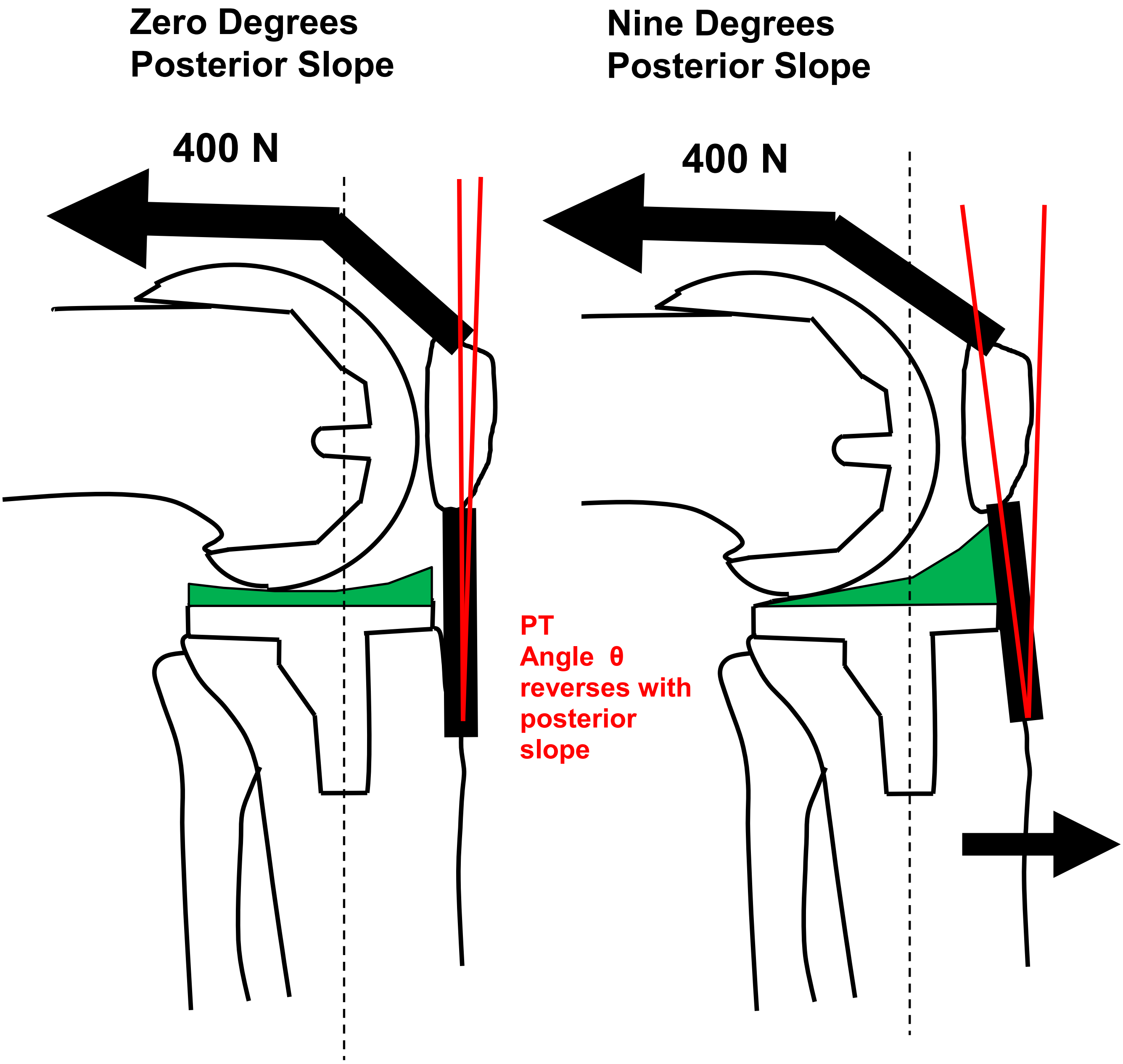

Figure 202: Diagrams of 70% life size 7 Scorpio CR TKRs, the left with a standard un-sloped tibial insert and the right with a 9º posteriorly sloped tibial tray insert. The posterior slope of the insert on the right unloads the posterior structures of the knee resulting in greater AP laxity. The resultant force of the femoral condyles against the sloped polyethylene insert results in a resultant thrust that causes the tibia to sublux anteriorly in the presence of the extra AP laxity. This reverses the patella tendon angle θ. Although this reduces the anterior moment of the simulated quadriceps force (400N . Sin PT Angle θ), the change is not significant and the net effect is the observed anterior translation of the tibia.

Combined misalignments of the tibial tray insert:

20º external rotation combined with 9º posterior slope of the tibial insert

When compared with the navigated insert (Figure 192), there were statistically significant changes observed in the neutral pathways of motion towards internal rotation ($p<0.05$), an anterior position ($p<0.05$) and towards valgus ($p<0.05$). These forces applied to the tibia were also evident as statistically significant changes in the envelopes of laxity, towards internal rotation ($p<0.05$), an anterior position ($p<0.05$) and towards varus ($p<0.05$).

The translations observed by the combined misalignment may be explained by the compounding actions of the individual effects of the 9º slope and 20º external tibial rotation in isolation as discussed previously in this chapter. The 9º posterior slope results in an alteration in the resultant force applied across the tibial joint surface and also significantly alters the joint laxity by unloading the posterior soft tissue elements. The 20º of external rotation misalignment results in a significant incongruence with the overlying femoral condyles that lie posteriorly due to the excessive laxity in the joint (figure 203).

As the knee is loaded and flexed, the 400N simulated quadriceps contraction force acting through the patella to the tibial tuberosity, results in the generation of an overwhelming anterior thrust. This force in combination with the extra posterior laxity, results in anterior translation of the tibia (even in the presence of the relatively small posterior thrust generated by the incongruent articulation of the femoral condyles on the posterior slope of the tibial tray). The rotational incongruence of the severely rotated tibial tray results in the internal rotation observed, and the very posterior position of the femur on the rotated tibial tray insert may also result in the medial condyle of the femur overlying and falling behind or into the posterior cruciate recess (figure 204). With the lateral condyle of the femur still on the tibial tray, this difference in the heights of the condyles may explain the observed translation towards varus (figure 205).

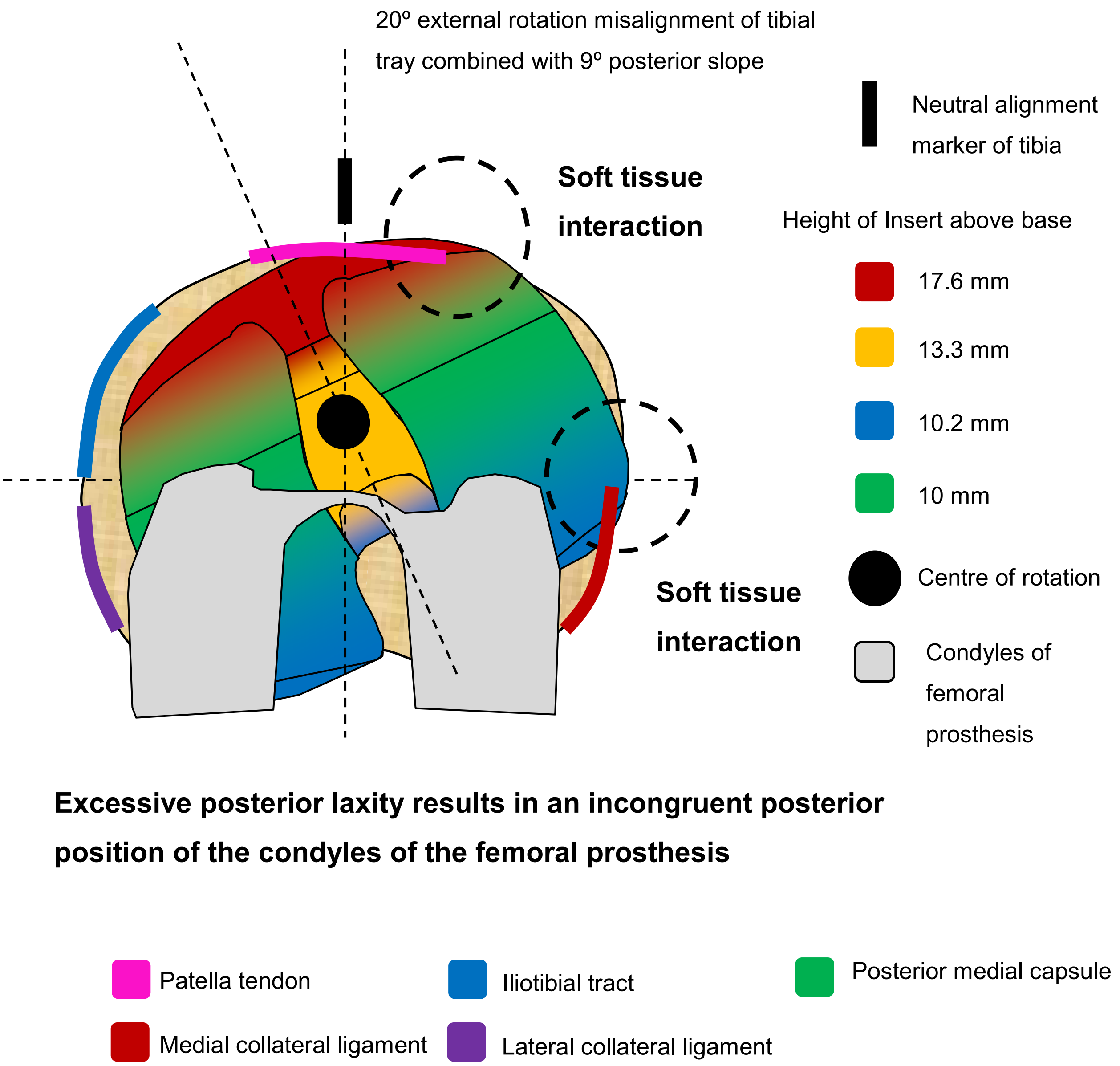

Figure 203: Diagram of a life size image of a 20º externally rotated misaligned tibial tray component rotated about its central axis combined with 9º of posterior tibial slope, demonstrating the posterior position of the femoral component due to the excessive posterior laxity and anterior tibial translation generated by the slope of the insert. The resulting articulation is incongruent with significant overhang of the tibial tray. The medial condyle of the femur overlies and can sublux behind the tibial tray or into the posterior cruciate recess whilst the lateral condyle of the femur remains on the incongruent tibial tray and may explain the observed translation towards varus. Note also the soft tissue interaction in the region of the LCL, iliotibial tract, patella tendon and Posterior medial capsule.

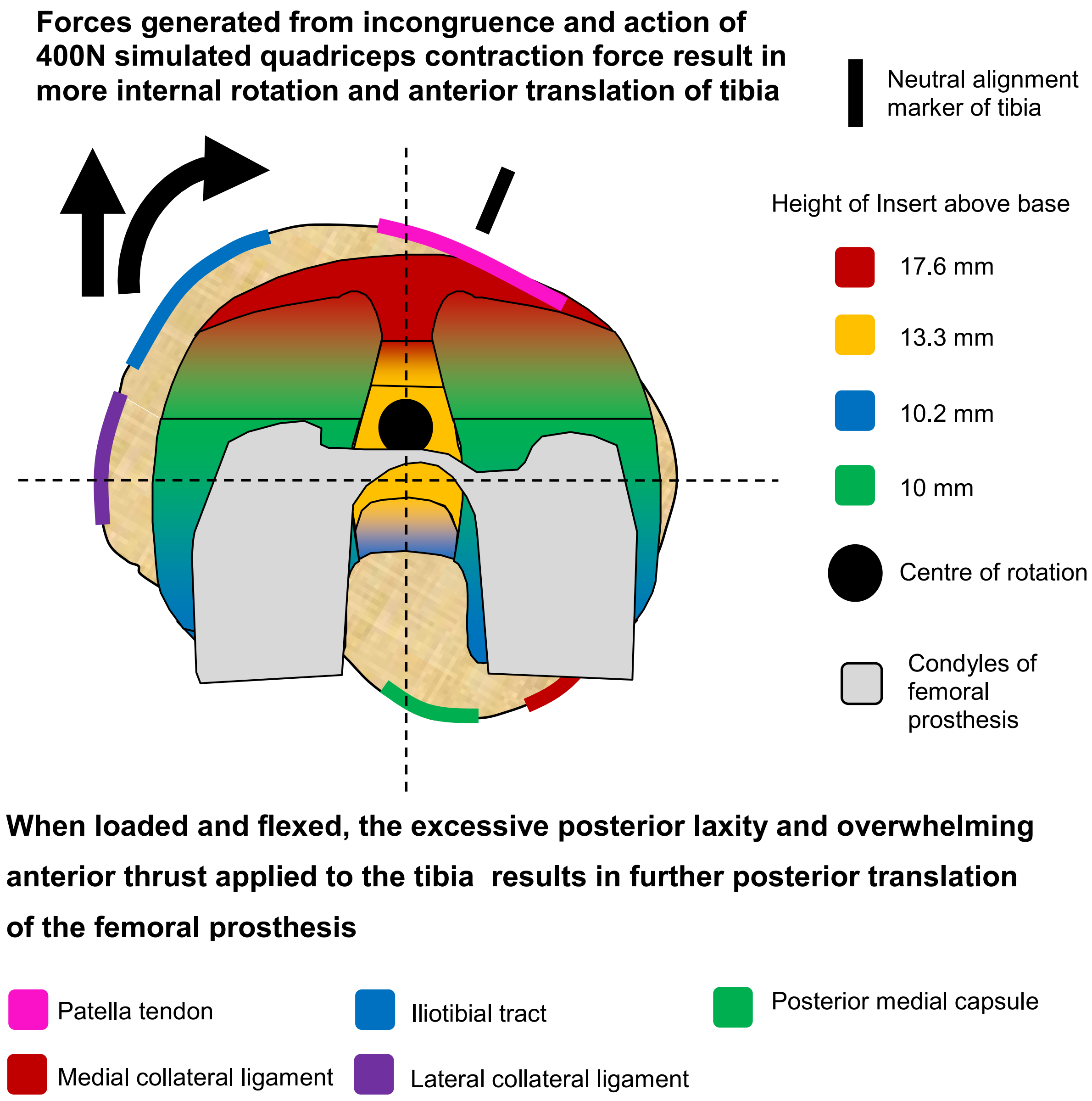

Figure 204: Diagram of a life size image of a 20º externally rotated misaligned tibial tray component rotated about its central axis combined with 9º of posterior tibial slope, demonstrating the resultant internal rotation and anterior translation of the tibia when the knee is loaded and flexed. The excessive laxity also results in further posterior translation of the femoral prosthesis. The medial femoral condyle may also sublux behind or into the posterior cruciate recess resulting in the translation towards varus that is also observed.

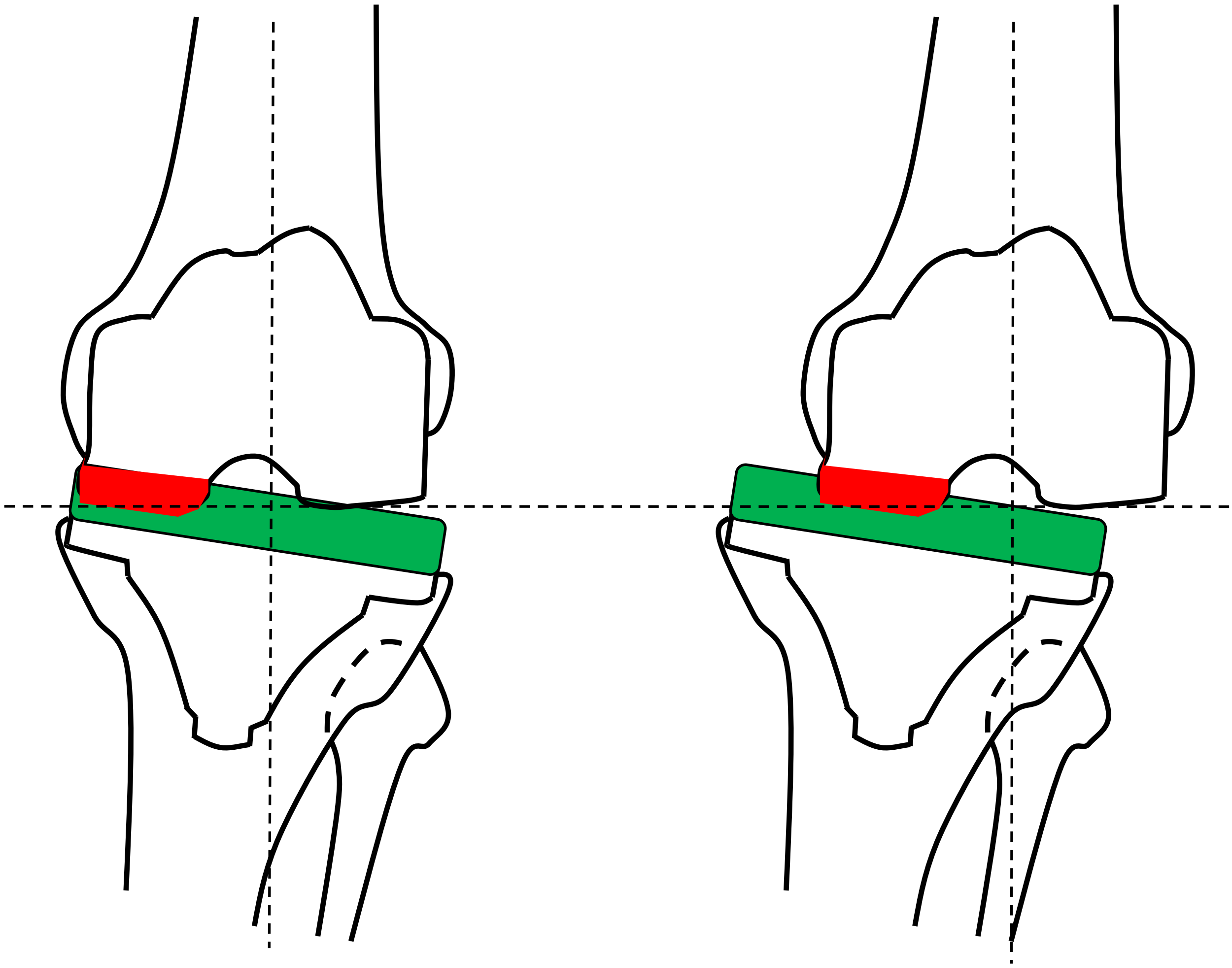

Figure 205: Diagram of a 70% of life size coronal image of size 7 Scorpio CR TKR with an added 20º externally rotated 9º posteriorly sloped tibial insert, demonstrating the varus angulation caused by the excessive laxity after posterior slope of the tibial insert, resulting in a posterior dislocation of the medial femoral condyle (image on left) or a subluxation of the medial femoral condyle into the posterior cruciate recess (image on right).

20º internal rotation combined with 9º posterior slope of the tibial insert

When compared with the navigated insert, there were statistically significant changes observed in the neutral pathways of motion towards external rotation ($p<0.05$), an anterior position ($p<0.05$) and towards valgus ($p<0.05$). These forces applied to the tibia were also evident as statistically significant changes in the envelopes of laxity, towards external rotation ($p<0.05$), an anterior position ($p<0.05$) and towards valgus ($p<0.05$).

The translations observed by the combined misalignment may be explained by the compounding actions of the individual effects of the 9º slope and 20º internal tibial rotation in isolation as discussed previously in this chapter. The 9º posterior slope results in an alteration in the resultant force applied across the tibial joint surface and also significantly alters the joint laxity by unloading the posterior soft tissue elements. The 20º of internal rotation misalignment results in a significant incongruence with the overlying femoral condyles that lie posteriorly due to the excessive laxity in the joint (figure 206).

As the knee is loaded and flexed, the 400N simulated quadriceps contraction force acting through the patella to the tibial tuberosity, results in the generation of an overwhelming anterior thrust. This force in combination with the extra posterior laxity, results in anterior translation of the tibia (even in the presence of the relatively small posterior thrust generated by the incongruent articulation of the femoral condyles on the posterior slope of the tibial tray). The rotational incongruence of the severely rotated tibial tray results in the external rotation observed, and the very posterior position of the femur on the rotated tibial tray insert may also result in the medial condyle of the femur overlying and falling behind or into the posterior cruciate recess (figure 207). With the lateral condyle of the femur still on the tibial tray, this difference in the heights of the condyles may explain the observed translation towards valgus (figure 208).

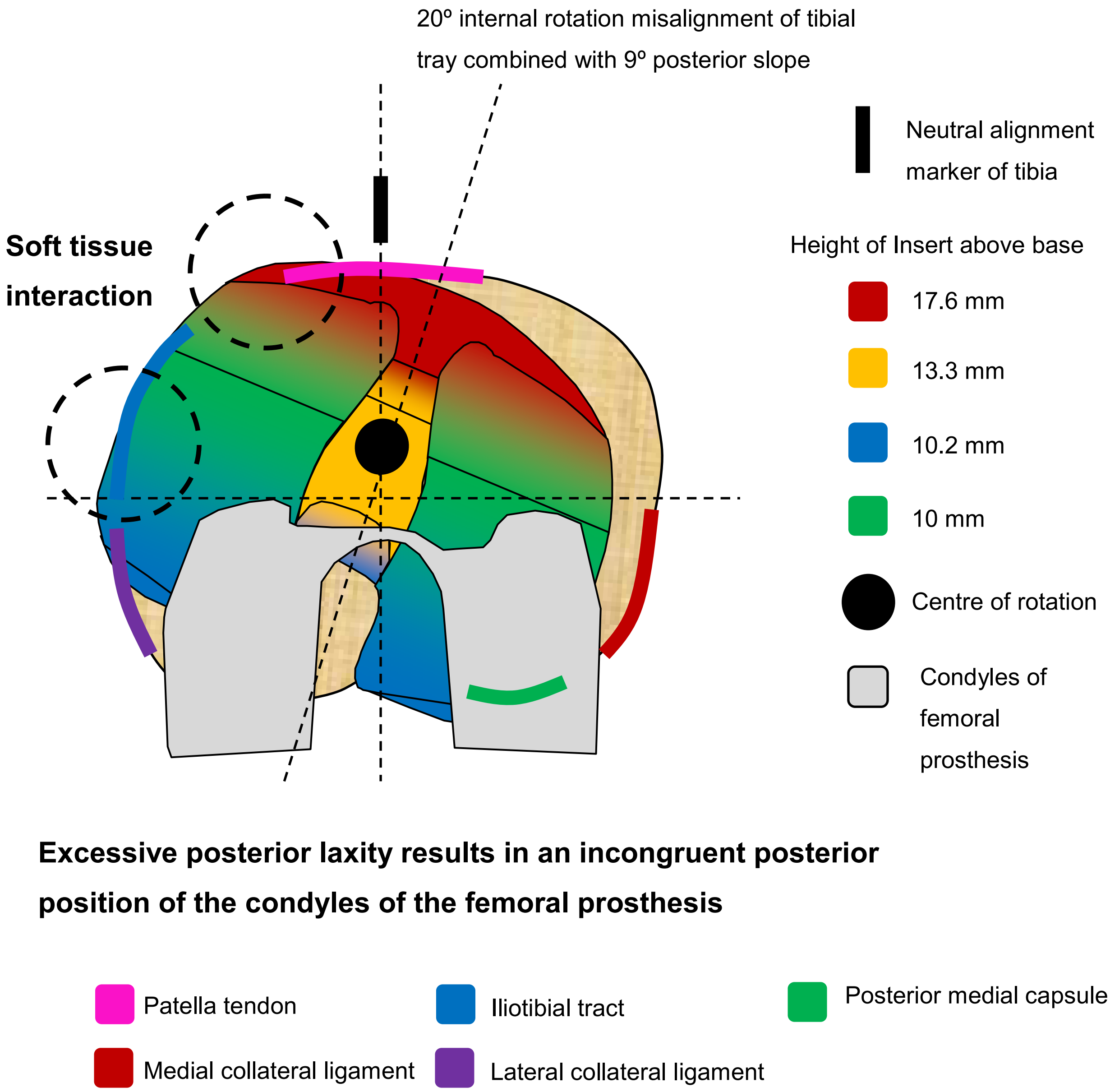

Figure 206: Diagram of a life size image of a 20º internally rotated misaligned tibial tray component rotated about its central axis combined with 9º of posterior tibial slope, demonstrating the posterior position of the femoral component due to the excessive posterior laxity and anterior tibial translation generated by the slope of the insert. The resulting articulation is incongruent with significant overhang of the tibial tray. The lateral condyle of the femur overlies and can sublux behind the tibial tray or into the posterior cruciate recess, whilst the medial condyle of the femur remains on the incongruent tibial tray. This may explain the observed translation towards valgus. Note also the soft tissue interaction in the region of the LCL, iliotibial tract, patella tendon and Posterior medial capsule.

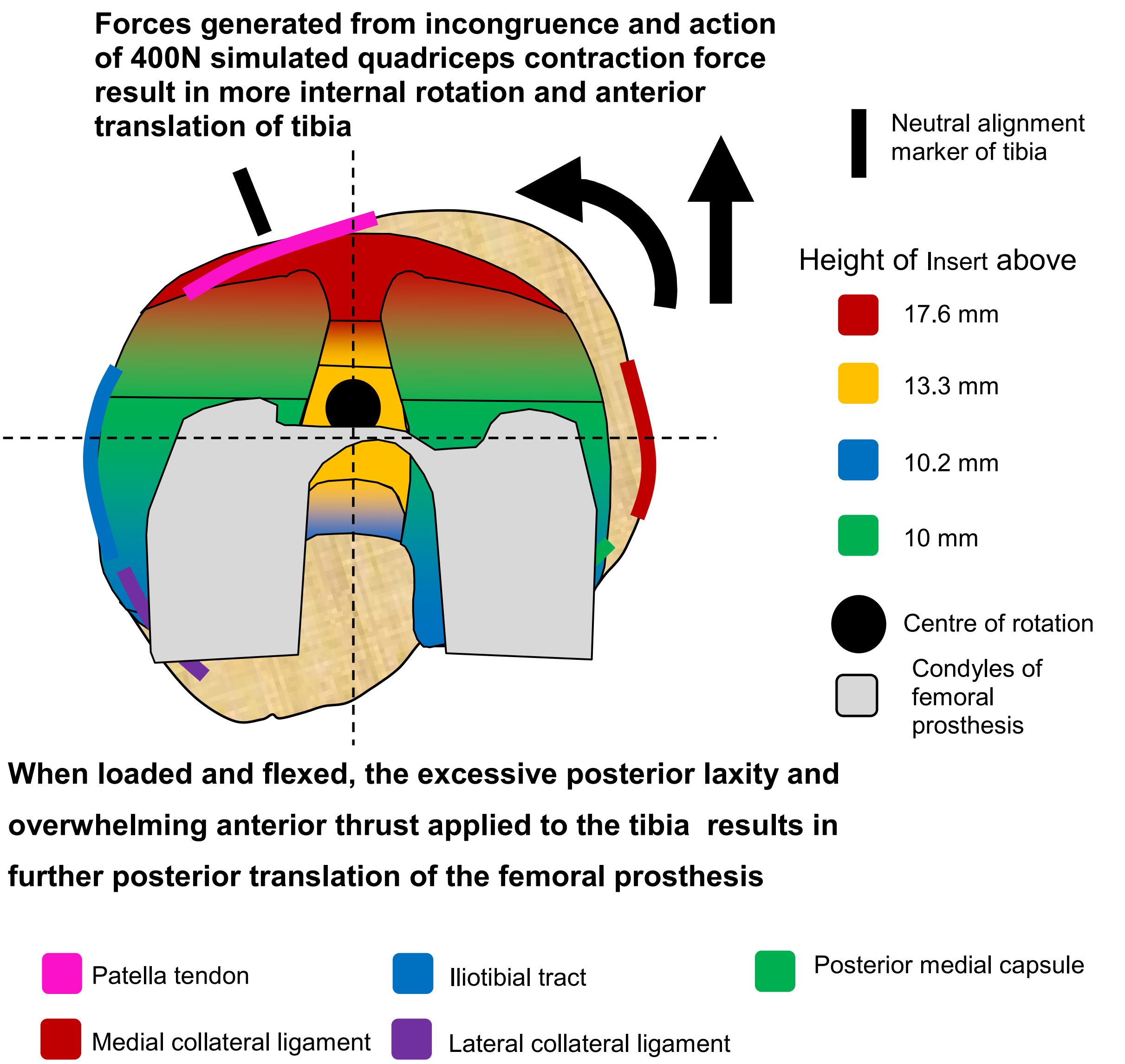

Figure 207: Diagram of a life size image of a 20° internally rotated misaligned tibial tray component rotated about its central axis combined with 9° of posterior tibial slope, demonstrating the resultant external rotation and anterior translation of the tibia when the knee is loaded and flexed. The excessive laxity also results in further posterior translation of the femoral prosthesis. The lateral femoral condyle may also sublux behind or into the posterior cruciate recess resulting in the translation towards valgus that is also observed.

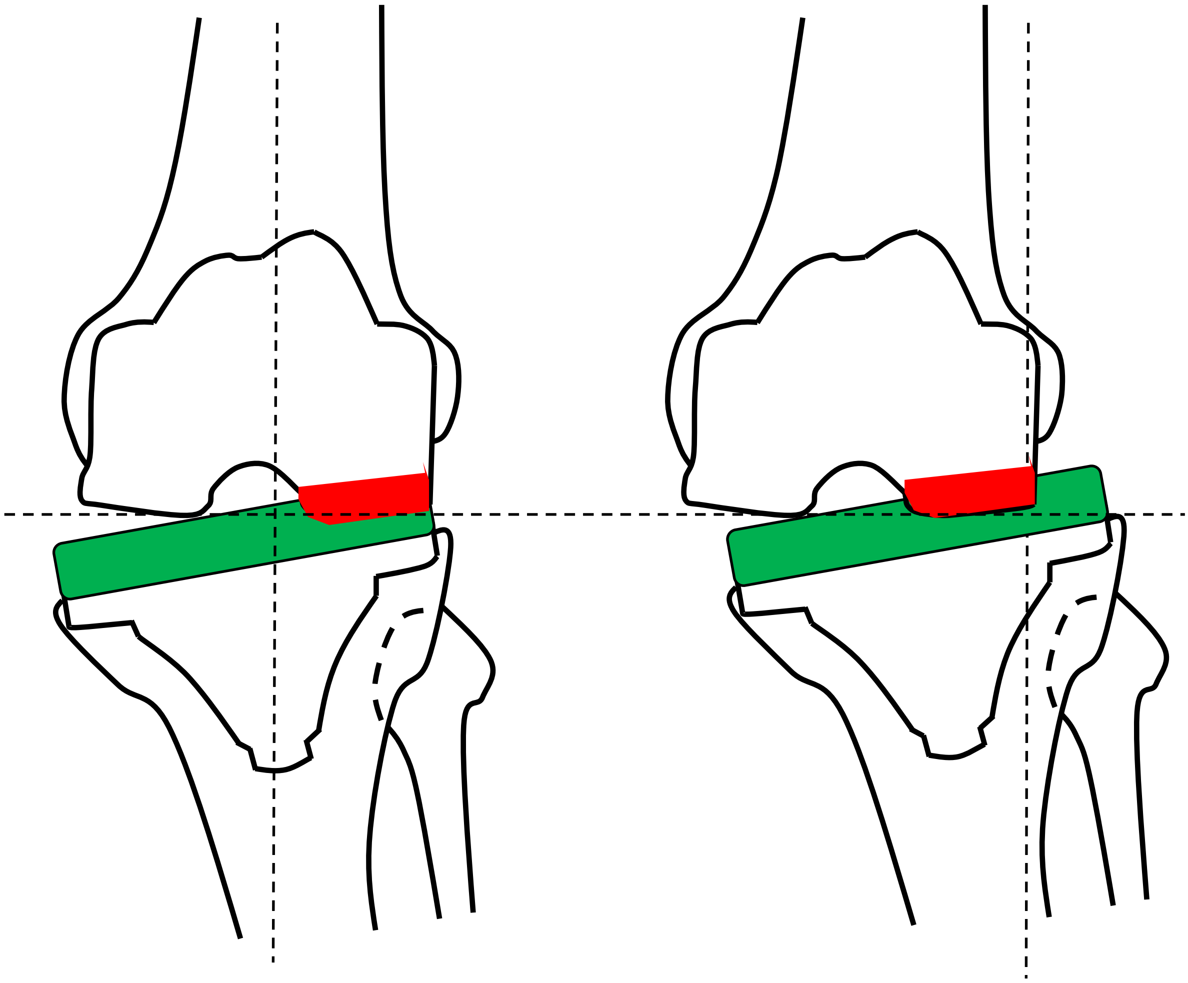

Figure 208: Diagram of a 70% of life size coronal image of size 7 Scorpio CR TKR with an added 20º internally rotated 9º posteriorly sloped tibial insert, demonstrating the varus angulation caused by the excessive laxity after posterior slope of the tibial insert resulting in a posterior dislocation of the medial femoral condyle (image on left) or a subluxation of the medial femoral condyle into the posterior cruciate recess (image on right).

SUMMARY

Knee kinematics were significantly different from the native knee after navigated TKR using this implant. The knee adopted a single axis profile with obliteration of the screw-home and femoral roll back mechanisms. The tibia also adopted a paradoxical posterior position as the knee was flexed. The varus / valgus laxity of the knee was unchanged, but this may have depended on the bony cuts and soft tissue releases.

External rotation of the tibial tray resulted in a change of the neutral path of motion of the tibia towards internal rotation and an anterior position, with matching changes in the envelope of laxity anteriorly and towards internal rotation. The magnitudes of deviation from normal kinematics were proportional to the amount of external rotation misalignment applied to the tibial tray.

Internal rotation of the tibial tray resulted in a change in the neutral path of motion of the tibia towards external rotation, an anterior position and into a valgus alignment, with a change in the envelope of laxity anteriorly and towards external rotation. The magnitudes of deviation from normal kinematics were proportional to the amount of internal rotation misalignment applied to the tibial tray.

The addition of posterior slope to the tibial tray resulted in a change in the neutral path of motion of the tibia towards an anterior position and towards increasing degrees of external rotation as the magnitude of the slope applied increased, with an average anterior tibial translation of 2mm for every 3º of posterior slope applied. At the greatest slope of 9º, there was also a change in the neutral pathway of motion towards valgus. The envelopes of laxity also moved anteriorly, towards external rotation and valgus with increasing posterior slope.

The combined misalignment of 20º of external rotation and 9º of posterior slope of the tibial insert resulted in a change of the neutral path of motion anteriorly, into internal rotation and towards a varus angulation, with a change in the envelope of laxity towards an anterior position, external rotation and varus.

The combined misalignment of 20º of internal rotation and 9º of posterior slope of the tibial insert resulted in a change of the neutral path anteriorly, into external rotation and towards a valgus angulation, with a change in the envelope of laxity towards an anterior position, external rotation and valgus.

The results of this study have demonstrated that tibial tray rotational misalignment in isolation, posterior slope and extreme combinations of slope and rotation of the tibial tray all modify the neutral path of motion and the envelope of laxity of the knee following TKR, resulting in a deviation from normal navigated TKR kinematics.

CLINICAL IMPLICATIONS

The number of total joint replacements performed per year is growing rapidly and estimated to reach 3.5 million new procedures per year in the United States alone by 2030 (65). After infection, misalignment and aseptic loosening are the most frequent reasons today for revision surgery following TKR ([34;116]), with rates as high as 9% ([74]) and costs exceeding $3 billion per year in the USA alone (23).

Tibial component misalignment encompasses component varus & valgus position, correct coronal positioning, component fit, rotational alignment, joint line and tibial slope. Of all these, tibial component rotational misalignment is the commonest positioning error in TKR, with studies demonstrating as much as 96% of components incorrectly placed in a wide range from 10º of external rotation to 28º of internal rotation ([56;92;115]). The addition of posterior tibial slope is also still controversial although widely practiced, with most published clinical studies showing no advantage from the addition of tibial slope ([14;68;97;120]). Furthermore, TKR retrieval studies suggest that any posterior slope can result in excessive posterior loading of the components with subsequent increased wear ([142]). But there is also evidence for the use of posterior slope, with reported gains of 1.7^{o} of extra flexion per applied degree of posterior slope and statistically significant clinical gains in knee flexion ([24;91]).

This study has demonstrated significant deviations from normal kinematics following 10 degrees of tibial tray rotation and 3º of posterior slope with a tibial component that utilises a femoral component with symmetrical condyles, articulating with a symmetrical tibial tray and fixed bearing tibial tray insert. It was presumed that the symmetry of this implant combined with its single radius design would be tolerant and forgiving in the face of component misalignment compared to some more recent commercially available designs that utilise asymmetric femoral condyles, tibial trays and inserts, of the fixed or mobile bearing kind. However, it must be noted that there has not been sufficient follow up of these newer asymmetric knee implant designs to determine if, given the same incidence of misalignment, that there will be more wear and / or a higher failure rate.

Computer assisted surgery devices or navigation systems are being used increasingly for TKR, and have been shown to improve the accuracy of tibial and femoral bone resections and to improve component positioning ([21;44;86;110;135]). However, navigation systems are expensive and add significant costs to the procedure in terms of extra equipment required and time expended compared to traditional jig-based implantation systems ([55]) with an extra average surgical time of 10 to 20 minutes of surgical time expended for tracker fixation in experienced hands ([32]) and significantly longer during the surgeons 'learning curve' period, which may affect patient outcome adversely and reduce theatre efficiency. Also, any system which uses additional ionising radiation (e.g. CT scanning) introduces extra costs and a small but definite cancer risk in such a large patient population.

Tracker pin placements for navigation are not without surgical morbidity: Neurovascular damage, pin track infections, fractures through pin sites and breakages of devices within the bone have all been reported ([55]). A further source of error can be incorrect interpretation or use of the computer software and a poor fix of the trackers or reflector arrays, especially in the porotic bone frequently encountered in patients undergoing TKR.

Despite published evidence that navigation systems used in TKR can result in more accurate bone resections and component positioning ([21;44;86;110;135]), this increased accuracy has not demonstrated any significant clinical improvement postoperatively, or at a follow up at the 2 ([127]) or 5 year ([65;99]) mark.

It must also be noted, that computer-assisted navigation is purely a tool. It does not replace the surgeon, but merely provides him/her with information, that must be evaluated and assessed prior to proceeding by an experienced surgeon. The machine cannot substitute for knowledge and skill. The use of a navigation system requires training and experience or inadvertent surgical errors can be concealed and compounded by the computer system, resulting in a potential disaster.

Optimum knee kinematics allows for increased surface conformity and subsequent balanced implant loading throughout the range of motion. Incompatibilities of alignment, joint loading or implant geometry may result in increased ligament tension and incongruence or dysfunction of the component articulations with the generation of localised stress concentrations in the gain cycle. These may contribute to premature wear and loosening of the implants resulting in patient dissatisfaction and symptoms that may necessitate revision knee surgery. However, it is impossible in this study or any other so far published, to determine the clinical significance of the statistically significant translations with as little magnitude as ±1mm of translation or ±1 degree of rotation as detected by our navigation equipment.

Finally, it is still unknown if the “navigated” position chosen for implant placement by a computer aided guidance system will produce the best physiological kinematics in vivo, or that the reproduction of native knee kinematics in a prosthetic knee will improve patient satisfaction, performance and the longevity of the implants.

LIMITATIONS OF THIS STUDY

1. Specimen numbers

Ten fresh cadaver specimens were used for the kinematic and misalignment experiments. However, the results of two of the specimens were excluded from the study due to failure. The first excluded specimen was extremely porotic and failed whilst being loaded, due to a fracture of the femur. The second excluded specimen had a very poor soft tissue envelope and failed with complete avulsion of the medial and posterior knee capsule and muscles, an avulsion that was not repairable.

A post hoc power calculation using the standard deviations obtained from the results of the remaining 8 specimens demonstrated an 80% power at the 95% confidence level to detect translations of 5 mm or angulations of 9º. Although this power level is satisfactory to meet the aims of this study, increasing the number of specimens would have increased the statistical power of the results. It is suggested that for any subsequent experiments, a greater number of specimens are used.

2. Repetitive opening and closing of the knee

The posterior slope of the implant was altered by using a sloped polyethylene machined insert. Although this insert did not change the level of the joint line of the implant, it was necessary to open the soft tissue envelope of the knee in order to physically change the polyethylene insert. Although the soft tissue envelope was meticulously repaired using commercially available sutures following the change of polyethylene insert, the repeated opening and closing of the knee may have affected the integrity of the soft tissue envelope and may account for some of the laxity observed in some of the experiments. It is suggested that for subsequent studies, a jig be devised to allow the adjustment of tibial slope without having to repetitively open and close the knee. It would also have been wise to repeat the initial kinematic measurements after using all the polyethylene inserts and completing the cycle of experiments. By going back to the first zero degrees insert, any changes in the envelope of laxity attributable to the instrumentation of the soft tissue envelope could be measured. Similarly a random order of insert use might have avoided any related systematic bias.

3. Range of recorded movement

The aim of this study was to record knee kinematics for the full range of knee motion, from full extension to deep flexion (0 to >120º of flexion). During the experiments, the knee specimens were extended from deep flexion to full extension. However, at the extremes of flexion and extension (in deep flexion and in full extension), there was visible soft tissue impingement and tightness, resulting in inaccurate data collection of the knee kinematics at these extremes of movement, clearly visible on the plotted curves as prominent deviations in the data. Resultantly, the kinematic data collected between 0 and 5º of knee flexion and after 110º of knee flexion was deemed unreliable, removed from the graphs and disregarded in the subsequent analyses. In future studies, it is suggested that the specimens chosen be tested prior to experimentation to ensure they have a full range of motion (0 to >120º of flexion) without significant soft tissue impingement.

4. Simulated quadriceps force applied through patella

The simulated quadriceps extension force of 400 N was applied to the knee via a trans-osseous pin placed transversely through the thickest portion of the bony patella. A centrally mounted pneumatic piston was used to apply the constant load of 400 N via a half ring and cable assembly, parallel to the anterior aspect of the femur. Therefore, the individual actions and magnitudes of force applied by each of the quadriceps muscles were not considered. Neither was the distribution of force through the quadriceps retinaculum / tendon. In future studies, it is suggested that the quadriceps muscles should be loaded independently to better replicate the actions of the native knee, in line with the protocols and anatomical data in the literature ([13;45]).

5. Simulated quadriceps force not applied parallel to femur

The pneumatic piston used to apply the constant 400 N simulated quadriceps force was mounted centrally and slightly higher than the level of the femur. This was to ensure that the cable assembly did not snag on the specimen or the mounted trackers during the loading cycles. The resultant simulated quadriceps force was not applied parallel to the femur as is the case with true quadriceps muscular contraction. In future studies, it is suggested that the quadriceps muscles should be loaded independently to better replicate the actions of the native knee, but this would have only a minor effect on tibial kinematics.

6. Single surgeon

In this study, all the surgical dissection, digitisation and experimentation was performed by a single surgeon (AK), guided by the navigation system. It is recommended that subsequent experiments should be performed by 2 or more experienced surgeons working in combination. This should reduce any errors in digitisation and implantation as well as decrease the time required to perform the experimental cycle, which helps preserve the fresh condition of the specimen.

7. Single implant design.

The implant chosen and used for the experiments was a Scorpio CR (cruciate retaining) fixed bearing total knee replacement. This utilised a polyethylene fixed bearing and a full radius, single, fixed axis design. It is unknown what effect if any, modifying the implant design would have on the observed kinematics. It is therefore suggested that in subsequent studies, a variety of implant designs be tested to compare and contrast the kinematics inferred by the differences in design.

8. Absent co-contractions of the hamstring muscles

In this study, only the quadriceps muscles were simulated using a pneumatic piston. No attempt was made to simulate the co-contractions of the hamstring muscles normally observed during gait and deep flexion of the knee ([51]). These muscular co-

contractions stabilise the knee, particularly during descent, ascent and holding stages in knee flexion and extension. In subsequent experiments, it is suggested that both the quadriceps and hamstring muscles be loaded independently to better re-create the muscle tension in the soft tissue envelope during flexion and extension as is observed in the native knee. The situation studied therefore replicated open-chain knee extension actions.

9. Averaging of data for analyses.

In this study, the recorded kinematic data sets of each of the tested specimens were combined and averaged to produce an “average normal knee” and an “average implanted knee” data set for each of the component positions. These averaged data sets were then used for the subsequent results and statistical analyses. A criticism of this method of analysis is that no two human knees are identical in structure or function and the specimens should therefore have been compared independently.

The specimens utilised in this study were all selected at random from a tissue bank. Although they were devoid of significant arthritic defects and from an age group likely to benefit from knee arthroplasty, there were significant differences in the bone quality, extent of arthritic change and soft tissue bulk and quality between them.

Averaging of the specimen data sets was required to achieve sufficient power for the statistical analyses, and to minimise errors generated from the individual specimens. 95% confidence intervals were also calculated and displayed on all the graphs generated from the combination of data sets in order to minimise the averaging bias. In future experiments, it is suggested that the specimens be examined prior to selection, possibly with pre-experimental MRI or CT scans, to ensure that anatomy, bone quality, arthritic change and soft tissue bulk and quality are as closely matched as possible.

10. Patella not resurfaced

During normal surgical protocol for total knee replacement, it is common in some hospitals to resurface the patella by excising the articular surface and subchondral bone and replacing it with a domed or contoured polyethylene patella button. In this study, the patella was not resurfaced and this step was excluded from the experimental protocol. Previous experiments conducted in the lab using a realistic simulated saw bone ([3;7]) demonstrated that following resurfacing, the patella was unable to withstand the 400N simulated quadriceps contraction force applied through it using the transosseous pin.

It is not known what effect, if any, that resurfacing the patella has on the tibio-femoral kinematics of total knee replacement, however it is suggested that in subsequent studies, if the loading conditions allow, then the patella should be resurfaced to reflect the current practice in total knee replacement in some centres, and to find out whether resurfacing contributes significantly to the motion of the tibia.

11. Constant simulated quadriceps load

In this study, a simulated quadriceps contraction force of 400N was utilised as this equated to half the anticipated body weight for an average 80 kg human being. This value was constant throughout the full range of flexion and extension. This value provided sufficient quadriceps simulation to ensure a compressive joint load while still allowing the envelope of laxity to be investigated using moderate precise loading forces in the other planes of movement. It was known from prior experience that larger forces led to a risk of failure of the trans-osseous pin in the porotic patellae of the elderly knees available and used in the experiments.

The physiological load applied through the native knee varies depending on activity and knee position in the flexion / extension cycle. It has been shown that loads can approach 3.1 times body weight when walking and 5.4 times body weight when stair climbing, as suggested by *Taylor et al* ([133]). It is presumed that weight distribution for TKA is similar to that of the native knee during the gait cycle, and it is therefore suggested that in subsequent studies, a method for loading the knee physiologically be devised to better replicate the loading conditions for the knee for kinematic analysis.

12. Misalignment rotations not navigated.

In this study, the rotational misalignments of the tibial tray about its centre point were measured using a large printed protractor that was affixed to the superior surface of the nylon rotation disc and measured with a control rod screwed into the inner tibial rod. Although this method for determining the rotational misalignment angle was adequate for this study, it would have been more accurate to have devised a fitment for the inner tibial rod that would have allowed the rotational misalignment to be more precisely guided by the navigation system.

13. Alignment of the femur specimen in the rig

In this study, the specimen femurs were potted in a bone cement block in a vertical alignment using a spirit level and a plumb line as reference markers, before being mounted in the rig and further adjusted so that they hung vertically in the rig and the epicondyles were in line with the hinge of the rig. Although this method proved satisfactory, it would have been more accurate to devise a jig to allow the alignment of the femur in the rig using the navigation system, to better align the rotation of the femurs using the bony landmarks as well as the position of the hanging tibia.

14. Patella tracking was not monitored

Abnormal patellar tracking and instability are significant causes of symptoms and may necessitate revision surgery following TKR. Rotational component misalignment, in particular, as well as the addition of posterior slope, can result in abnormal patellar tracking and instability. In this study, the position of the patella was not monitored. Ideally, the patella should have been resurfaced (as per normal surgical protocol) and an additional navigation tracker modified and applied to the patella to allow its movements and displacements to be tracked during all the loading cycles and component configurations. Unfortunately such technology was not available at the time and we suggest that future experiments incorporate patellar tracking as part of the kinematic analyses of the knee.

FUTURE EXPERIMENTS

1. Use of a tibial force platform in a loaded TKR in cadaver specimens.

From the results of this study, it has been possible to ascertain the envelope of laxity of the knee but not the centre of force. That is, the resultant tibio-femoral force. It is presumed that as the envelope of laxity of the knee changes through a flexion-extension cycle; that the resultant force will also translate between the medial and lateral sides of the implanted knee.

As a follow-up study, it is suggested that a standard tibial tray be modified into a force platform by machining 3 equidistant recesses in a triangular formation into its top surface. These recesses would then accommodate micro load cells. A standard polyethylene insert would then be used as per normal surgical protocol. The force platform would then be implanted using a navigated surgical technique into a fresh cadaver knee specimen. This specimen would then be mounted into a suitable rig and loaded with a variety of loading cycles through a full range of flexion / extension. Continuous data would be recorded from the load cells for all the loading conditions and cross referenced with the navigation systems recorded flexion / extension data.

The data collected from the load cells would be analysed and used to triangulate the movements of the resultant force crossing the knee through the various loading conditions. This knowledge will further enhance the understanding of load transmission in the implanted knee and may influence polyethylene designs to ensure central and even loading of the medial and lateral compartments in knee replacement prostheses.

2. Strain Gauges.

From the results of this study, it has been possible to ascertain the envelope of laxity of the knee and how tibial component misalignment affects this envelope. It is presumed that the observed changes and constraints of the envelope of laxity of the knee are due to the restraining properties of the ligaments.

As a following study, it is suggested that a fresh cadaver knee specimen be dissected to allow the implantation of small strain gauges within the various ligament complexes of the medial and lateral sides of the knee. The specimen would then be mounted into a suitable rig and undergo navigated knee replacement as per normal surgical protocol, then loaded with a variety of loading cycles through a full range of flexion / extension. Continuous data would be recorded from the strain gauges for all the loading conditions and cross referenced with the navigation systems recorded flexion / extension data.

The data collected from the strain gauges would be analysed and used to determine the ligament tensions and resultant force transmission to the medial and lateral sides of the knee through the various loading conditions. Alternatively, this data could be obtained using robotic technology. This knowledge will further enhance the understanding of load transmission in the implanted knee and may influence the design and soft tissue balancing of TKR components.

3. Mobile bearings.

From the results of this study, it has been possible to ascertain the envelope of laxity of the knee and the effects of misalignment on the envelope of laxity of the knee using a standard cruciate retaining tibial tray. The effect of misalignment of mobile bearing knee designs is not known.

As a following study, it is suggested that the experiments performed in this study be repeated using a mobile bearing knee design.

The collected data would then be used to compare the kinematics and effects of misalignment between fixed bearing and mobile bearing designs to determine the tolerances of misalignment of mobile bearings and to determine if they are more forgiving, particularly in cases of rotational misalignment of the tibial tray.

4. Pressure film measurements

From the results of this study, it has been possible to ascertain the envelope of laxity of the knee and the effects of misalignment on the envelope of laxity of the knee.

As a following study, it is suggested that pressure film measurements of the medial and lateral compartment polyethylene insert following navigated TKR are performed at various degrees of flexion under a protocol of loading conditions. These pressure film measurements would then be repeated following component misalignment to determine if misalignment affects pressure distribution across the polyethylene insert that may lead to overloading and accelerated wear of the insert.

5. Patellar kinematics

Abnormal patellar tracking and instability are significant causes of symptoms and may necessitate revision surgery following TKR. In this study, the kinematics of the patella were ignored as there was not sufficient technology to mount an IR kinematic tracker to the patella. We suggest that in future experiments, a kinematic tracker be modified and used to incorporate patellar tracking as part of the kinematic analyses of the knee.

REFERENCES

Reference List

1. Application for Ethical Approval with Ealing Hospital Research Ethical Committee - COREC Ref No: 06/Q046/8. COREC website . 23-1-2006.
Ref Type: Journal (Full)

2. Joint Replacement Institute. Internet ref . 2007.
Ref Type: Journal (Full)

3. Sawbones USA. Pacific Research Laboratories Inc . 2007.
Ref Type: Journal (Full)

4. Total Knee Replacement Statistics. American Academy of Orthoppaedic Surgeons Website . 2007.
Ref Type: Journal (Full)

5. Arthritis Foundation USA. 2008.
Ref Type: Generic

6. Google Medical Image Library. 2008.
Ref Type: Generic

7. **Pacific Research Laboratories, Inc.** 2008.
Ref Type: Generic

8. Wikipedia Internet Resource. 2008.
Ref Type: Generic

9. www.medicinenet.com. 2008.
Ref Type: Generic

10. Images Used With Patient Permission and Courtesy of Southampton General Hospital. 2009.
Ref Type: Generic

11. Aglietti, P., Buzzi, R., and Gaudenzi, A.: Patellofemoral functional results and complications with the posterior stabilized total condylar knee prosthesis. J. Arthroplasty. 3:17-25, 1988.

12. Akagi, M., Ueo, T., Matsusue, Y., Akiyama, H., and Nakamura, T.: Improved range of flexion after total knee arthroplasty. The total condylar knee versus the KU knee. Bull. Hosp. Jt. Dis. 56:225-232, 1997.

13. Amis, A. A., Senavongse, W., and Bull, A. M.: Patellofemoral kinematics during knee flexion-extension: an in vitro study
2. J. Orthop. Res. 24:2201-2211, 2006.

14. Andriacchi T.P, Stanwyck T.S., and Galante J.O. Knee Biomechanics and Total Knee
Replacement. J.Arthroplasty 1, 211-219. 1994.
Ref Type: Journal (Full)

15. Arthritis Statistics CDC.2008. The National Women's Health Information Center. 2008.
Ref Type: Generic

16. Ateshian G, Colman W Mow V. Quantitative Anatomy of the Knee Joint. Knee Surgery 1, 55-76. 1994.
Ref Type: Journal (Full)

17. Bai, B., Baez, J., Testa, N., and Kummer, F. J.: Effect of posterior cut angle on tibial component loading
1. J. Arthroplasty. 15:916-920, 2000.

18. Banks S.A. and Hodge W.A. Accurate measurement of three-dimensional knee replacement kinematics using single-plane fluoroscopy. IEEE Trans.Biomed.Eng [345], 65-69. 1996.
Ref Type: Journal (Full)

19. Banks, S. A., Markovich, G. D., and Hodge, W. A.: In vivo kinematics of cruciate-retaining and -substituting knee arthroplasties. J. Arthroplasty. 12:297-304, 1997.

20. Bathis, H., Perlick, L., Tingart, M., Perlick, C., Luring, C., and Grifka, J.: Intraoperative cutting errors in total knee arthroplasty. Arch Orthop Trauma Surg. 125:16-20, 2005.

21. Bathis, H., Shafizadeh, S., Paffrath, T., Simanski, C., Grifka, J., and Luring, C.: [Are computer assisted total knee replacements more accurately placed? A meta-analysis of comparative studies]. Orthopade. 35:1056-1065, 2006.

22. Beadling L. Better Extensor Mechanism Function. Orthopaedics Today . 1999.
Ref Type: Journal (Full)

23. Bellemans, J., Robijns, F., Duerinckx, J., Banks, S., and Vandenneucker, H.: The influence of tibial slope on maximal flexion after total knee arthroplasty. Knee Surg Sports Traumatol. Arthrosc. 13:193-196, 2005.

24. Bergman RA, Adel K, Jew J, and Reimann P. Atlas of human anatomy in cross section. Section 7 Lower Limb. 2009.
Ref Type: Generic

25. Best, J. T.: Revision total hip and total knee arthroplasty. Orthop Nurs. 24:174-179, 2005.

26. Blankevoort, L., Huiskes, R., and de Lange, A.: The envelope of passive knee joint motion. J. Biomech. 21:705-720, 1988.

27. Blunn, G. W., Walker, P. S., Joshi, A., and Hardinge, K.: The dominance of cyclic sliding in producing wear in total knee replacements. Clin. Orthop Relat Res.253-260, 1991.

28. Bull, A. M., Kessler, O., Alam, M., and Amis, A. A.: Changes in knee kinematics reflect the articular geometry after arthroplasty. Clin. Orthop. Relat Res. 466:2491-2499, 2008.

29. Catani, F., Fantozzi, S., Ensini, A., Leardini, A., Moschella, D., and Giannini, S.: Influence of tibial component posterior slope on in vivo knee kinematics in fixed-bearing total knee arthroplasty

1. J. Orthop. Res. 24:581-587, 2006.

30. Chang, C. W. and Yang, C. Y.: Kinematic navigation in total knee replacement--experience from the first 50 cases. J. Formos. Med. Assoc. 105:468-474, 2006.

31. Charnley, J.: The long-term results of low-friction arthroplasty of the hip performed as a primary intervention. 1972. Clin. Orthop Relat Res.4-15, 1995.

32. Chauhan, S. K., Scott, R. G., Breidahl, W., and Beaver, R. J.: Computer-assisted knee arthroplasty versus a conventional jig-based technique. A randomised, prospective trial

1. J. Bone Joint Surg. Br. 86:372-377, 2004.

33. Clemantine C. A regional atlas to the human body. Baltimore: Williams and Wilkins , 452-459. 1987.

Ref Type: Journal (Full)

34. Cloutier, J. M.: Results of total knee arthroplasty with a non-constrained prosthesis. J. Bone Joint Surg Am. 65:906-919, 1983.

35. Davidson J.M. and Hedley W.S. A method of precise localisation and measurement by means of roentgen rays. lancet , 1001. 1897.

Ref Type: Journal (Full)

36. de Bruin, P. W., Kaptein, B. L., Stoel, B. C., Reiber, J. H., Rozing, P. M., and Valstar, E. R.: Image-based RSA: Roentgen stereophotogrammetric analysis based on 2D-3D image registration. J. Biomech. 41:155-164, 2008.

37. Defrate, L. E., Papannagari, R., Gill, T. J., Moses, J. M., Pathare, N. P., and Li, G.: The 6 degrees of freedom kinematics of the knee after anterior cruciate ligament deficiency: an in vivo imaging analysis. Am. J. Sports Med. 34:1240-1246, 2006.

38. Dennis, D. A., Komistek, R. D., Colwell, C. E., Jr., Ranawat, C. S., Scott, R. D., Thornhill, T. S., and Lapp, M. A.: In vivo anteroposterior femorotibial translation of total knee arthroplasty: a multicenter analysis. Clin. Orthop. Relat Res.47-57, 1998.

39. Dennis, D. A., Komistek, R. D., Stiehl, J. B., Walker, S. A., and Dennis, K. N.: Range of motion after total knee arthroplasty: the effect of implant design and weight-bearing conditions. J. Arthroplasty. 13:748-752, 1998.

40. Dowson D. Biotribology of natural and replacement synovial joints. Biomechanics of diarthrodial joints , 305-345. 1990. Springer verlag.
Ref Type: Generic

41. EBERHART, H. D. and INMAN, V. T.: An evaluation of experimental procedures used in a fundamental study of human locomotion. Ann. N. Y. Acad. Sci. 51:1213-1228, 1951.

42. Eisenhart-Rothe, R., Vogl, T., Englmeier, K. H., and Dennis, D. A.: [TKA kinematics. In vivo techniques and results]. Orthopade. 36:620-627, 2007.

43. El Masri, F., Rammal, H., Ghanem, I., El Hage, S., El Abiad, R., Kharrat, K., and Dagher, F.: [Computer-assisted surgery in total knee replacement. Preliminary results: report of 60 cases]. Rev. Chir Orthop. Reparatrice Appar. Mot. 94:261-267, 2008.

44. Ensini, A., Catani, F., Leardini, A., Romagnoli, M., and Giannini, S.: Alignments and clinical results in conventional and navigated total knee arthroplasty. Clin. Orthop Relat Res. 457:156-162, 2007.

45. Farahmand, F., Senavongse, W., and Amis, A. A.: Quantitative study of the quadriceps muscles and trochlear groove geometry related to instability of the patellofemoral joint
1. J. Orthop. Res. 16:136-143, 1998.

46. Fehring, T. K., Odum, S., Griffin, W. L., Mason, J. B., and Nadaud, M.: Early failures in total knee arthroplasty. Clin. Orthop Relat Res.315-318, 2001.

47. Felson, D. T., Zhang, Y., Hannan, M. T., Naimark, A., Weissman, B. N., Aliabadi, P., and Levy, D.: The incidence and natural history of knee osteoarthritis in the elderly. The Framingham Osteoarthritis Study. Arthritis Rheum. 38:1500-1505, 1995.

48. Figgie, H. E., III, Goldberg, V. M., Heiple, K. G., Moller, H. S., III, and Gordon, N. H.: The influence of tibial-patellofemoral location on function of the knee in patients with the posterior stabilized condylar knee prosthesis. J. Bone Joint Surg. Am. 68:1035-1040, 1986.

49. Fisher, J. and Dowson, D.: Tribology of total artificial joints. Proc. Inst. Mech. Eng [H.]. 205:73-79, 1991.

50. Giffin, J. R., Stabile, K. J., Zantop, T., Vogrin, T. M., Woo, S. L., and Harner, C. D.: Importance of tibial slope for stability of the posterior cruciate ligament deficient knee
1. Am. J. Sports Med. 35:1443-1449, 2007.

51. Gryzlo, S. M., Patek, R. M., Pink, M., and Perry, J.: Electromyographic analysis of knee rehabilitation exercises. J. Orthop. Sports Phys. Ther. 20:36-43, 1994.

52. Gunston, F. H.: Polycentric knee arthroplasty: prosthetic simulation of normal knee movement. 1971. Clin. Orthop Relat Res. 446:11-12, 2006.

53. Hallen, L. G. and Lindahl, O.: The "screw-home" movement in the knee-joint. Acta Orthop Scand. 37:97-106, 1966.

54. Hanson, G. R., Suggs, J. F., Freiberg, A. A., Durbhakula, S., and Li, G.: Investigation of in vivo 6DOF total knee arthoplasty kinematics using a dual orthogonal fluoroscopic system. J. Orthop. Res. 24:974-981, 2006.

55. Hernandez-Vaquero, D. and Suarez-Vazquez, A.: Complications of fixed infrared emitters in computer-assisted total knee arthroplasties
1. BMC. Musculoskelet. Disord. 8:71, 2007.

56. Hofmann, S., Romero, J., Roth-Schiffl, E., and Albrecht, T.: [Rotational malalignment of the components may cause chronic pain or early failure in total knee arthroplasty]. Orthopade. 32:469-476, 2003.

57. Hollister, A. M., Jatana, S., Singh, A. K., Sullivan, W. W., and Lupichuk, A. G.: The axes of rotation of the knee. Clin. Orthop Relat Res.259-268, 1993.

58. Ishii, Y., Terajima, K., Koga, Y., and Bechtold, J. E.: Screw home motion after total knee replacement. Clin. Orthop. Relat Res.181-187, 1999.

59. Jeffery, R. S., Morris, R. W., and Denham, R. A.: Coronal alignment after total knee replacement. J Bone Joint Surg Br. 73:709-714, 1991.

60. Jenny, J. Y., Clemens, U., Kohler, S., Kiefer, H., Konermann, W., and Miehlke, R. K.: Consistency of implantation of a total knee arthroplasty with a non-image-based navigation system: a case-control study of 235 cases compared with 235 conventionally implanted prostheses. J Arthroplasty. 20:832-839, 2005.

61. Jojima, H., Whiteside, L. A., and Ogata, K.: Effect of tibial slope or posterior cruciate ligament release on knee kinematics
1. Clin. Orthop. Relat Res.194-198, 2004.

62. Jones W.N., Aufranc O.E., and Kermond W.L. Mould arthroplasty of the knee. J.Bone Joint Surg 49[A], 1022. 1967.
Ref Type: Journal (Full)

63. Judet J., Judet R., and Crepin G.T. Essais de prosthese osteo-articulaire. Presse Med 52, 302. 1947.
Ref Type: Journal (Full)

64. Kadaba, M. P., Ramakrishnan, H. K., and Wootten, M. E.: Measurement of lower extremity kinematics during level walking. J. Orthop. Res. 8:383-392, 1990.

65. Kamat, Y. D., Aurakzai, K. M., Adhikari, A. R., Matthews, D., Kalairajah, Y., and Field, R. E.: Does computer navigation in total knee arthroplasty improve patient outcome at midterm follow-up?
1. Int. Orthop. 33:1567-1570, 2009.

66. Kansara, D. and Markel, D. C.: The effect of posterior tibial slope on range of motion after total knee arthroplasty
1. J. Arthroplasty. 21:809-813, 2006.

67. Kessler, O., Lacatusu, E., Sommers, M. B., Mayr, E., and Bottlang, M.: Malrotation in total knee arthroplasty: effect on tibial cortex strain captured by laser-based strain acquisition. Clin. Biomech. (Bristol. , Avon.). 21:603-609, 2006.

68. Kim, J. M. and Moon, M. S.: Squatting following total knee arthroplasty. Clin. Orthop Relat Res.177-186, 1995.

69. Kim, S. J., MacDonald, M., Hernandez, J., and Wixson, R. L.: Computer assisted navigation in total knee arthroplasty: improved coronal alignment. J. Arthroplasty. 20:123-131, 2005.

70. Kinzel, V., Ledger, M., and Shakespeare, D.: Can the epicondylar axis be defined accurately in total knee arthroplasty? Knee. 12:293-296, 2005.

71. Komistek, R. D., Kane, T. R., Mahfouz, M., Ochoa, J. A., and Dennis, D. A.: Knee mechanics: a review of past and present techniques to determine in vivo loads. J. Biomech. 38:215-228, 2005.

72. KUHNS, J. G.: NYLON MEMBRANE ARTHROPLASTY OF THE KNEE IN CHRONIC ARTHRITIS. J. Bone Joint Surg Am. 46:448-449, 1964.

73. Kurtz, S., Mowat, F., Ong, K., Chan, N., Lau, E., and Halpern, M.: Prevalence of primary and revision total hip and knee arthroplasty in the United States from 1990 through 2002. J. Bone Joint Surg Am. 87:1487-1497, 2005.

74. Kurtz, S., Ong, K., Lau, E., Mowat, F., and Halpern, M.: Projections of primary and revision hip and knee arthroplasty in the United States from 2005 to 2030. J. Bone Joint Surg Am. 89:780-785, 2007.

75. Lacoste, C., Granizo, J. J., and Gomez-Barrena, E.: Reliability of a simple fluoroscopic method to study sagittal plane femorotibial contact changes in total knee arthroplasties during flexion. Knee. 14:289-294, 2007.

76. Landy, M. M. and Walker, P. S.: Wear of ultra-high-molecular-weight polyethylene components of 90 retrieved knee prostheses. J. Arthroplasty. 3 Suppl:S73-S85, 1988.

77. Laskin R.S. Alignment of total knee arthroplasty components. Orthopaedics [7], 62-68. 1984.
Ref Type: Journal (Full)

78. Laskin, R. S.: Articular constraint: use only what you need. Orthopedics. 26:975-976, 2003.

79. Lee, K. Y., Slavinsky, J. P., Ries, M. D., Blumenkrantz, G., and Majumdar, S.: Magnetic resonance imaging of in vivo kinematics after total knee arthroplasty. J. Magn Reson. Imaging. 21:172-178, 2005.

80. Li, G., Most, E., Otterberg, E., Sabbag, K., Zayontz, S., Johnson, T., and Rubash, H.: Biomechanics of posterior-substituting total knee arthroplasty: an in vitro study. Clin. Orthop. Relat Res.214-225, 2002.

81. Logan, M. C., Williams, A., Lavelle, J., Gedroyc, W., and Freeman, M.: What really happens during the Lachman test? A dynamic MRI analysis of tibiofemoral motion. Am J. Sports Med. 32:369-375, 2004.

82. Lombardi, A. V., Jr., Berend, K. R., Aziz-Jacobo, J., and Davis, M. B.: Balancing the flexion gap: relationship between tibial slope and posterior cruciate ligament release and correlation with range of motion
1. J. Bone Joint Surg. Am. 90 Suppl 4:121-132, 2008.

83. Lotke PA and Ecker ML. Influence of positioning of prosthesis in total knee replacement. J Bone Joint Surg Am [59], 77-79. 1977.
Ref Type: Journal (Full)

84. Macdonald, W., Styf, J., Carlsson, L. V., and Jacobsson, C. M.: Improved tibial cutting accuracy in knee arthroplasty
1. Med. Eng Phys. 26:807-812, 2004.

85. Macintosh D.L. Arthroplasty of the knee. J.Bone Joint Surg 48[B], 179. 1966.
Ref Type: Journal (Full)

86. Macule-Beneyto, F., Hernandez-Vaquero, D., Segur-Vilalta, J. M., Colomina-Rodriguez, R., Hinarejos-Gomez, P., Garcia-Forcada, I., and Seral, G. B.: Navigation in total knee arthroplasty. A multicenter study. Int. Orthop. 30:536-540, 2006.

87. Maestro, A., Harwin, S. F., Sandoval, M. G., Vaquero, D. H., and Murcia, A.: Influence of intramedullary versus extramedullary alignment guides on final total knee arthroplasty component position: a radiographic analysis. J. Arthroplasty. 13:552-558, 1998.

88. Magnoni J.M. Genou en resine acrylique. Rev.Orthop 35, 556. 1949.
Ref Type: Journal (Full)

89. Mahoney, O. Improved extensor mechanism (function with the Scorpio total knee replacement). Presented at the 45th Annual meeting of the orthopaedic research society . 1999.
Ref Type: Journal (Full)

90. Mahoney, O. M. and Kinsey, T. L.: 5- to 9-year survivorship of single-radius, posterior-stabilized TKA. Clin. Orthop. Relat Res. 466:436-442, 2008.

91. Malviya, A., Lingard, E. A., Weir, D. J., and Deehan, D. J.: Predicting range of movement after knee replacement: the importance of posterior condylar offset and tibial slope
9. Knee. Surg. Sports Traumatol. Arthrosc. 17:491-498, 2009.

92. Matsuda, S., Miura, H., Nagamine, R., Urabe, K., Hirata, G., and Iwamoto, Y.: Effect of femoral and tibial component position on patellar tracking following total knee arthroplasty: 10-year follow-up of Miller-Galante I knees. Am J. Knee Surg. 14:152-156, 2001.

93. Matsumoto, H., Seedhom, B. B., Suda, Y., Otani, T., and Fujikawa, K.: Axis location of tibial rotation and its change with flexion angle. Clin. Orthop Relat Res.178-182, 2000.

94. Matziolis, G., Mehlhorn, S., Schattat, N., Diederichs, G., Hube, R., Perka, C., and Matziolis, D.: How much of the PCL is really preserved during the tibial cut?
1. Knee. Surg. Sports Traumatol. Arthrosc. 2011.

95. McKee, G. K. and Watson-Farrar, J.: Replacement of arthritic hips by the McKee-Farrar prosthesis. J. Bone Joint Surg Br. 48:245-259, 1966.

96. Merkow, R. L., Soudry, M., and Insall, J. N.: Patellar dislocation following total knee replacement. J. Bone Joint Surg. Am. 67:1321-1327, 1985.

97. Migaud, H., De Ladoucette, A., Dohin, B., Cloutier, J. M., Gougeon, F., and Duquennoy, A.: [Influence of the tibial slope on tibial translation and mobility of non-constrained total knee prosthesis]. Rev. Chir Orthop Reparatrice Appar. Mot. 82:7-13, 1996.

98. Miller, M. C., Berger, R. A., Petrella, A. J., Karmas, A., and Rubash, H. E.: Optimizing femoral component rotation in total knee arthroplasty. Clin. Orthop Relat Res.38-45, 2001.

99. Molfetta, L. and Caldo, D.: Computer navigation versus conventional implantation for varus knee total arthroplasty: a case-control study at 5 years follow-up
1. Knee. 15:75-79, 2008.

100. Moran, C. G. and Horton, T. C.: Total knee replacement: the joint of the decade. A successful operation, for which there's a large unmet need. BMJ. 320:820, 2000.

101. Moro-oka, T. A., Hamai, S., Miura, H., Shimoto, T., Higaki, H., Fregly, B. J., Iwamoto, Y., and Banks, S. A.: Can magnetic resonance imaging-derived bone models be used for accurate motion measurement with single-plane three-dimensional shape registration? J. Orthop Res. 25:867-872, 2007.

102. Moro-oka, T. A., Hamai, S., Miura, H., Shimoto, T., Higaki, H., Fregly, B. J., Iwamoto, Y., and Banks, S. A.: Dynamic activity dependence of in vivo normal knee kinematics. J. Orthop. Res. 26:428-434, 2008.

103. Muller, W.: Form and function of the knee. Its relation to high performance and to sports. Am J. Sports Med. 24:S104-S106, 1996.

104. Murphy M.C., Zarins B., Jasty M, and Mann R.W. In Vivo Measurement of the Three-
Dimensional Skeletal Motion at the Normal Knee. Trans.Orthop Res.Soc. 142-144. 1995.
Ref Type: Journal (Full)

105. Murphy, J. B.: I. Arthroplasty. Ann. Surg. 57:593-647, 1913.

106. Nabeyama, R., Matsuda, S., Miura, H., Mawatari, T., Kawano, T., and Iwamoto, Y.: The accuracy of image-guided knee replacement based on computed tomography. J Bone Joint Surg Br. 86:366-371, 2004.

107. Nadzadi, M. E., Nielsen, J. K., Ecker, T. M., and Murphy, S. B.: Passive kinematics and laxity of prosthetic knees and intact knees as measured by a novel computer-assisted system. Orthopedics. 30:92-96, 2007.

108. Nilsson, K. G., Karrholm, J., and Ekelund, L.: Knee motion in total knee arthroplasty. A roentgen stereophotogrammetric analysis of the kinematics of the Tricon-M knee prosthesis. Clin. Orthop Relat Res.147-161, 1990.

109. Ostermeier, S., Hurschler, C., Windhagen, H., and Stukenborg-Colsman, C.: In vitro investigation of the influence of tibial slope on quadriceps extension force after total knee arthroplasty
1. Knee. Surg. Sports Traumatol. Arthrosc. 14:934-939, 2006.

110. Picard, F., Deakin, A. H., Clarke, J. V., Dillon, J. M., and Gregori, A.: Using Navigation Intraoperative Measurements Narrows Range of Outcomes in TKA. Clin. Orthop Relat Res. 463:50-57, 2007.

111. Plaskos, C., Hodgson, A. J., Inkpen, K., and McGraw, R. W.: Bone cutting errors in total knee arthroplasty. J. Arthroplasty. 17:698-705, 2002.

112. Putti, V. I. Arthroplasty. Am J.Orthop.Surg 19, 421. 1953.
Ref Type: Journal (Full)

113. Ranawat, C. S., Flynn, W. F., Jr., Saddler, S., Hansraj, K. K., and Maynard, M. J.: Long-term results of the total condylar knee arthroplasty. A 15-year survivorship study. Clin. Orthop Relat Res.94-102, 1993.

114. Rodriguez, J. A., Bhende, H., and Ranawat, C. S.: Total condylar knee replacement: a 20-year followup study. Clin. Orthop Relat Res.10-17, 2001.

115. Romero, J., Stahelin, T., Wyss, T., and Hofmann, S.: [Significance of axial rotation alignment of components of knee prostheses]. Orthopade. 32:461-468, 2003.

116. Rousseau, M. A., Lazennec, J. Y., and Catonne, Y.: Early mechanical failure in total knee arthroplasty. Int. Orthop. 32:53-56, 2008.

117. Sampson, J. E. Arthroplasty of the knee joint. J.Bone Joint Surg [31-B], 50. 1949.
Ref Type: Journal (Full)

118. Scarvell, J. M., Smith, P. N., Refshauge, K. M., and Galloway, H. R.: Magnetic resonance imaging analysis of kinematics in osteoarthritic knees. J. Arthroplasty. 22:383-393, 2007.

119. Schepers, H. M., Koopman, H. F., and Veltink, P. H.: Ambulatory assessment of ankle and foot dynamics. IEEE Trans. Biomed. Eng. 54:895-902, 2007.

120. Schurman, D. J., Parker, J. N., and Ornstein, D.: Total condylar knee replacement. A study of factors influencing range of motion as late as two years after arthroplasty. J. Bone Joint Surg Am. 67:1006-1014, 1985.

121. Selvik, G.: Roentgen stereophotogrammetry. A method for the study of the kinematics of the skeletal system. Acta Orthop Scand. Suppl. 232:1-51, 1989.

122. Selvik, G., Alberius, P., and Aronson, A. S.: A roentgen stereophotogrammetric system. Construction, calibration and technical accuracy. Acta Radiol. Diagn. (Stockh). 24:343-352, 1983.

123. Serpe, L. Conformity without constraint. 45th annual meeting of orthopaedic research society . 1999.
Ref Type: Journal (Full)

124. Shefelbine, S. J., Ma, C. B., Lee, K. Y., Schrumpf, M. A., Patel, P., Safran, M. R., Slavinsky, J. P., and Majumdar, S.: MRI analysis of in vivo meniscal and tibiofemoral kinematics in ACL-deficient and normal knees. J. Orthop Res. 24:1208-1217, 2006.

125. Sikorski, J. M. and Blythe, M. C.: Learning the vagaries of computer-assisted total knee replacement. J Bone Joint Surg Br. 87:903-910, 2005.

126. Simmons, E. D., Jr., Sullivan, J. A., Rackemann, S., and Scott, R. D.: The accuracy of tibial intramedullary alignment devices in total knee arthroplasty. J. Arthroplasty. 6:45-50, 1991.

127. Spencer, J. M., Chauhan, S. K., Sloan, K., Taylor, A., and Beaver, R. J.: Computer navigation versus conventional total knee replacement: no difference in functional results at two years
1. J. Bone Joint Surg. Br. 89:477-480, 2007.

128. Stiehl, J. B., Dennis, D. A., Komistek, R. D., and Crane, H. S.: In vivo determination of condylar lift-off and screw-home in a mobile-bearing total knee arthroplasty. J. Arthroplasty. 14:293-299, 1999.

129. Stiehl, J. B., Komistek, R. D., and Dennis, D. A.: Detrimental kinematics of a flat on flat total condylar knee arthroplasty. Clin. Orthop. Relat Res.139-148, 1999.

130. Stryker. Operative Reference Guide for Scorpio CR Total Knee Prosthesis. 2008.
Ref Type: Generic

131. Stryker. Operative Technique Guide For Stryker Scorpio Navigation System. 2008.
Ref Type: Generic

132. Takatsu, T., Itokazu, M., Shimizu, K., and Brown, T. D.: The function of posterior tilt of the tibial component following posterior cruciate ligament-retaining total knee arthroplasty. Bull. Hosp. Jt. Dis. 57:195-201, 1998.

133. Taylor, W. R., Heller, M. O., Bergmann, G., and Duda, G. N.: Tibio-femoral loading during human gait and stair climbing. J. Orthop. Res. 22:625-632, 2004.

134. Teter, K. E., Bregman, D., and Colwell, C. W., Jr.: Accuracy of intramedullary versus extramedullary tibial alignment cutting systems in total knee arthroplasty. Clin. Orthop Relat Res.106-110, 1995.

135. Tingart, M., Luring, C., Bathis, H., Beckmann, J., Grifka, J., and Perlick, L.: Computer-assisted total knee arthroplasty versus the conventional technique: how precise is navigation in clinical routine? Knee Surg Sports Traumatol. Arthrosc. 2007.

136. Toksvig-Larsen, S. and Ryd, L.: Surface flatness after bone cutting. A cadaver study of tibial condyles
1. Acta Orthop. Scand. 62:15-18, 1991.

137. Uvehammer, J., Karrholm, J., and Brandsson, S.: In vivo kinematics of total knee arthroplasty. Concave versus posterior-stabilised tibial joint surface. J. Bone Joint Surg. Br. 82:499-505, 2000.

138. Uvehammer, J., Karrholm, J., Brandsson, S., Herberts, P., Carlsson, L., Karlsson, J., and Regner, L.: In vivo kinematics of total knee arthroplasty: flat compared with concave tibial joint surface. J. Orthop. Res. 18:856-864, 2000.

139. Verneviul A. De la création d'une fausse articulation par section ou ressection partielle de l'os maxillaire inférieur, comme moyen de rémedier a l'ankylose vraie ou fausse de la machoire inférieure. Arch Gen Med 15[174]. 1840.
Ref Type: Journal (Full)

140. WALLDIUS, B.: Arthroplasty of the knee joint employing an acrylic prosthesis. Acta Orthop. Scand. 23:121-131, 1953.

141. WALLDIUS, B.: Arthroplasty of the knee using an endoprosthesis. Clin. Orthop Relat Res.4-10, 1996.

142. Wasielewski, R. C., Galante, J. O., Leighty, R. M., Natarajan, R. N., and Rosenberg, A. G.: Wear patterns on retrieved polyethylene tibial inserts and their relationship to technical considerations during total knee arthroplasty. Clin. Orthop Relat Res.31-43, 1994.

143. Weber, W and Weber, E. Mechanik der menschlichen Gehwerkzeuge. Göttingen Dieterich. 1836. 1836.
Ref Type: Generic

144. Werner, F. W., Ayers, D. C., Maletsky, L. P., and Rullkoetter, P. J.: The effect of valgus/varus malalignment on load distribution in total knee replacements. J. Biomech. 38:349-355, 2005.

145. Whiteside, L. A. and Amador, D. D.: The effect of posterior tibial slope on knee stability after Ortholoc total knee arthroplasty
1. J. Arthroplasty. 3 Suppl:S51-S57, 1988.

146. Whiteside, L. A. and Amador, D. D.: Rotational stability of a posterior stabilized total knee arthroplasty. Clin. Orthop Relat Res.241-246, 1989.

147. Whiteside, L. A., Kasselt, M. R., and Haynes, D. W.: Varus-valgus and rotational stability in rotationally unconstrained total knee arthroplasty. Clin. Orthop Relat Res.147-157, 1987.

148. Wimmer, M. A. and Andriacchi, T. P.: Tractive forces during rolling motion of the knee: implications for wear in total knee replacement. J. Biomech. 30:131-137, 1997.

149. Windsor, R. E., Scuderi, G. R., Moran, M. C., and Insall, J. N.: Mechanisms of failure of the femoral and tibial components in total knee arthroplasty. Clin. Orthop Relat Res.15-19, 1989.

150. Woo, S. L., Debski, R. E., Withrow, J. D., and Janaushek, M. A.: Biomechanics of knee ligaments. Am J. Sports Med. 27:533-543, 1999.

151. Wright, T. M., Rimnac, C. M., Stulberg, S. D., Mintz, L., Tsao, A. K., Klein, R. W., and McCrae, C.: Wear of polyethylene in total joint replacements. Observations from retrieved PCA knee implants. Clin. Orthop Relat Res.126-134, 1992.

152. Yingying, S., Chengtao, W., Yuanshuai, Q., Shiju, Y., and Lixu, G.: Development of an imageless navigation system for total knee arthroplasty. Conf. Proc. IEEE Eng Med Biol. Soc. 6:6060-6063, 2005.

153. Zuppinger H. Die active flexion im unbelastien Knigelenk. Wiesbaden Bergamann , 703. 1904.
Ref Type: Journal (Full)